

Doctoral Thesis

**Modeling of Film Blowing Process
for Non-Newtonian Fluids by using
Variational Principles**

Modelování procesu vyfukování fólií
pro neneutonské kapaliny
s využitím variačního počtu

Roman Kolařík

June 2012

Zlín, Czech Republic

Study program: P2808 Chemistry and Material Technology
2808V006 Technology of Macromolecular Substances

Supervisor: Prof. Ing. Martin Zatloukal, Ph.D.

© Ing. Roman Kolařík

Published by Tomas Bata University in Zlín in 2012

ACKNOWLEDGEMENT

At this place, I would like to express my heartfelt thanks to all people who made this thesis possible.

I wish to express my deepest gratitude to my supervisor, Professor Martin Zatloukal, for his permanent support, valuable advices and patience not only during the time I worked on this thesis.

Besides, my grateful thanks belong to my co-authors, Professor Costas Tzoganakis and Dr. Mike Martyn for their cooperation.

My acknowledgement also belongs to all my colleagues, friends, from Faculty of Technology for their friendly environment and kind help. I am especially thankful to my best friend, Jan Musil, who involved me in cleaning procedure (550 times) of laboratory extruder during my doctoral study. ☺

Finally, I would like to express my special gratitude and thanks to my parents, sisters, brother-in-law and his family and to my little niece, for their permanent support, patience and beautiful moments of my life that filled me with new energy needed for my studies.

Thank you all. This thesis would not have been possible without your support.

ABSTRACT

The first part of this work introduces the tubular film blowing process for polymer films production together with the process instabilities which represent the main limiting factors for this technology. Specific attention has been paid to the summarization and description of different models in chronological order, which can be utilized for single-layer and multi-layer film blowing modeling.

In the second part of this work, a novel numerical scheme for variational principle based modeling of the non-isothermal, single-layer film blowing process which takes into consideration the generalized Newtonian model depending on three principal invariants of the deformation rate tensor, D , and its absolute value (defined as the square root of $D \cdot D$), is proposed and successfully tested in order to understand the complicated relationship between processing conditions (i.e. internal bubble pressure, heat transfer coefficient, mass flow rate, cooling air temperature, melt/die temperature), material parameters (i.e. extensional viscosity, rupture stress, Newtonian viscosity, flow activation energy, power law index) and film blowing stability. It was discovered that the processing parameters, together with the flow activation energy, have a greater effect on the film blowing stability than the basic rheological characteristics of the polymer melt and the relationship between the film blowing stability window size (and/or minimum achievable final film thickness) and the extensional strain hardening has a non-monotonic character for a given range of melt strengths.

In the last part of this work, the proposed variational principle based modeling approach for the multi-layer film blowing process was tested on the experimental data obtained from a 9-layer film blowing line which was used to produce a LDPE/LDPE/tie/PA6/EVOH/PA6/tie/LDPE/LDPE film under different processing conditions. It was established that the utilized model can be used to describe the bubble shape and to predict the internal bubble pressure reasonably well for all applied processing conditions.

Keywords: Applied rheology • mathematical modeling • film blowing process • extrusion • polymer melts • non-Newtonian fluids • stability analysis

ABSTRAKT

První část této práce se věnuje popisu jak procesu vyfukování, který se používá k výrobě polymerních fólií, tak různých typů nestabilit, které představují hlavní limitující faktor této technologie. Zvláštní pozornost byla věnována shrnutí a popisu jednotlivých matematických modelů, které mohou být využity k modelování tohoto procesu.

Ve druhé části této práce bylo navrženo a úspěšně otestováno stabilní numerické schéma pro modelování neizotermálního procesu vyfukování jednovrstvé polymerní fólie pomocí variačního počtu s využitím generalizovaného Newtonského modelu beroucí v úvahu funkční závislost viskozity na třech základních invariantech deformačně rychlostního tenzoru D a jeho absolutní hodnotě (definované jako odmocnina z $D:D$), a to s cílem porozumět komplikovanému vztahu mezi procesními podmínkami (vnitřní přetlak, koeficient přestupu tepla, hmotnostní průtok, teplota chladicího vzduchu, teplota taveniny/vytlačovací hlavy), materiálovými parametry (tahová viskozita, pevnost taveniny, Newtonská viskozita, aktivační energie toku, index neneutonského chování) a stabilitou procesu vyfukování. Bylo odhaleno, že procesní parametry společně s aktivační energií toku mají větší vliv na stabilitu procesu vyfukování fólií než základní reologické charakteristiky polymerní taveniny, přičemž vzájemný vztah mezi velikostí stabilitního okna (a/nebo minimální dosažitelnou finální tloušťkou fólie) a stupněm zatvrzení při protahování polymerní taveniny má nemonotónní charakter v daném rozsahu pevnosti taveniny.

V poslední části této práce byla testována využitelnost a aplikovatelnost variačního počtu na modelování procesu vyfukování vícevrstevných fólií s využitím experimentálních dat získaných vyfukováním koextrudované fólie typu LDPE/LDPE/pojivo/PA6/EVOH/PA6/pojivo/LDPE/LDPE při různých zpracovatelských podmínkách. Bylo prokázáno, že použitý model popisuje jak tvar vyfukovaného rukávu, tak velikost vnitřního přtlaku s dostatečnou přesností, a to pro všechny aplikované zpracovatelské podmínky.

Klíčová slova: Aplikovaná reologie • matematické modelování • vyfukování fólií • vytlačování • polymerní taveniny • neneutonské kapaliny • stabilitní analýza

LIST OF PAPERS

The following papers are included in the present doctoral thesis:

PAPER I

Modeling of Nonisothermal Film Blowing Process for Non-Newtonian Fluids by using Variational Principles

Roman Kolarik, Martin Zatloukal

Journal of Applied Polymer Science 2011, vol. 122, no. 4, pp. 2807-2820.

PAPER II

Stability Analysis of Non-Isothermal Film Blowing Process for Non-Newtonian Fluids using Variational Principles

Roman Kolarik, Martin Zatloukal and Costas Tzoganakis

Chemical Engineering and Science 2012, vol. 73, pp. 439-453.

PAPER III

The Effect of Polyolefin Extensional Rheology on Film Blowing Process Stability

Roman Kolarik, Martin Zatloukal and Mike Martyn

Submitted for publication in *Rheologica Acta* in 2012.

PAPER IV

Evaluation of the 9-Layer Film Blowing Process by using Variational Principles

Roman Kolarik, Martin Zatloukal

Considered for publication in *Chemical Engineering and Science* in 2012.

CONTENT

ACKNOWLEDGEMENT

ABSTRACT

ABSTRAKT

LIST OF PAPERS

CONTENT

STATE OF THE FILM BLOWING PROCESS	8
1. The Film Blowing Process	8
1.1 <i>Description of the Process</i>	8
1.2 <i>Bubble Instabilities</i>	10
2. Mathematical Modeling of the Film Blowing Process.....	13
2.1 <i>Review of the Current Models Describing Single-Layer Film Blowing Process</i>	13
2.2 <i>Review of the Current Models Describing Multi-Layer Film Blowing Process</i>	20
2.3 <i>Pearson and Petrie Formulation</i>	21
2.4 <i>Zatloukal and Vlcek Formulation</i>	26
THE AIMS OF THE DOCTORAL RESEARCH WORK.....	29
SUMMARY OF THE PAPERS	30
CONCLUSION	33
REFERENCES.....	35
PAPER I	43
PAPER II.....	59
PAPER III	77
PAPER IV	145
CURRICULUM VITAE	
LIST OF PUBLICATIONS	

STATE OF THE FILM BLOWING PROCESS

1. The Film Blowing Process

The film blowing process belongs to an important polymer processing operation continuously producing thin biaxially oriented thermoplastic films at constant mass flow rate. A biaxial orientation of a single or multi layer film structure is caused by the take-up force and internal bubble pressure effect in the machine (axial) and transverse (circumferential) direction, respectively. Typical applications of blown films include packaging (grocery sacks, carrier bags, garbage bags, food wrapping films, shrink films, stretch films), barrier films (meat or cheese packaging), agricultural films (greenhouse films, silage stretch films), medical films and separators for Li-ion batteries. All these biaxially oriented products are mostly made of polyolefines, polystyrene, polyvinylchloride and polyamide. The entire film blowing process is described below in compliance with Figure 1.1 introducing the most often used film blowing line, i.e. nip rolls are situated on the top [1-3].

1.1 Description of the Process

At the beginning of a single-layer film blowing process (see Figure 1.1), the extruder is fed through the hopper by solid polymer pellets. Inside the extruder, pellets are transported, homogenized, compressed and melted between the rotating screw and stationary barrel of the extruder. Then, polymer melt is extruded through an annular die to a continuous tube. When the tube is first time extruded, closing of this future cylindrical tube is necessary. In this case, the end of the tube is tied by a rope and consequently drawn upward towards the nip rolls. At the same time, the tube is inflated into a bubble by the internal pressure. These both actions, which have to be done very carefully, to protect the bubble from tearing, are stretching the biaxially oriented film in two directions, as was mentioned above. Simultaneously, the bubble is cooled outside by an air ring. Inside of the bubble an internal bubble cooling system (IBC) can be used for more efficient cooling. Then, above the freezeline height, the cooled bubble is in a solid state with the final mechanical and optical properties. From the point of view of bubble stabilization, a calibration cage is usually used. Then, the

bubble is folded with the help of the collapsing frames changing the film from bubble shape to a lay-flat tube of film which can be then used in the tube form or the tube is slit to form a sheet. Finally, the resulting film is drawn by the nip rolls to a wind-up roll [1-2, 4-6].

In the case of a multi-layer film blowing production (coextrusion), the above presented description of a single-layer film blowing process can be used as well, with only modifications that two or more different polymer melts are extruded from individual extruders through a coextrusion die (flat spiral dies) to a continuous tube [1-2].

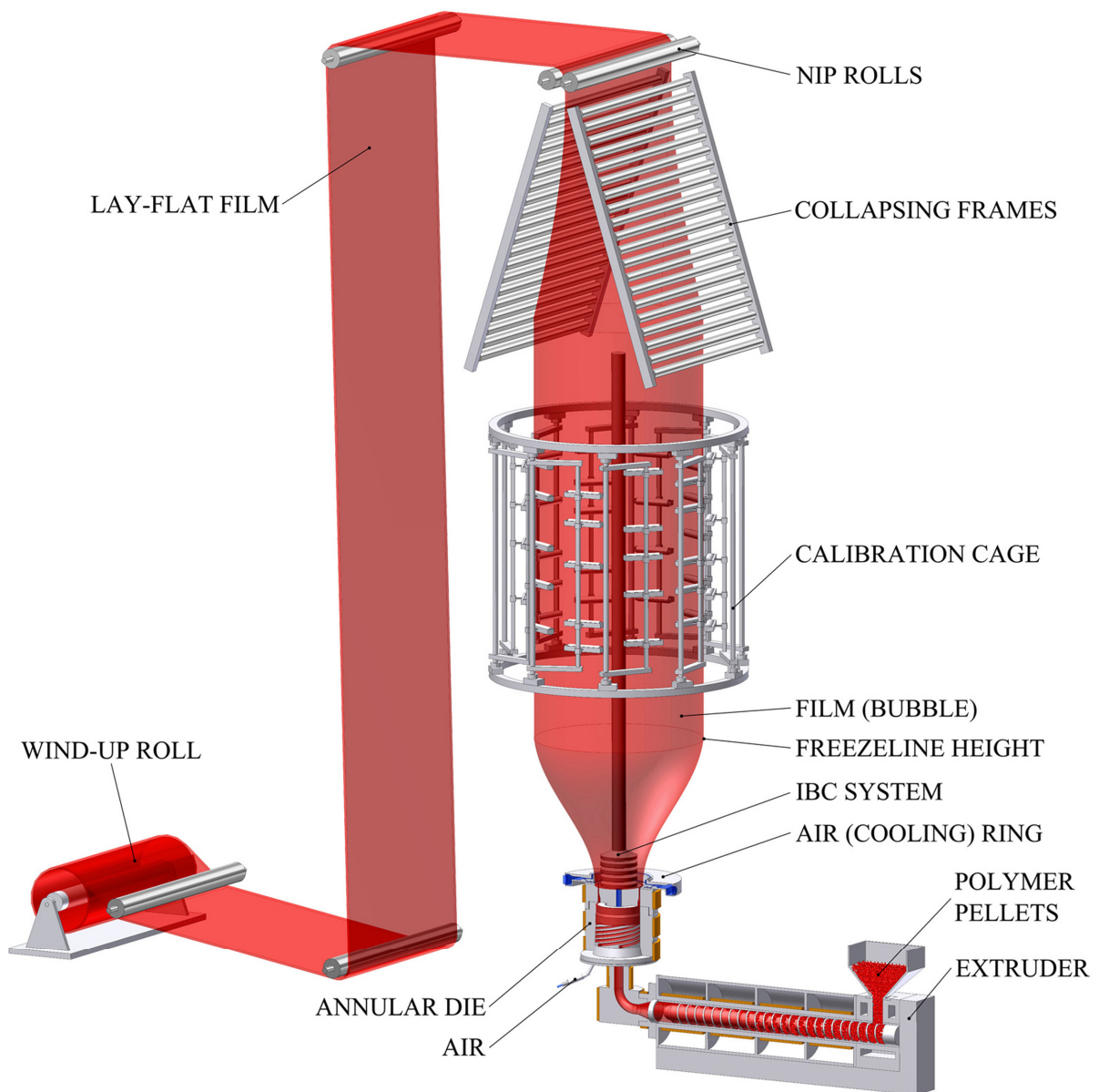


Figure 1.1. The single-layer film blowing line.

The frequently used terms generally describing the film blowing process are summarized below [1-2, 7-8]:

The **blow-up ratio, BUR**, is expressed as a ratio of the final bubble diameter, D_1 , at the freezeline height to the die diameter, D_0 , which usually varies from 1 to 5. This ratio describes mainly the melt stretching in the transverse direction.

The **take-up ratio, TUR**, is a ratio of the film velocity above the freezeline height, v_f , to melt velocity at the die exit, v_d . The take-up ratio is usually kept between 5 and 40 and determines the melt stretching in the axial machine direction. It should be noted, that TUR can also be expressed as a *draw-down ratio, DDR*, defined as a ratio of the die gap, H_0 , to the final film thickness, H_1 and blow-up ratio.

The **thickness reduction, TR**, describes relationship between the die gap, H_0 , and the final film thickness, H_1 . This ratio is typically in the range of 20 to 200.

Finally, the **freezeline height, L**, is defined as a ring shaped zone of frosty appearance located at the point where the resin solidifies, caused by a reduction in film temperature below the melting point of the polymer [2]. Thus, the freezeline height represents transition between the liquid and solid phases where no bubble deformation above this height is assumed.

It is clear that the objective of the film blowing process is to produce a thin stable film of a uniform gauge with good optical and mechanical properties at a maximum production rate. Thus, for the continuous film blowing process operation and production of an acceptable film, a stable bubble of constant bubble diameter is required otherwise thickness-variation instability may appear and limit the film blowing process, as described in the following section [1-3, 7].

1.2 Bubble Instabilities

During the film blowing process the instability called “thickness variation” can arise and significantly decrease a processing window of a stable blown film. This instability changes bubble shape in the area between the die exit and freezeline height (see Figure 1.2) which causes reduction of the film production-rate, worse mechanical

and optical product properties, formation of failures and large amounts of film scrap. Moreover, the film blowing process can be interrupted by one of the thickness-variation instability types. Typical film blowing instabilities, their formation and elimination, are briefly introduced below [1, 9-15].

Draw resonance, called also “Hourglassing”, happens especially when take-up ratio is high, thus, strain rates are high and the melt is stretched too quickly which appears as a continuous variation in bubble diameter, as can be seen in Figure 1.2a. The most popular stabilization way is increasing melt speed (screw speed) to get a higher freezeline height and lower take-up ratio. The same effect has also increasing melt temperature, narrowing die gap and material with higher melt index [1, 9, 11-14].

Helical instability, known as “Snaking”, appears when freezeline is too low because of an unsuitable setting of air ring. Then, the right side of the bubble is cooled more than the left side (see Figure 1.2b). To solve this problem, increasing extruder output is needed. Other remedies include reduction of melt temperature, material with lower melt index or wider die gap [1, 9, 11-14].

Instability of the freezeline height (FLH instability) is described by periodic oscillations at the interval from 30 seconds to 5 minutes in the area of freezeline (as presented in Figure 1.2c) where a little thickness variation in the machine direction arises. This can be caused by surging as the result of extruder motor amps and back pressure. To eliminate this varying extruder output and provide better mixing, an improvement in solids feeding and melting is necessary as well as application of an appropriate air ring, haul of speed or unworn screws [1, 9, 11, 14].

Heavy-bubble instability (also known as “Bubble sag”) occurs when cooling of a bubble is insufficient (Figure 1.2d). The preferred solution is to lower the freezeline height. So, extruder output should decrease as well as melt temperature. Another possibility is narrower die gap or material with lower melt index [1, 9-10].

Bubble flutter (Figure 1.2e) appears below the freezeline when a high velocity of cooling air is impinging on the bubble surface. Solutions consist in higher freezeline height (lower blower speed), lower melt temperature, higher melt index resin or narrower die gap [1, 9-10].

Bubble breathing happens if air volume inside the bubble changes periodically. This “breathing” (see Figure 1.2f) causes various film thickness in machine direction and fluctuations in layflat width. The main problem is usually with internal bubble cooling system. Thus, cooling valves, blowers and sensors are controlled. The other solutions of this instability are reduction of melt temperature, using material with higher melt index or decrease of extruder output [1, 9-10].

Bubble tear, also called as “Snap off”, appears when the take-up force, needed to draw up the bubble, is higher than the tensile strength of the molten film. Thus, the bubble is torn (which is clear in Figure 1.2g) if it is cooled too quickly or drawn too fast. This problem can be solved by suitable adjustment of the air ring, reduction of extruder output (slower screw and nip speed), increase of the die and melt temperature, using a material with a higher melt index without strain hardening or by a narrower die gap [1, 9-10].

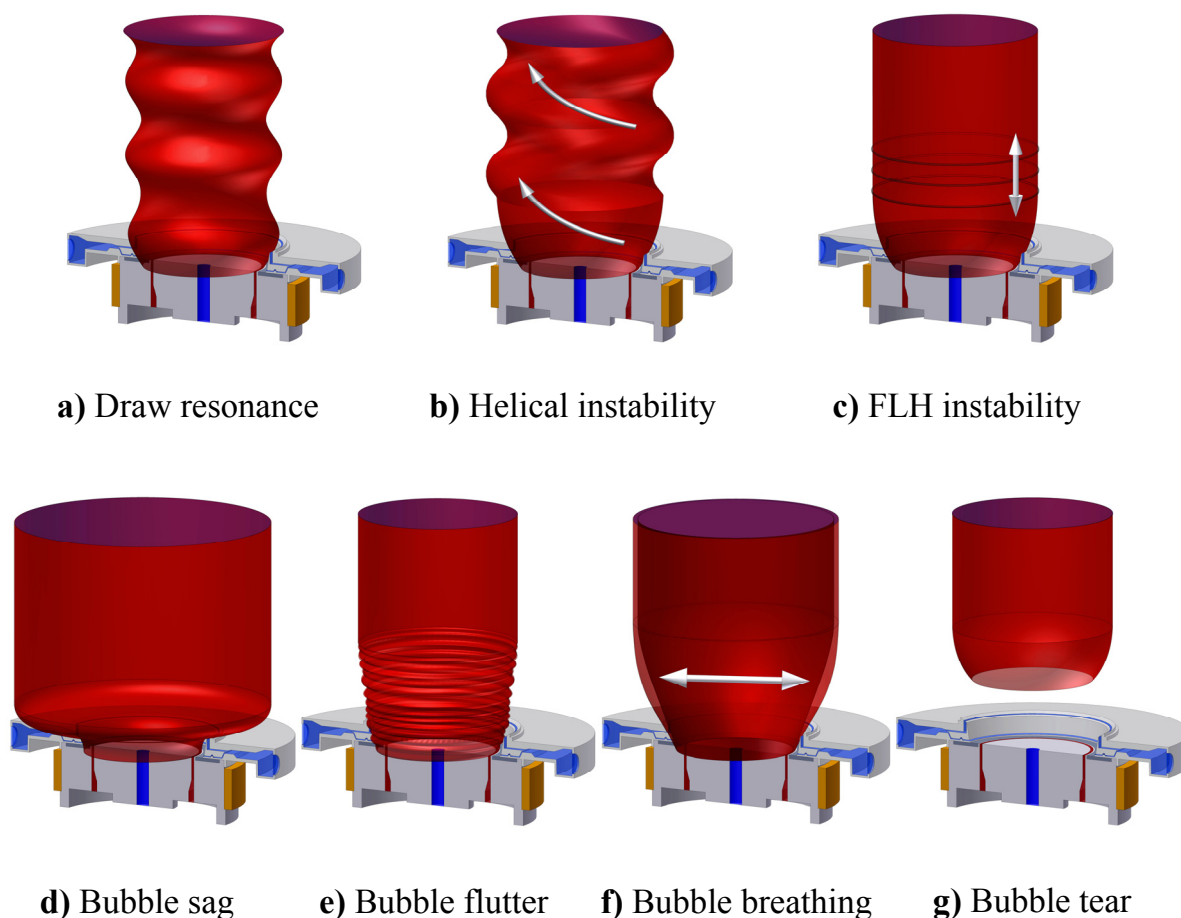


Figure 1.2. Different types of bubble instabilities in film blowing process.

As can be seen, bubble instabilities of the film blowing process include various problems: from variation of bubble diameter, film thickness and film width to scratches and tears. In spite of the presented recommendations reducing the bubble instabilities, the relationship between the machine design, processing parameters, material characteristics and stresses is not fully understood yet. Thus, for process optimization and its better understanding, modeling of the film blowing process is necessary.

2. Mathematical Modeling of the Film Blowing Process

In the following two sections, modeling of the film blowing process describing single-layer as well as multi-layer film production is introduced. It is clear, that greater part of research studies on film blowing process has been focused on modeling and stability analysis of processing and material parameters relating to a single-layer blown film. In contrast to coextrusion, only a few experimental and modeling studies have been addressed to multi-layer process, despite its recent rapid growth and technological importance.

2.1 Review of the Current Models Describing Single-Layer Film Blowing Process

The first film blowing model was developed in 1970 by Pearson and Petrie [16-18]. In their pioneering work they employed a Newtonian model as the constitutive equation and the process has been considered isothermal. In more detail, film is assumed as a thin shell in tension in the machine and circumferential direction where the effect of inertia, surface tension, air drag, and gravity is neglected. This formulation became a basic idea for many of following researchers. In 1973, Petrie [19] extended the Pearson-Petrie formulation [16-17] to isothermal viscoelastic film blowing process using a constitutive equation of the Oldroyd type. In this work, bubble shapes for different Maxwell model types were numerically obtained. Afterwards, Petrie [20] derived equations describing bubble shape and velocity profile of the non-isothermal Newtonian film and isothermal elastic film, and then the

theoretical predictions compared with experimental data measured by Ast [21] and Farber [22]. It should be noted that accurate modeling of the heat transfer and the use of a suitable viscoelastic constitutive equation was required in this work. Further, experimental study of the film blowing process of low-density polyethylene (LDPE), high-density polyethylene (HDPE) and polypropylene (PP) was performed by Han and Park [23-24] who applied the power law model following Pearson and Petrie's approach based on theory of thin shells. In the first study [23], a uniaxial and biaxial elongational flow behavior of viscoelastic polymer melts at different melt temperatures was investigated through an internal bubble pressure control. It was found that the obtained data of elongational viscosity under uniaxial stretching in film blowing process are very well comparable with the data of the melt-spinning process. In their subsequent paper [24], they developed mathematical model, taking into account the heat transfer between the molten film and the cooling air and the effect of gravity, to perform non-isothermal film blowing process analysis. Then, the theoretical predictions were compared with experimentally observed bubble and film thickness profiles of LDPE and HDPE films. Another experimental and theoretical work has been performed by Ast [25] who investigated cooling of the film by using the energy equation. Then, it was possible to determine the temperature profile along the bubble as well as height of the freeze line using heat transfer coefficient parameter. In 1976, Wagner [26], in his Ph.D thesis, modeled non-isothermal film blowing process for a Newtonian, purely elastic and a Maxwell fluid where he was able to accurately measure the take-up force with a specially constructed device. In the same period, Wagner [27] tried to find an agreement between theoretical model predictions and experimental data of internal bubble pressure assuming an average Newtonian viscosity during the process. In 1978, Pearson and Gutteridge [28] first modeled film blowing behavior of polypropylene film by purely elastic non-isothermal model. Gupta et. al. [29] reported experimental study of non-isothermal film blowing process of polystyrene (PS) film where viscoelastic behavior was described by the White-Metzner equation. In this work, bubble shapes, velocities, stretch rates, stresses and temperatures were measured in the area between the die exit and the freezeline height. It was revealed that circumferential stresses of the film were not predicted

accurately. On the other hand, stresses in the axial direction were predicted well. Fisher [30], in his Ph.D. thesis, determined the stresses in the machine and transverse direction with the help of measured temperature and deformation profiles. These both stresses were compared with experimentally obtained stresses. In this work, Wagner's nonlinear integral equation was used as a constitutive equation. Luo and Tanner [31] applied to modeling of the film blowing process a non-isothermal viscoelastic model considering an Upper Convected Maxwell and Leonov models. Unfortunately, they found the solution highly unstable and were unable to obtain convergence with arbitrary values of the film-blowing parameters. Also, they compared their predictions of blown PS film with the experimental results of Gupta [29] and concluded that numerical instability issues present the greatest problem in the process modeling. Kanai and White [32-33] developed theoretical model assuming the melt as a Newtonian fluid with a temperature dependent viscosity characterized by an Arrhenius model and incorporating crystallization effect in their energy equation. They found good agreement between experimental data and their model predictions for LDPE, LLDPE and HDPE. It was concluded that the bubble shape, radius and film thickness profiles are mostly influenced by the activation energy. This conclusion is supported by the work of Yamane and White [34] who modeled the film blowing process by the power law non-linear model with temperature and crystallinity dependent properties. In this work, it was revealed that increase in the activation energy has much greater effect on the bubble shape than variations in non-Newtonian characteristics. In 1988, Cain and Denn [35] applied for modeling of the film blowing process the Newtonian model as well as the non-isothermal Upper Convected Maxwell and Marrucci model which were tested on PS experimental data from Gupta [29] with different numerical techniques. In this work, the existence of multiple steady state solutions (bubble shapes) for the certain value of processing parameters (internal bubble pressure and take-up force) was observed. In 1990, Cao and Campbell [36] introduced two-phase model describing the area between the die exit and freezeline height by the modified Maxwell and Hookean model employed to description of liquid-like film behavior and solid-like film behavior, respectively. Here, the transition is described as the plastic-elastic transition (PET) and occurs when the Vohn-Mises yield condition [37]

is satisfied. This developed viscoplastic-elastic model presents results, i.e. bubble shapes, velocity and temperature profiles, in good agreement with the experimental data of Gupta [29] for polystyrene. Two-phase constitutive model was also introduced in the work of Ashok and Campbell [38] where the film blowing process is divided into a liquid part, liquid-solid part and solid part. Predictions of the bubble shape, velocity and temperature profiles were found in qualitative agreement with experimental data taken from [32] for high-density polyethylene. In 1993, the non-isothermal film blowing process was analyzed by Alaie and Papanastasiou [39] using a nonlinear integral constitutive equation that incorporates shear history effects, spectrum of relaxation times, shear thinning and extension thinning or thickening. Solving system of integrodifferential equations using a finite element discretisation with Newton iteration, bubble shape, velocity, temperature, stress and thickness profiles are obtained and compared with polystyrene experimental data from open literature [29]. In 1995, Liu et al. [40-41] performed online experimental measurements of radius, velocity and temperature along the LDPE and LLDPE blown films. Moreover, they studied effect of internal bubble pressure on the blow-up ratio for different values of the take-up ratio, melt temperature and air flow rate for LDPE, LLDPE and HDPE blown films. It was revealed that mostly, an “intuitive” effect of the internal bubble pressure on the blow-up ratio was observed, i.e. increasing internal bubble pressure leads to increasing the final bubble radius. On the other hand, a “counterintuitive” behavior was noticed at high blow-up ratios, where increase in bubble radius is caused by decreasing internal bubble pressure. The presented experimental results were then successfully compared with the developed quasi-cylindrical model by Liu et al. [42] including crystallization effect of non-Newtonian polymer melt on film blowing process. The model showed disagreement with the “counterintuitive” results reported by Pearson and Petrie [16-17]. In 1996, Sidiropoulos et al. [43] introduced non-isothermal, purely viscous, temperature-dependent mathematical model simulating bubble formation and the biaxial film stretching. The predicted bubble shape and temperature profile has been found in very good agreement with the LLDPE experimental data measured by Butler et al. [44]. Another film blowing model was applied in 1998 by André et al. [45]. In

their study, the model is composed of the Newtonian as well as viscoelastic constitutive equations. It was revealed, that the initial blowing angle at the die exit has significant influence on the bubble shape stability. Further, multiple solutions (bubble shapes) have been introduced in the case of non-isothermal viscoelastic behavior. In 2002, the film blowing process of LDPE was experimentally and theoretically investigated by Khonakdar et al. [46]. The Experimental measurements were performed for axial tension, bubble diameter and film thickness under the different processing conditions (flow rate, internal bubble pressure and take-up speed). In the theoretical study, the polymer melt is considered as a non-Newtonian fluid of power law type in non-isothermal conditions. Then, the bubble shape, temperature profile and film thickness along the bubble were predicted by the developed mathematical model. In 2003, Muke et al. [47] developed a simple non-isothermal viscoelastic Kelvin model describing bubble diameter, film thickness and strain rate profiles in film blowing. In this work, the model predictions were obtained by numerical integration based on a finite element approach. Then, it was revealed that the experimentally measured film blowing data of PP are described by the non-isothermal Kelvin model more precisely than by the non-isothermal Newtonian model, which is probably caused by the relatively small Hencky strains and strain rates applied in the film blowing conditions. In 2003, Pirkle and Braatz [48] performed dynamic modeling of the film blowing process for LDPE experimental data of Liu et al. [40, 42]. A non-Newtonian constitutive equation including crystallization effect was used in the numerical method of lines solving the algebraic and partial differential equations. Then, the effect of operating parameters (heat transfer coefficient and internal bubble pressure) on the bubble radius, film thickness and film crystallinity was described. It was observed, that increasing internal bubble pressure leads to increasing bubble radius, which is in contradiction with the counterintuitive simulation results of Liu et al. [40, 42] who probably applied an incorrect boundary condition or numerical method in their simulation. In 2004, Muslet and Kamal [49] developed a mathematical model where the liquid-like region is described by the Phan-Thien and Tanner constitutive equation and the solid-like region by the neo-Hookean constitutive equation. The two-phase proposed model, taking into account crystallization effect and

variable heat transfer coefficient, predicts bubble shape, film thickness, velocity and temperature profiles and crystallinity in good agreement with the experimental results in the literature (Tas [50]). The transient behavior and nonlinear dynamics of the nonisothermal film blowing process were introduced by Hyun et al. [51]. In this study, the viscoelastic Phan-Thien and Tanner constitutive equation was incorporated into the numerical scheme overcoming numerical problems, such as periodic oscillations called draw resonance. In 2004, Zatloukal and Vlcek [52] introduced an opposite view on modeling of the film blowing process by using variational principle based model derived on the assumptions of Pearson and Petrie of a thin shell in tension. Here, the general equation for the bubble shape is a priori known and is understood as an elastic membrane which is deformed due to the internal bubble pressure and the take-up force, in such a way that the resulting stable bubble satisfies the minimum energy requirements. In more detail, modeling of the film blowing process considering isothermal elastic model for bubble with and without neck has been introduced in [52]. A very good agreement between the experimentally measured [50] and predicted bubble shapes, take-up force and internal bubble pressure values for LDPE and HDPE was observed. In 2006, Zatloukal and Vlcek [53] presented variational principle based model describing high stalk bubble formation (a bubble having an extremely long neck). The isothermal Newtonian model revealed high capability to describe experimentally obtained high molecular weight HDPE bubble shapes as well as velocity and thickness profiles. This model was then extended to a non-Newtonian polymer melt behavior considering non-isothermal process conditions of high stalk bubbles, stated in [54]. Following the classical analysis of Pearson and Petrie [16-17], in 2007, Beaulne and Mitsoulis [8] used K-BKZ integral constitutive equation with a spectrum of relaxation times to perform numerical viscoelastic simulations with the isothermal Newtonian and Upper-Convected Maxwell models. It was concluded that the poor agreement between LDPE experimental data [50] and the bubble shape and velocity profile predictions is attributed to an inability of the model to take into account aerodynamic forces supporting bubble cooling. Therefore, reasonable agreement is observed between the experimental and the simulated temperature profiles of LDPE. Extended Pom-Pom constitutive equation, describing rheological

behavior of branched polymers, together with crystallization kinetics and a variable heat transfer coefficient was applied to analysis of the non-isothermal film blowing process performed by Sarafrazi and Sharif [55] based on [16-17]. The investigated predictions of bubble shape, velocity and temperature profiles, strain rates, stresses in the machine and transverse direction, take-up force and internal bubble pressure are found in good agreement with the experimental data of Tas [50]. In 2011, Kolarik and Zatloukal [56] introduced variational principle based non-isothermal film blowing model describing non-Newtonian polymer melts. This model is based on minimum energy approach developed in [52] and novel generalized Newtonian model [57] used as a constitutive equation describing the strain rate dependent steady shear and uniaxial extensional viscosities of linear and branched polyolefines as well as providing correct behavior in steady planar/equibiaxial extensional viscosity. Two developed iteration schemes (fixed bubble shape or internal bubble pressure) present similar predictions very well comparable with theoretical (Beaulne and Mitsoulis [8] and Sarafrazi and Sharif [55]) as well as experimental data (internal bubble pressure, take-up force, bubble shape, velocity and temperature profiles) taken from the open literature (Tas [50]). In 2011, Demay and Clamond [58] developed non-isothermal membrane model including the balance equations based on a stretching force and a curvature equation. A nonlinear system of differential equations for velocity, thickness, radius and stress components along the bubble was then involved to the computational procedure together with the take-up force and internal bubble pressure obtained by shooting method. In 2012, Kim et al. [59] applied transient simulation techniques to investigate the frequency response of the non-isothermal film blowing process to the ongoing sinusoidal disturbances. In this work, the process sensitivity, defined by amplitude ratio of the film cross-sectional area at the freezeline height, was investigated under the various operating conditions, such as draw-down ratio, blow-up ratio, and cooling. It was observed, that the middle of three multiple steady states is the most sensitive to the disturbance due to the lowest stability caused by the nearest unstable draw resonance region.

2.2 Review of the Current Models Describing Multi-Layer Film Blowing Process

In 1978, Han and Shetty [60] experimentally investigated blown film coextrusion of two polymers in various combinations of LDPE, HDPE, PP and ethylene-vinyl acetate (EVA). Then, the experiment was theoretically analyzed by using a power-law non-Newtonian model included in a computational procedure predicting the number of layers, layer thickness and the volumetric flow rate compared with the experiment. Theoretical investigation of two-layer blown film was also studied by Yoon and Park [61] in 1992. In their work, considering isothermal processing conditions, two film layers are described by a Newtonian and an Upper-Convected Maxwell fluid. In their following study [62] a linear stability analysis of this system has been performed. In 2000, Stasiek [63] investigated the heat transfer between three-layer blown film and cooling medium by a developed mathematical model estimating length of a cooling path. In 2005, Gamache et al. [64] performed experimental study evaluating axial and transverse stresses in a two-layer coextruded blown film of LDPE, ultra low density polyethylene (ULDPE), LDPE/ULDPE and ULDPE/LDPE under various processing conditions. Then, these stresses were successfully compared with theoretically calculated ones by the non-isothermal Newtonian model. In 2009, a 2-D model describing non-isothermal two-layer blown film process was developed by Xu and McHugh [65]. This model is based on the 1-D model of Henrichsen and McHugh [66] taking into account viscoelasticity and flow-enhanced crystallinity. The 2-D model presents numerical results showing influence of the rheological, thermal and crystallization properties on the crystallinity development and stresses in particular layers. It was observed, that the individual layers of the same materials contain significantly different stresses due to the temperature difference. Further, different material properties in a certain layer affect stresses and crystallinity in its own layer as well as in another layer through heat transfer. Finally, it was concluded that stresses and semi-crystalline phase orientation at the freezeline, i.e. final film properties, are affected by the layer arrangement.

It is clear, that most of the studies focused on modeling of the single-layer film blowing process are based on the Pearson and Petrie formulation [16-17]. For this purpose, the Pearson and Petrie pioneering work is introduced below in more detail.

2.3 Pearson and Petrie Formulation

As was mentioned above, in 1970, Pearson and Petrie [16-17] developed simple mathematical film blowing model including the following assumptions:

- the polymer melt behaves as a homogenous Newtonian fluid,
- the formulation is considering non-isothermal processing conditions,
- the bubble is described as a thin shell ($h \ll r$) where the film thickness, h , is much smaller than the bubble radius, r ,
- the bubble movement is time steady and symmetrical around the bubble axis,
- the velocity gradient across the film is not assumed,
- the effects of gravity, surface tension, air drag and the inertia of the liquid are neglected due to their low values.

The Pearson and Petrie formulation is based on a local Cartesian co-ordinate system (Figure 2.1) defined at a point P with the tangential (machine) direction ξ_1 , thickness direction (normal to the film) ξ_2 and the transverse (circumferential) direction ξ_3 .

In this co-ordinate system, the velocity components (v_1, v_2, v_3) are suggested and utilized to obtain approximations to the velocity gradients $\frac{\partial v_i}{\partial \xi_j}$ included in the following deformation rate tensor

$$D = \begin{pmatrix} \frac{\partial v_1}{\partial \xi_1} & 0 & 0 \\ 0 & \frac{\partial v_2}{\partial \xi_2} & 0 \\ 0 & 0 & \frac{\partial v_3}{\partial \xi_3} \end{pmatrix} \quad (2.1)$$

It should be noted, that the shear components of the strain rate are neglected due to the membrane approximation. Moreover, the origin point P is assumed to be on the inner surface of the film. Thus, on the inner surface, the velocity normal to the film thickness, v_2 , is equal to zero ($\xi = 0$) and on the outer surface $v_2 = Dh/Dt$. Then,

$$\frac{\partial v_2}{\partial \xi_2} = \frac{1}{h} \frac{Dh}{Dt} \quad (2.2)$$

Taking into account the condition of axisymmetric bubble and the relation $\xi_3 = r \tan \Theta$, the velocity gradient in the circumferential direction is obtained in the following form

$$\frac{\partial v_3}{\partial \xi_3} = \frac{1}{r} \frac{Dr}{Dt} \quad (2.3)$$

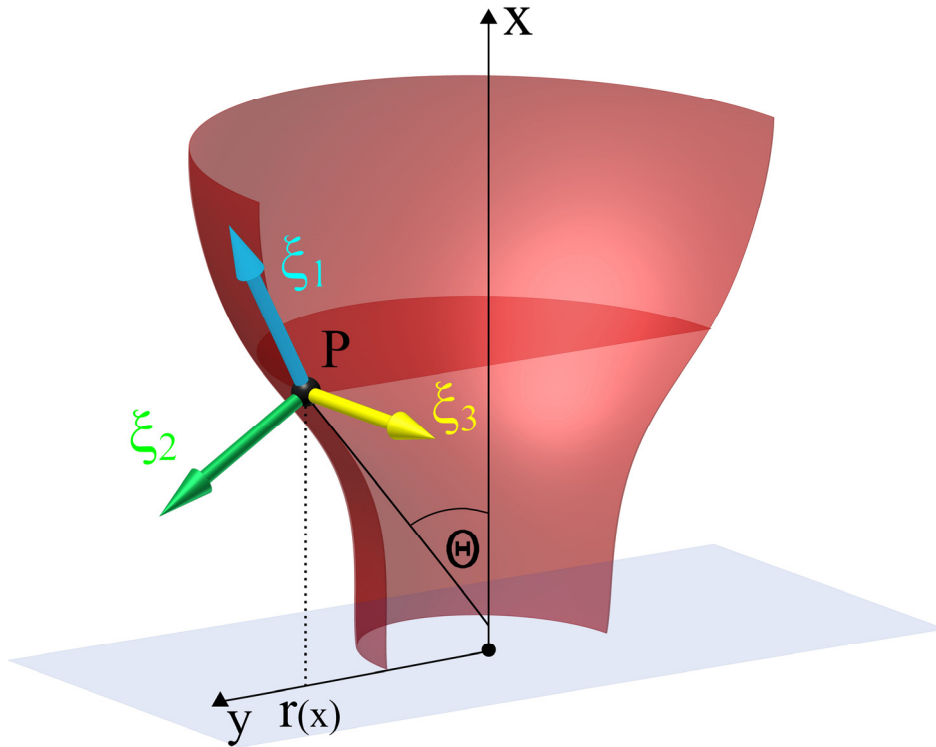


Figure 2.1. Cartesian co-ordinate system.

Finally, by applying the assumption of polymer incompressibility, the velocity gradient in the machine direction is revealed as

$$\frac{\partial v_1}{\partial \xi_1} = -\left(\frac{\partial v_2}{\partial \xi_2} + \frac{\partial v_3}{\partial \xi_3}\right) = -\left(\frac{1}{h} \frac{Dh}{Dt} + \frac{1}{r} \frac{Dr}{Dt}\right) \quad (2.4)$$

Then, r and h can be expressed as functions of x , and if term $\frac{dx}{d\xi_1} = \cos \Theta$ is taken

together with the velocity gradient in the machine direction $\frac{D\xi_1}{Dt} = v_1$ into account, the

particular velocity gradients are then obtained in the following forms

$$\frac{\partial v_1}{\partial \xi_1} = -v_1 \cos \Theta \left(\frac{1}{h} \frac{dh}{dx} + \frac{1}{r} \frac{dr}{dx}\right) \quad (2.5)$$

$$\frac{\partial v_2}{\partial \xi_2} = v_1 \cos \Theta \frac{1}{h} \frac{dh}{dx} \quad (2.6)$$

$$\frac{\partial v_3}{\partial \xi_3} = v_1 \cos \Theta \frac{1}{r} \frac{dr}{dx} \quad (2.7)$$

Using the equation of continuity

$$Q = 2\pi r h v_1 \quad (2.8)$$

where Q is the volumetric flow rate, and substituting Eqs. (2.5)-(2.7) into the above presented deformation rate tensor (Eq. (2.1)), leads to the following form

$$D = \frac{Q \cos \Theta}{2\pi r h} \begin{pmatrix} -\left(\frac{1}{h} \frac{dh}{dx} + \frac{1}{r} \frac{dr}{dx}\right) & 0 & 0 \\ 0 & \frac{1}{h} \frac{dh}{dx} & 0 \\ 0 & 0 & \frac{1}{r} \frac{dr}{dx} \end{pmatrix} \quad (2.9)$$

The principal stresses are defined by the below presented generalized Newtonian model

$$\sigma = -p + 2\eta D \quad (2.10)$$

where p is the pressure, η is the liquid viscosity and σ represents total stress tensor, defined as

$$\sigma = \begin{pmatrix} \sigma_{xx} & 0 & 0 \\ 0 & \sigma_{yy} & 0 \\ 0 & 0 & \sigma_{zz} \end{pmatrix} \quad (2.11)$$

where σ_{xx} , σ_{yy} , σ_{zz} are normal components of total stress tensor. If the condition of the free surface ($\sigma_{yy} = 0$) is taken into account, then, with the help of the Eq. (2.11), the pressure, p , is obtained in the following form

$$p = 2\eta v_1 \cos \Theta \frac{1}{h} \frac{dh}{dx} \quad (2.12)$$

Applying the bubble assumption of a thin shell, the bubble is affected by the forces, $F_m = h\sigma_{11}$ and $F_t = h\sigma_{33}$, defined per unit length, in the machine and transverse direction, respectively, where σ_{11} describes total stress in the machine direction and σ_{33} represents total stress in the circumferential direction. Solving these equations together with Eq. (2.12) and (2.11), the final expressions of these forces are following

$$F_m = -\frac{\eta Q \cos \Theta}{\pi r} \left(\frac{1}{r} \frac{dr}{dx} + \frac{2}{h} \frac{dh}{dx} \right) \quad (2.13)$$

$$F_t = \frac{\eta Q \cos \Theta}{\pi r} \left(\frac{1}{r} \frac{dr}{dx} - \frac{1}{h} \frac{dh}{dx} \right) \quad (2.14)$$

It should be noted, that the overall force balance in the machine direction is given as follows [41, 23-24]:

$$F_{\text{rheo}} = F - F_{\text{grav}} - F_{\text{drag}} - F_{\text{surf}} - F_{\text{inert}} - F_{\Delta p} \quad (2.15)$$

where F_{rheo} is the rheological force in the film, F is the take-up force, F_{grav} is the gravitational force caused by the film's weight, F_{drag} is the force between the air and the film surface, F_{surf} is the surface tension of the bubble, F_{inert} is the inertial force required to accelerate the fluid and $F_{\Delta p}$ describes the pressure difference across the film.

If the above presented assumptions are taken into account (i.e. gravity, surface tension, air drag and the inertia of the liquid are neglected), force balance in the vertical direction has the following form

$$2\pi r h \sigma_{11} \cos(\theta) = F - \pi \Delta p (R_1^2 - r^2) \quad (2.16)$$

where R_1 describes the bubble radius at the freezeline height.

Then, after the momentum equation and membrane theory are taken into account, the internal bubble pressure, Δp , can be expressed in the following form:

$$\Delta p = \frac{h\sigma_{11}}{R_m} + \frac{h\sigma_{33}}{R_t} \quad (2.17)$$

Here, parameters R_m and R_t represents the curvature radii in the machine and transverse direction, respectively. The presented curvature radii have a form

$$R_t = \frac{r}{\cos(\theta)} \quad (2.18)$$

$$R_m = \frac{-1}{\frac{d^2r}{dx^2} \cos^3(\theta)} \quad (2.19)$$

Term $\cos(\theta)$ in Eqs. (2.18) and (2.19) is calculated as:

$$\cos(\theta) = \frac{1}{\sqrt{1 + \left(\frac{dr}{dx}\right)^2}} \quad (2.20)$$

From Eq. (2.16), stress σ_{11} can be expressed as

$$\sigma_{11}(x) = \frac{F - \pi\Delta p(R_1^2 - r(x)^2)}{2\pi r(x)h(x)\cos(\theta(x))} \quad (2.21)$$

Stress $\sigma_{11}(x)$ is a distance function from the annular die, x , as well as a function of parameters $r(x)$, $h(x)$ and $\cos(\theta(x))$. The equation for stress $\sigma_{11}(x)$ has a specific form in the area of the freeze line height, L . If the line slope $\left(\frac{dr}{dx}\right)$ is equal to zero, the stress in the machine direction $\sigma_{11}(L)$ at the freeze line height can be rewritten into the following form:

$$\sigma_{11}(L) = \frac{F}{2\pi R_1 H_1} \quad (2.22)$$

where the bubble radius at the freezeline height is $R_1 = R_0 BUR$, and H_1 is the bubble thickness at the same place.

With the help of Eq. (2.17), the stress in the transverse direction is stated in the form

$$\sigma_{33}(x) = \frac{R_t(x)}{h(x)} \left(\Delta p - \frac{h(x)}{R_m(x)} \sigma_{11}(x) \right) \quad (2.23)$$

Finally, the stress at the freeze line height is introduced as

$$\sigma_{33}(L) = \frac{R_1}{H_1} \Delta p \quad (2.24)$$

Let us now briefly introduce the Zatloukal-Vlcek model [52] applied in this Ph.D. study for modeling of the film blowing process taking into account non-isothermal conditions and non-Newtonian fluid behavior.

2.4 Zatloukal and Vlcek Formulation

The Zatloukal-Vlcek model describes the film blowing process as a stable bubble which satisfies minimum energy requirements by using variational principles. The bubble is considered as a deformed elastic membrane due to the load, p , and the take-up force, F , where thickness is a neglected parameter because the membrane is very thin. Then, two bubble shapes can occur. One of them is the bubble shape before deformation (Figure 2.2) where this shape is understood as a line element of the membrane dx . Then, after deformation (Figure 2.2), shape of the element is changed and described by the following equation [52]:

$$\sqrt{1 + (y')^2} dx \approx \left[1 + \frac{1}{2} (y')^2 \right] dx \quad (2.25)$$

This approximation of bubble-shape change is followed by zero contribution to the potential energy of the membrane. Then, the potential energy is composed of the elastic strain energy increase and negative work of the applied load.

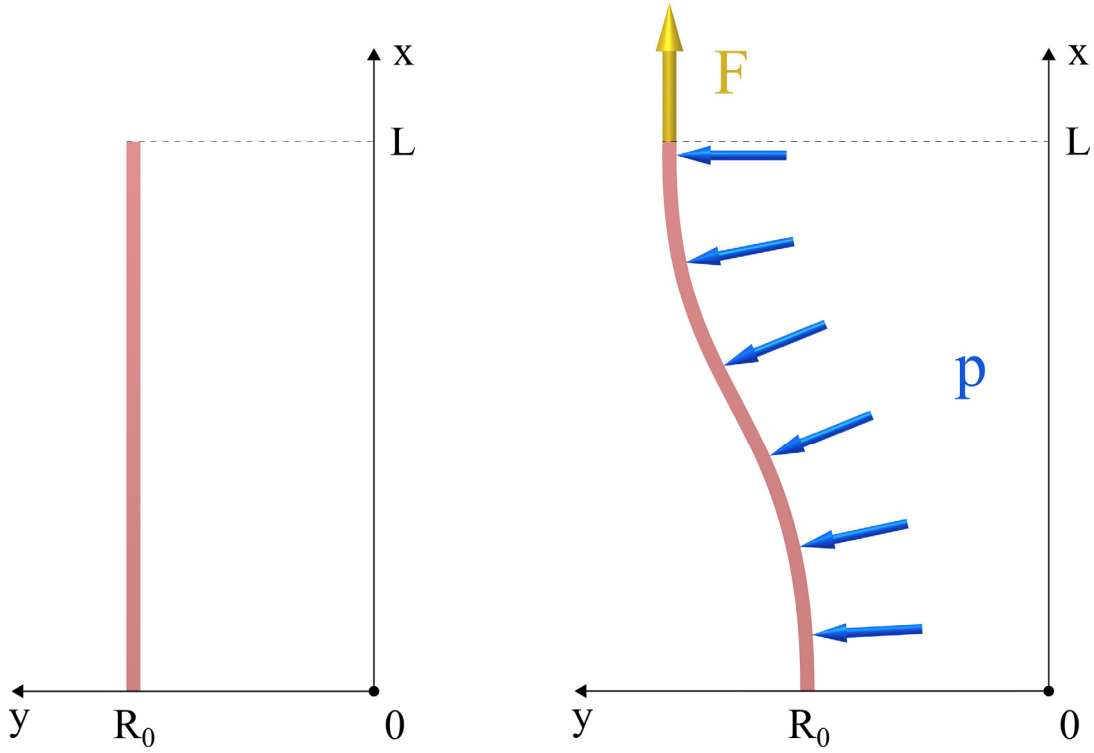


Figure 2.2. Membrane before deformation (left), membrane after deformation (right) [52].

As presented in more detail in [52], through definition of bubble volume and minimization of potential energy functional I , the following differential equation is reached:

$$Fy'' - \lambda_1 2\pi y + p = 0 \quad (2.26)$$

Here, λ_1 represents the Lagrange multiplier, p is the internal load and y indicates the equation of the bubble shape described in the following form:

$$y = (R_0 - pJ)\cos\left(\frac{x\varphi}{L}\right) - \alpha'(pJ - BURR_0)\sin\left(\frac{x\varphi}{L}\right) + pJ \quad (2.27)$$

where the parameter x means a positive number from zero to the freezeline height, L , parameter pJ is bubble curvature (which is given by membrane compliance, J , and the internal load, p), parameter α' is defined as

$$\alpha' = \sqrt{\frac{2pJ - R_0 - BURR_0}{pJ - BURR_0} \left| \frac{R_0(BUR - 1)}{pJ - BURR_0} \right|} \quad (2.28)$$

and parameter φ is presented in Table 2.1, where A is given by the following equation

$$A = \frac{pJ - R_0}{pJ - BURR_0} \quad (2.29)$$

Biaxial orientation of the blown film is caused by the take-up force, F , which is expressed as

$$F = -\frac{L^2}{J\phi^2} \quad (2.30)$$

and internal bubble pressure, Δp , defined in the following form

$$\Delta p = \frac{pL}{2\pi \int_0^L y \sqrt{1+(y')^2} dx} \quad (2.31)$$

where the term $2\pi \int_0^L y \sqrt{1+(y')^2} dx$ in Eq. (2.31) means the bubble surface and the term pL is the force acting in the thickness direction of the bubble, $F_{\text{thickness}}$. Eq. (2.31) represents the calculation of the internal bubble pressure in such a way that the bubble is represented by an equivalent cylinder, which has the same surface as the real bubble.

The total number of parameters needed to describe the bubble shape is equal to four (pJ , L , R_0 , BUR). Just note that pJ/R_0 (dimensionless form of pJ) determines the total deformation (curvature) of the bubble which varies between 0 and $R_0(1+BUR)/2$ for the bubbles without the neck [52].

Table 2.1. Parameters A and ϕ for different bubble shapes (y) [52].

Equation	A	ϕ	y
1.	1	0	R_0
2.	$0 < A < 1$	$\arctan \left(\frac{\sqrt{1-A^2}}{A} \right)$	The form of Eq. (2.27).
3.	0	$\pi/2$	$R_0 \left\{ 1 - \sin \left(\frac{x\pi}{2L} \right) (1 - BUR) \right\}$
4.	$-1 < A < 0$	$\pi + \arctan \left(\frac{\sqrt{1-A^2}}{A} \right)$	The form of Eq. (2.27).
5.	-1	π	$\frac{R_0}{2} \left\{ 1 + \cos \left(\frac{x\pi}{L} \right) (1 - BUR) + BUR \right\}$

THE AIMS OF THE DOCTORAL RESEARCH WORK

The main goal of the doctoral research work is to develop and test a stable numerical scheme for modeling of non-isothermal film blowing process considering non-Newtonian fluids by using variational principles in order to understand the complicated relationship between the processing conditions, material characteristics and bubble stability. The individual aims are provided bellow:

- Development and predicting capabilities testing of stable numerical scheme for variational principle based film blowing modeling by using particular set of experimental data taken from the open literature such as internal bubble pressure, take-up force, bubble shape, velocity and temperature profiles.
- Investigation the effect of processing conditions (internal bubble pressure, heat transfer coefficient, mass flow rate, cooling air temperature, melt/die temperature) and material parameters (extensional viscosity, melt strength, Newtonian viscosity, flow activation energy, power law index) on the film blowing stability.
- Evaluation of variational principles based modeling approach for multi-layer film blowing process.

SUMMARY OF THE PAPERS

In this current doctoral thesis, novel numerical scheme for variational principles based modeling of non-isothermal film blowing process considering generalized Newtonian model, taking steady shear and extensional viscosity of the polymer melts properly into account, has been proposed and successfully tested in order to understand the complicated relationship between the equipment design, processing conditions, material characteristics and process stability. The main results of the four enclosed papers are highlighted in the following parts.

Paper I

Modeling of Nonisothermal Film Blowing Process for Non-Newtonian Fluids by using Variational Principles

In this work, non-isothermal film blowing process analysis for non-Newtonian polymer melts has been performed theoretically by using minimum energy approach and the obtained predictions were compared with both, theoretical and experimental data (internal bubble pressure, take-up force, bubble shape, velocity and temperature profiles) taken from the open literature. For this purpose, recently proposed generalized Newtonian model depending on three principal invariants of the deformation rate tensor, D , and its absolute value defined as the square root of $D \cdot D$ has been used. It has been found that film blowing model predictions are in very good agreement with the corresponding experimental data.

Paper II

Stability Analysis of Non-Isothermal Film Blowing Process for Non-Newtonian Fluids using Variational Principles

This study is focused on a numerical stability analysis of the film blowing process. The numerical scheme used is based on a variational principle model of the film blowing operation. This model employs non-isothermal processing conditions, non-Newtonian behavior of the polymer and physically limiting criteria (maximum tensile and/or hoop stress) to investigate the complex relationship between processing

conditions (internal bubble pressure, heat transfer coefficient, mass flow rate, cooling air temperature, melt/die temperature), material parameters (rupture stress, Newtonian viscosity, flow activation energy, power law index) and film blowing stability. It has been shown that the melt/die temperature has the highest impact on the film blowing stability window size as well as on the maximum and minimum achievable film thickness. In more detail, it has been found that processing parameters together with flow activation energy have much higher effect on the film blowing stability and maximum achievable film thickness than the basic rheological characteristics of the polymer melt. On the other hand, the effect of basic rheological parameters of the polymer melt become much more important than processing parameters (except of melt/die temperature) in order to reach minimum film thickness.

Paper III

The Effect of Polyolefin Extensional Rheology on Film Blowing Process Stability

In this work, the effect of polyolefin extensional rheology on the film blowing stability and minimum achievable final film thickness has been investigated experimentally as well as theoretically utilizing variational principle model for the film blowing operation. It has been revealed experimentally as well as theoretically that the relationship between film blowing stability window size (and/or minimum achievable final film thickness) and the extensional strain hardening is non-monotonic in character, i.e. there is existence of the optimal values for both variables to reach maximum stability window size and/or the smallest minimum achievable final film thickness.

Paper IV

Evaluation of the 9-Layer Film Blowing Process by using Variational Principles

In this work, coextrusion experiments utilizing an industrial 9-layer Brampton Engineering coextrusion film blowing line for LDPE/LDPE/tie/PA6/EVOH/PA6/tie/LDPE/LDPE film production has been performed under different processing conditions (different air cooling intensity and

mass flow rate) in order to evaluate variational principles based modeling approach for the multi-layer film blowing process. It has been revealed that the variational principle based model can describe the bubble shape and predict internal bubble pressure reasonably well for all applied processing conditions even if the multi-layer film has been viewed as the static elastic membrane characterized only by one material parameter - bubble compliance J , which was not allow to vary along the multi-layer bubble.

Thus, it is believed, that the variational principle based modeling approach can be used and explored for the multi-layer film blowing process to understand complex rheological, heat transfer and crystallization phenomena occurring in multi-layer film blowing process with respect to process stability and final film properties.

CONCLUSION

In this work, novel and stable numerical scheme for modeling of non-isothermal film blowing process, considering non-Newtonian polymer melts by using variational principles, has been proposed and validated in order to understand the complicated relationship between processing conditions (internal bubble pressure, heat transfer coefficient, mass flow rate, cooling air temperature, melt/die temperature), material characteristics (extensional viscosity, rupture stress, Newtonian viscosity, flow activation energy, power law index) and bubble stability. For this purpose, recently proposed generalized Newtonian model depending on three principal invariants of the deformation rate tensor, D , and its absolute defined value as square root of $D \cdot D$ has been used and the following findings have been discovered:

- The film blowing model predictions are in very good agreement with the corresponding experimental data (internal bubble pressure, take-up force, bubble shape, velocity and temperature profiles) taken from the open literature for single-layer LDPE film production.
- The role of biaxial extensional viscosity on the film blowing process is significant suggesting that film blowing model predictions might be rather erroneous when the equibiaxial extensional viscosity is not correctly taken into account by the utilized constitutive equation.
- The melt/die temperature has the highest impact on the film blowing stability window size as well as on the maximum and minimum achievable final film thickness.
- Processing parameters together with flow activation energy have much higher effect on the film blowing stability and maximum achievable final film thickness than basic rheological characteristics of the polymer melt.
- The effect of basic rheological parameters of the polymer melt become much more important than processing parameters (except of melt/die temperature) in order to reach minimum final film thickness.

- The relationship between film blowing stability window size (and/or minimum achievable final film thickness) and extensional strain hardening is of non-monotonic character for a given range of melt strengths i.e. there exists some optimal values for both variables to reach maximum stability window size and/or the smallest minimum achievable final film thickness.
- The film blowing stability increases (or minimum achievable film thickness decreases) if the melt strength, σ , increases with the increased extensional strain hardening parameter, $\frac{\eta_{E,\max}}{3\eta_0}$, more than according to the follow simple relationship: $\sigma = A' \left(\frac{\eta_E}{3\eta_0} \right)^2 + B' \left(\frac{\eta_E}{3\eta_0} \right) + C'$, where A' , B' and C' are constants.
- There is always existence of some minimum melt strength for the given extensional strain hardening parameter at which the film blowing stability is maximized or at which the achievable final film thickness is at its minimum.
- The utilized variational principle based model can describe quantitatively as well as qualitatively the experimentally determined film blowing stability contours for linear as well as branched mLLDPEs.
- Variational principles based modeling approach is applicable to correctly capture the bubble shape as well as to predict the internal bubble pressure during production of LDPE/LDPE/tie/PA6/EVOH/PA6/tie/LDPE/LDPE barrier films on 9-layer film blowing line even if the multilayer film has been viewed as the static elastic membrane characterized only by one material parameter - bubble compliance J , which was not allow to vary along the bubble.

REFERENCES

- [1] CANTOR, K. Blown Film Extrusion. Munich: Carl Hanser Verlag, 2006. ISBN 3-446-22741-5.
- [2] BUTLER, T.I. Film Extrusion Manual: Process, Materials, Properties. Atlanta: Tappi Press, 2005. ISBN 1-59510-075-X.
- [3] KANAI, T., CAMPBELL, G.A. Film Processing, Munich: Carl Hanser Verlag, 1999. ISBN 3-446-17882-1.
- [4] MAYAVARAM, R.S. Modeling and Simulation of Film Blowing Process. *Ph.D. Thesis*, Texas A&M University, 2005.
- [5] FANG, Y. Rheological Effect in Film Blowing. *Ph.D. Thesis*, Université de Montréal, 1999.
- [6] MAJUMDER, K.K. Blown Film Extrusion: Experimental, Modeling and Numerical Study. *Ph.D. Thesis*. RMIT University, Melbourne, 2008.
- [7] BAIRD, D.G., COLLIAS, D.I. Polymer Processing: Principles and Design. New York: John Wiley & Sons, Inc., 1998. ISBN 0-471-25453-3.
- [8] BEAULNE, M., MITSOULIS, E. Effect of Viscoelasticity in the Film-Blowing Process. *J. Appl. Polym. Sci.* 2007, vol. 105, no. 4, pp. 2098-2112.
- [9] BUTLER, T.I. Blown Film Bubble Instability Induced by Fabrication Conditions, *SPE ANTEC Tech. Papers* 2000, vol. 1, pp. 1120-1129.
- [10] WALLER, P. What To Do When the Bubble Won't Behave, *Plastic Technology* 2002 (December), pp. 36-37.
- [11] OBIJESKI, T.J., PRUITT, K.R. Improving the Output and Bubble Stability of Thick Gauge Blown Helical Instability. *Annual Technical Conference - ANTEC, Conference Proceedings* 1992, vol. 1, pp. 150-153.
- [12] LAFFARGUE, J., PARENT, L., LAFLEUR, P.G., CARREAU, P.J., DEMAY, Y., AGASSANT, J.F. Investigation of Bubble Instabilities in Film Blowing Process. *Int. Polym. Proc.* 2002, vol. 17, pp. 347-353.
- [13] KIM, S., FANG, Y.L., LAFLEUR, P.G., CARREAU, P.J. Dynamics and Criteria for Bubble Instabilities in a Single Layer Film Blowing Extrusion. *Polym. Eng. Sci.* 2004, vol. 44, no. 2, pp. 283-302.

- [14] GHANEH-FARD, A., CARREAU, P.J., LAFLEUR, P.G. Study of Instabilities in Film Blowing, *AICHE J.* 1996, vol. 42, no. 5, pp. 1388-1396.
- [15] HAN, C.D., PARK, J.Y. Studies on Blown Film Extrusion. III. Bubble Instability. *J. Appl. Polym. Sci.* 1975, vol. 19, no. 12, pp. 3291-3297.
- [16] PEARSON, J.R.A., PETRIE, C.J.S. The Flow of a Tubular Film. Part 1. Formal Mathematical Representation. *J. Fluid Mech.* 1970, vol. 40, no. 1, pp. 1–19.
- [17] PEARSON, J.R.A., PETRIE, C.J.S. The Flow of a Tubular Film. Part 2. Interpretation of the Model and Discussion of Solutions. *J. Fluid Mech.* 1970, vol. 42, no. 3, pp. 609–625.
- [18] PEARSON, J.R.A., PETRIE, C.J.S. A Fluid-Mechanical Analysis of the Film-Blowing Process. *Plastic Polym.* 1970, vol. 38, pp. 85–94.
- [19] PETRIE, C.J.S. Memory Effects in a Non-Uniform Flow: A Study of the Behaviour of a Tubular Film of Viscoelastic Fluid. *Rheol. Acta* 1973, vol. 12, no. 2, pp. 92-99.
- [20] PETRIE C.J.S. A Comparison of Theoretical Predictions with Published Experimental Measurements on the Blown Film Process. *AICHE J.* 1975, vol. 21, no. 2, pp. 275-282.
- [21] AST, W. The Cooling Process in the Manufacture of Blown Film from Low Density Polyethylene. (in German) *Kunststoffe* 1973, vol. 63, p. 427.
- [22] FARBER, R. Measurement of Deformation Rates in the Film Blowing of Polyethylene. *M. Eng. Thesis*, McGill University, Montreal, 1973.
- [23] HAN, C.D., PARK, J.Y. Studies on Blown Film Extrusion. I. Experimental Determination of Elongational Viscosity. *J. Appl. Polym. Sci.* 1975, vol. 19, no.12, pp. 3257–3276.
- [24] HAN, C.D., PARK, J.Y. Studies on Blown Film Extrusion. II. Analysis of the Deformation and Heat Transfer Processes. *J. Appl. Polym. Sci.* 1975, vol. 19, no. 12, pp. 3277-3290.
- [25] AST, W. Extrusion von Schlauchfolien. Theoretische und Experimentelle Untersuchungen des Abkühlvorganges, *Ph.D. Thesis*, IKT Stuttgart, 1976.
- [26] WAGNER, M.H. Ein Rheologisch-thermodynamisches Prozessmodell des Folien-blasverfahrens, *Ph.D. Thesis*, IKT Stuttgart, 1976.

- [27] WAGNER, M.H. Das Folienblasverfahren als Rheologisch-Thermodynamischer PozeB. *Rheol. Acta* 1976, vol. 15, no. 1, pp. 40–51.
- [28] PEARSON, J.R.A, GUTTERIDGE, P.A. Stretching Flows for Thin Film Production. Part 1. Bubble Blowing in the Solid Phase. *J. Non-Newton. Fluid Mech.* 1978, vol. 4, no. 1-2, pp. 57-72.
- [29] GUPTA, R.K., METZNER, A.B., WISSBRUN, K.F. Modeling of Polymeric Film-Blowing Processes. *Polym. Eng. Sci.* 1982, vol. 22, no. 3, pp. 172–181.
- [30] FISHER, E. Ein Rheologisches Modell zur Beschreibung der Produktqualität bei der Verarbeitung von Hochdruckpolyethylen, *Ph.D. Thesis*, IKT Stuttgart, 1983.
- [31] LUO, X.-L., TANNER, R.I. Computer Study of Film Blowing. *Polym. Eng. Sci.* 1985, vol. 25, no. 10, pp. 620-629.
- [32] KANAI, T., WHITE, J.L. Kinematics, Dynamics and Stability of the Tubular Film Extrusion of Various Polyethylenes. *Polym. Eng. Sci.* 1984, vol. 24, no. 15, pp. 1185-1201.
- [33] KANAI, T., WHITE, J.L. Dynamics, Heat Transfer and Structure Development in Tubular Film Extrusion of Polymer Melts: A Mathematical Model and Predictions. *J. Polym. Eng.* 1985, vol. 5, no. 2, pp. 135–157.
- [34] YAMANE, H., WHITE, J.L. Simulation of Tubular Film Extrusion of Polymer Melts. Non-Newtonian and Non-Isothermal Effects on Bubble Shape. *Int. Polym. Proc.* 1987, vol.2, no. 2, pp. 107-112,
- [35] CAIN, J.J., DENN, M.M. Multiplicities and Instabilities in Film Blowing. *Polym. Eng. Sci.* 1988, vol. 28, no. 23, pp. 1527-1541.
- [36] CAO, B., CAMPBELL, G.A. Viscoplastic-Elastic Modeling of Tubular Blown Film Processing. *AICHE J.* 1990, vol. 36, no. 3, pp. 420-430.
- [37] HILL, R. The Mathematical Theory of Plasticity. Oxford: Clarendon Press, 1950.
- [38] ASHOK, B.K., CAMPBELL, G.A. Two-Phase Simulation of Tubular Film Blowing of Crystalline Polymers. *Int. Polym. Proc.* 1992, vol. 7, no. 3, pp. 240-247.

- [39] ALAIE, S.M., PAPANASTASIOU, T.C. Modeling of Nonisothermal Film Blowing with Integral Constitutive Equations. *Int. Polym. Proc.* 1993, vol. 8, no. 1, pp. 51-65.
- [40] LIU, C.C., BOGUE, D.C., SPRUIELL, J.E. Tubular Film Blowing. Part 1: On-line Experimental Studies. *Int. Polym. Proc.* 1995, vol. 10, no. 3, pp. 226–229.
- [41] LIU, C.C. Studies of Mathematical Modelling and Experimental On-line Measurement for the Tubular Film Blowing Process. *Ph.D. Thesis*, University of Tennessee, Knoxville, 1991.
- [42] LIU, C.C., BOGUE, D.C., SPRUIELL, J.E. Tubular Film Blowing. Part 2: Theoretical Modelling. *Int. Polym. Proc.* 1995, vol. 10, no. 3, pp. 230–236.
- [43] SIDIROPOULOS, V., TIAN, J.J., VLACHOPOULOS, J. Computer Simulation of Film Blowing. *TAPPI J.* 1996, vol. 79, no. 8, pp. 113-118.
- [44] BUTLER, T.I., PATEL, R., LAI, S., et al. Blown Film Frost Line–Freeze Line Interactions. 1993 TAPPI, Polymers, Laminations and Coatings Conference Proceedings, Atlanta: TAPPI PRESS, 1993.
- [45] ANDRÉ, J.-M., AGASSANT, J.-F., DEMAY, Y., HAUDIN, J.-M., MONASSE, B. Numerical Modelling of the Polymer Film Blowing Process. *Int. J. Form. Proc.* 1998, vol. 1, no. 2, pp. 187-210.
- [46] KHONAKDAR, H.A., MORSHEDIAN, J., NODEHI, A.O. Mathematical and Computational Modeling of Heat Transfer and Deformation in Film Blowing Process. *J. App. Polym. Sci.* 2002, vol. 86, no. 9, pp. 2115-2123.
- [47] MUKE, S., CONNELL, H., SBARSKI, I., BHATTACHARYA, S.N. Numerical Modelling and Experimental Verification of Blown Film Processing. *J. Non-Newton. Fluid Mech.* 2003, vol. 116, no. 1, pp. 113-138.
- [48] PIRKLE, J.C., BRAATZ, R.D. Dynamic Modeling of Blown-Film Extrusion. *Polym. Eng. Sci.* 2003, vol. 43, no. 2, pp. 398-418.
- [49] MUSLET, I.A., KAMAL, M.R. Computer Simulation of the Film Blowing Process Incorporating Crystallization and Viscoelasticity. *J. Rheol.* 2004, vol. 48, no. 3, pp. 525-550.

- [50] TAS, P.P. Film Blowing from Polymer to Product. *Ph.D. Thesis*. Technische Universiteit Eindhoven, 1994. ISBN 90-386-0204-9.
- [51] HYUN, J.C., KIM, H., LEE J.S., SONG, H.-S, JUNG, H.W. Transient Solutions of the Dynamics in Film Blowing Process. *J. Non-Newton. Fluid Mech.* 2004, vol. 121, no. 2-3, pp. 157-162.
- [52] ZATLOUKAL, M., VLCEK, J. Modeling of the Film Blowing Process by using Variational Principles. *J. Non-Newton. Fluid Mech.* 2004, vol. 123, no. 2-3, pp. 201-213.
- [53] ZATLOUKAL, M., VLCEK, J. Application of Variational Principles in Modeling of the Film Blowing Process for High Stalk Bubbles. *J. Non-Newton. Fluid Mech.* 2006, vol. 133, no. 1, pp. 63-72.
- [54] ZATLOUKAL, M., MAVRIDIS, H., VLCEK, J., SAHA, P. Modeling of Non-Isothermal Film Blowing Process by using Variational Principles. *Annual Technical Conference - ANTEC, Conference Proceedings 2006*, vol. 2, pp. 825-829.
- [55] SARAFRAZI, S. SHARIF, F. Non-Isothermal Simulation of the Film Blowing Process Using Multi-Mode Extended Pom-Pom Model. *Int. Polym. Proc.* 2008, vol. 23, no. 1, pp. 30-37.
- [56] KOLARIK, R., ZATLOUKAL, M. Modeling of Nonisothermal Film Blowing Process for Non-Newtonian Fluids by Using Variational Principles. *J. Appl. Polym. Sci.* 2011, vol. 122, no. 4, pp. 2807-2820.
- [57] ZATLOUKAL, M. A Simple Phenomenological Non-Newtonian Fluid Model, *J. Non-Newton. Fluid* 2010, vol. 165, no. 11-12, pp. 592-595.
- [58] DEMAY, Y., CLAMOND, D. A New Model for the Blown Film Process. *C. R. Mec.* 2011, vol. 339, no. 11, pp. 692–699.
- [59] KIM, H.M., SUNG LEE, J., JUNG, H.W., HYUN, J.C. Frequency Response Analysis of Nonisothermal Film Blowing Process Using Transient Simulations. *J. Appl. Polym. Sci.* 2012, vol. 123, no. 5, pp. 3028-3035.
- [60] HAN, C.D., SHETTY, R. Studies on Multilayer Film Coextrusion III. The Rheology of Blown Film Coextrusion. *Polym. Eng. Sci.* 1978, vol. 18, no. 3, pp. 187-199.

- [61] YOON, K.-S., PARK, C.-W. Analysis of Isothermal Two-layer Blown Film Coextrusion. *Polym. Eng. Sci.* 1992, vol. 32, no. 23, pp. 1771-1777.
- [62] YOON, K.-S., PARK, C.-W. Stability of a Two-layer Blown Film Coextrusion. *J. Non-Newtonian Fluid Mech.* 2000, vol. 89, no.1-2, pp. 97-116.
- [63] STASIEK, J. Review of a Mathematical Treatment of the Heat Transfer in Multi-layer Film Blowing. *Prog. Rubber Plast. Recycl. Technol.* 2000, vol. 16, no. 3, pp. 183-192.
- [64] GAMACHE, E., AGASSANT, J.-F., DEMAY, Y., LAFLEUR, P.G. Evaluation of Stresses in a Two-layer Co-extruded LDPE Melt Blown Film. *J. Plast. Film Sheeting* 2005, vol. 21, no. 2, pp. 127-144.
- [65] XU, F., McHUGH, A.J. A Model for the Two-layer Blown Film Process with Flow-enhanced Crystallization. *Chem. Eng. Sci.* 2009, vol. 64, no. 22, pp. 4787-4795.
- [66] HENRICHSEN, L.K., McHUGH, A.J. Analysis of Film Blowing with Flow-enhanced Crystallization: part 1. Steady-State Behavior. *Int. Polym. Proc.* 2007, vol. 22, no. 2, pp. 179–189.
- [67] DOUFAS, A.K., McHUGH, A.J. Simulation of Film Blowing Including Flow-Induced Crystallization. *J. Rheol.* 2001, vol. 45, no. 5, pp. 1085-1104.

PAPER I

Modeling of Nonisothermal Film Blowing Process for Non-Newtonian Fluids by Using Variational Principles

Roman Kolarik, Martin Zatloukal

Centre of Polymer Systems, Polymer Centre, Tomas Bata University in Zlin, nam. T. G. Masaryka 5555, 760 01 Zlin, Czech Republic

Received 4 August 2010; accepted 12 February 2011

DOI 10.1002/app.34392

Published online 29 June 2011 in Wiley Online Library (wileyonlinelibrary.com).

ABSTRACT: In this work, nonisothermal film blowing process analysis for non-Newtonian polymer melts has been performed theoretically by using minimum energy approach and the obtained predictions were compared with both, theoretical and experimental data (internal bubble pressure, take-up force, bubble shape, velocity and temperature profiles) taken from the open literature. For this purpose, recently proposed generalized Newtonian model depending on three principal invariants of the deformation rate tensor, D , and its absolute defined as

$\sqrt{D \cdot D}$ has been used. It has been found that film blowing model predictions are in very good agreement with the corresponding experimental data. © 2011 Wiley Periodicals, Inc. *J Appl Polym Sci* 122: 2807–2820, 2011

Key words: extrusion; films; mathematical modeling; non-newtonian fluids; numerical analysis; polymers; polymer processing; rheology

INTRODUCTION

The film blowing process is an important polymer processing operation which is widely used for thin polymer films production.^{1–29} At the beginning of the process, polymer pellets go through the extruder hopper to the thread of the screw, where pellets are transported, homogenized, compressed, and melted. Then, the polymer melt is extruded at a constant flow rate through an annular die to a continuous tube, as can be seen in Figure 1, which describes the most often used film blowing line type, the nip rolls situated on the top of the line. The continuous tube is stretched in two directions: the axial drawing (machine direction) by the nip rolls and the circumferential drawing (transverse direction) by the internal air pressure. Simultaneously, the bubble is cooled by an air ring (with/without internal bubble cooling system IBC) situated around the bubble level with the die exit. Then, above the freezeline height, the bubble is in a solid state, with the final mechanical and optical properties. Calibration bub-

ble cage is usually used to stabilize the system. The dimensions of the bubble are defined by the terms blow-up ratio, BUR, which is the ratio of the final bubble diameter at the freezeline height to the bubble diameter at the die exit, and the take-up ratio, TUR, which is the ratio of the film velocity above the freezeline to the melt velocity through die exit. Above the calibration cage, the bubble is folded between two table flaps and drawn by the nip rolls to a wind-up roll. These biaxially oriented films of a small thickness are used in commodity applications, such as food wrapping and carrier bags in food processing, medical films, scientific balloons, garbage bags, and waste land fill liners in the waste industry.³

The relationships between the machine design, processing parameters, material and the extensional stresses within the extending bubble are still not fully understood although they have been investigated by many researchers from the late 1930's.^{1–14} The most popular way to optimize the film blowing process is modeling. The first film blowing model was developed by Pearson and Petrie^{20,22} for isothermal process and Newtonian fluid where the film is assumed to be a thin shell in tension in the axial and circumferential directions. This model became the basis of the most subsequent film blowing models.^{15–17,24,26,30–36} However, numerical instabilities,^{26,29} inability to describe the full range of the bubble shapes²⁷ and existence of anomalous predictions^{37,38} were identified in the open literature if one tried to solve the Pearson-Petrie

Correspondence to: M. Zatloukal (mzatloukal@ft.utb.cz).

Contract grant sponsor: GA CR; contract grant number: P108/10/1325.

Contract grant sponsor: MSMT (project Centre of Polymer Systems); contract grant number: CZ.1.05/2.1.00/03.0111.

Journal of Applied Polymer Science, Vol. 122, 2807–2820 (2011)
© 2011 Wiley Periodicals, Inc.

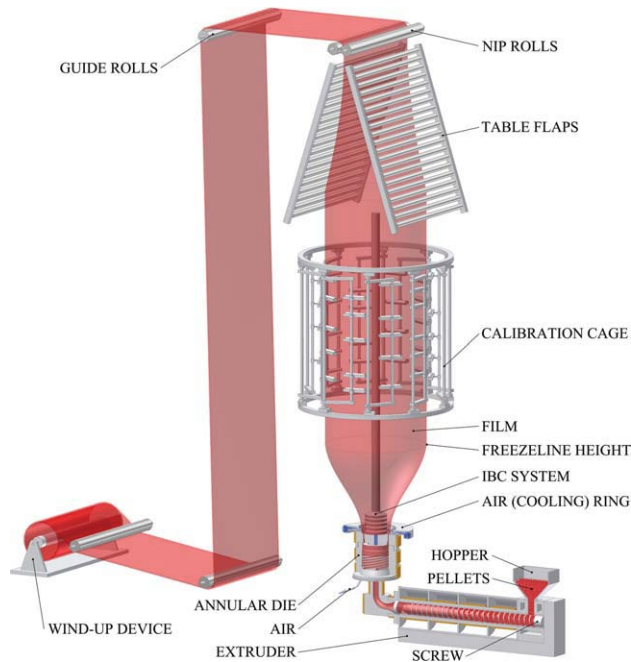


Figure 1 The film blowing line. [Color figure can be viewed in the online issue, which is available at wileyonlinelibrary.com.]

equations with particular constitutive equations. It has been recently found that these problems can be overcome by the use of the Zatloukal-Vlcek model,^{30–36} which describes the formation of the bubble, because of the internal bubble pressure and the take-up force, in such a way that the resulting bubble satisfies the minimum energy requirements.

The main aim in this work is to investigate predicting capabilities of the Zatloukal-Vlcek model if nonisothermal conditions and non-Newtonian fluid behavior are taken into account. The studied model behavior will be compared with Tas's Ph.D. thesis experimental data¹⁸ and predictions of the following two different Pearson and Petrie based models: Sarafrazi and Sharif model¹⁶ (extended Pom-Pom constitutive equation is used; a variable heat transfer coefficient and stress induced crystallization is taken into account) and Beaulne and Mitsoulis model¹⁵ (integral constitutive equation of the K-BKZ type is utilized; constant heat transfer coefficient and no crystallization effects are assumed).

MATHEMATICAL MODELING

It has been shown by Zatloukal and Vlcek³¹ that the bubble during blowing can be viewed as a bended elastic membrane due to the load p and the take-up force F , where the line element of the membrane

after loading can be simplified as $\sqrt{1 + (y')^2} dx \approx \left[1 + \frac{1}{2}(y')^2\right] dx$ (see Fig. 2). In such a case, the membrane potential energy can be expressed by the following form:

$$E_p = \frac{F}{2} \int_0^L (y')^2 dx - p \int_0^L y dx \quad (1)$$

which takes into account two basic contributions to the potential energy: elastic strain energy increase and negative work done by the applied load. Having the bubble volume, $V = \pi \int_0^L y^2 dx$, as the main geometrical constrain, the equation for the bubble shape, y , can be derived through minimization of the potential energy functional, I , in the following form:

$$I = \left[\frac{1}{2} F (y')^2 - p y \right] + \lambda_1 (\pi y^2) \quad (2)$$

i.e., $I = f(x, y, y')$ where λ_1 is the Lagrange multiplier. The functional I is minimized if the following equation is satisfied:

$$\frac{\partial I}{\partial y} - \frac{\partial}{\partial x} \frac{\partial I}{\partial y'} = 0 \quad (3)$$

Equations (2) and (3) yield the following differential equation:

$$F y'' - \frac{1}{J} y + p = 0 \quad (4)$$

Where J is the compliance of the membrane defined as positive constant taking the following form:

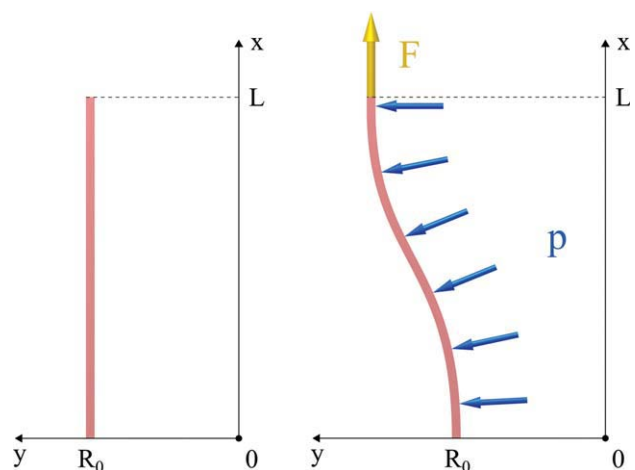


Figure 2 Membrane before deformation (left), membrane after deformation (right). [Color figure can be viewed in the online issue, which is available at wileyonlinelibrary.com.]

TABLE I
Relationship Between A and φ Functions

Equation number	A	φ
(1)	1	0
(2)	$0 < A < 1$	$\arctg\left(\frac{\sqrt{1-A^2}}{A}\right)$
(3)	0	$\pi/2$
(4)	$-1 < A < 0$	$\pi + \arctg\left(\frac{\sqrt{1-A^2}}{A}\right)$
(5)	-1	π

$$J = \frac{1}{2\pi\lambda_1} \tag{5}$$

Let us use the following boundary conditions for the bubble shape:

$$\frac{\partial y(x=L)}{\partial x} = 0, \quad y(x=0) = R_0 \tag{6}$$

and

$$y(x=L) = R_0BUR = R_2 \tag{7}$$

where R_0 is the extrusion die radius, L the freezeline height and R_2 is the bubble radius at the freezeline, i.e., $x = L$. Since above the freezing line there is no deformation, it can be assumed that $y(x > L) = const. = y(x = L)$. It is not difficult to show (see Ref. ³¹ for detailed derivation) that the solution of eq. (4), considering the aforementioned boundary conditions, takes the following form:

$$y = (R_0 - pJ) \cos\left(\frac{x\varphi}{L}\right) - \alpha'(pJ - BURR_0) \sin\left(\frac{x\varphi}{L}\right) + pJ \tag{8}$$

where force F is given by the following expression:

$$F = -\frac{L^2}{J\varphi^2} \tag{9}$$

Here α' and A are given below and the value of $\varphi(A)$ is calculated according to Table I:

$$\alpha' = \sqrt{\frac{2pJ - R_0 - BUR R_0}{pJ - BUR R_0} \left| \frac{R_0(BUR - 1)}{pJ - BUR R_0} \right|} \tag{10}$$

$$A = \frac{pJ - R_0}{pJ - BUR R_0} \tag{11}$$

The total number of parameters needed to describe the bubble shape is equal to four (pJ , L , R_0 , BUR). Just note that pJ/R_0 (dimensionless form of pJ) determines the total deformation (curvature) of the bubble which varies between 0 and $R_0*(1+BUR)/2$ for the bubbles without the neck.³¹

According to,³¹ the internal bubble pressure and the take-up force for a 3D bubble can be directly calculated from parameters of the proposed model and the force balance by taking the 3D nature of a real bubble into account through following equations:

$$\Delta p = \frac{pL}{2\pi \int_0^L y \sqrt{1 + (y')^2} dx} \tag{12}$$

$$F_{total} = |F| \tag{13}$$

where the term $2\pi \int_0^L y \sqrt{1 + (y')^2} dx$ in eq. (12) means the bubble surface and the term pL is the force acting in the thickness direction of the bubble, $F_{thickness}$. Eq. (12) represents the calculation of the internal bubble pressure in such a way that the bubble is represented by an equivalent cylinder, which has the same surface as the real bubble. Force F in eq. (13) is defined by eq. (9).

Nonisothermal film blowing with non-Newtonian fluid

In this section, the assumptions about the static (not moving) and elastic only bubble having constant thickness will be relaxed. It is done here by considering an additional set of equations, which are summarized below.

Continuity equation:

$$Q = 2\pi y(x)h(x)v(x) \tag{14}$$

where Q is the volume flow rate, $y(x)$, the radius of the bubble, $h(x)$, the thickness of the film and $v(x)$ is the film velocity, all as functions of the distance from the die x .

Constitutive equation (generalized Newtonian fluid recently proposed in³⁹):

$$\tau = 2\eta(I_{|D|}, II_D, III_D)D \tag{15}$$

where τ means the extra stress tensor, D represents the deformation rate tensor and η stands for the viscosity, which is not constant (as in the case of standard Newtonian law), but it is allowed to vary with the first invariant of the absolute value of deformation rate tensor $I_{|D|} = tr(|D|)$, (where $|D|$ is defined as the square root of D^2) as well as on the second $II_D = 2tr(D^2)$, and third, $III_D = det(D)$, invariants of D according to eq. (16)

$$\eta(I_{|D|}, II_D, III_D) = \eta(III_D)^{f(I_{|D|}, II_D, III_D)} \tag{16}$$

where $\eta(II_D)$ is given by the well known Carreau-Yasuda model, eq. (17) and $f(I_{|D|}, II_D, III_D)$ is given by eq. (18).

$$\eta(II_D) = \frac{\eta_0 a_T}{[1 + (\lambda a_T \sqrt{II_D})^a]^{\frac{1-a}{a}}} \tag{17}$$

$$f(I_{|D|}, II_D, III_D) = \left\{ \tanh \left[\alpha a_T \left(1 + \frac{1}{4(\sqrt{3})^3} \right)^{-\psi} \right. \right. \\ \left. \left. \left(\left| 1 + \frac{III_D}{II_D^{3/2}} \right| \right)^\psi \frac{\sqrt[3]{4|III_D| + I_{|D|}}}{3} + \beta \right] \frac{1}{\tanh(\beta)} \right\}^\zeta \tag{18}$$

Here η_0 , λ , a , n , α , ψ , β , ζ are adjustable parameters and a_T is temperature shift factor defined by the Arrhenius equation:

$$a_T = \exp \left[\frac{E_a}{R} \left(\frac{1}{273.15 + T} - \frac{1}{273.15 + T_r} \right) \right] \tag{19}$$

where E_a is the activation energy, R is the universal gas constant, T_r is the reference temperature and T is local bubble temperature. This recently proposed constitutive equation in³⁹ has been chosen for the film blowing modeling because it has high flexibility to represent the strain rate dependent steady shear and uniaxial extensional viscosities for linear and branched polyolefines as well as it provides correct behavior in steady planar/equibiaxial extensional viscosity. Moreover, the model allows independent strain hardening level control for planar/equibiaxial extensional viscosity with respect to uniaxial extensional viscosity through parameter ψ .³⁹

It is not difficult to show that the equation of continuity ($Q = Sv_f$) together with the generalized Newtonian model (applied for the machine direction stress $\tau_{xx} = 2\bar{\eta}\dot{\epsilon}_1$) yields the following expression for the internal force ($F_N = \tau_{xx}S$) at the freezeline in the machine direction:

$$F_N = 2\bar{\eta}\dot{\epsilon}_1 \frac{Q}{v_f} \tag{20}$$

where $\bar{\eta}$ and $\dot{\epsilon}_1$ represent the mean values of the melt viscosity ($\bar{\eta} = \frac{1}{L} \int_0^L \eta dx$) and the extensional rate ($\dot{\epsilon}_1 = \frac{1}{L} \int_0^L \dot{\epsilon} dx$), respectively, for the whole bubble, Q , the volume flow rate, v_f , the velocity of the film at the freezeline. The equation for bubble compliance J can be obtained by solving eqs. (9), (13), and (20) in the following form:

$$J = \frac{L^2 v_f}{2\bar{\eta}^2 \dot{\epsilon}_1 Q} \tag{21}$$

Energy equation

With the aim to take nonisothermal conditions into account, cross sectionally averaged energy equation taken from,⁴⁰ has been considered:

$$\rho C_p \frac{dT}{dx} = - \frac{2\pi y \rho}{\dot{m}} [HTC(T - T_{air}) + \sigma_B \bar{\epsilon} (T^4 - T_{air}^4)] \\ + \tau : \nabla v + \rho \Delta H_f \frac{d\phi}{dx} \tag{22}$$

where C_p stands for the specific heat capacity, ρ is the polymer density, y means the local bubble radius, \dot{m} is the mass flow rate, HTC represents the heat transfer coefficient, T is the bubble temperature, T_{air} means the air temperature used for the bubble cooling, σ_B stands for the Stefan-Boltzmann constant, $\bar{\epsilon}$ represents the emissivity, τ is the extra stress tensor, ∇v means velocity gradient tensor, ΔH_f indicates the heat of crystallization per unit mass and ϕ is the average absolute crystallinity degree of the system at the axial position, x .

To reduce the problem complexity, the axial conduction, dissipation, radiation effects, and crystallization are neglected. For such simplifying assumptions, eq. (22) is reduced in the following, the simplest version of the cross sectionally averaged energy equation:

$$\dot{m} C_p \frac{dT}{dx} = 2\pi y [HTC(T - T_{air})] \tag{23}$$

where the local bubble radius y is given by eq. (8). It should be mentioned that neglecting several terms in eq. (22) for the energy equation (especially crystallization) may be the reason for the poor predicted of the temperature profile along the bubble in the range of the polymer freezing point. The eq. (23) applied for the whole part of the bubble takes the following form:

$$\int_{T_{die}}^{T_{solid}} \frac{\dot{m} C_p}{HTC(T - T_{air})} dT = 2\pi \int_0^L y dx \tag{24}$$

where T_{die} and T_{solid} represents the temperature of the melt at the die exit and solidification temperature of the polymer, respectively. After integration from die temperature, T_{die} , up to freezeline temperature, T_{solid} , we can obtain equation defining the relationship between freezeline height, L , and heat transfer coefficient, HTC , which takes the following simple analytical expression:

$$L = - \frac{1}{2} \dot{m} C_p \ln \left(- \frac{(T_{die} - T_{air})}{(-T_{solid} + T_{air})} \right) \frac{\phi}{\pi HTC (\alpha p J - \alpha BURR_0 - \sin(\phi) R_0 - p J \phi + \sin(\phi) p J - \alpha \cos(\phi) p J + \alpha \cos(\phi) BURR_0)} \tag{25}$$

With the aim to get equations for the temperature profile along the bubble, it is necessary to apply the eq. (23) for any arbitrary point at the bubble, i.e., in the following way:

$$\int_{T_{\text{die}}}^T \frac{\dot{m}C_p}{HTC(T - T_{\text{air}})} dT = 2\pi \int_0^x y dx \quad (26)$$

After the integration of eq. (26), the temperature profile takes the following analytical expression:

$$T = T_{\text{air}} + (T_{\text{die}} - T_{\text{air}}) \exp \left\{ -\frac{2\pi L HTC}{\dot{m}C_p \varphi} \left(-\alpha [R_0 BUR - p] \right) \times \left[\cos \left(\frac{x\varphi}{L} \right) - 1 \right] + \sin \left(\frac{x\varphi}{L} \right) [R_0 - p] + pJ\varphi \frac{x}{L} \right\} \quad (27)$$

Velocity profile calculation

With the aim to calculate the velocity profile and the film thickness in the nonisothermal film blowing process, the force balance in vertical direction (gravity and upward force due to the airflow are neglected) proposed by Pearson and Petrie is considered in the following form:

$$\frac{2\pi y h \sigma_{11}}{\sqrt{1 + (y')^2}} = F - \pi \Delta p (R_0^2 BUR^2 - y^2) \quad (28)$$

where σ_{11} is the total stress in the machine direction and F and Δp are defined by eqs. (9), (13), and (12). The deformation rate tensor in the bubble forming region takes the following form:

$$D = \begin{pmatrix} \dot{\epsilon}_1 & 0 & 0 \\ 0 & \dot{\epsilon}_2 & 0 \\ 0 & 0 & \dot{\epsilon}_3 \end{pmatrix} = \begin{pmatrix} \frac{dv}{dx} & 0 & 0 \\ 0 & \frac{v}{h} \frac{dh}{dx} & 0 \\ 0 & 0 & \frac{v}{y} y' \end{pmatrix} \quad (29)$$

where v and h is bubble velocity and thickness, respectively. Assuming that $h \ll y$, then

$$\sigma_{11} = \tau_{11} - \tau_{22} \quad (30)$$

By combination of eqs. (15), (29), (30), the σ_{11} takes the following form:

$$\sigma_{11} = 2\eta \left(2 \frac{dv}{dx} + \frac{v}{y} y' \right) \quad (31)$$

After substituting eq. (31) into eq. (28), the equation for the bubble velocity in the following form can be obtained.

$$v = v_d \exp \left(\int_0^L \left\{ \frac{\sqrt{1 + (y')^2} [F - \pi \Delta p (R_0^2 BUR^2 - y^2)]}{4Q\eta} - \frac{1}{2y} y' \right\} dx \right) \quad (32)$$

where v_d is bubble velocity at the die exit. Having the velocity profile, the deformation rates and the thickness can be properly calculated along the bubble. The key film blowing variables are depicted in Figure 3.

MODELING VERSUS EXPERIMENTAL DATA

In this part, the above described film blowing model will be tested by using experimental data taken from the Tas's Ph.D. thesis.¹⁸ Moreover, theoretical predictions will be compared with two different film blowing models^{15–17} (those predictions will be taken from the literature), which has already been utilized for the same experimental data set.

Material definition

In this work, LDPE L8 taken from Tas's Ph.D. thesis¹⁸ is considered. Material characteristics together

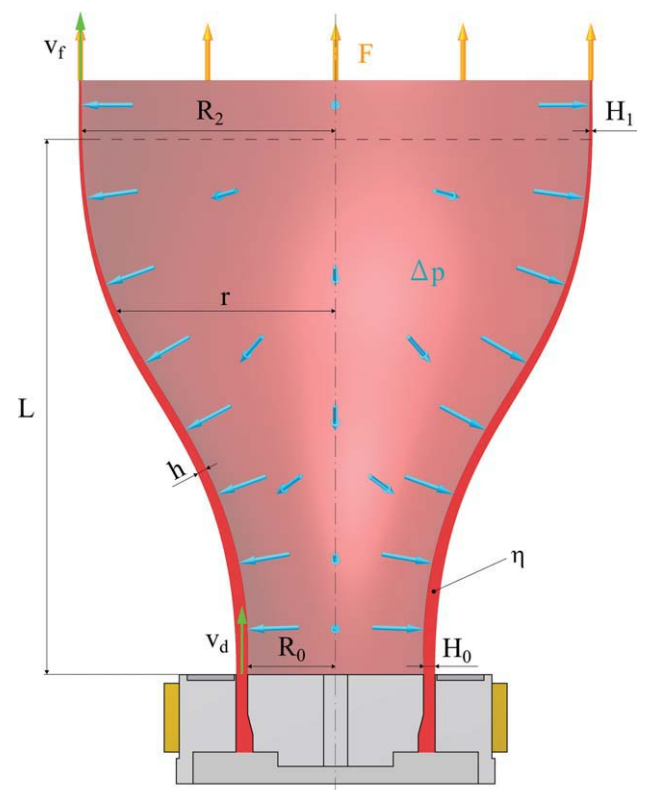


Figure 3 Film blowing variables. [Color figure can be viewed in the online issue, which is available at [wiley onlinelibrary.com](http://www.interscience.wiley.com).]

TABLE II
Characteristics of the L8 Stamyln LDPE Used in the Experiments by Tas¹⁸

LDPE material	Grade (Stamyln LD)	Melt Index (dg.min ⁻¹)	Molecular weight averages			Density (kg m ⁻³)	Crystallization temperature T_c (°C)
			M_n (g mol ⁻¹)	M_w (g mol ⁻¹)	M_z (g mol ⁻¹)		
L8	2008XC43	8	13,000	155,000	780,000	920	98.6

with corresponding viscoelastic Phan-Thien-Tanner (PTT) model parameters are provided in Tables II and III. It should be mentioned that predictions of the PTT model⁴¹ for steady state shear and steady uniaxial extensional viscosities have been used as the measurements for LDPE L8 to obtain all adjustable parameters of the proposed model [eqs. (16–18)], which is utilized here as the constitutive equation. This procedure has been chosen due to the fact that steady state rheological data for tested LDPE L8 is not available in Tas's Ph.D. thesis.

In Figure 4, it is clearly visible that the used generalized Newtonian model has very good capabilities to describe steady shear and steady uniaxial extensional viscosities for the Tas's LDPE L8 sample, which justifies its utilization in the film blowing modeling. The generalized Newtonian

model parameters are provided in Table IV and the parameter ψ has been chosen to be 20 as suggested in.³⁹

Numerical scheme

To determine the heat transfer coefficients for the Tas's film blowing experimental data, first, the eq. (8) has been used to fit the Tas's bubble shapes to obtain all model parameters (R_0 , L , BUR and p). In the second step, the heat transfer coefficient HTC for each specific condition has been determined by using eq. (25).

On the basis of the input parameters (see numerical scheme in Fig. 5) and guess values for p , Δp , $\overline{I_{|D|}}$, $\overline{II_D}$, and $\overline{III_D}$, so called average bubble viscosity $\overline{\eta}$ can be determined according to eq. (33)

$$\overline{\eta} = \left\{ \frac{\eta_0 \overline{a_T}}{\left[1 + \left(\lambda \overline{a_T} \sqrt{\overline{II_D}} \right)^a \right]^{\left(\frac{1-a}{a} \right)}} \right\} \left\{ \tanh \left[\alpha \overline{a_T} \left(1 + \frac{1}{4(\sqrt{3})^3} \right) \left(\left| 1 + \frac{\overline{III_D}}{\overline{II_D}^2} \right| \right)^\psi \frac{\sqrt[3]{4|\overline{III_D}| + \overline{I_{|D|}}}}{3} + \beta \right] \frac{1}{\tanh(\beta)} \right\}^\zeta \quad (33)$$

where $\overline{I_{|D|}}$ is the mean value of the first invariant of the square root of D^2 , $\overline{II_D}$, and $\overline{III_D}$ represent the mean value of the second and third invariants of deformation rate tensor, respectively, and $\overline{a_T}$ is the average temperature shift factor [eq. (33)]:

$$\overline{I_{|D|}} = \sqrt{\dot{\varepsilon}_1^2} + \sqrt{\dot{\varepsilon}_2^2} + \sqrt{\dot{\varepsilon}_3^2} \quad (34)$$

$$\overline{II_D} = 2 \left(\dot{\varepsilon}_1^2 + \dot{\varepsilon}_2^2 + \dot{\varepsilon}_3^2 \right)$$

$$\overline{III_D} = \dot{\varepsilon}_1 \dot{\varepsilon}_2 \dot{\varepsilon}_3 \quad (35)$$

$$\overline{a_T} = \exp \left[\frac{E_a}{R} \left(\frac{1}{273.15 + T_s} - \frac{1}{273.15 + T_r} \right) \right] \quad (36)$$

Here, the average bubble temperature T_s and mean values of the deformation rate components $\dot{\varepsilon}_1$, $\dot{\varepsilon}_2$, $\dot{\varepsilon}_3$ are defined as follows

$$T_s = \frac{T_{die} + T_{solid}}{2} \quad (37)$$

$$\overline{\varepsilon}_1 = \frac{1}{L} \int_0^L \dot{\varepsilon}_1 dx \quad (38)$$

$$\overline{\varepsilon}_2 = \frac{\overline{v} \overline{h} - H_0}{\overline{h} L} \quad (39)$$

TABLE III
Discrete Relaxation Time Spectra Together With Nonlinear PTT⁴¹ Model Parameters ξ and ε at 190°C for L8 Stamyln LDPE Sample

L8 ($\xi = 0.13$, $\varepsilon = 0.05$)	
λ_i (s)	G_i (Pa)
4.28×10^{-5}	2.17×10^5
2.07×10^{-4}	9.18×10^4
1.34×10^{-3}	5.75×10^4
9.02×10^{-3}	2.43×10^4
5.69×10^{-2}	8.91×10^3
3.53×10^{-1}	2.34×10^3
1.82×10^0	3.21×10^2
9.94×10^0	1.24×10^1

Data are taken from Tas's Ph.D. thesis.¹⁸

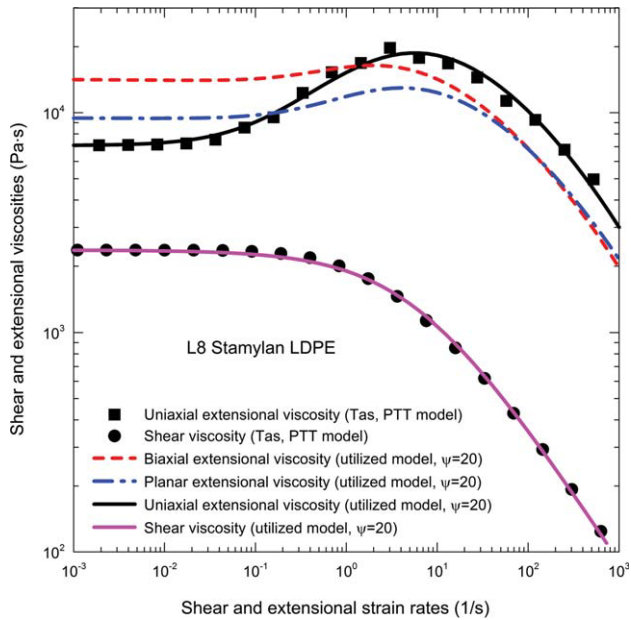


Figure 4 Comparison between the generalized Newtonian model fit (solid lines)³⁹ and PTT model predictions (symbols) characterizing L8 Stamyran LDPE material according to Tas’s Ph.D. thesis.¹⁸ [Color figure can be viewed in the online issue, which is available at wileyonlinelibrary.com.]

$$\bar{\epsilon}_3 = -(\bar{\epsilon}_1 + \bar{\epsilon}_2) \tag{40}$$

where L is freezeline height, H_0 is bubble thickness at the die, \bar{v} and \bar{h} is mean value of bubble velocity and thickness along the bubble, respectively, which are defined below:

$$\bar{v} = \frac{1}{L} \int_0^L v(x) dx \tag{41}$$

$$\bar{h} = \frac{1}{L} \int_0^L h(x) dx \tag{42}$$

It is well known that during the film blowing process, the melt viscosity is changing dramatically between the extrusion die exit and freezeline height. To take such strong temperature dependence of the viscosity during velocity calculation of the film [by using eq. (32)] into account, the following expression for the viscosity η has been proposed and used:

$$\eta = \bar{\eta} a_{T,Bubble} \tag{43}$$

where $a_{T,Bubble}$ is the normalized bubble temperature shift factor defined as:

$$a_{T,Bubble} = \frac{a_T}{a_{TS}} \tag{44}$$

where a_{TS} represents the mean value of the Arrhenius temperature shift factor a_T [see eq. (19)], which is given as follows:

$$a_{TS} = \frac{1}{L} \int_0^L a_T dx \tag{45}$$

The velocity profile is calculated by the help of eq. (32) where the take-up force F is varied until the calculated film velocity at the freezeline height reached the desirable value (according to defined TUR). For the obtained velocity profile, the average bubble viscosity $\bar{\eta}$ is upgraded (based on the new values of three deformation rate tensor invariants $\overline{I_{|D|}}$, $\overline{II_D}$, and $\overline{III_D}$) and the velocity calculation is repeated again until the average bubble viscosity $\bar{\eta}$

TABLE IV
Film Blowing Model Parameters for Tas’s Experiments No. 23 and 29 and L8 Stamyran LDPE Material

Input parameters for the Zatloukal-Vlcek film blowing model								
Exp.	BUR (-)	L (m)	p/l (m)	Δp (Pa)	R_0 (m)	H_0 (m)	TUR (-)	\dot{m} (kg s ⁻¹)
23	2.273	0.13365	0.027605	85	0.0178	0.0022	21.5083	0.00100
29	2.749	0.13882	0.029818	70	0.0178	0.0022	19.4437	0.00100
Parameters of the generalized Newtonian constitutive equation ($\psi = 20$)								
η_0 (Pa s)	λ (s)	a (-)	n (-)	α (s)	β (-)	ζ (-)		
2,365	0.17242	0.71597	0.37108	1.10^{-5}	$9.21.10^{-7}$	0.054384		
Temperature parameters								
T_{air} (°C)	T_{solid} (°C)	T_{die} (°C)	T_r (°C)	E_a (J mol ⁻¹)	R (J K ⁻¹ mol ⁻¹)	C_p (J kg ⁻¹ K ⁻¹)		
25	92	145	190	59,000	8.314	2,300		

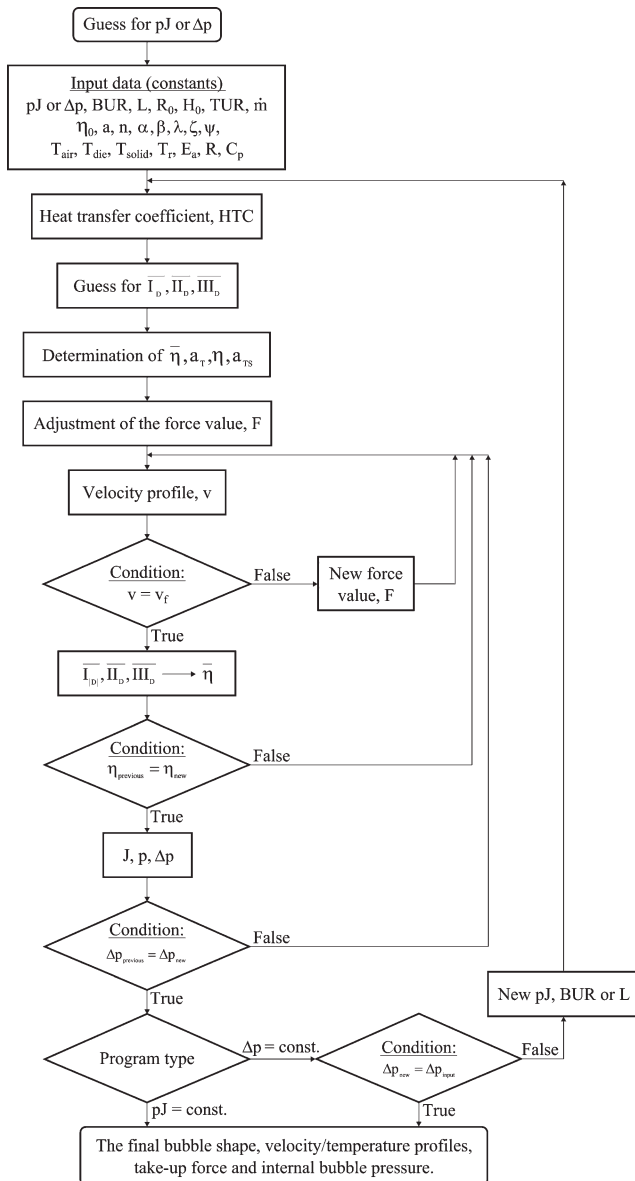


Figure 5 Iteration scheme for the proposed film blowing model.

remains unchanged for the given take-up force F and velocity profile.

In the final case, the bubble compliance J is calculated according to eq. (21). For the given pJ value (bubble curvature) the internal load is determined and consequently used for the internal bubble pressure Δp [eq. (12)] calculation. By using this new Δp value the velocity profile calculation is repeated again until the Δp becomes constant. Above described numerical scheme is summarized in Figure 5. In this way, the internal bubble pressure and take-up force can be calculated for the given bubble shape. If the internal bubble pressure is fixed, whereas the take-up force and bubble shapes (i.e., pJ), are calculated variables, the above described numerical scheme can be repeated for different values of pJ until desirable Δp is obtained.

Film blowing experiment versus model prediction

In this section, proposed model predictions for the bubble shape (Figs. 6 and 7), film velocity (Fig. 8 and 9), and temperature profiles (Figs. 10 and 11), for the processing conditions summarized in Table IV, are compared with Tas's experimental data¹⁸ together with theoretical predictions by Sarafrazi and Sharif¹⁶ model and Beaulne and Mitsoulis model,¹⁵ which are based on the classical approach of Pearson and Petrie.²⁰

It should be mentioned that two possible numerical schemes have been tested for the proposed model. First procedure consider that the bubble shape (i.e., pJ , BUR) is a priori known and take-up force F and internal bubble pressure Δp are unknowns parameters, whereas in the second case Δp is known and bubble shape (i.e., pJ , BUR) and F are unknown parameters (see numerical scheme in Fig. 5).

As can be clearly seen in Figures 6–11, both numerical approaches leads to very similar predictions for all investigated variables (bubble shape, velocity, and temperature) and it can be concluded that the agreement between the proposed model predictions are in very good agreement with the corresponding experimental data. Moreover, tested model predictions are comparable with the Sarafrazi and Sharif¹⁶ model predictions (which is based on the advanced extended Pom-Pom constitutive equation; a variable heat transfer coefficient and stress induced crystallization).

Complete set of calculated variables in the proposed model for theoretical predictions depicted in Figures 6–11 are summarized in Tables V and VI. It is visible that predicted F and Δp for all tested polymers and processing conditions are in fairly good agreement with the corresponding Tas's experimental data. These predictions are comparable with Sarafrazi and Sharif¹⁶ model predictions and even better than Beaulne and Mitsoulis model¹⁵ behaviour, which is based on the viscoelastic integral constitutive equation of the K-BKZ type assuming constant heat transfer coefficient and no crystallization effects. Just note that for the die volume rate calculation (from the experimentally known mass flow rate), the following definition of the LDPE density taken from¹⁸ was used:

$$\rho = \frac{1,000}{0.934 \cdot 0.001 \cdot (273.15 + T_{\text{die}}) + 0.875} \quad (46)$$

As it can be seen, the proposed approach for the film blowing modeling is comparable with the Pearson and Petrie based models for the tested polymers and processing conditions. It should be

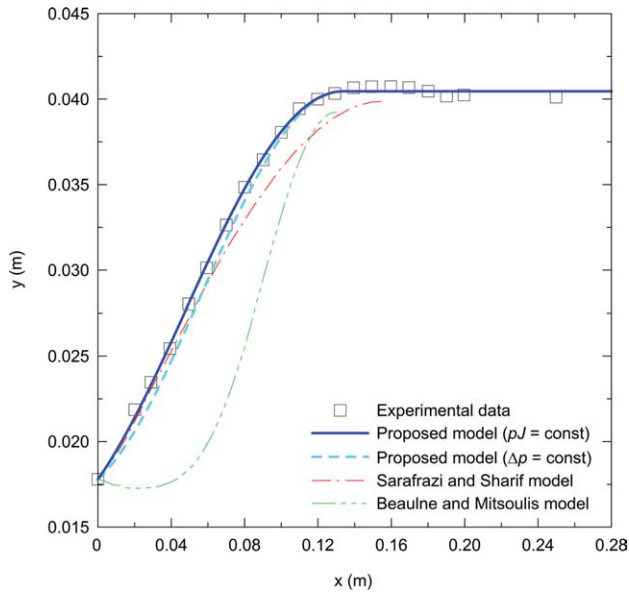


Figure 6 Comparison of the bubble shapes between the proposed model prediction,³⁰ experiment No. 23 taken from Tas's Ph.D. thesis¹⁸ and the Beaulne/Mitsoulis model prediction¹⁵ and the Sarafrazi/Sharif model prediction.¹⁶ [Color figure can be viewed in the online issue, which is available at wileyonlinelibrary.com.]

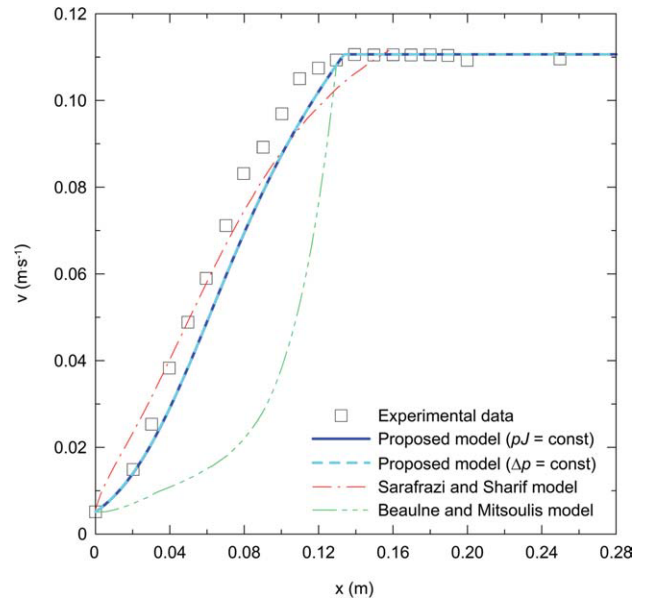


Figure 8 Comparison of the velocity profiles between the proposed model prediction,³⁰ experiment No. 23 taken from Tas's Ph.D. thesis¹⁸ and the Beaulne/Mitsoulis model prediction¹⁵ and the Sarafrazi/Sharif model prediction.¹⁶ [Color figure can be viewed in the online issue, which is available at wileyonlinelibrary.com.]

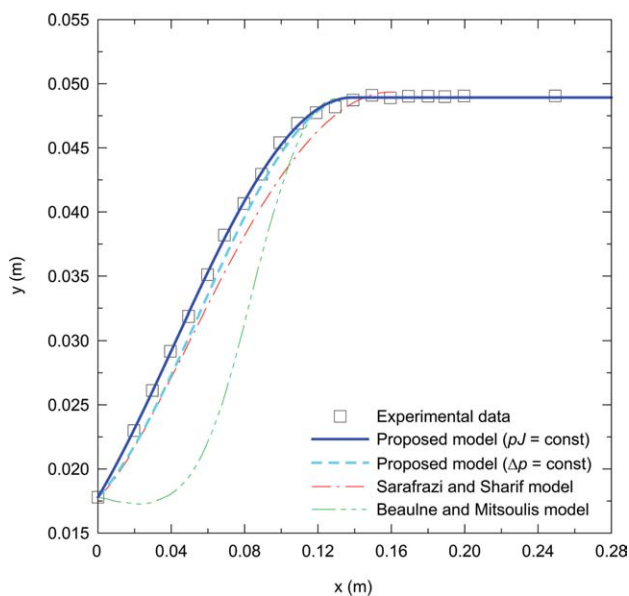


Figure 7 Comparison of the bubble shapes between the proposed model prediction,³⁰ experiment No. 29 taken from Tas's Ph.D. thesis¹⁸ and the Beaulne/Mitsoulis model prediction¹⁵ and the Sarafrazi/Sharif model prediction.¹⁶ [Color figure can be viewed in the online issue, which is available at wileyonlinelibrary.com.]

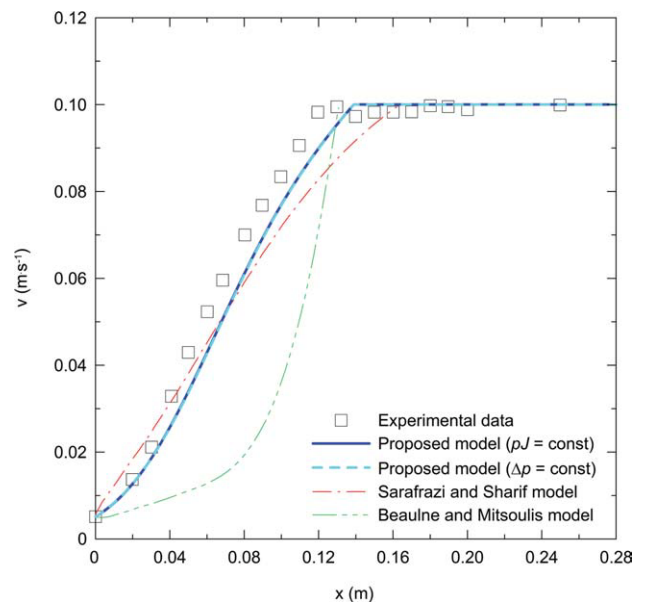


Figure 9 Comparison of the velocity profiles between the proposed model prediction,³⁰ experiment No. 29 taken from Tas's Ph.D. thesis¹⁸ and the Beaulne/Mitsoulis model prediction¹⁵ and the Sarafrazi/Sharif model prediction.¹⁶ [Color figure can be viewed in the online issue, which is available at wileyonlinelibrary.com.]

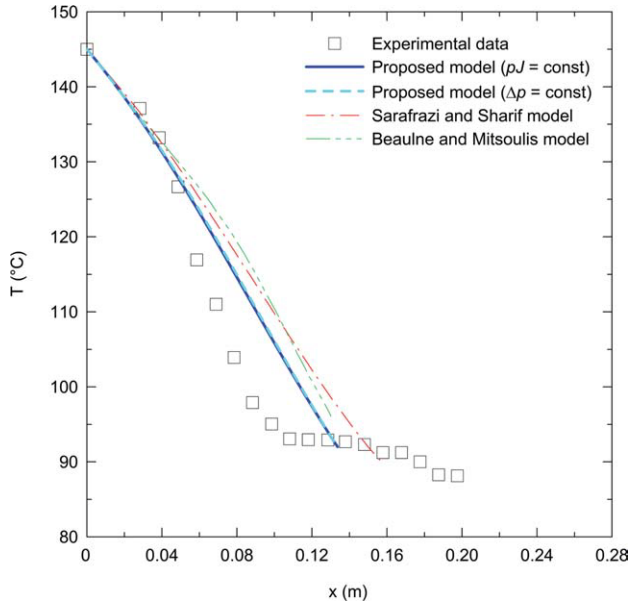


Figure 10 Comparison of the temperature profiles between the proposed model prediction,³⁰ experiment No. 23 taken from Tas’s Ph.D. thesis¹⁸ and the Beaulne/Mitsoulis model prediction¹⁵ and the Sarafrazi/Sharif model prediction.¹⁶ [Color figure can be viewed in the online issue, which is available at wileyonlinelibrary.com.]

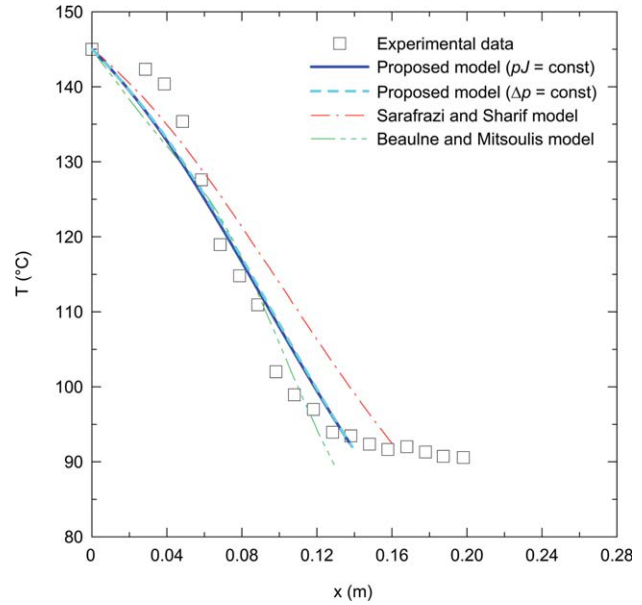


Figure 11 Comparison of the temperature profiles between the proposed model prediction,³⁰ experiment No. 29 taken from Tas’s Ph.D. thesis¹⁸ and the Beaulne/Mitsoulis model prediction¹⁵ and the Sarafrazi/Sharif model prediction.¹⁶ [Color figure can be viewed in the online issue, which is available at wileyonlinelibrary.com.]

mentioned that an additional value of the proposed model is availability of analytical expressions for the freezeline height/heat transfer coefficient, bubble shape, internal bubble pressure and take-up force, which significantly stabilizes numerical scheme and anomalous predictions are avoided.

To the author’s knowledge, the effect of biaxial extensional viscosity on the film blowing experiment has not been clearly investigated, yet in the open literature because the measurement of the

biaxial extensional viscosity of the polymer melt is very complicated.⁴² To fill this gap, the effect of strain hardening level in equibiaxial extensional viscosity (by keeping unchanged shear and uniaxial extensional viscosities) on the film blowing process is investigated here through parameter ψ occurring in eq. (18). In this model, the parameter ψ increase causes the equibiaxial extensional strain hardening decrease for the LDPE L8 as shown in Figure 12 and vice versa. Film blowing modeling of the Tas’s experiment No. 23, where parameter ψ was varied

TABLE V
Summarization of Tas’s Experimental Data,¹⁸ Zatloukal-Vlcek^a the Calculated Results for the Fixed Bubble Shape ρJ and Internal Bubble Pressure Δp are provided in the Parentheses and Without Parentheses, Respectively), Sarafrazi/Sharif [16] and Beaulne/Mitsoulis [15] Model Predictions

Material L8 Models	Experiment 23				Experiment 29			
	Δp (Pa)	F (N)	σ_{11} (MPa)	σ_{33} (MPa)	Δp (Pa)	F (N)	σ_{11} (MPa)	σ_{33} (MPa)
Experimental data (Tas)	85	4.30	0.410	0.068	70	3.50	0.270	0.070
Zatloukal-Vlcek (this work) ^a	85.000 (64.910)	5.895 (5.834)	0.515 (0.510)	0.076 (0.058)	70.000 (46.341)	5.724 (5.619)	0.452 (0.444)	0.083 (0.055)
Sarafrazi and Sharif	69.60	4.80	0.462	0.018	55.84	3.34	0.311	0.038
Beaulne and Mitsoulis	186	1.86	0.196 ^b	0.201 ^b	168	2.13	0.206 ^b	0.245 ^b

^a Zatloukal-Vlcek model considering nonisothermal conditions and non-Newtonian fluid behavior in this work.

^b σ_{11} , σ_{33} at the freezeline were calculated by using v_d , R_0 , H_0 , F , Δp , BUR, v_f provided in¹⁵ and Pearson and Petrie

$$\text{equations } \sigma_{11} = \frac{F}{2\pi R_0 \text{BUR} H_1} \text{ and } \sigma_{33} = \frac{R_0 \text{BUR} \Delta p}{H_1}$$

TABLE VI
Summarization of the Proposed Film Blowing Model Predictions for Tas's LDPEs and Processing Conditions

	pJ (m)	v_d (m s ⁻¹)	v_f (m s ⁻¹)	\dot{Q} (10 ⁻⁷ m ³ s ⁻¹)	H_1 (10 ⁻⁵ m)	J (Pa ⁻¹)
Exp. 23	0.028611 (0.027605)	0.005143 (0.005143)	0.110627 (0.110627)	12.656 (12.656)	4.5007 (4.5008)	0.001763 (0.002183)
Exp. 29	0.032311 (0.029818)	0.005143 (0.005143)	0.100008 (0.100008)	12.656 (12.656)	4.1161 (4.1163)	0.002076 (0.002812)
	HTC (W m ⁻² K ⁻¹)	η (Pa s)	$\bar{\eta}$ (Pa s)	a_{TS} (-)	\bar{a}_T (-)	A (-)
Exp. 23	52.53 (51.47)	3,494.6 (3,482.0)	72,273.48 (72,657.1)	20.68 (20.87)	16.40 (16.40)	-0.91280 (-0.76304)
Exp. 29	43.43 (42.20)	3,637.9 (3,626.0)	73,425.8 (74,171.0)	20.18 (20.46)	16.40 (16.40)	-0.87342 (-0.62896)
	$\bar{\dot{\epsilon}}_1$ (s ⁻¹)	$\bar{\dot{\epsilon}}_2$ (s ⁻¹)	$\bar{\dot{\epsilon}}_3$ (s ⁻¹)	\bar{I}_D (s ⁻¹)	\bar{II}_D (s ⁻²)	\bar{III}_D (s ⁻³)
Exp. 23	0.82771 (0.82768)	-2.39027 (-2.45498)	1.56257 (1.62730)	4.78055 (4.90996)	4.20479 (4.32668)	-3.09145 (-3.30656)
Exp. 29	0.72051 (0.72046)	-2.13999 (-2.24335)	1.41949 (1.52289)	4.27999 (4.48671)	3.77191 (3.96759)	-2.18868 (-2.46137)

The calculated results for the fixed bubble shape pJ and internal bubble pressure Δp are provided in the parentheses and without parentheses, respectively.

from 0 up to 30, reveals that ψ increase leads to more neck-in like behavior of the bubble and reduction of take-up force (see Figs. 13 and 14, $\Delta p = \text{const.}$), as well as to reduction of the internal bubble pressure if the bubble shape is fixed (see Fig. 15, $pJ = \text{const.}$). The obtained results clearly show that the role of the biaxial extensional viscosity in the film blowing process is significant. This suggests that the film blowing model predictions might be rather erroneous for the cases when the equibiaxial extensional viscosity is not correctly taken into account by the utilized constitutive equation.

CONCLUSIONS

In this work film blowing process has been model by using variational principles considering minimum energy approach, nonisothermal processing conditions and novel generalized Newtonian model taking steady shear and extensional viscosity of the polymer melts properly into account. The obtained theoretical predictions have been compared with the corresponding experimental data (internal bubble pressure, take-up force, bubble shape, velocity, and temperature profiles) as well as with theoretical predictions of two different Pearson and Petrie based models. It has been

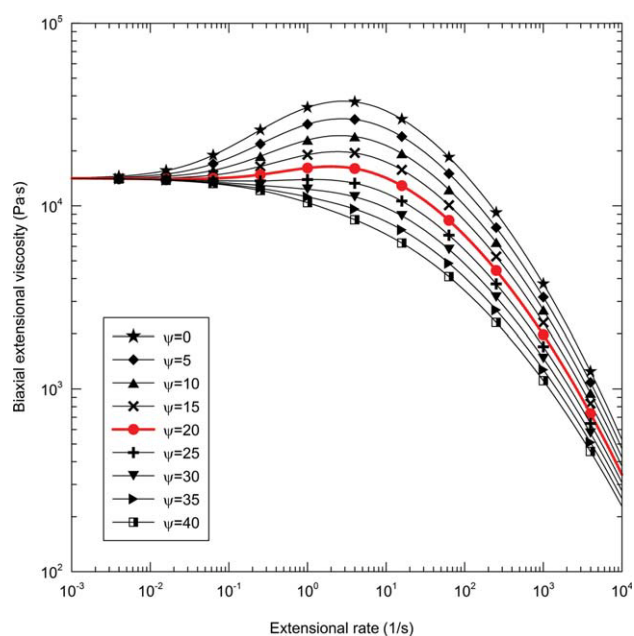


Figure 12 The effect of ψ parameter in the utilized generalized Newtonian model³⁹ on the biaxial extensional viscosity for LDPE L8. [Color figure can be viewed in the online issue, which is available at wileyonlinelibrary.com.]

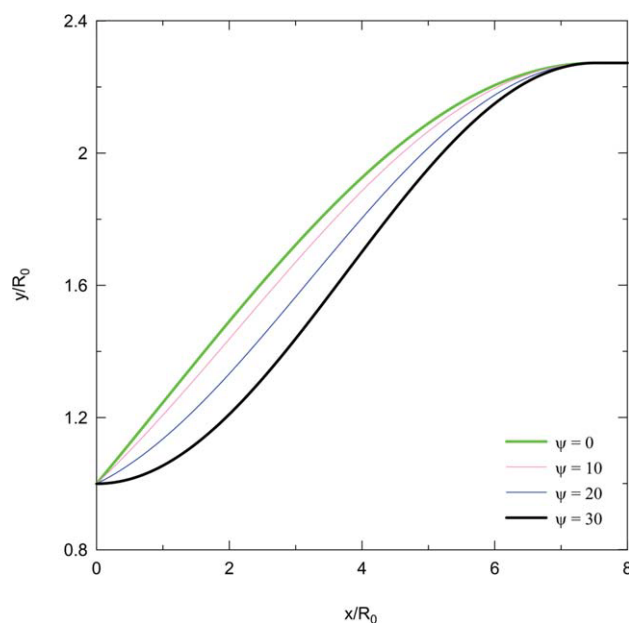


Figure 13 The effect of ψ parameter in the utilized generalized Newtonian model³⁹ on the bubble shape for experiment No. 23 in Tas's Ph.D. thesis¹⁸ for the fixed Δp . [Color figure can be viewed in the online issue, which is available at wileyonlinelibrary.com.]

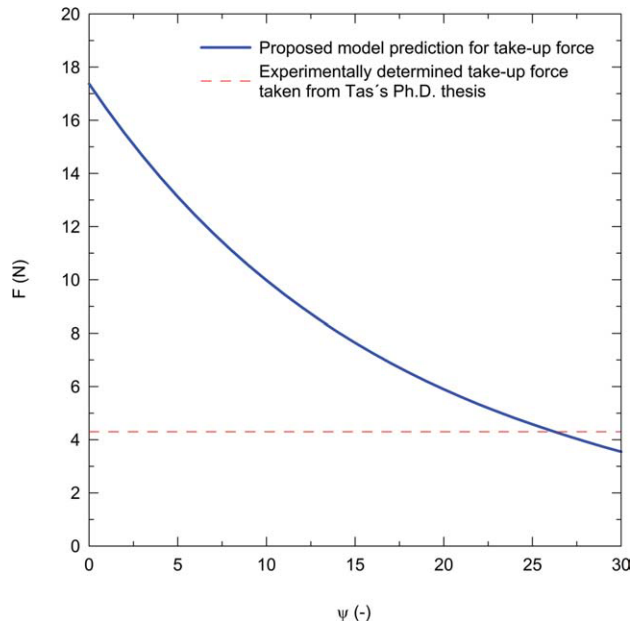


Figure 14 The effect of ψ parameter in the utilized generalized Newtonian model³⁹ on the predicted take-up force for experiment No. 23 in Tas's Ph.D. thesis¹⁸ for the fixed Δp . [Color figure can be viewed in the online issue, which is available at wileyonlinelibrary.com.]

revealed that both numerical approaches leads to very similar predictions for all investigated variables and the model predictions are in good agreement with corresponding experimental data. The theoretical analysis has revealed that the role of biaxial extensional viscosity on the film blowing process is significant which suggests that film

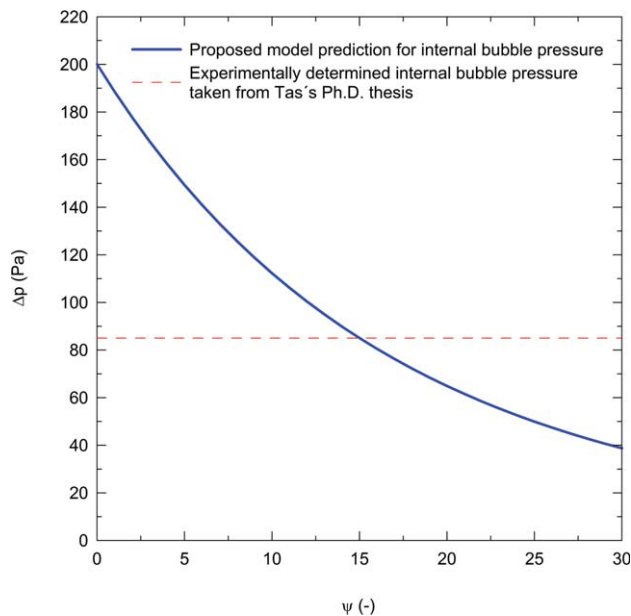


Figure 15 The effect of ψ parameter in the utilized generalized Newtonian model³⁹ on the predicted internal bubble pressure for experiment No. 23 in Tas's Ph.D. thesis¹⁸ for the fixed bubble shape. [Color figure can be viewed in the online issue, which is available at wileyonlinelibrary.com.]

blowing model predictions might be rather erroneous for the cases when the equibiaxial extensional viscosity is not correctly taken into account by the utilized constitutive equation.

NOMENCLATURE

A	Zatloukal-Vlcek model function (1)
a	Generalized Newtonian model parameter (1)
a_T	Arrhenius temperature shift factor (1)
$a_{T,\text{Bubble}}$	Bubble temperature shift factor (1)
a_{TS}	Mean value of the Arrhenius temperature shift factor a_T (1)
\bar{a}_T	Average temperature shift factor (1)
BUR	Blow-up ratio (1)
C_p	Specific heat capacity ($\text{J kg}^{-1} \text{K}^{-1}$)
D	Deformation rate tensor (s^{-1})
dx	Element length in x direction (m)
E_a	Activation energy (J mol^{-1})
F, F_{total}, F_N	Take-up force (N)
$F_{\text{thickness}}$	Force acting in the thickness direction of the bubble (N)
G_i	Relaxation modulus in the " i " th relaxation mechanism (Pa)
HTC	Heat transfer coefficient ($\text{W m}^{-2} \text{K}^{-1}$)
H_0	Bubble thickness at the die exit (m)
H_1	Bubble thickness at the freezeline height (m)
$h(x), h$	Local film thickness (m)
\bar{h}	Mean value of bubble thickness along the bubble (m)
$I_{ D }$	First invariant of the absolute value of deformation rate tensor (s^{-1})
$\bar{I}_{ D }$	Mean value of the first invariant of deformation rate tensor (s^{-1})
II_D	Second invariant of deformation rate tensor (s^{-2})
\bar{II}_D	Mean value of the second invariant of deformation rate tensor (s^{-2})
III_D	Third invariants of deformation rate tensor (s^{-3})
\bar{III}_D	Mean value of the third invariant of deformation rate tensor (s^{-3})
I	Potential energy functional (N)
J	Bubble compliance (Pa^{-1})
L	Freezeline height (m)
M_n	Number average molecular weight (g.mol^{-1})
M_w	Weight average molecular weight (g.mol^{-1})
M_z	Z average molecular weight (g mol^{-1})
\dot{m}	Mass flow rate (kg.s^{-1})
n	Power-law index (1)
p	Internal load (Pa m)
Q	Volumetric flow rate ($\text{m}^3 \text{s}^{-1}$)
R	Universal gas constant ($\text{J K}^{-1} \text{mol}^{-1}$)

R_0	Die radius (m)	ξ	Phan-Thien-Tanner model parameter (1)
R_2	Bubble radius at the freezeline height (m)	π	Ludolf's number (1)
T	Local bubble temperature ($^{\circ}\text{C}$)	ρ	Polymer density (kg m^{-3})
T_{air}	Air temperature ($^{\circ}\text{C}$)	σ_B	Stefan-Boltzmann constant ($\text{W m}^{-2} \text{K}^{-4}$)
T_c	Crystallization temperature ($^{\circ}\text{C}$)	σ_{11}	Total stress tensor in machine direction (Pa)
T_{die}	Die exit melt temperature ($^{\circ}\text{C}$)	σ_{33}	Total stress tensor in circumferential direction (Pa)
T_r	Reference temperature ($^{\circ}\text{C}$)	τ	Extra stress tensor (Pa)
T_s	Average bubble temperature ($^{\circ}\text{C}$)	τ_{11}	Extra stress in the machine directions (Pa)
T_{solid}	Solidification (freezeline) temperature ($^{\circ}\text{C}$)	τ_{22}	Extra stress in the thickness directions (Pa)
TUR	Take-up ratio 1	ϕ	Average absolute degree of crystallinity (1)
V	Bubble volume (m^3)	φ	Zatloukal-Vlcek model function (1)
$v(x), v$	Local film velocity (m s^{-1})	ψ	Generalized Newtonian model parameter (1)
v_d	Bubble velocity at the die exit (m s^{-1})	∇v	Velocity gradient tensor (s^{-1})
v_f	Bubble velocity at the freezeline (m s^{-1})		
\bar{v}	Mean value of bubble velocity along the bubble (m.s^{-1})		
x	Particular distance from the die exit (m)		
$y(x), y$	Local bubble radius (m)		

Greek symbols

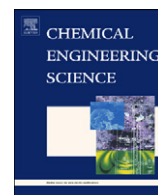
α	Generalized Newtonian model parameter (s)
α'	Zatloukal-Vlcek model function (1)
β	Generalized Newtonian model parameter (1)
ΔH_f	Heat of crystallization per unit mass (J kg^{-1})
Δp	Internal bubble pressure (Pa)
ε	Phan-Thien-Tanner model parameter (1)
$\dot{\varepsilon}_1$	Extensional rate in machine direction (s^{-1})
$\dot{\varepsilon}_2$	Extensional rate in thickness direction (s^{-1})
$\dot{\varepsilon}_3$	Extensional rate in circumferential direction (s^{-1})
$\bar{\varepsilon}$	Emissivity (1)
$\bar{\varepsilon}_1$	Mean value of extensional rate in machine direction (s^{-1})
$\bar{\varepsilon}_2$	Mean value of extensional rate in thickness direction (s^{-1})
$\bar{\varepsilon}_3$	Mean value of extensional rate in circumferential direction (s^{-1})
ζ	Generalized Newtonian model parameter (1)
η	Viscosity (Pa s)
η_0	Newtonian viscosity (Pa s)
$\bar{\eta}$	Average bubble viscosity (Pa s)
λ	Relaxation time (s)
λ_1	Lagrange multiplier (Pa)
λ_i	Relaxation time in the "i" th relaxation mechanism (s)

References

- Kim, S.; Fang, Y. L.; Lafleur, P. G.; Carreau, P. J. *Polym Eng Sci* 2004, 44, 283.
- Mayavaram, R. S. Modeling and simulation of film blowing process," Ph.D. Thesis, A&M University, Texas 2005.
- Cantor, K. *Blown Film Extrusion*; Carl Hanser Verlag: Munich, 2006.
- Han, C. D.; Park, J. Y. *J Appl Polym Sci* 1975, 19, 3277.
- Han, C. D.; Park, J. Y. *J Appl Polym Sci* 1975, 19, 3291.
- Yeow, Y. L. *J Fluid Mech* 1976, 75, 577.
- Han, C. D.; Shetty, R. *Ind Eng Chem Fund* 1977, 16, 49.
- Muke, S.; Connell, H.; Sbarski, I.; Bhattacharya, S. N. *J Non-Newtonian Fluid Mech* 2003, 116, 113.
- Minoshima, W.; White, J. L. *J Non-Newtonian Fluid Mech* 1986, 19, 275.
- Kanai, T.; White, J. L. *Polym Eng Sci* 1984, 24, 1185.
- T. J, Obijeski; Pruitt, K. R. *SPE ANTEC Tech Papers* 1992, 1, 150.
- Sweeney, P. A.; Campbell, G. A. *SPE ANTEC Tech Papers* 1993, 39, 461.
- Kanai, T.; Campbell, G. A. *Film Processing: Progress in Polymer Processing*; Hanser Gardner Publications: Munich, 1999.
- Butler, T. I. *SPE ANTEC Tech Papers* 2000, 1, 1120.
- Beaulne, M.; Mitsoulis, E. *J Appl Polym Sci* 2007, 105, 2098.
- Sarafrazi, S.; Sharif, F.; *Int Polym Process* 2008, 23, 30.
- Muslet, I. A.; Kamal, M. R. *J Rheol* 2004, 48, 525.
- Tas, P. P. *Film blowing from polymer to product*, Ph.D. Thesis, Technische Universiteit Eindhoven, 1994.
- Gupta, R. K. A new non-isothermal rheological constitutive equation and its application to industrial film blowing, Ph.D. Thesis, University of Delaware, 1981.
- Pearson, J. R. A.; Petrie, C. J. S. *J Fluid Mech* 1970, 40, 1.
- Pearson, J. R. A.; Petrie, C. J. S. *J Fluid Mech* 1970, 42, 609.
- Pearson, J. R. A.; Petrie, C. J. S. *Plast Polym* 1970, 38, 85.
- Petrie, C. J. S., "Film blowing, blow moulding and thermoforming," in *Computational Analysis of Polymer Processing*, edited by J. R. A. Pearson and S. M. Richardson; Applied Science: London, 1983, pp. 217-241.
- Han, C. D.; Park, J. Y. *J Appl Polym Sci* 1975, 19, 3257.

25. Petrie, C. J. *S. Am Inst Chem Eng J* 1975, 21, 275.
26. Luo, X. L.; Tanner, R. I. *Polym Eng Sci* 1985, 25, 620.
27. Ashok, B. K.; Campbell, G. A. *Int Polym Proc* 1992, 7, 240.
28. Alaie, S. M.; Papanastasiou, T. C. *Int Polym Proc* 1993, 8, 51.
29. André, J. M.; Demay, Y.; Haudin, J. M.; Monasse, B.; Agassant, J. F. *Int J Form Proc* 1998, 1, 187.
30. Zatloukal, M. *J Non-Newtonian Fluid Mech* 2003, 113, 209.
31. Zatloukal, M.; Vlcek, J. *J Non-Newtonian Fluid Mech* 2004, 123, 201.
32. Zatloukal, M.; Vlcek, J.; Saha, P. *Annual Technical Conference - ANTEC, Conference Proceedings* 2004, 1, 235.
33. Zatloukal, M.; Vlcek, J. *Annual Technical Conference - ANTEC, Conference Proceedings* 2005, 1, 139.
34. Zatloukal, M.; Vlcek, J. *J Non-Newtonian Fluid Mech* 2006, 133, 63.
35. Zatloukal, M.; Mavridis, H.; Vlcek, J.; Saha, P. *Annual Technical Conference - ANTEC, Conference Proceedings* 2006, 2, 825.
36. Zatloukal, M.; Mavridis, H.; Vlcek, J.; Saha, P. *Annual Technical Conference - ANTEC, Conference Proceedings* 2007, 3, 1571 2007, 3, 1579.
37. Liu, C. C.; Bogue, D. C.; Spruiell, J. E. *Int Polym Proc* 1995, 10, 226.
38. Liu, C. C.; Bogue, D. C.; Spruiell, J. E. *Int Polym Proc* 1995, 10, 230.
39. Zatloukal, M. *J Non-Newtonian Fluid Mech* 2010, 165, 592.
40. Doufas, A. K.; McHugh, A. J., *J Rheol* 2001, 45, 1085.
41. Phan-Thien, N.; Tanner, R. I. *J Non-Newtonian Fluid Mech* 1977, 2, 353.
42. Macosko, C. W. *Rheology: Principles, Measurements, and Applications*; Wiley: New York, 1994.

PAPER II



Stability analysis of non-isothermal film blowing process for non-Newtonian fluids using variational principles

Roman Kolarik^{a,b}, Martin Zatloukal^{a,b,*}, Costas Tzoganakis^c

^a Centre of Polymer Systems, University Institute, Tomas Bata University in Zlin, Nad Ovcirnou 3685, 760 01 Zlin, Czech Republic

^b Polymer Centre, Faculty of Technology, Tomas Bata University in Zlin, TGM 275, 762 72 Zlin, Czech Republic

^c Institute for Polymer Research, Department of Chemical Engineering, University of Waterloo, Waterloo, Ontario, Canada N2L 3G1

ARTICLE INFO

Article history:

Received 14 July 2011

Received in revised form

11 January 2012

Accepted 17 January 2012

Available online 28 January 2012

Keywords:

Non-isothermal film blowing extrusion process

Non-Newtonian polymer fluids

Stability analysis

Variational principle

Polymer rheology

Numerical analysis

ABSTRACT

In this study, a numerical stability analysis of the film blowing process is performed. The numerical scheme used is based on a variational principle model of the film blowing operation. This model employs non-isothermal processing conditions, non-Newtonian behavior of the polymer and physically limiting criteria (maximum tensile and/or hoop stress) to investigate the complex relationship between processing conditions (internal bubble pressure, heat transfer coefficient, mass flow rate, cooling air temperature, melt/die temperature), material parameters (rupture stress, Newtonian viscosity, flow activation energy, power law index) and film blowing stability. It has been shown that the melt/die temperature has the highest impact on the film blowing stability window size as well as on the maximum and minimum achievable film thickness. In more detail, it has been found that processing parameters together with flow activation energy have much higher effect on the film blowing stability and maximum achievable film thickness than the basic rheological characteristics of the polymer melt. On the other hand, the effect of basic rheological parameters of the polymer melt become much more important than processing parameters (except of melt/die temperature) in order to reach minimum film thickness.

© 2012 Elsevier Ltd. All rights reserved.

1. Introduction

The film blowing process is one of the most commonly used industrial processes where thin biaxially oriented thermoplastic film is produced.

In this process, the polymer melt is extruded through an annular die to a rising continuous tube which is cooled by an air ring and is simultaneously axially stretched and circumferentially inflated by the take-up force, F , and the internal bubble pressure, Δp , respectively, until the freezeline height, L , is reached (see Fig. 1). Consequently, with the help of the collapsing frames and nip rolls, the solidified film bubble is changed from the bubble shape to a lay-flat tube of film. The obtained biaxially oriented polymer film has mechanical, physical, and optical properties (e.g. tensile strength, tear resistance, heat seal characteristics, transparency) that are desirable in daily used products, such as carrier bags, wrapping foils, garbage bags, medical films or as electrolytic membranes (where polyolefines, polystyrene, polyvinylchloride,

polyamide represents typical film blowing polymers) (Cantor, 2006; Butler, 2005).

The film blowing process is mostly characterized by the following three ratios. First, the blow-up ratio, BUR , is defined as a ratio of the final bubble diameter at the freezeline height to the die diameter. This ratio determines the magnitude of melt stretching in the transverse direction and normally takes values in the range from 1 to 5 (Baird and Collias, 1998; Beaulne and Mitsoulis, 2007). Second, the take-up ratio, TUR , is expressed as a ratio between the film velocity above the freezeline height (nip velocity) and melt velocity at the die exit. This ratio determines the magnitude of melt stretching in the axial machine direction which is usually kept between 5 and 40 (Baird and Collias, 1998; Beaulne and Mitsoulis, 2007). Third, the thickness reduction, TR , is the ratio of the die gap to the final film thickness and is typically in the range of 20–200 (Beaulne and Mitsoulis, 2007).

The main goal of the film blowing process is to manufacture a stable film with good physical and optical properties at a maximum production rate. Moreover, constant bubble diameter (affecting uniform lay-flat width and thickness of the film) is necessary otherwise thickness-variation instability may appear. In this case, the bubble shape is changed in the area between the die exit and freezeline height which leads to reduced product properties, line failures, and large amounts of film scrap. Such

* Corresponding author at: Polymer Centre, Faculty of Technology, Tomas Bata University in Zlin, TGM 275, 762 72 Zlin, Czech Republic. Tel.: +420 57 603 1320.
E-mail address: mzatloukal@ft.utb.cz (M. Zatloukal).

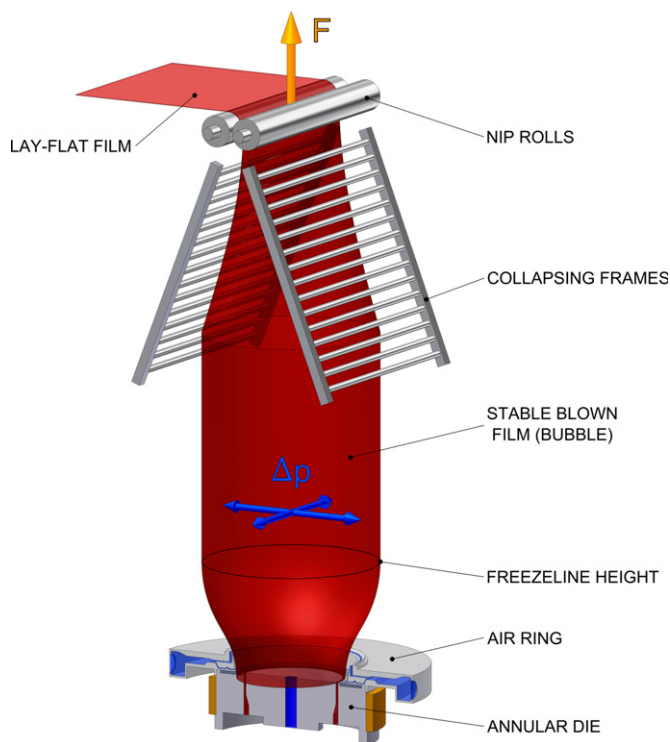


Fig. 1. Stable bubble formation during the film blowing process.

instabilities decrease significantly the window of stable processing conditions for blown film production.

The first report on film blowing instabilities was presented by Ast in 1974. Later on, Han and Park (1975) and Han and Shetty (1977) observed that lowering melt temperature leads to more stable bubble formation. The first theoretical study of bubble stability was shown in the work of Yeow (1976) for an isothermal film blowing process considering Newtonian polymer melts. Comprehensive experimental studies were presented by Kanai and White (1984), Minoshima and White (1986) and White and Yamane (1987) who revealed that film blowing stability for low-density polyethylene (LDPE) is higher than that for linear low-density polyethylene (LLDPE). In 1988, Cain and Denn extended Yeow's work to a viscoelastic upper convected Maxwell fluid. In another work, Huang (1988) used a pressure transducer to record variations of the internal bubble pressure corresponding to the bubble diameter oscillations which represent bubble instabilities. Ghijssels et al. (1990) observed that high polymer melt strength ensures good bubble stability of the film blowing process. In 1992, three types of bubble instabilities (draw resonance, freeze-line height instability and helical instability) were classified by Obijeski and Pruitt (1992) according to the variation in lay-flat width of LDPE, LLDPE and their blends. Sweeney et al. (1992) first used a noncontact real-time video analysis system to document instabilities in a film blowing process. Ghaneh-Fard et al. (1996) investigated three types of bubble instabilities for four different polymers. They found that the stability decreases in the following order LDPE > HDPE > LLDPE > PP. Butler (2000), in his work, firstly introduced six types of bubble instabilities, then examined the influence of process variables (blow-up ratio, film thickness, freeze-line height and melt temperature) on bubble stability and finally suggested various tools to limit an increase of these instabilities. In 2002, Laffargue et al. introduced an original on-line video device allowing quantitative investigation of various bubble instabilities in the film blowing process of LLDPE and

consequently it has been shown that increasing the take-up ratio, blow-up ratio and freeze-line height causes a growth of bubble instabilities. Similar to Butler (2000), seven types of bubble instabilities, their description and limitation, were presented by Waller (2002) who suggested elimination of the bubble instabilities mostly by suitable setting of the air ring, a material change or equipment modification. In 2004, Kim et al. extended the work of Laffargue et al. (2002) to investigate the dynamics and criteria of bubble instabilities. Moreover, a bubble stability map was proposed to describe the stable area of the film production for given processing parameters. In 2008, Zhang and Lafleur examined bubble instabilities induced by cooling airflow rate at different take-up and blow-up ratios. An in-line scanning camera system and manometer were used to record the bubble oscillations and the internal bubble pressure, respectively. It has been shown, that higher *TUR* provides a broader stable processing window due to greater aerodynamic forces acting on the bubble surface. Applying the linear stability analysis, Housiadas et al. (2007) have revealed that non-axisymmetric disturbances destabilize the film blowing process more than axisymmetric ones.

Typical film blowing instabilities are summarized below (Cantor, 2006; Butler, 2000; Waller, 2002):

Draw resonance, also known as “Hourglassing”, happens especially when the take-up ratio, *TUR*, is high, i.e. the melt is stretched too quickly at high strain rates. Then, due to strain hardening, the internal bubble pressure periodically decreases and increases at 2–10-s intervals, as can be seen in Fig. 2a and causes film thickness variation. In this case, the most popular stabilization method is increasing melt speed (screw and nip speed) to achieve a higher freeze-line height and lower take-up ratio. Similarly, the process can be stabilized by increasing melt temperature, narrowing die gap and using a material with higher melt index (Cantor, 2006; Obijeski and Pruitt, 1992; Butler, 2000; Laffargue et al., 2002; Waller, 2002; Kim et al., 2004).

Helical instability, known as “Snaking”, usually appears at the beginning of the process when freeze-line is too low because of unsuitable setting of the air ring. Then, the right side of the bubble is cooled more than the left side and subsequently the bubble is undulating at intervals of 5 up to 10 s, as presented in Fig. 2b. As in the previous case, to solve this problem, increasing extruder output is needed. Other remedies include reduction of melt temperature, material with lower melt index or wider die gap (Cantor, 2006; Obijeski and Pruitt, 1992; Butler, 2000; Laffargue et al., 2002; Waller, 2002; Kim et al., 2004).

Instability of the freeze-line height (FLH instability) is described by periodic oscillations at an interval from 30 s to 5 min. These oscillations are in the range of several centimeters. For that reason, at first glance the bubble seems to be stable (see Fig. 2c). However, more detailed observations reveal little thickness variation in the machine direction at the freeze-line area. This can be caused by surging as the result of extruder motor amps and back pressure. To eliminate this varying extruder output and provide better mixing, an improvement in solids feeding and melting is necessary. Thus, it is important to avoid blending polymers with very different melt flow indexes. On the contrary, appropriate air ring, haul off speed or unworn screws are necessary for good mixing (Cantor, 2006; Obijeski and Pruitt, 1992; Butler, 2000; Kim et al., 2004).

Bubble tear, also termed as “Snap off”, appears when the take-up force, drawing up the bubble, is higher than the tensile strength of the molten film. Then, the bubble is torn (which is clear in Fig. 2d) especially when it is cooled too quickly or drawn too fast. This problem can be solved by suitable adjustment of the air ring, reduction of extruder output (slower screw and nip speed), increase of the die and/or melt temperature, using a higher melt index non-strain hardening material or using narrower die gap (Cantor, 2006; Butler, 2000; Waller, 2002).

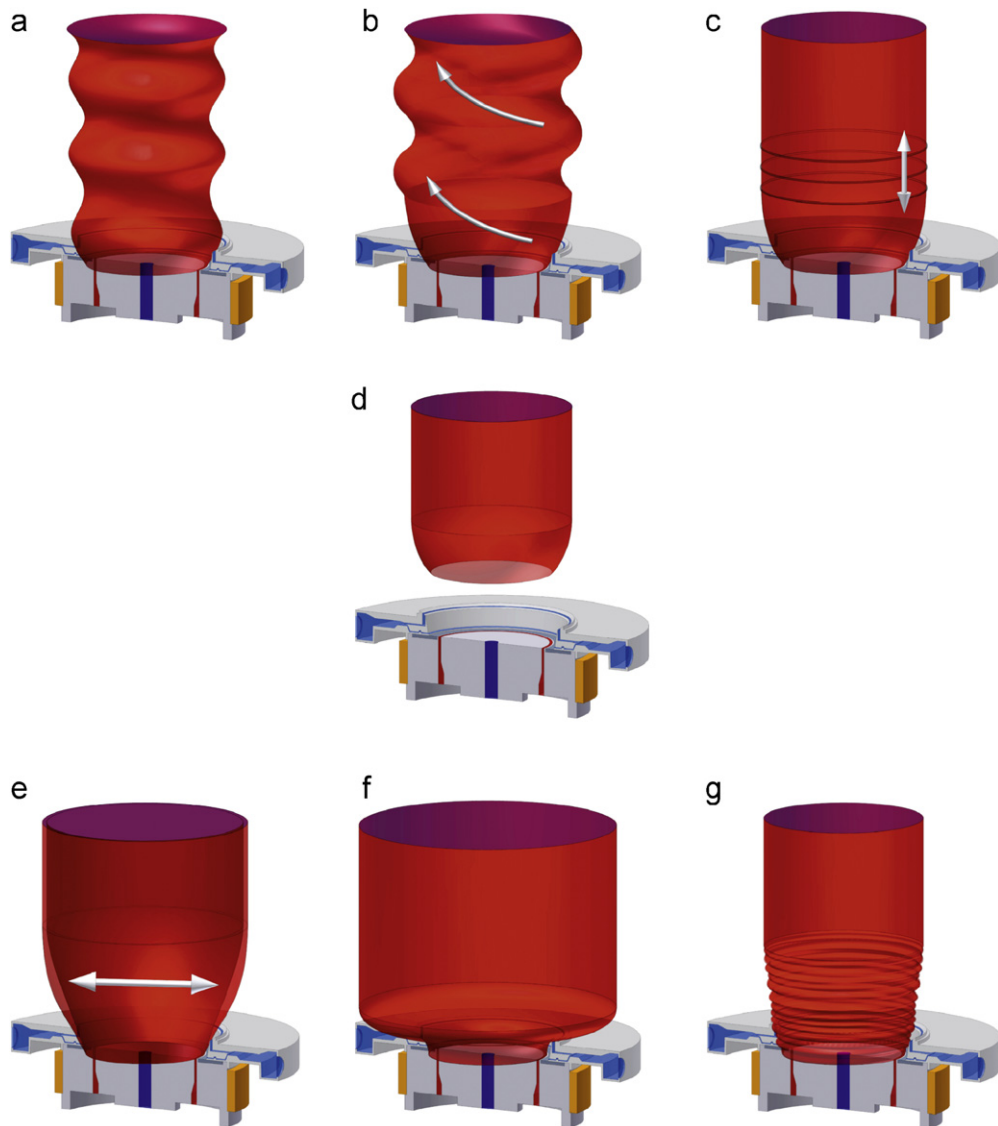


Fig. 2. Different types of bubble instabilities in film blowing process: (a) draw resonance, (b) helical instability, (c) FLH instability, (d) bubble tear, (e) bubble breathing, (f) bubble sag and (g) bubble flutter.

Bubble breathing happens if the air volume inside the bubble changes periodically. This “breathing” (see Fig. 2e) causes film thickness variation in the machine direction and fluctuations in lay-flat width. The main problem is usually in the internal bubble cooling system. Thus, cooling valves, blowers and sensors need to be controlled carefully. Other solutions consist of reducing melt temperature, using material with higher melt index or decreasing extruder output (Cantor, 2006; Butler, 2000; Waller, 2002).

Heavy-bubble instability (also known as “Bubble sag”) occurs when bubble cooling is insufficient. Then, the bubble diameter reaches its maximum at very short height, as can be seen in Fig. 2f, and consequently touches the air ring which makes flow marks or wrinkles on the film surface. These problems can be avoided by the freezeline height decrease through extruder output/melt temperature reduction. Another possibility is using material with lower melt index or narrower die gap enabling faster bubble cooling (Cantor, 2006; Butler, 2000; Waller, 2002).

Bubble flutter (Fig. 2g) appears below the freezeline when cooling air is impinging on the bubble surface at a high velocity. Then, “chatter marks” are created on the film in the transverse direction. This type of instability can be controlled using higher freezeline height (lower blower speed), lower melt temperature,

higher melt index resin or narrower die gap (Cantor, 2006; Butler, 2000; Waller, 2002).

It is evident that the stability of the film blowing process has been investigated for a long time. Although there are numerous general recommendations for film blowing instabilities reduction, the direct relationship between the processing parameters, equipment design and material characteristics, resulting in stable processing window, is not fully understood yet. For better understanding of film blowing instabilities, stability and multiplicity analyses, the Pearson–Petrie (Pearson and Petrie, 1970a, 1970b, 1970c) and Cain–Denn (Cain and Denn, 1988) formulations are usually employed. However, it has been shown (Cain and Denn, 1988) that the Pearson–Petrie model has limited capability for describing a full range of bubble shapes observed experimentally and, equally important, may lead to a variety of numerical instabilities. With the aim to overcome some of these limitations, a stable numerical scheme has been recently developed and applied for the variational principle based Zatloukal–Vlcek film blowing model (Zatloukal and Vlcek, 2004) (where the stable bubble satisfies minimum energy requirements) considering non-isothermal processing conditions and non-Newtonian polymer behavior (Kolarik and Zatloukal, 2011).

The main objective of this work is to perform a detailed theoretical analysis of the film blowing stability using the Zatloukal–Vlcek film blowing model considering physically limiting criteria (maximum tensile and/or hoop stress). Specifically, the effect of processing parameters (internal bubble pressure, heat transfer coefficient, mass flow rate, cooling air temperature, melt/die temperature) as well as material properties (rupture stress, Newtonian viscosity, flow activation energy, power law index) on the film blowing stability window size will be investigated theoretically and the obtained results will be compared with experimental data taken from the open literature.

2. Mathematical modeling

2.1. Zatloukal–Vlcek formulation

The variational principle based Zatloukal–Vlcek formulation (Zatloukal and Vlcek, 2004) describes a stable film blowing process as a state when the bubble shape satisfies minimum energy requirements. In more detail, the bubble during blowing is viewed as a bended elastic membrane due to the internal load p and the take-up force F , considering that the membrane potential energy E_p takes into account both, elastic strain energy increase and negative work done by the applied load:

$$E_p = \frac{F}{2} \int_0^L (y')^2 dx - p \int_0^L y dx \quad (1)$$

Having the bubble volume, $V = \pi \int_0^L y^2 dx$, as the main geometrical constrain, the equation for the bubble shape, y , can be derived through minimization of the potential energy functional, I , in the following form:

$$I = \left[\frac{1}{2} F (y')^2 - p y \right] + \lambda_1 (\pi y^2) \quad (2)$$

i.e., $I = f(x, y, y')$ where λ_1 is the Lagrange multiplier. The functional I is minimized if the following equation is satisfied:

$$\frac{\partial I}{\partial y} - \frac{\partial}{\partial x} \frac{\partial I}{\partial y'} = 0 \quad (3)$$

Eqs. (2) and (3) yield the following differential equation:

$$F y'' - \frac{1}{J} y + p = 0 \quad (4)$$

where J is the compliance of the membrane defined as positive constant taking the following form:

$$J = \frac{1}{2\pi\lambda_1} \quad (5)$$

The following boundary conditions for the bubble shape can be considered:

$$\frac{\partial y(x=L)}{\partial x} = 0, \quad y(x=0) = R_0 \quad (6)$$

and

$$y(x=L) = R_0 BUR \quad (7)$$

where R_0 is the extrusion die radius, L the freezeline height and $R_0 BUR$ is the bubble radius at the freezeline, i.e. $x=L$. Since above the freezing line there is no deformation, it can be assumed that $y(x>L) = \text{const.} = y(x=L)$. It is not difficult to show (see Zatloukal and Vlcek (2004) for detailed derivation) that the solution of Eq. (4), considering the above mentioned boundary conditions, takes the following form:

$$y = (R_0 - pJ) \cos\left(\frac{x\varphi}{L}\right) - \alpha'(pJ - BURR_0) \sin\left(\frac{x\varphi}{L}\right) + pJ, \quad x \in \langle 0; L \rangle \quad (8)$$

Table 1

Parameters A and φ for different bubble shapes (y) (Zatloukal and Vlcek 2004).

Equation	A	φ	y
1.	1	0	R_0
2.	$0 < A < 1$	$\arctan\left(\frac{\sqrt{1-A^2}}{A}\right)$	The form of Eq. (8)
3.	0	$\pi/2$	$R_0 \left\{ 1 - \sin\left(\frac{x\pi}{2L}\right) (1 - BUR) \right\}$
4.	$-1 < A < 0$	$\pi + \arctan\left(\frac{\sqrt{1-A^2}}{A}\right)$	The form of Eq. (8)
5.	-1	π	$\frac{R_0}{2} \left\{ 1 + \cos\left(\frac{x\pi}{L}\right) (1 - BUR) + BUR \right\}$

where the take-up force F is given by the following expression:

$$F = -\frac{L^2}{J\varphi^2} \quad (9)$$

Here α' and A are given below and the value of $\varphi(A)$ is calculated according to Table 1:

$$\alpha' = \sqrt{\frac{2pJ - R_0 - BURR_0}{pJ - BURR_0} \left| \frac{R_0(BUR - 1)}{pJ - BURR_0} \right|} \quad (10)$$

$$A = \frac{pJ - R_0}{pJ - BURR_0} \quad (11)$$

The total number of parameters needed to describe the bubble shape is equal to four (pJ , L , R_0 , BUR). Just note that pJ/R_0 (dimensionless form of pJ) determines the total deformation (curvature) of the bubble. It is important to mention that the A parameter defined by Eq. (11) determine whether the particular bubble shape satisfies the minimum energy requirement (i.e. whether the minimum potential energy functional I defined by Eq. (2) can be found) or not (i.e. if $A < -1$ as shown in Zatloukal and Vlcek (2004)). According to Zatloukal and Vlcek (2004), the internal bubble pressure and the take-up force for a 3D bubble can be directly calculated from parameters of the proposed model and the force balance by taking the 3D nature of a real bubble into account through following equations:

$$\Delta p = \frac{pL}{2\pi \int_0^L y \sqrt{1 + (y')^2} dx} \quad (12)$$

$$F_{\text{total}} = |F| \quad (13)$$

where the term $2\pi \int_0^L y \sqrt{1 + (y')^2} dx$ in Eq. (12) means the bubble surface and the term pL is the force acting in the thickness direction of the bubble, $F_{\text{thickness}}$. Eq. (12) represents the calculation of the internal bubble pressure in such a way that the bubble is represented by an equivalent cylinder, which has the same surface as the real bubble. Force F in Eq. (13) is defined by Eq. (9).

The equations describing the freezeline height, Eq. (14), and temperature profile along the bubble, Eq. (15), have been derived in Kolarik and Zatloukal (2011) from the cross-sectionally averaged energy equation (Doufas and McHugh, 2001) neglecting axial conduction, dissipation, radiation effects and crystallization.

$$L = -\frac{1}{2} \dot{m} C_p \ln\left(-\frac{(T_{\text{melt(die)}} - T_{\text{air}})}{(T_{\text{solid}} + T_{\text{air}})}\right) \times \frac{\varphi}{\pi \text{HTC} (x p J - \alpha BURR_0 - \sin(\varphi) R_0 - p J \varphi + \sin(\varphi) p J - \alpha \cos(\varphi) p J + \alpha \cos(\varphi) BURR_0)} \quad (14)$$

$$T = T_{\text{air}} + (T_{\text{melt(die)}} - T_{\text{air}}) \exp\left\{-\frac{2\pi \text{LHTC}}{\dot{m} C_p \varphi} \left(-\alpha [R_0 BUR - pJ] \left[\cos\left(\frac{x\varphi}{L}\right) - 1\right] + \sin\left(\frac{x\varphi}{L}\right) [R_0 - pJ] + pJ \varphi \frac{x}{L}\right)\right\} \quad (15)$$

The particular symbols have the following meaning: C_p represents the specific heat capacity, HTC is the heat transfer coefficient, \dot{m} is the mass flow rate, $T_{melt(die)}$ represent the die exit melt temperature, T_{solid} is the solidification temperature and T_{air} is the cooling air temperature.

It has to be mentioned that even if the assumption of constant bubble compliance J along the bubble defined by Eq. (5) has already been justified for standard range of processing conditions and polymers (Zatloukal and Vlcek, 2004; Kolarik and Zatloukal, 2011), it can also be considered that J is a general function of x , local film thickness, rheology, temperature, heat transfer, crystallization effects, surface tension, etc., however, in such a case, the potential energy functional given by Eq. (2) has to be treated numerically and the problem becomes mathematically more complicated because the analytical expressions for the bubble shape, take-up force, internal bubble pressure, freezeline height and temperature profile will not be available.

2.2. Continuity equation

$$Q = 2\pi y(x)h(x)v(x) \tag{16}$$

In this equation, Q represents the volumetric flow rate, $y(x)$, the radius of the bubble, $h(x)$, the thickness of the film and $v(x)$, the film velocity, all as functions of the distance from the die, x .

2.3. Constitutive equation

Non-Newtonian behavior of the polymer melt is taken into account through the constitutive equation derived from the generalized Newtonian model as recently proposed in (Zatloukal 2010):

$$\tau = 2\eta(I_{|D|}, II_D, III_D)D \tag{17}$$

where τ is the extra stress tensor, D represents the deformation rate tensor and η stands for the viscosity which varies with the first invariant of the absolute value of deformation rate tensor $I_{|D|} = \text{tr}(|D|)$, (where $|D|$ is defined as the square root of D^2) as well as on the second $II_D = 2\text{tr}(D^2)$, and third, $III_D = \det(D)$, invariants of D according to the following:

$$\eta(I_{|D|}, II_D, III_D) = \eta(II_D)^{f(I_{|D|}, II_D, III_D)} \tag{18}$$

where $\eta(II_D)$ is given by the well known Carreau–Yasuda model, Eq. (19) and $f(I_{|D|}, II_D, III_D)$ is given by the following equation:

$$\eta(II_D) = \frac{\eta_0 a_T}{[1 + (\lambda a_T \sqrt{II_D})^a]^{(1-n)/a}} \tag{19}$$

$$f(I_{|D|}, II_D, III_D) = \left\{ \tanh \left[\alpha a_T \left(1 + \frac{1}{4(\sqrt{3})^3} \right)^{-\psi} \left(\left| 1 + \frac{III_D}{II_D^{3/2}} \right| \right)^\zeta \right. \right. \\ \left. \left. \times \frac{\sqrt[3]{4|III_D| + I_{|D|}}}{3} + \beta \right] \frac{1}{\tanh(\beta)} \right\} \tag{20}$$

In these equations, η_0 , λ , a , n , α , β , ζ represent adjustable parameters, whereas parameter ψ is equal to 20 (as suggested in Zatloukal, 2010) and a_T is temperature shift factor defined according to the Arrhenius equation:

$$a_T = \exp \left[\frac{E_a}{R} \left(\frac{1}{273.15 + T} - \frac{1}{273.15 + T_r} \right) \right] \tag{21}$$

where E_a is the flow activation energy, R is the universal gas constant, T_r is the reference temperature and T is the local bubble temperature.

This recently proposed constitutive equation has been chosen for the film blowing modeling because it has high flexibility to represent the strain rate dependent steady shear and uniaxial

extensional viscosities for linear and branched polyolefins as well as it provides correct behavior in steady planar/equibiaxial extensional viscosity. Moreover, the model allows independent strain hardening level control for planar/equibiaxial extensional viscosity with respect to uniaxial extensional viscosity through parameter ψ (Zatloukal, 2010).

It has been shown (Kolarik and Zatloukal, 2011) that the equation for the bubble compliance J is defined in the following form:

$$J = \frac{L^2 v_f}{2\phi^2 \bar{\eta} \bar{\dot{\epsilon}}_1 Q} \tag{22}$$

where $\bar{\eta}$ and $\bar{\dot{\epsilon}}_1$ represent the mean values of the melt viscosity ($\bar{\eta} = (1/L) \int_0^L \eta dx$) and the extensional rate ($\bar{\dot{\epsilon}}_1 = (1/L) \int_0^L \dot{\epsilon} dx$), respectively, for the whole bubble and v_f is the velocity of the film at the freezeline ($v_f = Q/(2\pi R_0 BURH_1)$) defined by Eq. (16) where $x=L$.

2.4. Velocity profile

The non-linear velocity profile along the bubble is derived from the force balance in the vertical direction (gravity and upward force due to the airflow are neglected) proposed by Pearson and Petrie (1970a) in the following form:

$$\frac{2\pi y h \sigma_{11}}{\sqrt{1+(y')^2}} = F - \pi \Delta p (R_0^2 BUR^2 - y^2) \tag{23}$$

where σ_{11} is the total stress in the machine direction and F and Δp are defined by Eqs. (9), (13) and (12). The deformation rate tensor in the bubble forming region takes the following form:

$$D = \begin{pmatrix} \dot{\epsilon}_1 & 0 & 0 \\ 0 & \dot{\epsilon}_2 & 0 \\ 0 & 0 & \dot{\epsilon}_3 \end{pmatrix} = \begin{pmatrix} \frac{dv}{dx} & 0 & 0 \\ 0 & \frac{v}{h} \frac{dh}{dx} & 0 \\ 0 & 0 & \frac{v}{y} y' \end{pmatrix} \tag{24}$$

where v and h are the bubble velocity and the thickness, respectively. Assuming that $h \ll y$, then

$$\sigma_{11} = \tau_{11} - \tau_{22} \tag{25}$$

by combination of Eqs. (17), (24) and (25), σ_{11} can be written as

$$\sigma_{11} = 2\eta \left(2 \frac{dv}{dx} + \frac{v}{y} y' \right) \tag{26}$$

After substituting Eq. (26) into Eq. (23), the following equation for the bubble velocity can be obtained:

$$v = v_d \exp \left(\int_0^L \left\{ \frac{\sqrt{1+(y')^2} [F - \pi \Delta p (R_0^2 BUR^2 - y^2)]}{4Q\eta} - \frac{1}{2y} y' \right\} dx \right) \tag{27}$$

Having the velocity profile, the deformation rates and the thickness can be properly calculated along the bubble.

2.5. Stability contours determination

In this work, the stability processing window is defined as the closed area in the figure at which the relative final film thickness, H_1/H_0 , (film thickness at the freezeline height divided by the film thickness at the die) is plotted as a function of the blow-up ratio, BUR (see Fig. 3 as an example). The film blowing process is viewed here as unstable if the process does not satisfy minimum energy requirements (Zatloukal and Vlcek, 2004) ($A < -1$ where A is defined by Eq. (11)) or if the film stress in the machine or circumferential direction reach the rupture stress. A typical stability processing window for a particular internal bubble pressure range $\Delta p \in \langle \Delta p_{min}; \Delta p_{max} \rangle$ is formed by four different contours; AB , BC (where $A = -1$) and AD , DC where the film stress in machine (σ_{11}) and circumference (σ_{33}) directions, respectively, reached the

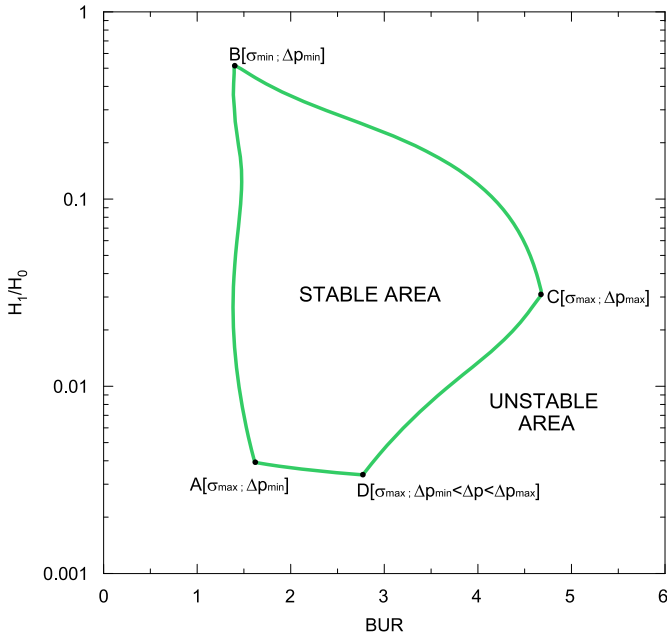


Fig. 3. Description of the stability processing window predicted by the Zatloukal-Vlcek model.

rupture stress σ_{max} (see Fig. 3). It should be mentioned that the both stresses are calculated according to the Pearson and Petrie formulation (Pearson and Petrie, 1970a) as

$$\sigma_{11}(x) = \frac{F - \pi \Delta p (r_i^2 - r(x)^2)}{2\pi r(x) h(x) \cos(\theta(x))} \quad (28)$$

$$\sigma_{33}(x) = \frac{R_t(x)}{h(x)} \left(\Delta p - \frac{h(x)}{R_m(x)} \sigma_{11}(x) \right) \quad (29)$$

where R_t and R_m are the curvature radius in the transverse and machine directions, respectively. The presented curvature radii have the form

$$R_t = \frac{r}{\cos(\theta)} \quad (30)$$

$$R_m = \frac{-1}{(d^2r/dx^2)\cos^3(\theta)} \quad (31)$$

The $\cos(\theta)$ term in Eqs. (30) and (31) is calculated as

$$\cos(\theta) = \frac{1}{\sqrt{1 + (dr/dx)^2}} \quad (32)$$

2.6. Numerical scheme

In the first step, a regular grid of H_1/H_0 versus BUR with equidistant steps in both variables is created. For a given grid node, the input parameters (see numerical scheme in Fig. 4) and guessed values for \bar{I}_{D1}, \bar{II}_D and \bar{III}_D are specified, and the average bubble viscosity $\bar{\eta}$ can be determined according to

$$\bar{\eta} = \left\{ \frac{\eta_0 \bar{a}_T}{[1 + (\lambda \bar{a}_T \sqrt{\bar{II}_D})^a]^{(1-\psi)}} \right\} \left\{ \tanh \left[\frac{z \bar{a}_T}{2} \left(1 + \frac{1}{4(\sqrt{\beta})^2} \right)^{-\psi} \left(1 + \frac{\bar{III}_D}{\bar{II}_D^{3/2}} \right)^{\psi} \frac{\sqrt{4|\bar{III}_D| + \bar{II}_D} + \beta}{\tanh(\beta)} \right] \right\}^{\zeta} \quad (33)$$

where \bar{I}_{D1} is the mean value of the first invariant of the square root of D^2 , \bar{II}_D and \bar{III}_D represent the mean value of the second and third invariants of deformation rate tensor, respectively, and \bar{a}_T is

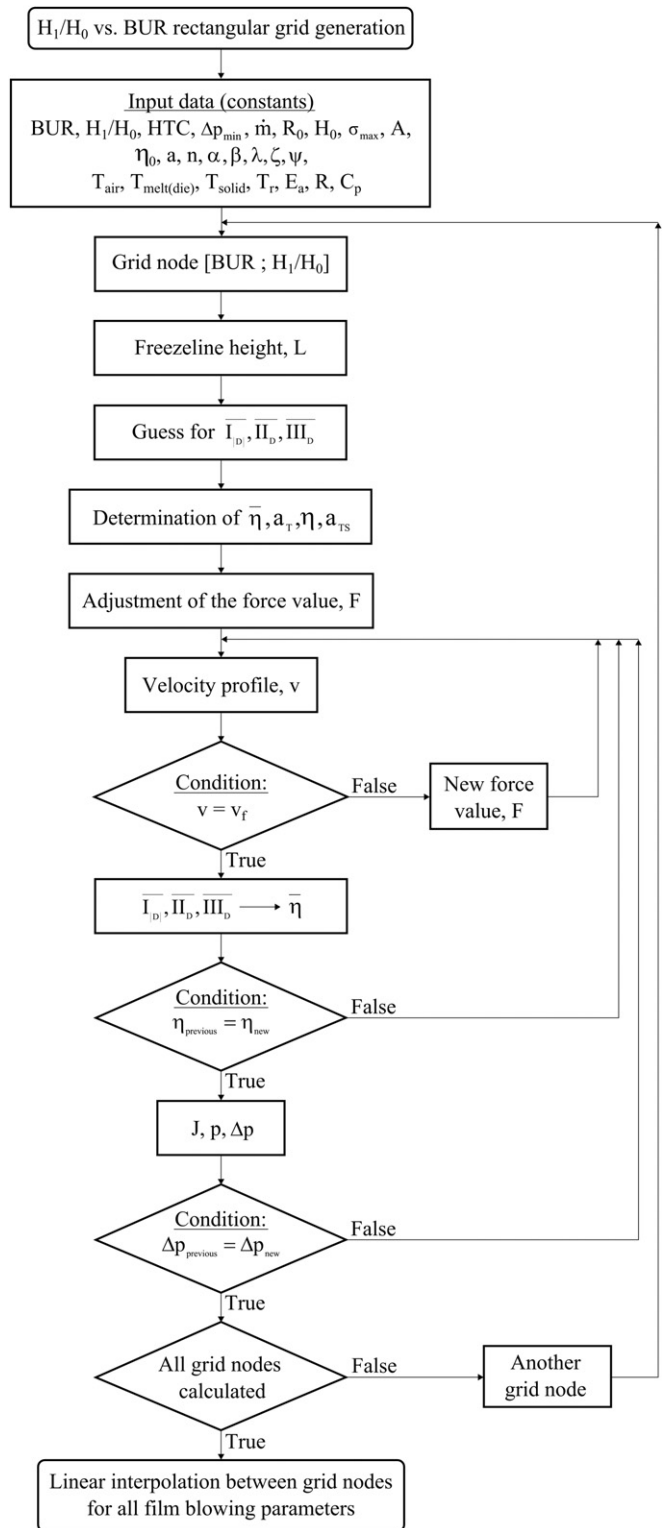


Fig. 4. Iteration scheme of the Zatloukal-Vlcek model utilized for the theoretical film blowing stability analysis.

the average temperature shift factor:

$$\bar{I}_{D1} = \sqrt{\dot{\epsilon}_1^2} + \sqrt{\dot{\epsilon}_2^2} + \sqrt{\dot{\epsilon}_3^2} \quad (34)$$

$$\bar{II}_D = 2 \left(\dot{\epsilon}_1^2 + \dot{\epsilon}_2^2 + \dot{\epsilon}_3^2 \right) \quad (35)$$

$$\overline{III_D} = \overline{\dot{\epsilon}_1 \dot{\epsilon}_2 \dot{\epsilon}_3} \quad (36)$$

$$\overline{a_T} = \exp \left[\frac{E_a}{R} \left(\frac{1}{273.15 + T_S} - \frac{1}{273.15 + T_r} \right) \right] \quad (37)$$

Here, the average bubble temperature T_S and mean values of the deformation rate components $\overline{\dot{\epsilon}_1}$, $\overline{\dot{\epsilon}_2}$, $\overline{\dot{\epsilon}_3}$ are defined as follows:

$$T_S = \frac{T_{\text{melt(die)}} + T_{\text{solid}}}{2} \quad (38)$$

$$\overline{\dot{\epsilon}_1} = \frac{1}{L} \int_0^L \dot{\epsilon}_1 dx \quad (39)$$

$$\overline{\dot{\epsilon}_2} = \frac{\overline{v} \overline{h} - H_0}{\overline{h} L} \quad (40)$$

$$\overline{\dot{\epsilon}_3} = -(\overline{\dot{\epsilon}_1} + \overline{\dot{\epsilon}_2}) \quad (41)$$

where L is the freezeline height, H_0 is the bubble thickness at the die, \overline{v} and \overline{h} are the mean values of bubble velocity and the thickness along the bubble, respectively, which are defined below

$$\overline{v} = \frac{1}{L} \int_0^L v(x) dx \quad (42)$$

$$\overline{h} = \frac{1}{L} \int_0^L h(x) dx \quad (43)$$

It is well known that during the film blowing process, the melt viscosity is changing dramatically between the extrusion die exit and freezeline height. In order to consider such strong temperature dependence of the viscosity during the film velocity calculation (using Eq. (27)) into account, the following expression for the viscosity η has been proposed and used:

$$\eta = \overline{\eta} a_{T, \text{Bubble}} \quad (44)$$

where $a_{T, \text{Bubble}}$ is the normalized bubble temperature shift factor defined as

$$a_{T, \text{Bubble}} = \frac{a_T}{a_{T_S}} \quad (45)$$

where a_{T_S} represents the mean value of the Arrhenius temperature shift factor a_T (see Eq. (21)) which is given as follows:

$$a_{T_S} = \frac{1}{L} \int_0^L a_T dx \quad (46)$$

The velocity profile is calculated by the help of Eq. (27), where the take-up force F is varied until the calculated film velocity at the freezeline height has reached the desirable value (according to defined TUR). For the obtained velocity profile, the average bubble viscosity $\overline{\eta}$ is updated (based on the new values of three deformation rate tensor invariants $\overline{I_{|D|}}$, $\overline{II_D}$ and $\overline{III_D}$) and the velocity calculation is repeated again until the average bubble viscosity $\overline{\eta}$ remains unchanged for the given take-up force F and velocity profile.

Then, the bubble compliance J is calculated according to Eq. (22). For the given pJ value (bubble curvature) the internal load, p , is determined and consequently used for the internal bubble pressure Δp (Eq. (12)) calculation. By using this new Δp value the velocity profile loop is repeated again until the Δp value remains unchanged.

The above described procedure is repeated for all H_1/H_0 versus BUR grid nodes. A continuous field of the given film blowing variables is determined using linear interpolation between grid nodes. The film blowing stability window is then generated on the H_1/H_0 versus BUR mesh for a given internal bubble pressure range by all grid nodes for which the stability limit (i.e. for $A = -1$) and/or the rupture stress in the machine/circumferential film direction is reached. Just note that if $A < -1$ the film blowing process is viewed as unstable because it does not satisfy the minimum energy requirements (Zatloukal and Vlcek, 2004).

3. Results and discussion

The film blowing model described in the previous section has been utilized in order to theoretically investigate the effect of internal bubble pressure, Δp , heat transfer coefficient, HTC , mass flow rate, \dot{m} , cooling air temperature, T_{air} , melt/die temperature, $T_{\text{melt(die)}}$, rupture stress, σ_{max} , Newtonian viscosity, η_0 , flow activation energy, E_a , and power law index, n , on the film blowing process stability. This theoretical stability analysis was examined for particular processing/material parameters summarized in Table 2, taken from Tas's Ph.D. thesis (Tas, 1994) for LDPE L8 sample, Experiment no. 23, i.e. for the material and processing conditions for which the utilized film blowing model correctly predicts basic film blowing parameters such as internal bubble pressure, take-up force, bubble shape, velocity and temperature profiles as shown in our previous work (Kolarik and Zatloukal, 2011). Figs. 5–16 and Tables 3–11 summarize the results of the numerical film blowing stability analysis. It also should be mentioned that the stability window size is characterized here as its area, which is calculated for each investigated parameter.

3.1. Effect of investigated parameters on the film blowing stability window size

It is clearly visible in Figs. 5–7, 8a,c,e, 9–11, 12a,c,e, 14, 16c, that an increase in Δp , \dot{m} , T_{air} , $T_{\text{melt(die)}}$, or decrease in HTC , σ_{max} , E_a leads to reduction of the film blowing stability window and vice versa. On the other hand, the relationship between the Newtonian viscosity, η_0 , power law index of non-Newtonian fluid behavior, n , and the film blowing stability window size has interestingly non-monotonic character i.e. there is existence of the optimal value for the η_0 and n to reach maximum stability window size (see Figs. 13, 15, 16a,e).

Table 2
Film blowing model parameters used for theoretical stability analysis on Tas's Ph.D. thesis data for LDPE L8 (Experiment no. 23) (Tas, 1994).

Input parameters for the Zatloukal-Vlcek film blowing model						
HTC ($\text{W m}^{-2} \text{K}^{-1}$)	Δp_{min} (Pa)	\dot{m} (kg s^{-1})	R_0 (m)	H_0 (m)	σ_{max} (MPa)	A (dimensionless)
52.731	85	0.00100	0.0178	0.0022	1	-1
Parameters of the generalized Newtonian constitutive equation ($\psi=20$)						
η_0 (Pa s)	λ (s)	a (dimensionless)	n (dimensionless)	α (s)	β (dimensionless)	ζ (dimensionless)
2365	0.17242	0.71597	0.37108	$1.10 \cdot 10^{-5}$	$9.21 \cdot 10^{-7}$	0.054384
Temperature parameters						
T_{air} ($^{\circ}\text{C}$)	T_{solid} ($^{\circ}\text{C}$)	$T_{\text{melt(die)}}$ ($^{\circ}\text{C}$)	T_r ($^{\circ}\text{C}$)	E_a (J mol^{-1})	R ($\text{J K}^{-1} \text{mol}^{-1}$)	C_p ($\text{J kg}^{-1} \text{K}^{-1}$)
25	92	145	190	59,000	8.314	2300

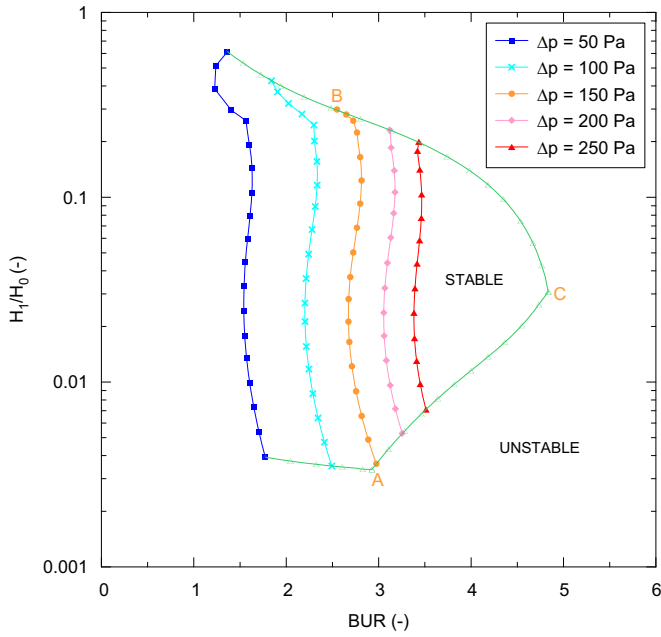


Fig. 5. Predicted film blowing stability window shape for different levels of the internal bubble pressure.

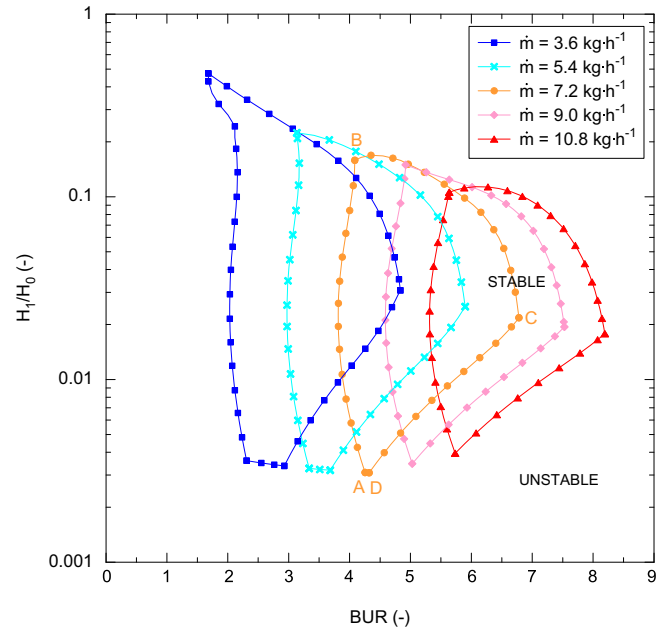


Fig. 7. Predicted film blowing stability window shape for different levels of the mass flow rate.

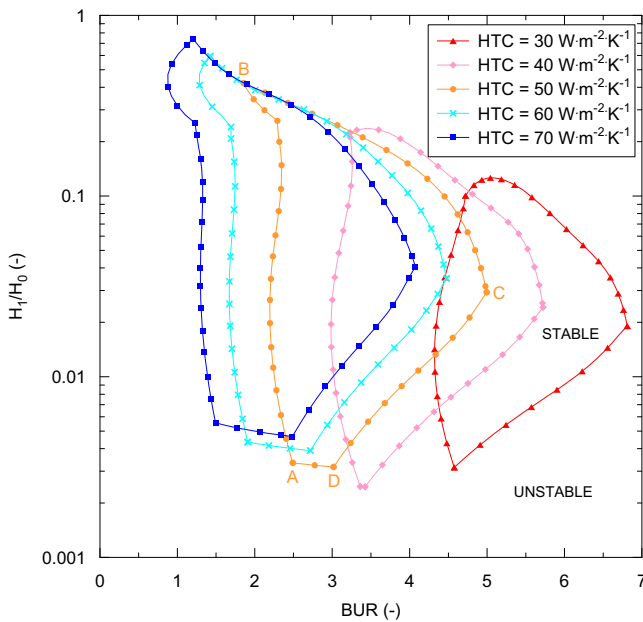


Fig. 6. Predicted film blowing stability window shape for different levels of the heat transfer coefficient.

The effect of each parameter on the film blowing stability size decreases in the following order as shown in Figs. 8, 12 and 16: $T_{\text{melt}(\text{die})}(3.102) > E_a(0.823) > HTC(0.392) > T_{\text{air}}(0.380) > \Delta p(0.295) > \dot{m}(0.168) > \sigma_{\text{max}}(0.139) > \eta_0(0.107) > n(0.097)$, where values in the brackets represent the sensitivity of the stability window size change with respect to each parameter, which is defined as $(\partial(\text{stability window size})/(\partial(\text{normalized parameter})))$.

3.2. Effect of investigated parameters on the maximum attainable film thickness

Based on Figs. 5–7, 8b,d,f, 9, 10, 12b,d, 13, 14, 16b,d, it can be concluded that increases in HTC , η_0 , E_a or decreases in Δp , \dot{m} , T_{air} , $T_{\text{melt}(\text{die})}$ allow to reach maximum attainable film thickness at low

$BURs$ and vice versa. Interestingly, the power law index, n , and rupture stress, σ_{max} , have practically no effect on the maximum attainable film thickness (see Figs. 11, 12f, 15, 16f).

The effect of each parameter on the maximum attainable film thickness according to Figs. 8, 12 and 16 decreases in the following order: $T_{\text{melt}(\text{die})}(3.175) > E_a(0.767) > HTC(0.576) > T_{\text{air}}(0.370) > \dot{m}(0.310) > \Delta p(0.122) > \eta_0(0.119) > n(0.019) > \sigma_{\text{max}}(0)$, where again values in the brackets represent the sensitivity of the maximum achievable film thickness change with respect to each parameter.

3.3. Effect of investigated parameters on the minimum attainable film thickness

The theoretically predicted data depicted in Figs. 5–7, 8b,d,f, 9–11, 12b,d,f, 13–15, 16b,d,f clearly show that, first, a decrease in n , η_0 , Δp allows to reach lower minimum attainable film thickness at high $BURs$ and vice versa (except of Δp for which minimum attainable film thickness is achievable at low $BURs$, see Fig. 8b). Second, an increase in E_a , $T_{\text{melt}(\text{die})}$, HTC , \dot{m} and T_{air} causes first decrease in the minimum achievable film thickness, which is followed by a subsequent increase in this parameter (at decreased $BURs$ for E_a , HTC and increased $BURs$ for $T_{\text{melt}(\text{die})}$, \dot{m} and T_{air}). Finally, an increase in rupture stress, σ_{max} , allows interestingly reaching of lower minimum attainable film thickness at constant BUR .

The effect of each parameter on the minimum attainable film thickness according to Figs. 8, 12 and 16 decreases in the following order: $T_{\text{melt}(\text{die})}(0.821) > n(0.620) > E_a(0.302) > \eta_0(0.183) > \sigma_{\text{max}}(0.180) > HTC(0.128) > \Delta p(0.081) > \dot{m}(0.035) > T_{\text{air}}(0.030)$, where again values in the brackets represent the sensitivity of the maximum achievable film thickness change with respect to each parameter.

It is also important to mention that at low and high $BURs$ the film rupture is caused by the machine and circumference direction stresses, respectively.

4. Summary

Based on the performed theoretical film blowing stability analysis, it has been shown that processing parameters ($T_{\text{melt}(\text{die})}$,

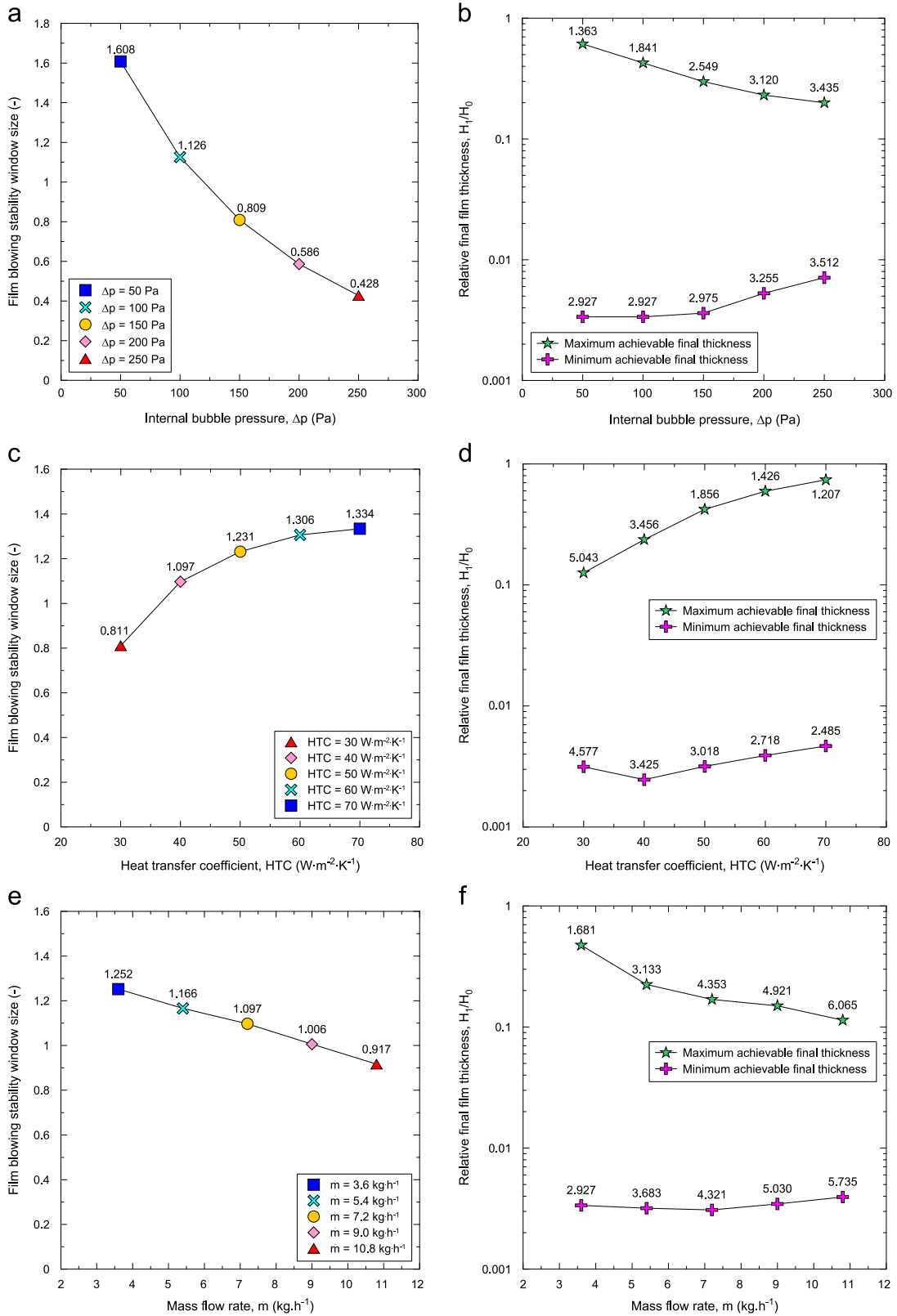


Fig. 8. The effect of internal bubble pressure, Δp , heat transfer coefficient, HTC , and mass flow rate, m on the film blowing stability window size (a), (c), (e) and maximum/minimum attainable film thickness (b), (d), (f).

HTC , T_{air} , \dot{m} , Δp) together with flow activation energy E_a have a larger effect on the film blowing stability window size and on maximum achievable film thickness than the basic rheological characteristics of the polymer melt (σ_{max} , η_0 , n). More specifically,

$T_{melt(die)}$ and E_a parameters were found to have the highest impact on the process stability and maximum achievable film thickness. This suggests that in order to reach highly stable film blowing processes or for heavy-duty bags production (thick final film

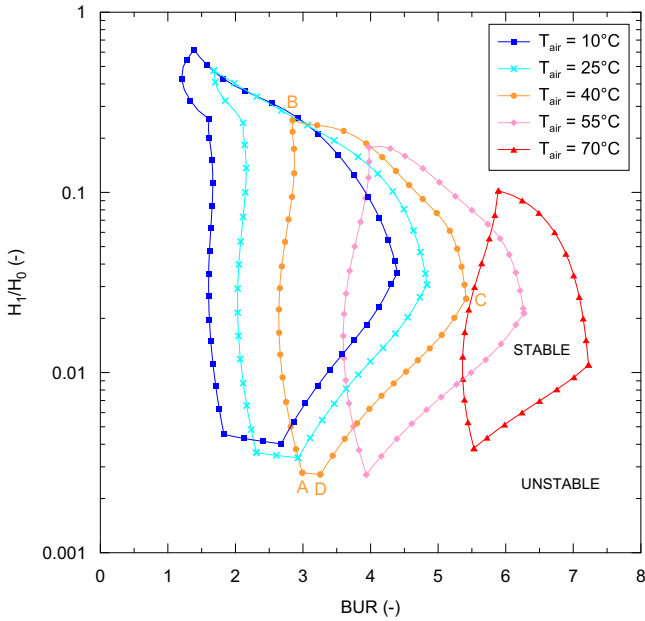


Fig. 9. Predicted film blowing stability window shape for different levels of the cooling air temperature.

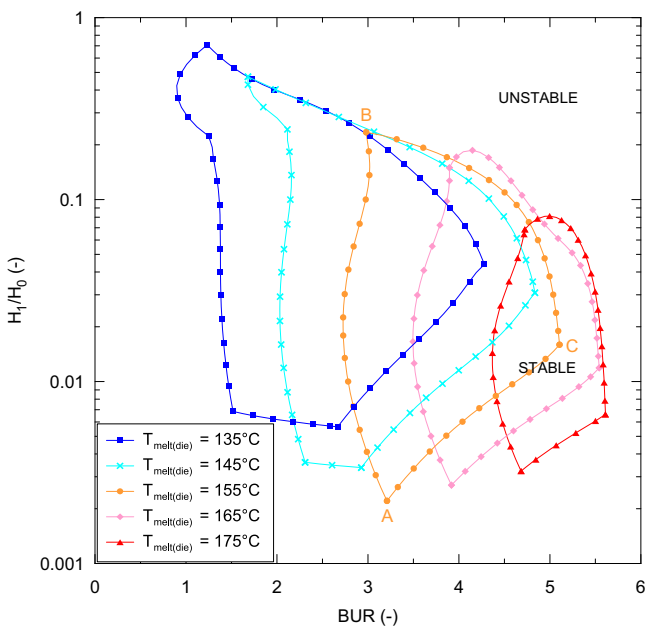


Fig. 10. Predicted film blowing stability window shape for different levels of the melt/die temperature.

thickness is required), highly effective cooling systems and polymers with as high as possible E_a should be utilized. This is in good agreement with the experimental work of Kim et al. (2004) and Kanai and White (1984) where it is reported that reduction of the freezeline height (i.e. increasing of the cooling efficiency) or utilization of polymers with higher activation energies (LDPE instead of LLDPE) stabilizes the film blowing process. On the other hand, the effect of basic rheological parameters of the polymer melt (n , E_a , η_0 , σ_{max}), becomes much more important than that of processing parameters (i.e. HTC , T_{air} , \dot{m} , Δp) in order to reach minimum film thickness. Interestingly, the theoretical film blowing stability analysis has also revealed that an increase in melt strength, σ_{max} , allows to decrease minimum achievable film thickness at constant BUR , which is not the case for the other

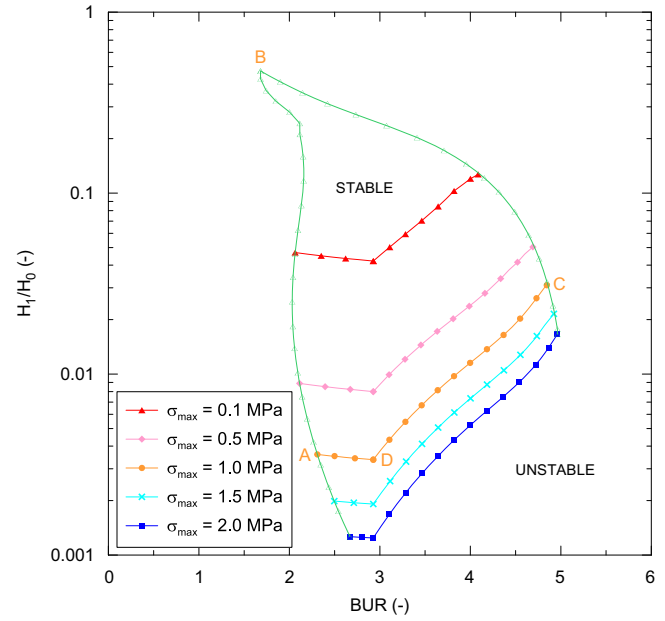


Fig. 11. Predicted film blowing stability window shape for different levels of the rupture stress.

studied rheological parameters. This suggests that specific attention has to be paid during polymer system selection with respect to its basic rheological characteristics and minimum achievable film thickness during the film blowing process.

5. Conclusion

In this work, a numerical stability analysis of the film blowing process has been performed using a variational principle based approach considering non-isothermal processing conditions, non-Newtonian behavior of the polymer and physically limiting criteria (maximum tensile and/or hoop stress). It has been shown that the melt/die temperature has the highest impact on the film blowing stability window size as well as on the maximum and minimum achievable film thickness. Also, it has been found that processing parameters together with flow activation energy have much higher effect on the film blowing stability and maximum achievable film thickness than the basic rheological characteristics of the polymer melt. On the other hand, the effect of basic rheological parameters of the polymer melt become much more important than processing parameters (except of melt/die temperature) in order to reach minimum film thickness.

Nomenclature

A	Zatloukal–Vlcek model function (1)
a	generalized Newtonian model parameter (1)
a_T	Arrhenius temperature shift factor (1)
$a_{T, \text{Bubble}}$	bubble temperature shift factor (1)
a_{TS}	mean value of the Arrhenius temperature shift factor a_T (1)
\bar{a}_T	average temperature shift factor (1)
BUR	blow-up ratio (1)
C_p	specific heat capacity ($\text{J kg}^{-1} \text{K}^{-1}$)
D	deformation rate tensor (s^{-1})
dx	element length in x direction (m)
E_a	flow activation energy (J mol^{-1})
F	take-up force (N)
HTC	heat transfer coefficient ($\text{W m}^{-2} \text{K}^{-1}$)

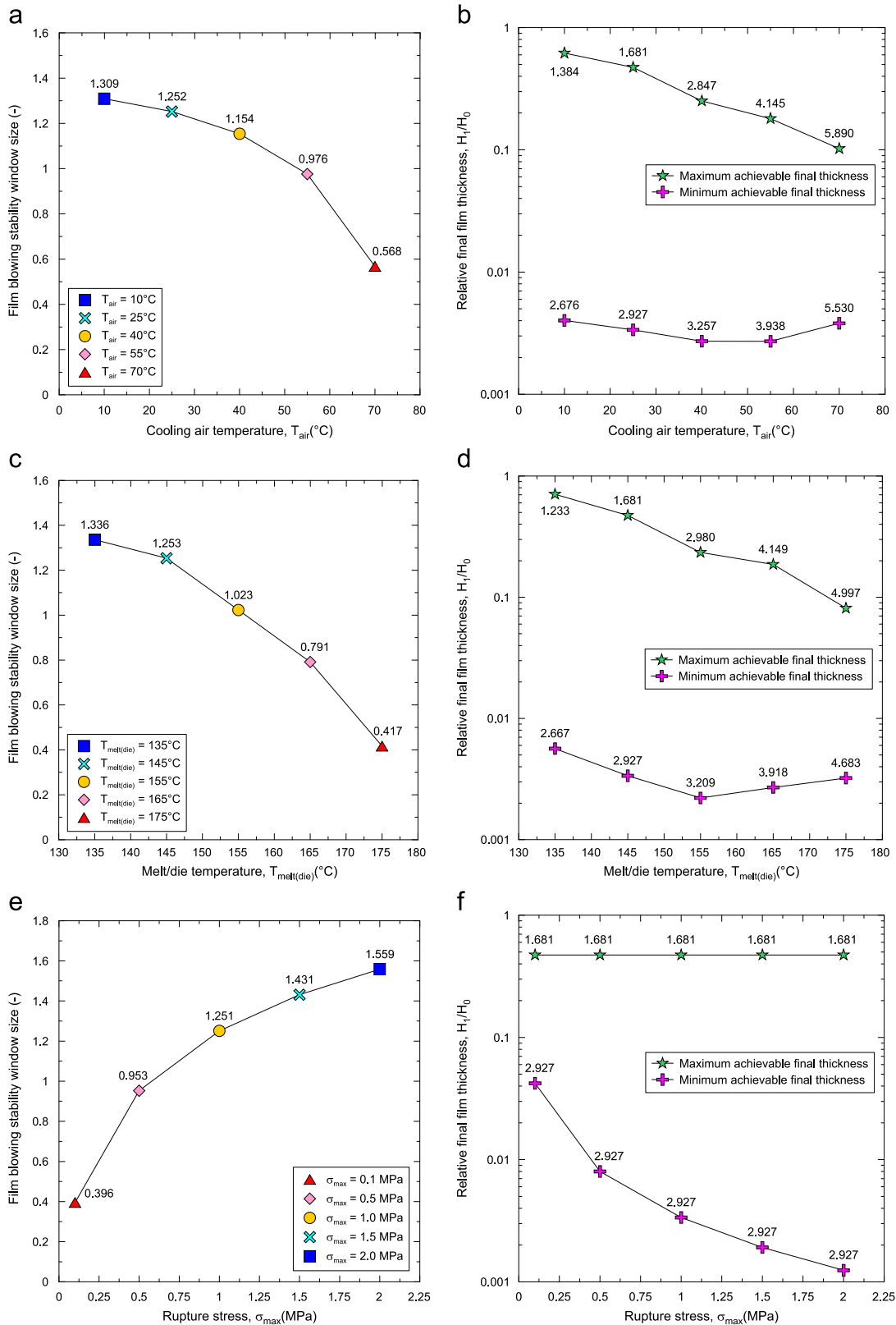


Fig. 12. The effect of cooling air temperature, T_{air} , melt/die temperature, $T_{melt(die)}$, and rupture stress, σ_{max} on the film blowing stability window size (a), (c), (e) and maximum/minimum attainable film thickness (b), (d), (f).

H_0 bubble thickness at the die exit (m)
 H_1 bubble thickness at the freezeline height (m)
 $h(x), h$ local film thickness (m)
 \bar{h} mean value of bubble thickness along the bubble (m)

$I_{|D|}$ first invariant of the absolute value of deformation rate tensor (s^{-1})
 $\bar{I}_{|D|}$ mean value of the first invariant of deformation rate tensor (s^{-1})

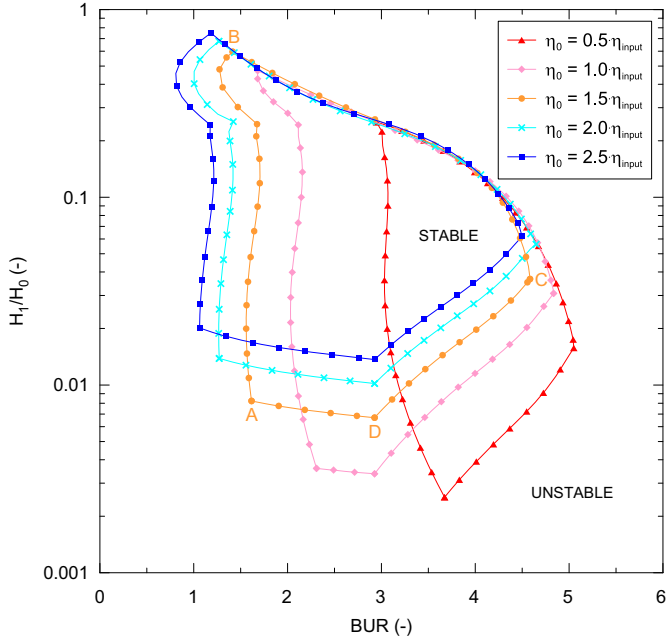


Fig. 13. Predicted film blowing stability window shape for different levels of the Newtonian viscosity.

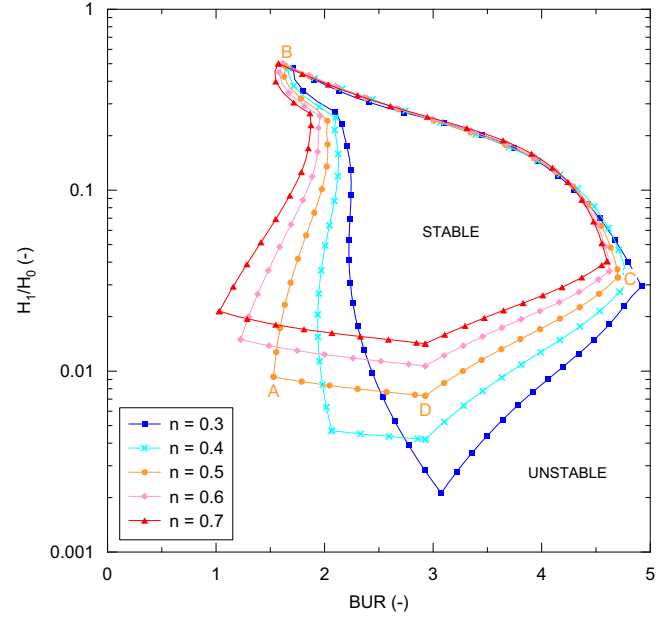


Fig. 15. Predicted film blowing stability window shape for different levels of the power law index.

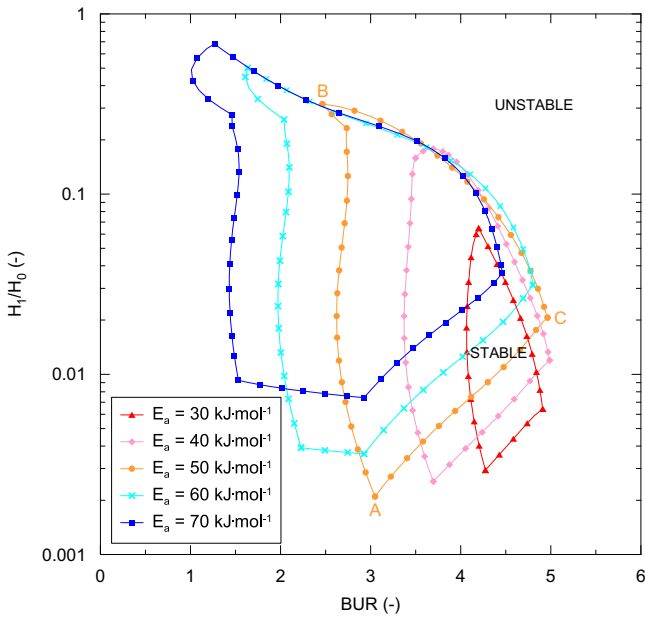


Fig. 14. Predicted film blowing stability window shape for different levels of the flow activation energy.

II_D	second invariant of deformation rate tensor (s^{-2})
\overline{II}_D	mean value of the second invariant of deformation rate tensor (s^{-2})
III_D	third invariant of deformation rate tensor (s^{-3})
\overline{III}_D	mean value of the third invariant of deformation rate tensor (s^{-3})
I	potential energy functional (N)
J	bubble compliance (Pa^{-1})
L	freezeline height (m)
\dot{m}	mass flow rate ($kg\ s^{-1}$)
n	power law index (1)
p	internal load (Pa m)
Q	volumetric flow rate ($m^3\ s^{-1}$)
R	universal gas constant ($J\ K^{-1}\ mol^{-1}$)

R_0	die radius (m)
R_m	curvature radius in the machine direction (m)
R_t	curvature radius in the transverse direction (m)
r_f	bubble radius at the freezeline height (m)
$r(x)$	local bubble radius (m)
T	local bubble temperature ($^{\circ}C$)
T_{air}	cooling air temperature ($^{\circ}C$)
$T_{melt/(die)}$	melt/die temperature ($^{\circ}C$)
T_r	reference temperature ($^{\circ}C$)
T_s	average bubble temperature ($^{\circ}C$)
T_{solid}	solidification (freezeline) temperature ($^{\circ}C$)
T_R	thickness reduction (1)
T_{UR}	take-up ratio (1)
V	bubble volume (m^3)
$v(x), v$	local film velocity ($m\ s^{-1}$)
v_d	bubble velocity at the die exit ($m\ s^{-1}$)
v_f	bubble velocity at the freezeline ($m\ s^{-1}$)
\bar{v}	mean value of bubble velocity along the bubble ($m\ s^{-1}$)
x	particular distance from the die exit (m)
$y(x), y$	local bubble radius (m)

Greek symbols

α	generalized Newtonian model parameter (s)
α'	Zatloukal-Vlcek model function (1)
β	generalized Newtonian model parameter (1)
Δp	internal bubble pressure (Pa)
Δp_{min}	minimum internal bubble pressure (Pa)
Δp_{max}	maximum internal bubble pressure (Pa)
$\dot{\epsilon}_1$	extensional rate in machine direction (s^{-1})
$\dot{\epsilon}_2$	extensional rate in thickness direction (s^{-1})
$\dot{\epsilon}_3$	extensional rate in circumferential direction (s^{-1})
$\bar{\dot{\epsilon}}_1$	mean value of extensional rate in machine direction (s^{-1})
$\bar{\dot{\epsilon}}_2$	mean value of extensional rate in thickness direction (s^{-1})
$\bar{\dot{\epsilon}}_3$	mean value of extensional rate in circumferential direction (s^{-1})
ζ	generalized Newtonian model parameter (1)
η	viscosity (Pa s)

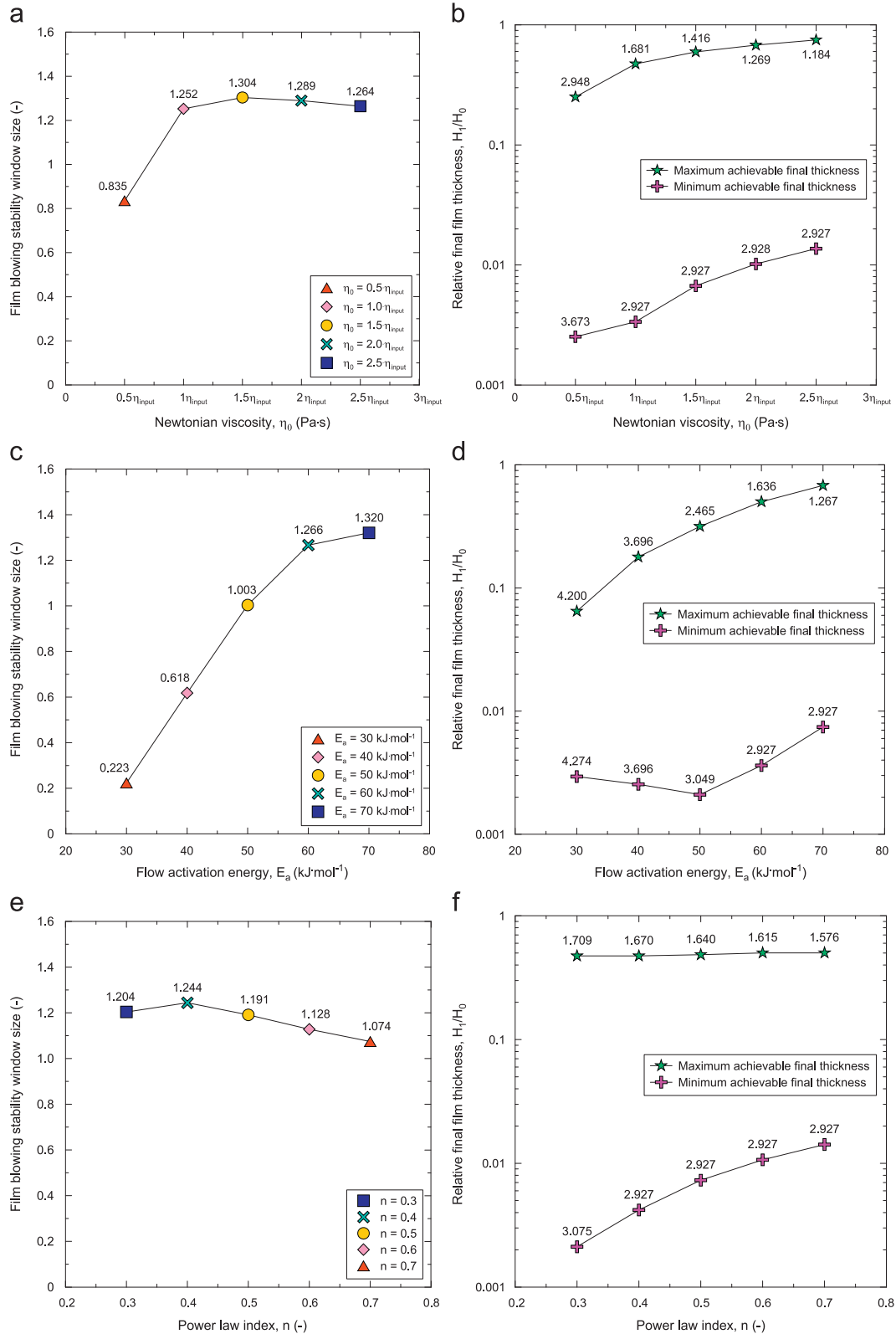


Fig. 16. The effect of Newtonian viscosity, η_0 , flow activation energy, E_a , and power law index, n , on the film blowing stability window size (a), (c), (e) and maximum/minimum attainable film thickness (b), (d), (f).

η_{input} input Newtonian viscosity (Pa s)
 η_0 Newtonian viscosity (Pa s)
 $\bar{\eta}$ average bubble viscosity (Pa s)
 θ bubble angle (deg.)
 λ relaxation time (s)

λ_1 Lagrange multiplier (Pa)
 π Ludolf's number (1)
 σ_{max} rupture stress (maximum value) (Pa)
 σ_{min} rupture stress (minimum value) (Pa)
 σ_{11} total stress tensor in machine direction (Pa)

Table 3

Summary of the calculated data in Fig. 5 for the internal bubble pressure effect analysis ($\Delta p = 150$ Pa).

Point	A	B	C
BUR (dimensionless)	2.975	2.549	4.835
H_1/H_0 (dimensionless)	0.0036	0.2985	0.0308
Δp (Pa)	150	150	785
F (N)	8.154	1.997	20.652
L (m)	0.1143	0.1281	0.0779
σ_{11} (MPa)	0.9447	0.0167	0.1660
σ_{33} (MPa)	1.0000	0.0104	1.0000
TUR (dimensionless)	93.09	1.31	6.73
TR (dimensionless)	276.78	3.35	32.51

Table 4

Summary of the calculated data in Fig. 6 for the heat transfer coefficient effect analysis ($HTC = 50$ W m⁻² K⁻¹).

Point	A	B	C	D
BUR (dimensionless)	2.490	1.856	4.995	3.018
H_1/H_0 (dimensionless)	0.0033	0.4217	0.0294	0.0032
Δp (Pa)	85	85	725	130
F (N)	6.686	1.151	20.343	7.810
L (m)	0.1374	0.1679	0.0799	0.1193
σ_{11} (MPa)	1.0000	0.0158	0.1638	1.0000
σ_{33} (MPa)	0.5137	0.0030	1.0000	1.0000
TUR (dimensionless)	120.51	1.28	6.83	104.71
TR (dimensionless)	299.96	2.37	34.06	315.97

Table 5

Summary of the calculated data in Fig. 7 for the mass flow rate effect analysis ($\dot{m} = 7.2$ kg h⁻¹).

Point	A	B	C	D
BUR (dimensionless)	4.254	4.086	6.781	4.321
H_1/H_0 (dimensionless)	0.0031	0.1585	0.0218	0.0031
Δp (Pa)	85	85	396	88
F (N)	10.296	3.263	22.381	10.446
L (m)	0.1730	0.1788	0.1168	0.1709
σ_{11} (MPa)	1.0000	0.0217	0.1898	1.0000
σ_{33} (MPa)	0.9453	0.0177	1.0000	1.0000
TUR (dimensionless)	75.96	1.54	6.79	75.02
TR (dimensionless)	322.91	6.31	45.93	323.89

Table 6

Summary of the calculated data in Fig. 9 for the cooling air temperature effect analysis ($T_{\text{air}} = 40$ °C).

Point	A	B	C	D
BUR (dimensionless)	2.990	2.847	5.414	3.257
H_1/H_0 (dimensionless)	0.0028	0.2512	0.0257	0.0027
Δp (Pa)	85	85	585	103
F (N)	6.821	1.564	19.326	7.334
L (m)	0.1374	0.1425	0.0855	0.1288
σ_{11} (MPa)	1.0000	0.0125	0.1593	1.0000
σ_{33} (MPa)	0.7407	0.0078	1.0000	1.0000
TUR (dimensionless)	120.52	1.40	7.20	112.98
TR (dimensionless)	360.09	3.98	38.98	367.63

Table 7

Summary of the calculated data in Fig. 10 for the melt/die temperature effect analysis ($T_{\text{melt(die)}} = 155$ °C).

Point	A	B	C
BUR (dimensionless)	3.209	2.980	5.106
H_1/H_0 (dimensionless)	0.0022	0.2344	0.0159
Δp (Pa)	85	85	585
F (N)	4.969	1.338	11.979
L (m)	0.1228	0.1299	0.0847
σ_{11} (MPa)	0.9374	0.0106	0.1759
σ_{33} (MPa)	1.0000	0.0088	1.0000
TUR (dimensionless)	141.27	1.43	12.31
TR (dimensionless)	452.99	4.27	62.76

Table 8

Summary of the calculated data in Fig. 11 for the rupture stress effect analysis ($\sigma_{\text{max}} = 1.0$ MPa).

Point	A	B	C	D
BUR (dimensionless)	2.309	1.681	4.835	2.927
H_1/H_0 (dimensionless)	0.0036	0.4732	0.0308	0.0034
Δp (Pa)	85	85	785	142
F (N)	6.627	1.016	20.652	7.998
L (m)	0.1374	0.1695	0.0780	0.1157
σ_{11} (MPa)	1.0000	0.0159	0.1660	1.0000
σ_{33} (MPa)	0.4417	0.0024	1.0000	1.0000
TUR (dimensionless)	120.51	1.26	6.73	101.59
TR (dimensionless)	278.10	2.11	32.51	297.31

Table 9

Summary of the calculated data in Fig. 13 for the Newtonian viscosity effect analysis ($\eta_0 = 1.5 \cdot \eta_{\text{input}}$).

Point	A	B	C	D
BUR (dimensionless)	1.616	1.416	4.582	2.927
H_1/H_0 (dimensionless)	0.0082	0.5957	0.0366	0.0067
Δp (Pa)	85	85	985	283
F (N)	9.202	0.834	24.869	14.010
L (m)	0.1738	0.1882	0.0814	0.1157
σ_{11} (MPa)	1.0000	0.0185	0.2020	1.0000
σ_{33} (MPa)	0.1353	0.0016	1.0000	1.0000
TUR (dimensionless)	75.34	1.18	5.98	51.02
TR (dimensionless)	121.64	1.68	27.34	149.33

Table 10

Summary of the calculated data in Fig. 14 for the flow activation energy effect analysis ($E_a = 50$ kJ mol⁻¹).

Point	A	B	C
BUR (dimensionless)	3.049	2.465	4.964
H_1/H_0 (dimensionless)	0.0021	0.3162	0.0206
Δp (Pa)	85	85	513
F (N)	5.511	1.202	14.780
L (m)	0.1123	0.1312	0.0762
σ_{11} (MPa)	0.8674	0.0097	0.1507
σ_{33} (MPa)	1.0000	0.0054	1.0000
TUR (dimensionless)	156.46	1.28	9.77
TR (dimensionless)	476.82	3.16	48.48

Table 11

Summary of the calculated data in Fig. 15 for the power law index effect analysis ($n = 0.5$).

Point	A	B	C	D
BUR (dimensionless)	1.529	1.640	4.704	2.927
H_1/H_0 (dimensionless)	0.0093	0.4843	0.0331	0.0073
Δp (Pa)	85	85	868	308
F (N)	9.636	1.021	22.397	15.006
L (m)	0.1797	0.1722	0.0997	0.1158
σ_{11} (MPa)	1.0000	0.0164	0.1835	1.0000
σ_{33} (MPa)	0.1133	0.0023	1.0000	1.0000
TUR (dimensionless)	70.38	1.26	6.43	46.82
TR (dimensionless)	107.57	2.06	30.24	136.94

- σ_{33} total stress tensor in circumferential direction (Pa)
 τ extra stress tensor (Pa)
 τ_{11} extra stress in the machine directions (Pa)
 τ_{22} extra stress in the thickness directions (Pa)
 φ Zatloukal–Vlcek model function (1)
 ψ generalized Newtonian model parameter (1)

Acknowledgments

The authors wish to acknowledge the Grant Agency of the Czech Republic (Grant no. P108/10/1325) for the financial support. This article was written with support of Operational Program Research and Development for Innovations co-funded by the European Regional Development Fund (ERDF) and national budget of Czech Republic, within the framework of project Centre of Polymer Systems (reg. number: CZ.1.05/2.1.00/03.0111).

References

- Ast, W., 1974. Air cooling on blown film lines. *Kunststoffe* 64, 146.
- Baird, D.G., Collias, D.L., 1998. *Polymer Processing: Principles and Design*. John Wiley & Sons, Inc., New York, ISBN: 0-471-25453-3.
- Beaulne, M., Mitsoulis, E., 2007. Effect of viscoelasticity in the film-blowing process. *J. Appl. Polym. Sci.* 105 (4), 2098–2112.
- Butler, T.L., 2000. Blown film bubble instability induced by fabrication conditions. *SPE ANTEC Tech. Pap.* 1, 1120–1129.
- Butler, T.L., 2005. *Film Extrusion Manual: Process, Materials, Properties*. Tappi Press, Atlanta, ISBN: 1-59510-075-X.
- Cain, J.J., Denn, M.M., 1988. Multiplicities and instabilities in film blowing. *Polym. Eng. Sci.* 28 (23), 1527–1541.
- Cantor, K., 2006. *Blown Film Extrusion*. Carl Hanser Verlag, Munich, ISBN: 3-446-22741-5.
- Doufas, A.K., McHugh, A.J., 2001. Simulation of film blowing including flow-induced crystallization. *J. Rheol.* 45 (5), 1085–1104.
- Ghaneh-Fard, A., Carreau, P.J., Lafleur, P.G., 1996. Study of instabilities in film blowing. *AIChE J.* 42 (5), 1388–1396.
- Ghijssels, A., Ente, J.J.S.M., Raadsen, J., 1990. Melt strength behavior of PE and its relation to bubble stability in film blowing. *Int. Polym. Proc.* 04, 284–286.
- Han, C.D., Park, J.Y., 1975. Studies on blown film extrusion. 3. Bubble instability. *J. Appl. Polym. Sci.* 19 (12), 3291–3297.
- Han, C.D., Shetty, R., 1977. Flow instability in tubular film blowing. 1. Experimental Study. *Ind. Eng. Chem. Fund.* 16 (1), 49–56.
- Housiadas, K.D., Klidis, G., Tsamopoulos, J., 2007. Two- and three-dimensional instabilities in the film blowing process. *J. Non-Newtonian Fluid* 141, 193–220.
- Huang, T.A., 1988. Instrumentation development for sensing modes of bubble motion of a blown-film process. *Adv. Polym. Technol.* 8 (1), 69–75.
- Kanai, T., White, J.L., 1984. Kinematics, dynamics and stability of the tubular film extrusion of various polyethylenes. *Polym. Eng. Sci.* 24 (15), 1185–1201.
- Kim, S., Fang, Y.L., Lafleur, P.G., Carreau, P.J., 2004. Dynamics and criteria for bubble instabilities in a single layer film blowing extrusion. *Polym. Eng. Sci.* 44 (2), 283–302.
- Kolarik, R., Zatloukal, M., 2011. Modeling of nonisothermal film blowing process for non-Newtonian fluids by using variational principles. *J. Appl. Polym. Sci.* 122, 2807–2820.
- Laffargue, J., Parent, L., Lafleur, P.G., Carreau, P.J., Demay, Y., Agassant, J.F., 2002. Investigation of bubble instabilities in film blowing process. *Int. Polym. Proc.* 17, 347–353.
- Minoshima, W., White, J.L., 1986. Instability phenomena in tubular film, and melt spinning of rheologically characterized high-density, low-density and linear low-density polyethylenes. *J. Non-Newtonian Fluid* 19 (3), 275–302.
- Objeski, T.J., Pruitt, K.R., 1992. Improving the output and bubble stability of thick gauge blown helical instability. *SPE ANTEC Tech. Pap.* 1, 150–153.
- Pearson, J.R.A., Petrie, C.J.S., 1970a. The flow of a tubular film. Part 1. Formal mathematical representation. *J. Fluid Mech.* 40 (1), 1–19.
- Pearson, J.R.A., Petrie, C.J.S., 1970b. The flow of a tubular film. Part 2. Interpretation of the model and discussion of solutions. *J. Fluid Mech.* 42 (3), 609–625.
- Pearson, J.R.A., Petrie, C.J.S., 1970c. A fluid-mechanical analysis of the film-blowing process. *Plastic Polym.* 38, 85–94.
- Sweeney, P.A., Campbell, G.A., Feeney, F.A., 1992. Real time video techniques in the analysis of blown film instability. *Int. Polym. Proc.* 03, 229–239.
- Tas, P.P., 1994. *Film Blowing from Polymer to Product*. Ph.D. Thesis. Technische Universiteit Eindhoven, ISBN:90-386-0204-9.
- Waller, P., 2002. What to do when the bubble won't behave. *Plastic Technol.*, 36–37.
- White, J.L., Yamane, H., 1987. A collaborative study of the stability of extrusion, melt spinning and tubular film extrusion of some high-, low- and linear-low density polyethylene samples. *Pure Appl. Chem* 59 (2), 193–216.
- Yeow, Y.L., 1976. Stability of tubular film flow: a model of the film-blowing process. *J. Fluid Mech.* 75 (3), 577–591.
- Zatloukal, M., 2010. A simple phenomenological non-Newtonian fluid model. *J. Non-Newtonian Fluid* 165, 592–595.
- Zatloukal, M., Vlcek, J., 2004. Modeling of the film blowing process by using variational principles. *J. Non-Newtonian Fluid* 123 (2–3), 201–213.
- Zhang, Z., Lafleur, P.G., 2008. Investigation of LDPE blown film instability induced by air cooling. *Polym. Eng. Sci.* 48 (8), 1504–1510.

PAPER III

The Effect of Polyolefin Extensional Rheology on Film Blowing Process Stability

Roman Kolarik^{1,2}, Martin Zatloukal^{1,2} * Mike Martyn³

¹*Centre of Polymer Systems, University Institute, Tomas Bata University in Zlin,
Nad Ovcirnou 3685, 760 01 Zlin, Czech Republic*

²*Polymer Centre, Faculty of Technology, Tomas Bata University in Zlin,
TGM 275, 762 72 Zlin, Czech Republic*

³*IRC in Polymer Science & Technology, School of Engineering, Design & Technology,
University of Bradford, Bradford, UK.*

*Corresponding author: mzatloukal@ft.utb.cz

ABSTRACT

The effect of polyolefin extensional rheology on the film blowing stability and minimum achievable final film thickness has been investigated experimentally as well as theoretically utilizing variational principle model for the film blowing operation. It has been revealed experimentally as well as theoretically that the relationship between film blowing stability window size (and/or minimum achievable final film thickness) and the extensional strain hardening is non-monotonic in character i.e. there is existence of the optimal values for both variables to reach maximum stability window size and/or the smallest minimum achievable final film thickness.

Keywords: Blown film stability, metallocene LLDPE, long chain branching, extensional viscosity, melt strength.

INTRODUCTION

The most common film production process is film blowing. The film blowing process is characterized by a high production of thin biaxially oriented thermoplastic polymer films applicable as high quality films (e.g. separators for Li-ion batteries, food packaging, medical films) or as daily used film products (e.g. grocery sacks, wrapping foils, garbage bags). Typical film blowing materials of such thin films are polyethylene, polypropylene, polystyrene and polyamide [1-3].

In this process, the polymer melt is extruded through an annular die to a rising continuous tube which is cooled by an air ring and is simultaneously axially stretched and circumferentially inflated by the take-up force, F , and the internal bubble pressure, Δp , respectively, until the freezeline height is reached. Once past the freezeline a stable bubble of a fixed diameter is created, as can be seen in Figure 1.

The film blowing process is mostly characterized by the following referred terminology. The freezeline height, L , defined as a ring shaped zone of frosty appearance located at the point where the resin solidifies, caused by a reduction in film temperature below the melting point of the resin [2]. Thus, the freezeline height represents transition between the liquid and solid phases where no bubble deformation above this height is assumed, as can be seen in Figure 2. The blow-up ratio, BUR , is defined as a ratio of the final bubble diameter, D_1 , at the freezeline height to the die diameter, D_0 , which usually varies from 1 to 5 and influences mainly the melt stretching in the transverse direction. The take-up ratio, TUR , is expressed as a ratio between the film velocity above the freezeline height, v_f , and melt velocity at the die exit, v_d , which is usually kept between 5 and 40 in order to control the melt stretching in the axial machine direction. The thickness reduction, TR , defined as the ratio of the die gap, H_0 , to the final film thickness, H_1 , is typically in the range of 20 to 200 [4,5].

The main goal of the film blowing process is to produce a stable film with good physical and optical properties at a maximum production rate. However, during the film blowing process, different types of bubble instabilities can take place (see Figure 3) which leads to time dependent bubble shape variation (film thickness and diameter) between the die exit and freezeline height causing creation of nonuniform film [6-9]. These instabilities leads to producing large amounts of film scrap, reduction

of film production-rate and film of inferior quality (nonuniform mechanical/optical properties). The most popular bubble stabilization methods consist in proper: set-up of screw and nip rolls speed, adjustment of air ring, height of freeze line, melt temperature, die design and material properties [1, 5, 10-11].

It is well known, that in the film blowing process the elongational flow plays a dominant role. Thus, stability of the film blowing process is also influenced by the relationship between the elongational viscosity and polymer melt strength. In more detail, the elongational viscosity is influenced by the presence of long chain branching that leads to increases in the flow activation energy, melt strength, and extensional strain hardening behavior in elongational flow which ensures good bubble stability in the film blowing process [12-16].

Long chain branching in polyethylene, as the major polymer in the film blowing process, can be introduced in many different ways, such as peroxide addition, radiation treatment, finishing/stabilization and through an appropriate choice of polymerization conditions [15]. Nowadays, the most ideal material used in film blowing processes is branched low-density polyethylene (LDPE). Its high use is associated with a high output rate, low cost, high clarity, high melt strength, flexibility, toughness and excellent bubble stability. On the other hand, LDPE films have lower tensile strength and elongational at break compared to linear low-density polyethylene (LLDPE) films. LLDPE film has outstanding film puncture resistance and greater stiffness. However, LLDPE film production is characterized by the low extruder outputs and has a tendency to be less stable in film blowing processes due to its low elongational viscosity associated with linear structure of its macromolecules. To overcome these problems, blending LDPE and LLDPE is performed in order to optimize the film blowing process, i.e. to achieve the most economic processing and desired film properties. Finally, recently developed metallocene catalyst polymerization process enables production of metallocene polyethylene (mPE) with very precise control over molecular structure, such as molecular weight distribution, comonomer content and its distribution and long-chain branches. There is therefore potential of polymerizing tailored polymers which are more suited the film blowing process as well as

optimizing the film structure in order to achieve required final film properties [13-15, 17-18].

Rheological properties of polymer melts as well as stability of the film blowing process are significantly influenced by the presence of long chain branching. Investigation of the relationship between the process stability and the elongational rheology behavior can be worthwhile. In 1977, Han and Shetty [19] experimentally studied the effect of processing variables (internal bubble pressure and take-up speed) on process stability of LDPE and HDPE films. They found that stability of the film blowing process is enhanced by an increase in elongational viscosity. In 1982, Speed [20-21] observed that increase in melt strength of LLDPE by blending of LDPE causes an improvement in bubble stability as well as lower haze. He also found that physical properties of LDPE film can be improved by blending LLDPE into LDPE. Comparison of different polyethylene molecular structures and bubble stability was summarized in the comprehensive experimental studies of Kanai and White [22], Minoshima and White [23] and White and Yamane [24]. It was shown, that the long chain branched polyethylenes (LDPEs) produce the most stable bubbles. On the other hand, the broader distribution linear polyethylenes (HDPEs) are less stable and the narrower molecular weight distribution polyethylenes (HDPEs and LLDPEs) are the most unstable during the film blowing process. Thus, the strain hardening behavior of LDPE in elongational flow plays major role in process stabilization. Fleissner [25] noted that bubble stability is related to rheological properties in elongation corroborating the previous result of Han and Shetty, i.e. process stability is enhanced by the strain hardening behavior. Ghijsels et al. [26] investigated the melt strength behavior of polyethylenes in relation to bubble stability in the film blowing process. He observed that high polymer melt strength (LDPE) ensures good bubble stability in contrast to LLDPEs and low molecular weight HDPEs. In this work, it was also stated that the melt strength is influenced by the molecular weight and the long chain branching. Sweeney et al. [27] analyzed bubble instability by a noncontact video-camera technique and in their work verified that long chain branching enables wider stable processing window of polyethylenes when blending up 5% LDPE in LLDPE. Obijeski and Pruitt [28] also noted an improvement of the bubble stability

when LLDPE is blended with LDPE. In 1996, Sukhadia [15] stated that increasing long chain branching level leads to decreasing film impact strength as well as film tear strength in transverse direction. Moreover, it was found that due to the very high long chain branching level, there is no possibility to achieve thin films during the film blowing process. The good correlation between the increasing strain hardening characteristics and greater processing window at increased temperature was found for LLDPE-rich blends by Micic et al. [18]. It was also concluded that elongational viscosity is a major factor in terms of predicting the bubble stability as a function of temperature. Field et al. [14] introduced importance of the macromolecular structure of the parent polymers and melt morphology (miscibility) on the film blowing process stability. Further, the experimentally measured increase in melt strength of LLDPE/LDPE blends showed very strong agreement with increasing bubble stability. In 2003, Kim et al. [29] studied effect of long chain branching level and width of molecular weight distribution (MWD) on bubble instabilities. In this experiment, metallocene and Ziegler-Natta catalyzed polyethylenes were used. It was revealed that branched metallocene catalyzed polyethylenes of a certain level of long chain branching leads to better bubble stability than polyethylenes with broad MWDs, i.e. long chain branching has higher stability effect than the broadening of the MWD. In 2005, Münstedt et al. [30] performed laboratory experiments on seven samples of polyethylenes (LDPE, LLDPE, mLLDPE) with different strain hardening behavior. It was found that increase in elongational viscosity causes an increase in take-up force and decrease in film blowing instabilities intensity. It was also observed that the homogeneity of film thickness is achieved due to the presence of strain hardening in the uniaxial elongational experiments. Finally, they concluded that knowledge about correlations between the molecular structure and strain hardening can play an important role in optimizing film blowing materials. In 2009, Zullo and Iannace [31] studied the film blowing of biodegradable films based on thermoplastic starch. In more detail, the material compositions and the technological procedures for preparing such films were investigated. Then, a composition based on high-amylose starch thermoplasticized with 30% of urea/formamide was found as the most suitable material for film blowing process due to its high elongation viscosity, melt

deformability and strain hardening behavior. In 2010, Oliviero et al. [32] investigated thermoplastic blown films processed from commercial zein (a cereal protein extracted from maize). It was revealed, that only samples having a pronounced strain hardening behavior and a large content of α -helices are able to produce a stable blown film. Improvement of process stability and polypropylene film properties was investigated by Auinger and Stadlbauer [33] in 2010. In this work, three polypropylene grades blended with two different high melt strength polypropylene grades were used. Enhanced output, bubble stability and mechanical properties were observed due to the addition of high melt strength polypropylene grades increasing the strain hardening index.

It is evident that the role of the extensional viscosity, strain hardening and the melt strength on the film blowing stability has been extensively investigated for different polymer systems. However the positive role of these rheological parameters on the reduction of the film blowing instabilities and minimum achievable final film thickness is still not fully understood yet. In order to elucidate the role of these rheological parameters on the film blowing process in more detail, variational principle based film blowing model [5,34-35] and laboratory film blowing line utilizing three metallocene based LLDPEs (chemically identical with different level of long chain branching) have been used.

MATHEMATICAL MODELING

Zatloukal-Vlcek Formulation

The variational principle based Zatloukal-Vlcek formulation [34] describes a stable film blowing process as a state when the bubble shape satisfies minimum energy requirements. The bubble shape is described by a set of simple analytical equations (see Table 1) utilizing four physical parameters: freezeline height, L , bubble curvature, pJ (which is given by membrane compliance, J , and the internal load, p), the inner die radius, R_0 and the blow-up ratio, BUR . It should be mentioned that the equations describing the freezeline height (Eq. (7)) and temperature profile (Eq. (8)) have been derived in [35] from the cross-sectionally averaged energy equation [36] neglecting axial conduction, dissipation, radiation effects and crystallization. The particular symbols with respect to model equations summarized in Table 1 have the following meaning: C_p represents the specific heat capacity, HTC is the heat transfer coefficient, \dot{m} is the mass flow rate, $T_{\text{melt}(\text{die})}$ represent the die exit melt temperature, T_{solid} is the solidification temperature and T_{air} is the cooling air temperature. Parameter φ is defined according to Table 2 where a parameter A is defined by Eq. (4).

Constitutive Equation

Non-Newtonian behavior of the polymer melt is taken into account through the constitutive equation derived from the generalized Newtonian model as recently proposed in [37]:

$$\tau = 2\eta \left(I_{|D|}, II_D, III_D \right) D \quad (9)$$

where τ is the extra stress tensor, D represents the deformation rate tensor and η stands for the viscosity which varies with the first invariant of the absolute value of deformation rate tensor $I_{|D|} = \text{tr}(|D|)$, (where $|D|$ is defined as the square root of D^2) as well as on the second $II_D = 2\text{tr}(D^2)$, and third, $III_D = \text{det}(D)$, invariants of D according to Eq. (10)

$$\eta \left(I_{|D|}, II_D, III_D \right) = A_1^{1-f(I_{|D|}, II_D, III_D)} \eta \left(II_D \right)^{f(I_{|D|}, II_D, III_D)} \quad (10)$$

where $\eta(I_{|D|})$ is given by the well known Carreau-Yasuda model, Eq. (11) and $f(I_{|D|}, II_D, III_D)$ is given by Eq. (12)

$$\eta(II_D) = \frac{\eta_0 a_T}{\left[1 + (\lambda a_T \sqrt{II_D})^a\right]^{\left(\frac{1-n}{a}\right)}} \quad (11)$$

$$f(I_{|D|}, II_D, III_D) = \left\{ \tanh \left[\alpha a_T \left(1 + \frac{1}{4(\sqrt{3})^3}\right)^{-\psi} \left(1 + \frac{III_D}{II_D^{3/2}}\right)^\psi \frac{\sqrt[3]{4|III_D| + I_{|D|}}}{3} + \beta \right] \frac{1}{\tanh(\beta)} \right\}^\zeta \quad (12)$$

In these equations, η_0 , λ , a , n , α , β , ζ , A_1 represent adjustable parameters, whereas parameter ψ is equal to 20 (as suggested in [37]) and a_T is temperature shift factor defined according to the Arrhenius equation:

$$a_T = \exp \left[\frac{E_a}{R} \left(\frac{1}{273.15 + T} - \frac{1}{273.15 + T_r} \right) \right] \quad (13)$$

where E_a is the flow activation energy, R the universal gas constant, T_r the reference temperature and T is the local bubble temperature.

It has been shown [35] that the equation for the bubble compliance J is defined in the following form:

$$J = \frac{L^2 v_f}{2\phi^2 \bar{\eta} \bar{\dot{\epsilon}}_1 Q} \quad (14)$$

where $\bar{\eta}$ and $\bar{\dot{\epsilon}}_1$ represent the mean values of the melt viscosity ($\bar{\eta} = \frac{1}{L} \int_0^L \eta dx$) and the

extensional rate ($\bar{\dot{\epsilon}}_1 = \frac{1}{L} \int_0^L \dot{\epsilon} dx$), respectively, for the whole bubble and v_f is the

velocity of the film at the freezeline ($v_f = \frac{Q}{2\pi R_0 BURH_1}$) defined by Eq. (15) where $x=L$.

Continuity Equation

$$Q = 2\pi y(x)h(x)v(x) \quad (15)$$

In this equation, Q represents the volumetric flow rate, $y(x)$, the radius of the bubble, $h(x)$, the thickness of the film and $v(x)$ is the film velocity, all as functions of the distance from the die, x .

Velocity Profile

$$v = v_d \exp \left(\int_0^L \left\{ \frac{\sqrt{1+(y')^2} [F - \pi \Delta p (R_0^2 BUR^2 - y^2)]}{4Q\eta} - \frac{1}{2y} y' \right\} dx \right) \quad (16)$$

Note that the Eq. (16) for the velocity profile along the bubble rises from the Pearson and Petrie [38] force balance in the vertical direction (gravity and upward force due to the airflow are neglected) as shown in [35].

Stability Contours Determination

In this work, the stability processing window is defined as the closed area in the figure at which the relative final film thickness, H_f/H_0 , (film thickness at the freezeline height divided by the film thickness at the die) is plotted as a function of the blow-up ratio, BUR (see Figure 4 as an example). The film blowing process is viewed here as unstable if the process does not satisfy minimum energy requirements [34] ($A < -1$ where A is defined by Eq. (4)) or if the film stress in the machine (σ_{11}) or circumferential (σ_{33}) direction reach the rupture stress σ_{max} . A typical stability processing window for a particular internal bubble pressure range $\Delta p \in (0; \Delta p_{max})$ is depicted in Figure 4. It should be mentioned that the both stresses are calculated according to the Pearson and Petrie formulation [38] as

$$\sigma_{11}(x) = \frac{F - \pi \Delta p (r_f^2 - r(x)^2)}{2\pi r(x) h(x) \cos(\theta(x))} \quad (17)$$

$$\sigma_{33}(x) = \frac{R_t(x)}{h(x)} \left(\Delta p - \frac{h(x)}{R_m(x)} \sigma_{11}(x) \right) \quad (18)$$

where R_t and R_m are the curvature radius in the transverse and machine direction, respectively. The presented curvature radii have the form

$$R_t = \frac{r}{\cos(\theta)} \quad (19)$$

$$R_m = \frac{-1}{\frac{d^2 r}{dx^2} \cos^3(\theta)} \quad (20)$$

The $\cos(\theta)$ term in Eqs. (19) and (20) is calculated as:

$$\cos(\theta) = \frac{1}{\sqrt{1 + \left(\frac{dr}{dx}\right)^2}} \quad (21)$$

Numerical Scheme

In this work, a recently proposed stable numerical scheme has been used to solve all above equations for both, film blowing process modeling (see Figure 5, left branch) and stability diagram determination (see Figure 5, right branch). More detailed information is provided in [35].

Theoretical Investigation of Film Blowing Stability

The above described film blowing model has been utilized in order to theoretically investigate the effect of uniaxial extensional strain hardening and melt strength, σ_{\max} , on the film blowing process stability. This theoretical stability analysis was examined for particular processing/material parameters summarized in Table 3, taken from the work of Tas [39] for LDPE L8 sample, experiment no. 23, i.e. for the material and processing conditions for which the utilized film blowing model correctly predicts basic film blowing parameters such as internal bubble pressure, take-up force, bubble shape, velocity and temperature profiles as shown in our previous work [35]. In this work, the level of uniaxial extensional strain hardening is characterized as the maximum steady-state uniaxial extensional viscosity, $\eta_{E,\max}$, normalized by the Trouton viscosity $3\eta_0$, and its value is controlled by the ζ parameter in the utilized generalized Newtonian law (Eqs. (9)-(13)), see Figure 6. The numerical film blowing stability analysis has been performed for the range of uniaxial extensional strain

hardening, $\frac{\eta_{E,\max}}{3\eta_0} \in \langle 0; 8.365 \rangle$ i.e. $\zeta \in \langle 0; 0.8 \rangle$, and melt strength, $\sigma_{\max} \in \langle 0.02; 3 \rangle$ MPa (which are typical for polyolefins [40-42]) in the following way. Firstly, stability processing windows has been generated for the varied $\frac{\eta_{E,\max}}{3\eta_0}$, i.e. $\zeta \in \langle 0; 0.8 \rangle$, but fixed σ_{\max} value (see Figure 7 for the example) and the minimum achievable film thickness has been recorded for the each case. Secondly, the stability window sizes have been determined for each ζ value as the area of the corresponding stability processing window. Finally, the above described procedure has been repeated for all considered σ_{\max} values.

Based on the performed film blowing stability analysis summarized in Figures 6-15 and Tables 3-6, it has been revealed that there are three different flow regimes depending on σ_{\max} and $\frac{\eta_{E,\max}}{3\eta_0}$ values: the stable film blowing process does not exist because σ_{\max} is too low (**Regime I**); the film blowing stability as well as minimum achievable final film thickness (for increased value of $\frac{\eta_{E,\max}}{3\eta_0}$), can be enhanced if the σ_{\max} increases significantly (**Regime II**) or σ_{\max} is increasing, remaining constant or even weakly decreasing (**Regime III**). Both the latter flow regimes are clearly visualized in the form of iso-stability and iso-minimum final film thickness contour maps depicted in Figures 9-10 and Figures 13-14 respectively. It should be noted that in practice, the increase in σ_{\max} of the polymer melt, as a consequence of introducing short/long chain branching, leads to an increase in $\frac{\eta_{E,\max}}{3\eta_0}$ too [43-49] and thus increase in both variables has to be considered during interpretation of the stability diagrams. Theoretical predictions depicted in Figures 6-15 reveals that the most effective way to increase the film blowing stability and/or to decrease minimum achievable final film thickness is to significantly increase σ_{\max} at small increase in $\frac{\eta_{E,\max}}{3\eta_0}$. However, if the increase in $\frac{\eta_{E,\max}}{3\eta_0}$ becomes very high (at rather small increase in σ_{\max}), the film blowing stability starts to decrease (followed by minimum achievable final film

thickness increase) and the relationship between the film blowing stability (minimum achievable final film thickness) and $\frac{\eta_{E,\max}}{3\eta_0}$ (for given range of σ_{\max}) becomes non-monotonic. The exact relationship between the melt strength and $\frac{\eta_{E,\max}}{3\eta_0}$ to keep the film blowing stability (or minimum achievable film thickness) constant in Regime II can be approximated by the following equation as shown in Figures 11 and 15:

$$\sigma = A' \left(\frac{\eta_E}{3\eta_0} \right)^2 + B' \left(\frac{\eta_E}{3\eta_0} \right) + C' \quad (22)$$

where A' , B' and C' are constants which are summarized in Tables 4-6.

Interestingly, there is very narrow range of $\frac{\eta_{E,\max}}{3\eta_0}$, σ_{\max} pairs (**Regime III** in Figures 10 and 14), at which simultaneous increase in both σ_{\max} and $\frac{\eta_{E,\max}}{3\eta_0}$ increases the film blowing stability and/or decreases minimum achievable final film thickness. Moreover, there is always a minimum σ_{\max} value for the given $\frac{\eta_{E,\max}}{3\eta_0}$ at which the film blowing stability is the highest or at which the minimum achievable final film thickness is the smallest. Such values are given by the boundary line between Regime II and Regime III which is determined by the iso-stability and iso-thickness contour minima depicted in Figures 10 and 14. The boundary lines can also be approximated by the Eq. (22) as shown in Figures 11 and 15.

Thus, it can be concluded that the most interesting result from the performed theoretical film blowing stability analysis is the finding that the relationship between film blowing stability window size (and/or minimum achievable final film thickness) and the extensional strain hardening (for given range of melt strengths) has non-monotonic character i.e. there exists some optimal values for which both variables reach maximum stability window size and/or the smallest minimum achievable final film thickness. In order to check the validity of the obtained theoretical findings, an additional experimental work followed by corresponding theoretical analysis described below has been done.

EXPERIMENTAL

Materials

In this work, three metallocene based LLDPEs (with chemically identical structure) having different level of the LCB were considered for the experiments on the film blowing line. The grades are referred to as mLLDPE low (virtually linear structure), mLLDPE middle (low level of LCB) and mLLDPE high (high level of LCB). The frequency dependent linear viscoelastic properties (storage modulus G' , loss modulus G''), of these three materials were measured with use of the Advanced Rheometric Expansion System (ARES 2000) Rheometrics rheometer. The transient uniaxial extensional viscosity of each melt was measured using the ARES 2000 rheometer equipped with the SER Universal Testing Platform (SER-HV-A01 model) from Xpansion Instruments [50-52].

The comparison between frequency dependent complex viscosity for all three samples is given in Figure 16. Clearly, the increase in the LCB slightly increases the Newtonian viscosity, however, at higher shear rates the viscosity for all three materials becomes almost identical. Data in Figure 17 clearly show that there is significantly greater difference in the measured frequency dependent recoverable shear between all three materials. It shows that recoverable shear (defined here as $\frac{G'}{\eta^* \omega}$) increases with increasing level of LCB especially at low frequencies, which is in agreement with the open literature [53]. Finally, the extensional viscosity data in Figure 18 show that increase in the LCB leads to strain hardening behavior and higher melt strength. These have been determined according to Eq. (23) and summarized in Table 7 for all samples as the mean value of the extensional strain dependent melt strength determined at different extensional strain rates ($0.1s^{-1}$ - $10s^{-1}$).

$$\overline{\sigma_{\max}} = \frac{1}{\varepsilon_{\max} - \varepsilon_{\min}} \int_{\varepsilon_{\min}}^{\varepsilon_{\max}} f(\sigma_{\max, \varepsilon}) d\varepsilon \quad (23)$$

where $\overline{\sigma_{\max}}$ is mean value of the melt strength, ε_{\min} and ε_{\max} represents minimum and maximum extensional strain, respectively, $f(\sigma_{\max, \varepsilon})$ is the melt strength vs. strain function.

In the next step, the ‘steady state’ extensional viscosity data were taken from the peaks appearing on the transient viscosity curves for corresponding extensional strain rates. Further, the generalized Newtonian law defined by Eqs. (9)-(12), has been used to fit extensional strain rate dependent extensional viscosity data for all three samples and the obtained model parameters have been summarized in Table 8. As can be seen in Figure 19, the utilized generalized Newtonian law has very high capability to describe the measured steady-state shear and uniaxial extensional viscosity data.

Film Blowing Experiment

Pertinent film blowing processing parameters such as internal bubble pressure, Δp , volumetric flow rate, Q , die gap, H_0 , bubble radius at the die exit, R_0 , and freeze line height, L , were obtained from measurements on the film blowing line depicted in Figures 20a-20b. The processing equipment comprised of a Betol BC 38mm single screw extruder equipped with a Davis Standard model DSBMT barrier screw (Figures 20d-20e) and spiral mandrel die (Figure 20c) having six feeding channels. The outer die annulus was 75 mm in diameter and had a gap equal to 1.34 mm. In-house software has been developed to measure the profile of the bubble. Bubble images taken with a Pulnix PEC 2010 CCD camera are captured using a bt878 based capture card. The edges of the bubble are determined by a simple thresholding technique. As no easily locatable features exist on the film to enable scaling, the dimensions of the bubble are determined following a calibration stage that identifies the positions of four Light Emitting Diodes (LEDs). The position of the LEDs is shown in Figure 21. It should be mentioned that during all experiments, the freezeline height was kept to be constant as suggested in [16].

RESULTS AND DISCUSSION

In the first step, the effect of the extensional strain hardening on the bubble shape/curvature and the take up force has been studied experimentally as well as theoretically by utilization of three previously characterized mLLDPEs having different LCB content. In order to create comparable processing conditions for all test samples, freezeline height and final film thickness (about 30 μm) have been kept virtually constant during the experiments. Theoretical film blowing process analysis has been conducted for each sample for the experimental die design ($R_0 = 0.03616$ m, $H_0 = 0.00134$ m) and process parameters (Δp , TUR , L , \dot{m} , T_{air}) utilizing the numerical scheme depicted in Figure 5 (left branch). The experimental and model parameters/predictions are summarized in Table 8 and Table 9, respectively, and graphical comparison between actual, measured and predicted bubble shapes are provided in Figures 22-24. It is clear the model is capable of correctly predicting the bubble shape for all three studied polymer samples. Moreover, closer inspection of the Table 10 reveals that the model predicts an increase of the take-up force with the increasing level of the LCB, which is in good agreement with the open literature [30] because LCB increases the extensional strain hardening hence resistance to the extensional flow [24, 54-59]. This supports the physics behind the utilized variational principle based film blowing model. It is also interesting to mention that increase of LCB leads to both, bubble neck disappearance and decrease of the total bubble deformation/curvature (see Figures 22-24) which is quantified through the parameter pJ/R_0 in Table 10. It should be noted that if pJ/R_0 increases the total bubble deformation/curvature also increases (see Figure 5 in [34]).

In the second step, film blowing stability analysis for linear and branched mLLDPE samples has been performed experimentally as well as theoretically (utilizing the numerical scheme depicted in Figure 5, right branch) in order to determine their processing windows. The main experimental results are depicted in Figure 25 where the experimentally determined stability diagrams (relative final film thickness at the freeze line vs. BUR) for linear and branched mLLDPEs are provided. The lines superimposed on Figure 25 demark areas of stable and unstable bubble. The areas above the lines are stable, while those below the lines are regions of bubble instability.

The experimental data clearly show that the branched mLLDPEs are much more stable compared to linear melts, i.e. branched mLLDPEs can be used to produce thinner film at a higher *BUR*. More importantly, these experimental results suggest that processibility of the mLLDPEs in film blowing process can be improved by increasing the content of LCB up to an optimum level. Increasing the LCB content beyond this level narrows the processing window for stable film production.

The comparison between the measured and predicted stability contours are depicted in Figure 26. As it can be seen, there is quantitative as well as qualitative agreement between the predicted and experimentally determined film stability contours. This suggests that the predictive capabilities of the utilized model with respect to film blowing stability and minimum achievable final film thickness is very high and thus, conclusions arising from the theoretical study described above in chapter ‘Theoretical investigation of film blowing stability’ are generally applicable to explain experimentally observed non-monotonic relationship between the strain hardening (LCB) and film blowing stability/minimum achievable final film thickness. As it has been shown, the LCB increases not only melt strength but also melt extensional strain hardening which promotes easier stress rise in the film bubble during the processing. It seems that at low LCB level the melt strength increase becomes more effective than extensional viscosity increase and the bubble may become more stable. However, if the LCB is increased too much, the strain hardening can dominate over the concomitant melt strength increase to the extent that melt strength can no longer compensate the corresponding stress rise and the bubble becomes more easily unstable or bubble tear takes place.

CONCLUSIONS

It has been revealed experimentally as well as theoretically that the relationship between film blowing stability window size (and/or minimum achievable final film thickness) and extensional strain hardening is of non-monotonic character for a given range of melt strengths i.e. there exists some optimal values for both variables to reach maximum stability window size and/or the smallest minimum achievable final film thickness.

Based on the theoretical investigation, it has been revealed that the film blowing stability increases (or minimum achievable film thickness decreases) if the melt strength increases with the increased $\frac{\eta_{E,\max}}{3\eta_0}$ more than according to the follow simple

relationship: $\sigma = A' \left(\frac{\eta_E}{3\eta_0} \right)^2 + B' \left(\frac{\eta_E}{3\eta_0} \right) + C'$, where A' , B' and C' are constants. It also

has been revealed that there is always some minimum melt strength value for the given $\frac{\eta_{E,\max}}{3\eta_0}$ at which the film blowing stability is maximized or at which the achievable final film thickness is at its minimum.

It has been found that the utilized variational principle based model can describe quantitatively as well as qualitatively the experimentally determined film blowing stability contours for linear as well as branched mLLDPEs.

ACKNOWLEDGMENTS

The authors wish to acknowledge the Grant Agency of the Czech Republic (grant No. P108/10/1325) for the financial support. This article was written with support of Operational Program Research and Development for Innovations co-funded by the European Regional Development Fund (ERDF) and national budget of Czech Republic, within the framework of project Centre of Polymer Systems (reg. number: CZ.1.05/2.1.00/03.0111).

The authors would also like to thank Ing. Jan Musil for his support during rheological characterization of tested polymer samples.

REFERENCES

- [1] CANTOR, K. *Blown Film Extrusion*. Munich: Carl Hanser Verlag, 2006. ISBN 3-446-22741-5.
- [2] BUTLER, T.I. *Film Extrusion Manual: Process, Materials, Properties*. Atlanta: Tappi Press, 2005. ISBN 1-59510-075-X.
- [3] KANAI, T., CAMPBELL, G.A. *Film Processing*, Munich: Carl Hanser Verlag, 1999. ISBN 3-446-17882-1.
- [4] BAIRD, D.G., COLLIAS, D.I. *Polymer Processing: Principles and Design*. New York: John Wiley & Sons, Inc., 1998. ISBN 0-471-25453-3.
- [5] KOLARIK, R., ZATLOUKAL, M., TZOGANAKIS, C. Stability Analysis of Non-Isothermal Film Blowing Process for Non-Newtonian Fluids using Variational Principles. *Chem. Eng. Sci.* 2012, vol. 73, pp. 439-453.
- [6] GHANEH-FARD, A., CARREAU, P.J., LAFLEUR, P.G. Study of Instabilities in Film Blowing. *AIChE J.* 1996, vol. 42, no. 5, pp. 1388–1396.
- [7] HAN, C.D., PARK, J.Y. Studies on Blown Film Extrusion. III. Bubble Instability. *J. Appl. Polym. Sci.* 1975, vol. 19, no. 12, pp. 3291–3297.
- [8] KIM, S., FANG, Y.L., LAFLEUR, P.G., CARREAU, P.J. Dynamics and Criteria for Bubble Instabilities in a Single Layer Film Blowing Extrusion. *Polym. Eng. Sci.* 2004, vol. 44, no. 2, pp. 283–302.
- [9] LAFFARGUE, J., PARENT, L., LAFLEUR, P.G., CARREAU, P.J., DEMAY, Y., AGASSANT, J.F. Investigation of Bubble Instabilities in Film Blowing Process. *Int. Polym. Proc.* 2002, vol. 17, pp. 347–353.
- [10] BUTLER, T.I. Blown Film Bubble Instability Induced by Fabrication Conditions. *Annual Technical Conference - ANTEC, Conference Proceedings* 2000, vol. 1, pp. 1120–1129.
- [11] WALLER, P. What to Do When the Bubble Won't Behave. *Plastic Technol.* 2002, pp. 36–37.
- [12] MÜNSTEDT, H., KURZBECK, S., STANGE, J. Advances in Film Blowing, Thermoforming, and Foaming by Using Long-Chain Branched Polymers. *Macromolecular Symposia* 2006, vol. 245-246, pp. 181-190.

- [13] STEFFL, T. Rheological and Film Blowing Properties of Various Low Density Polyethylenes and Their Blends. *Ph.D. Thesis*. Universität Erlangen-Nürnberg, 2004.
- [14] FIELD, G.J., MICIC, P., BHATTACHARYA, S.N. Melt Strength and Film Bubble Instability of LLDPE/LDPE Blends. *Polym. Int.* 1999, vol. 48, no. 6, pp. 461-466.
- [15] SUKHADIA, A.M. Effects of Long Chain Branching on the Processing-Structure-Property Behavior of Polyethylene Blown Film Resins. *Annual Technical Conference - ANTEC, Conference Proceedings* 1996, vol. 1, pp. 1157-1163.
- [16] TIANG, J.S., DEALY, J.M. Evaluating the Processability of Film Blowing Resins. *Polym. Eng. Sci.* 2009, vol. 49, no. 11, pp. 2132-2143.
- [17] MAJUMDER, K.K. Blown Film Extrusion: Experimental, Modeling and Numerical study. *Ph.D. Thesis*. RMIT University, Melbourne, 2008.
- [18] MICIC, P., BHATTACHARYA, S.N., FIELD, G. Transient Elongational Viscosity of LLDPE/LDPE Blends and Its Relevance to Bubble Stability in the Film Blowing Process. *Polym. Eng. Sci.* 1998, vol. 38, no. 10, pp. 1685-1693.
- [19] HAN, C.D., SHETTY, R. Flow Instability in Tubular Film Blowing. 1. Experimental Study. *Ind. Eng. Chem., Fundam.* 1977, vol. 16, no. 1, pp. 49-56.
- [20] SPEED, C.S. LLDPE Blends for Film Applications. *Annual Technical Conference - Society of Plastics Engineers* 1982, pp. 214-216.
- [21] SPEED, C.S. Formulating Blends of LLDPE and LDPE to Design Better Film. *Plast. Eng.* 1982, vol. 38, no. 7, pp. 39-42.
- [22] KANAI, T., WHITE, J.L. Kinematics, Dynamics and Stability of the Tubular Film Extrusion of Various Polyethylenes. *Polym. Eng. Sci.* 1984, vol. 24, no. 15, pp. 1185-1201.
- [23] MINOSHIMA, W., WHITE, J.L. Instability Phenomena in Tubular Film, and Melt Spinning of Rheologically Characterized High Density, Low Density and Linear Low Density Polyethylenes. *J. Non-Newton. Fluid Mech.* 1986, vol. 19, no. 3, pp. 275-302.

- [24] WHITE, J.L., YAMANE, H. A Collaborative Study of the Stability of Extrusion, Melt Spinning and Tubular Film Extrusion of some High-, Low-, and Linear-Low Density Polyethylene Samples. *Pure Appl. Chem.* 1987, vol. 59, no. 2, pp. 193-216.
- [25] FLEISSNER, M. Elongational Flow of HDPE Samples and Bubble Instability in Film Blowing, *Int. Polym. Proc.* 1988, vol. 2, no.3-4, pp. 229-233.
- [26] GHIJSELS, A., ENTE, J.J.S.M., RAADSEN, J. Melt Strength Behavior of PE and its Relation to Bubble Stability in Film Blowing. *Int. Polym. Proc.* 1990, vol. 5, no. 4, pp. 284-286.
- [27] SWEENEY, P.A., CAMPBELL, G.A., FEENEY, F.A. Real Time Video Techniques in the Analysis of Blown Film Instability. *Int. Polym. Proc.* 1992, vol. 7, no. 3, pp. 229-239.
- [28] OBIJESKI, T.J., PRUITT, K.R. Improving the Output and Bubble Stability of Thick Gauge Blown Helical Instability. *Annual Technical Conference - ANTEC, Conference Proceedings* 1992, vol. 1, pp. 150-153.
- [29] KIM, S., LAFLEUR, P.G., SAMMUT, P., MICHEL, H.A. Effects of Molecular Structure of Polyethylenes on their Bubble Instabilities in Film Blowing Extrusion. *Annual Technical Conference - ANTEC, Conference Proceedings* 2003, vol. 1, pp. 361-365.
- [30] MÜNSTEDT, H., STEFFL, T., MALMBERG, A. Correlation between Rheological Behavior in Uniaxial Elongation and Film Blowing Properties of Various Polyethylenes. *Rheol. Acta* 2005, vol. 45, no. 1, pp. 14-22.
- [31] ZULLO, R., IANNACE, S. The Effects of Different Starch Sources and Plasticizers on Film Blowing of Thermoplastic Starch: Correlation Among Process, Elongational Properties and Macromolecular Structure. *Carbohydr. Polym.* 2009, vol. 77, no. 2, pp. 376-383.
- [32] OLIVIERO, M., DI MAIO, E., IANNACE, S. Effect of Molecular Structure on Film Blowing Ability of Thermoplastic Zein. *J. Appl. Polym. Sci.* 2010, vol. 115, no. 1, pp. 277-287.
- [33] AUINGER, T., STADLBAUER, M. Inter-relationship between Processing Conditions and Mechanical Properties of Blown Film from Different

- Polypropylenes and High Melt Strength Polypropylene Blends. *J. Appl. Polym. Sci.* 2010, vol. 117, no. 1, pp. 155-162.
- [34] ZATLOUKAL, M., VLCEK, J. Modeling of the Film Blowing Process by using Variational Principles. *J. Non-Newton. Fluid Mech.* 2004, vol. 123, no. 2-3, p. 201-213.
- [35] KOLARIK, R., ZATLOUKAL, M. Modeling of Non-Isothermal Film Blowing Process for Non-Newtonian Fluids by Using Variational Principles. *J. Appl. Polym. Sci.* 2011, vol. 122, no. 4, pp. 2807-2820.
- [36] DOUFAS, A.K. McHUGH, A.J. Simulation of Film Blowing Including Flow-Induced Crystallization. *J. Rheol.* 2001, vol. 45, no. 5, pp. 1085-1104.
- [37] ZATLOUKAL, M. A Simple Phenomenological Non-Newtonian Fluid Model. *J. Non-Newton. Fluid Mech.* 2010, vol. 165, no. 11-12, pp. 592-595.
- [38] PEARSON, J.R.A., PETRIE, C.J.S. The Flow of a Tubular Film. Part 1. Formal Mathematical Representation. *J. Fluid. Mech.* 1970, vol. 40, no. 1, pp. 1-19.
- [39] TAS, P.P. Film Blowing from Polymer to Product. *Ph.D. Thesis*. Technische Universiteit Eindhoven, 1994. ISBN 90-386-0204-9.
- [40] ZATLOUKAL, M., ŠTACH, P., LIU, P., SÁHA, P. Tensile Strength Characteristics of Polymer Melts. *Int. Polym. Proc.* 2002, vol. 17, no. 3, pp. 223-227.
- [41] KIM, S., DEALY, J.M. Gross Melt Fracture of Polyethylene. I: A Criterion Based on Tensile Stress. *Polym. Eng. Sci.* 2002, vol. 42, no. 3, pp. 482-494.
- [42] KIM, S., DEALY, J.M. Gross Melt Fracture of Polyethylene. II: Effects of Molecular Structure. *Polym. Eng. Sci.* 2002, vol. 42, no. 3, pp. 495-503.
- [43] ROLÓN-GARRIDO, V.H., PIVOKONSKY, R., FILIP, P., ZATLOUKAL, M., WAGNER, M.H. Modelling Elongational and Shear Rheology of Two LDPE Melts. *Rheol. Acta* 2009, vol. 48, no. 6, pp. 691-697.
- [44] MUSIL, J., ZATLOUKAL, M. Experimental Investigation of Flow Induced Molecular Weight Fractionation During Extrusion of HDPE Polymer Melts. *Chem. Eng. Sci.* 2011, vol. 66, no. 20, pp. 4814-4823.

- [45] WAGNER, M.H., KHEIRANDISH, S., STANGE, J., MÜNSTEDT, H. Modeling Elongational Viscosity of Blends of Linear and Long-Chain Branched Polypropylenes. *Rheol. Acta* 2006, vol. 46, no. 2, pp. 211-221.
- [46] WAGNER, M.H., KHEIRANDISH, S., YAMAGUCHI, M. Quantitative Analysis of Melt Elongational Behavior of LLDPE/LDPE Blends. *Rheol. Acta* 2004, vol. 44, no. 2, pp. 198-218.
- [47] WOLFF, F., RESCH, J.A., KASCHTA, J., MÜNSTEDT, H. Comparison of Viscous and Elastic Properties of Polyolefin Melts in Shear and Elongation. *Rheol. Acta* 2010, vol. 49, no. 1, pp. 95-103.
- [48] STANGE, J., UHL, C., MÜNSTEDT, H. Rheological Behavior of Blends from a Linear and a Long-Chain Branched Polypropylene. *J. Rheol.* 2005, vol. 49, no. 5, pp. 1059-1079.
- [49] GABRIEL, C., MÜNSTEDT, H. Strain Hardening of Various Polyolefins in Uniaxial Elongational Flow. *J. Rheol.* 2003, vol. 47, no. 3, pp. 619-630.
- [50] SENTMANAT, M.L. Miniature Universal Testing Platform: From Extensional Melt Rheology to Solid-state Deformation Behavior. *Rheol. Acta* 2004, vol. 43, no. 6 pp. 657-669.
- [51] SENTMANAT, M.L. *Dual Wind-up Extensional Rheometer*, US Patent No. 6,578,413 (2003).
- [52] SENTMANAT, M.L., WANG, B.N., McKINLEY, G.H. Measuring the Transient Extensional Rheology of Polyethylene Melts using the SER Universal Testing Platform. *J. Rheol.* 2005, vol. 49, no. 3, pp 585-606.
- [53] MÜNSTEDT, H., AUHL, D., Rheological Measuring Techniques and their Relevance for the Molecular Characterization of Polymers. *J. Non-Newton. Fluid Mech.* 2005, vol. 128, no. 1 SPEC. ISS., pp. 62-69.
- [54] WAGNER, M.H., BASTIAN, H., HACHMANN, P., MEISSNER, J., KURZBECK, S., MÜNSTEDT, H., LANGOUCHE, F. The Strain-Hardening Behaviour of Linear and Long-Chain-Branched Polyolefin Melts in Extensional Flows. *Rheol. Acta* 2000, vol. 39, no. 2, pp. 97-109.
- [55] MALMBERG, A., GABRIEL, C., STEFFL, T., MÜNSTEDT, H., LÖFGREN, B. Long-Chain Branching in Metallocene-Catalyzed Polyethylenes Investigated

- by Low Oscillatory Shear and Uniaxial Extensional Rheometry. *Macromolecules* 2002, vol. 35, no. 3, pp. 1038-1048.
- [56] MÜNSTEDT, H., LAUN, H.M. Elongational Properties and Molecular Structure of Polyethylene Melts. *Rheol. Acta* 1981, vol. 20, no. 3, pp. 211-221.
- [57] WAGNER, M.H. The Rheology of Linear and Long-Chain Branched Polymer Melts. *Macromolecular Symposia* 2006, vol. 236, pp. 219-227.
- [58] STADLER, F.J., KASCHTA, J., MÜNSTEDT, H., BECKER, F., BUBACK, M. Influence of Molar Mass Distribution and Long-Chain Branching on Strain Hardening of Low Density Polyethylene. *Rheol. Acta* 2009, vol. 48, no. 5, pp. 479-490.
- [59] STADLER, F.J., NISHIOKA, A., STANGE, J., KOYAMA, K., MÜNSTEDT, H. Comparison of the Elongational Behavior of Various Polyolefins in Uniaxial and Equibiaxial Flows. *Rheol. Acta* 2007, vol. 46, no. 7, pp. 1003-1012.

LIST OF SYMBOLS

A	Zatloukal-Vlcek model function	1
A'	Iso-contour constant	Pa
A_1	Generalized Newtonian model parameter	1
a	Generalized Newtonian model parameter	1
a_T	Arrhenius temperature shift factor	1
a_{TS}	Mean value of the Arrhenius temperature shift factor a_T	1
B'	Iso-contour constant	Pa
BUR	Blow-up ratio	1
C'	Iso-contour constant	Pa
C_p	Specific heat capacity	$\text{J kg}^{-1} \cdot \text{K}^{-1}$
D	Deformation rate tensor	s^{-1}
D_1	Bubble diameter at the freezeline height	m
D_0	Bubble diameter at the die exit	m
dx	Element length in x direction	m
E_a	Flow activation energy	J mol^{-1}
F	Take-up force	N
F_{critical}	Critical take-up force causing bubble rupture	N
G'	Storage modulus	Pa
G''	Loss modulus	Pa
HTC	Heat transfer coefficient	$\text{W m}^{-2} \cdot \text{K}^{-1}$
H_0	Bubble thickness at the die exit	m
H_1	Bubble thickness at the freezeline height	m
$h(x), h$	Local film thickness	m
$I_{ D }$	First invariant of the absolute value of deformation rate tensor	s^{-1}
$\overline{I_{ D }}$	Mean value of the first invariant of deformation rate tensor	s^{-1}
II_D	Second invariant of deformation rate tensor	s^{-2}
$\overline{II_D}$	Mean value of the second invariant of deformation rate tensor	s^{-2}

	tensor	
III_D	Third invariants of deformation rate tensor	s^{-3}
$\overline{III_D}$	Mean value of the third invariant of deformation rate tensor	s^{-3}
	tensor	
J	Bubble compliance	Pa^{-1}
L	Freezeline height	m
\dot{m}	Mass flow rate	$kg \cdot s^{-1}$
n	Power law index	1
p	Internal load	$Pa \cdot m$
pJ	Bubble curvature	m
Q	Volumetric flow rate	$m^3 \cdot s^{-1}$
R	Universal gas constant	$J \cdot K^{-1} \cdot mol^{-1}$
R_0	Inner die radius	m
R_m	Curvature radius in the machine direction	m
R_t	Curvature radius in the transverse direction	m
r_f	Bubble radius at the freezeline height	m
$r(x)$	Local bubble radius	m
T	Local bubble temperature	$^{\circ}C$
T_{air}	Cooling air temperature	$^{\circ}C$
$T_{melt/(die)}$	Die exit melt temperature	$^{\circ}C$
T_r	Reference temperature	$^{\circ}C$
T_{solid}	Solidification (freezeline) temperature	$^{\circ}C$
TR	Thickness reduction	1
TUR	Take-up ratio	1
$v(x), v$	Local film velocity	$m \cdot s^{-1}$
v_d	Bubble velocity at the die exit	$m \cdot s^{-1}$
v_f	Bubble velocity at the freezeline	$m \cdot s^{-1}$
x	Particular distance from the die exit	m
$y(x), y$	Local bubble radius	m

Greek Symbols

α	Generalized Newtonian model parameter	s
α'	Zatloukal-Vlcek model function	1
β	Generalized Newtonian model parameter	1
Δp	Internal bubble pressure	Pa
Δp_{input}	Input internal bubble pressure value	Pa
Δp_{max}	Maximum internal bubble pressure	Pa
Δp_{new}	Internal bubble pressure calculated in the current iteration step	Pa
$\Delta p_{\text{previous}}$	Internal bubble pressure calculated in the previous iteration step	Pa
$\dot{\varepsilon}$	Extensional rate	s ⁻¹
$\overline{\dot{\varepsilon}}_1$	Mean value of extensional rate in machine direction	s ⁻¹
ε_{max}	Maximum extensional strain	1
ε_{min}	Minimum extensional strain	1
ζ	Generalized Newtonian model parameter (extensional strain hardening parameter)	1
η	Viscosity	Pa·s
$\overline{\eta}$	Mean value of melt viscosity	Pa·s
η^*	Complex viscosity	Pa·s
η_E	Extensional viscosity	Pa·s
$\eta_{E,\text{max}}$	Maximum steady-state uniaxial extensional viscosity	Pa·s
$\eta_E^+(t)$	Time-dependent uniaxial extensional viscosity	Pa·s
η_{new}	Viscosity calculated in the current iteration step	Pa·s
η_0	Newtonian viscosity	Pa·s
η_{previous}	Viscosity calculated in the previous iteration step	Pa·s
θ	Bubble angle	°
λ	Relaxation time	s
π	Ludolf's number	1
σ	Rupture stress	Pa

σ_{\max}	Rupture stress (maximum value)	Pa
$\overline{\sigma_{\max}}$	Mean value of melt strength	Pa
σ_{11}	Total stress tensor in machine direction	Pa
σ_{33}	Total stress tensor in circumferential direction	Pa
τ	Extra stress tensor	Pa
φ	Zatloukal-Vlcek model function	1
ψ	Generalized Newtonian model parameter	1
ω	Frequency	rad s ⁻¹

Table 1. Summary of the Zatloukal-Vlcek film blowing model equations [5, 34, 35].

Equation type	Equation form	Equation number
Bubble shape	$y = (R_0 - pJ)\cos\left(\frac{x\varphi}{L}\right) - \alpha'(pJ - BURR_0)\sin\left(\frac{x\varphi}{L}\right) + pJ$	(1)
Parameter	$x \in <0; L >$	(2)
Parameter	$\alpha' = \sqrt{\frac{2pJ - R_0 - BURR_0}{pJ - BURR_0} \left \frac{R_0(BUR - 1)}{pJ - BURR_0} \right }$	(3)
Parameter	$A = \frac{pJ - R_0}{pJ - BURR_0}$	(4)
Take-up force	$F = -\frac{L^2}{J\varphi^2}$	(5)
Internal bubble pressure	$\Delta p = \frac{pL}{2\pi \int_0^L y \sqrt{1 + (y')^2} dx}$	(6)
Freezeline height	$L = -\frac{1}{2} \dot{m} C_p \ln \left(-\frac{(T_{\text{melt}(\text{die})} - T_{\text{air}})}{(-T_{\text{solid}} + T_{\text{air}})} \right) \cdot \frac{\varphi}{\pi HTC [\alpha pJ - \alpha BURR_0 - pJ\varphi + (pJ - R_0)\sin(\varphi) + (BURR_0 - pJ)\alpha \cos(\varphi)]}$	(7)
Temperature profile	$T = T_{\text{air}} + (T_{\text{melt}(\text{die})} - T_{\text{air}}) \exp \left\{ -\frac{2\pi L HTC}{\dot{m} C_p \varphi} \left(-\alpha [R_0 BUR - pJ] \cdot \left[\cos\left(\frac{x\varphi}{L}\right) - 1 \right] + \sin\left(\frac{x\varphi}{L}\right) [R_0 - pJ] + pJ\varphi \frac{x}{L} \right) \right\}$	(8)

Table 2. Parameters A and φ for different bubble shapes (y) [34].

Equation	A	φ	y
1.	1	0	R_0
2.	$0 < A < 1$	$\arctan \left(\frac{\sqrt{1 - A^2}}{A} \right)$	The form of Eq. (1).
3.	0	$\pi/2$	$R_0 \left\{ 1 - \sin \left(\frac{x\pi}{2L} \right) (1 - BUR) \right\}$
4.	$-1 < A < 0$	$\pi + \arctan \left(\frac{\sqrt{1 - A^2}}{A} \right)$	The form of Eq. (1).
5.	-1	π	$\frac{R_0}{2} \left\{ 1 + \cos \left(\frac{x\pi}{L} \right) (1 - BUR) + BUR \right\}$

Table 3. Film blowing model parameters used for theoretical stability analysis on Tas's Ph.D. thesis data for LDPE L8 (experiment No. 23) [39].

<i>Input parameters for the Zatloukal-Vlcek film blowing model</i>						
L (m)	\dot{m} (kg.s ⁻¹)	R_0 (m)	H_0 (m)	σ_{\max} (MPa)		
0.10	0.001	0.0178	0.0022	< 0.02 ; 3 >		
<i>Parameters of the generalized Newtonian constitutive equation ($A_1 = 1$, $\psi = 20$)</i>						
η_0 (Pa's)	λ (s)	a (-)	n (-)	α (s)	β (-)	ζ (-)
2,365.0	0.17242	0.71597	0.37108	0.00001	$9.21 \cdot 10^{-7}$	< 0 ; 0.08 >
<i>Temperature parameters</i>						
T_{air} (°C)	T_{solid} (°C)	$T_{\text{melt(die)}}$ (°C)	T_r (°C)	E_a (J.mol ⁻¹)	R (J.K ⁻¹ .mol ⁻¹)	C_p (J.kg ⁻¹ .K ⁻¹)
25	92	145	190	59,000	8.314	2,300

Table 4. Summarization of all adjustable parameters for approximation function given by Eq. (22) for different iso-stability contour values.

<i>Iso-stability contour (-)</i>	<i>A'</i> (Pa)	<i>B'</i> (Pa)	<i>C'</i> (Pa)
0	-0.00037	0.00514	0.00123
1	-0.00145	0.02342	0.00022
2	-0.00293	0.05009	-0.02216
3	-0.00435	0.08335	-0.04100
4	-0.00748	0.13757	-0.07910
5	-0.00521	0.18573	-0.11852
6	-0.00500	0.26878	-0.18578
7	-0.00845	0.41375	-0.31530
8	-0.01116	0.58181	-0.46565
9	0.01184	0.64295	-0.52178
10	0.04323	0.71643	-0.58366
11	0.10896	0.67803	-0.56856
12	0.27358	0.31749	-0.27798
13	0.48483	-0.11802	0.02696
14	0.77460	-0.84009	0.65924
15	1.16650	-1.75204	1.34118
16	2.55162	-5.93888	4.68104
17	4.54027	-11.94640	9.47660
18	5.78796	-15.15831	11.76550
19	9.73394	-29.67070	25.44699

Table 5. Summarization of all adjustable parameters for approximation function given by Eq. (22) for different iso-minimum relative final film thickness contour values.

<i>Iso-minimum relative final film thickness contour</i> (-)	<i>A'</i> (Pa)	<i>B'</i> (Pa)	<i>C'</i> (Pa)
1×10^{-1}	-0.00114	0.02288	0.00326
8×10^{-2}	-0.00165	0.03198	-0.00233
6×10^{-2}	-0.00213	0.04696	-0.01483
4×10^{-2}	-0.00235	0.07419	-0.03184
2×10^{-2}	-0.00306	0.16710	-0.11404
1×10^{-2}	0.00702	0.28459	-0.23161
8×10^{-3}	0.01440	0.32997	-0.27437
6×10^{-3}	0.03785	0.33928	-0.29713
4×10^{-3}	0.08853	0.31743	-0.31595
2×10^{-3}	0.22363	0.21363	-0.31726
1×10^{-3}	0.51983	-0.24779	-0.12204
8×10^{-4}	0.62681	-0.44985	0.01988
6×10^{-4}	0.88881	-1.10415	0.49752
4×10^{-4}	1.10243	-1.33269	0.52463
2×10^{-4}	1.91737	-3.29791	1.95692
1×10^{-4}	5.85781	-15.90541	12.51535
8×10^{-5}	8.20777	-23.42111	18.64421
6×10^{-5}	12.39452	-38.22740	31.99265

Table 6. Summarization of all adjustable parameters for approximation function given by Eq. (22) for local extremes in iso-stability and iso-minimum relative final film thickness contour values.

<i>Description</i>	<i>A'</i> (Pa)	<i>B'</i> (Pa)	<i>C'</i> (Pa)
<i>Local extremes in iso-stability contours</i> (-)	4.27418	-5.85911	1.75994
<i>Local extremes in iso-minimum relative final film thickness contours</i> (-)	6.73714	-12.95280	6.36262

Table 7. Melt strength characteristics for all three tested polymer samples determined at 140°C.

Material	η_E (Pa's)	$\dot{\epsilon}$ (1/s)	σ (Pa)	<i>Time</i> (s)	<i>Hencky strain</i> (-)	$\overline{\sigma}_{max}$ (Pa)
Linear mLLDPE	38,106.92	10	381,069.17	0.48	4.8	50,526.19
	36,850.90	3.16	116,448.83	1.42	4.4872	
	36,686.18	1	36,686.18	4.765	4.765	
	35,075.19	0.316	11,083.76	14.235	4.49826	
	34,914.03	0.1	3,491.40	48.1	4.81	
Middle mLLDPE	51,388.96	10	513,889.57	0.48	4.8	168,990.28
	76,404.77	3.16	241,439.08	1.42	4.4872	
	84,238.48	1	84,238.48	4.765	4.765	
	96,682.60	0.316	30,551.70	14.235	4.49826	
	67,998.61	0.1	6,799.86	50.8	5.08	
High mLLDPE	69,919.05	10	699,190.48	0.48	4.8	238,898.26
	104,058.37	3.16	328,824.46	1.42	4.4872	
	135,458.95	1	135,458.95	4.765	4.765	
	168,786.46	0.316	53,336.52	14.235	4.49826	
	130,918.19	0.1	13,091.82	50.8	5.08	

Table 8. Material parameters utilized in the film blowing stability analysis for all tested polymer samples.

	Linear mLLDPE	Middle mLLDPE	High mLLDPE
η_0 (Pa's)	12,532.0	13,432.0	14,001.0
λ (s)	0.0319	0.0319	0.033
a (-)	0.853	0.853	0.8016
n (-)	0.13	0.1	0.1
α (s)	0.100249662	4.179239211	6.183603557
β (-)	3.407909759	3.255346092	3.090540474
ζ (-)	99.987888	99.991273	99.965923
A_1 (-)	1,000.0	1,000.0	1,000.0
ψ (-)	8	8	8
E_a (J·mol ⁻¹)	27,463.0	28,021.0	28,319.0
σ_{max} (Pa)	50,526.19	168,990.28	238,898.26
$T_{(melt)die}$ (°C)	190	190	190
T_{solid} (°C)	116	116	116
T_r (°C)	140	140	140
C_p (J·kg ⁻¹ ·K ⁻¹)	2,300	2,300	2,300
R (J·K ⁻¹ ·mol ⁻¹)	8.314	8.314	8.314

Table 9. Processing parameters utilized in the film blowing stability analysis for all tested polymer samples.

	Linear mLLDPE	Middle mLLDPE	High mLLDPE
Δp (Pa)	155.979	147.15	95.157
TUR (-)	20.816	27.784	25.743
L (m)	0.09	0.099	0.1145
\dot{m} (kg·s ⁻¹)	0.003258333	0.00223888	0.00385
T_{air} (°C)	25	25	25

Table 10. Film blowing model predictions.

	F (N)	pJ/R_0 (-)	BUR (-)	HTC (W·m ⁻² ·K ⁻¹)	p (Pa·m)
Linear mLLDPE	5.979	1.572012	2.14580	137.451	56.23177
Middle mLLDPE	6.968	1.407288	1.82	95.292	47.79762
High mLLDPE	11.306	1.245019	1.67912	143.648	30.48624

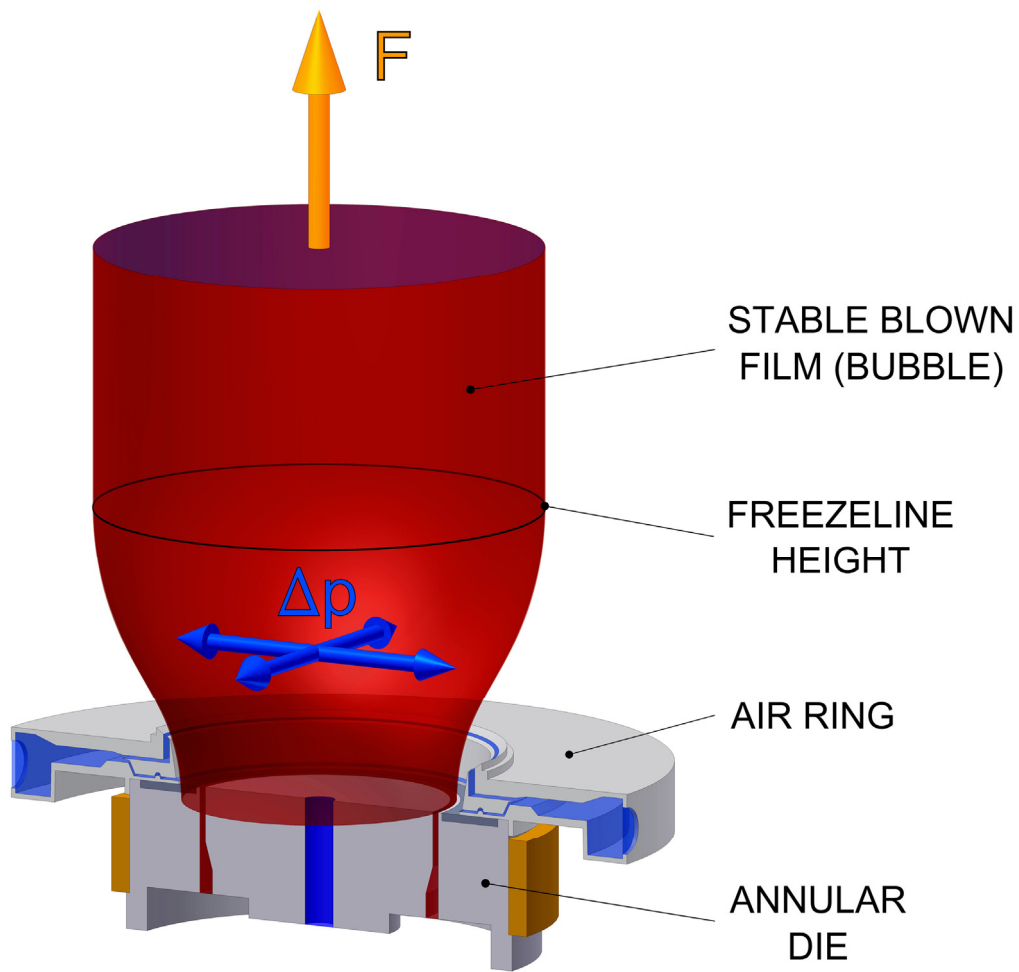


Figure1. Stable bubble formation during the film blowing process.

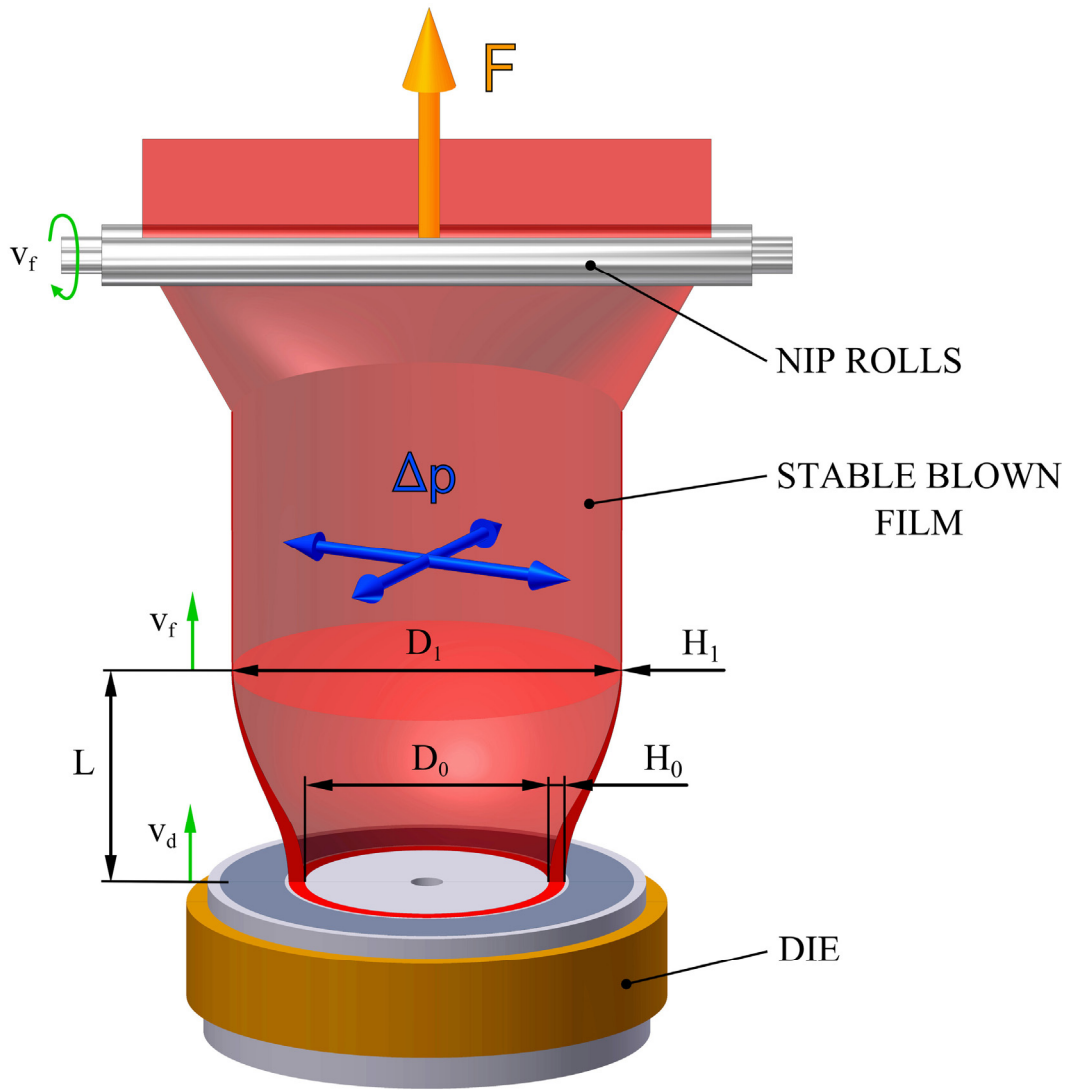


Figure 2. The film blowing process characterization.

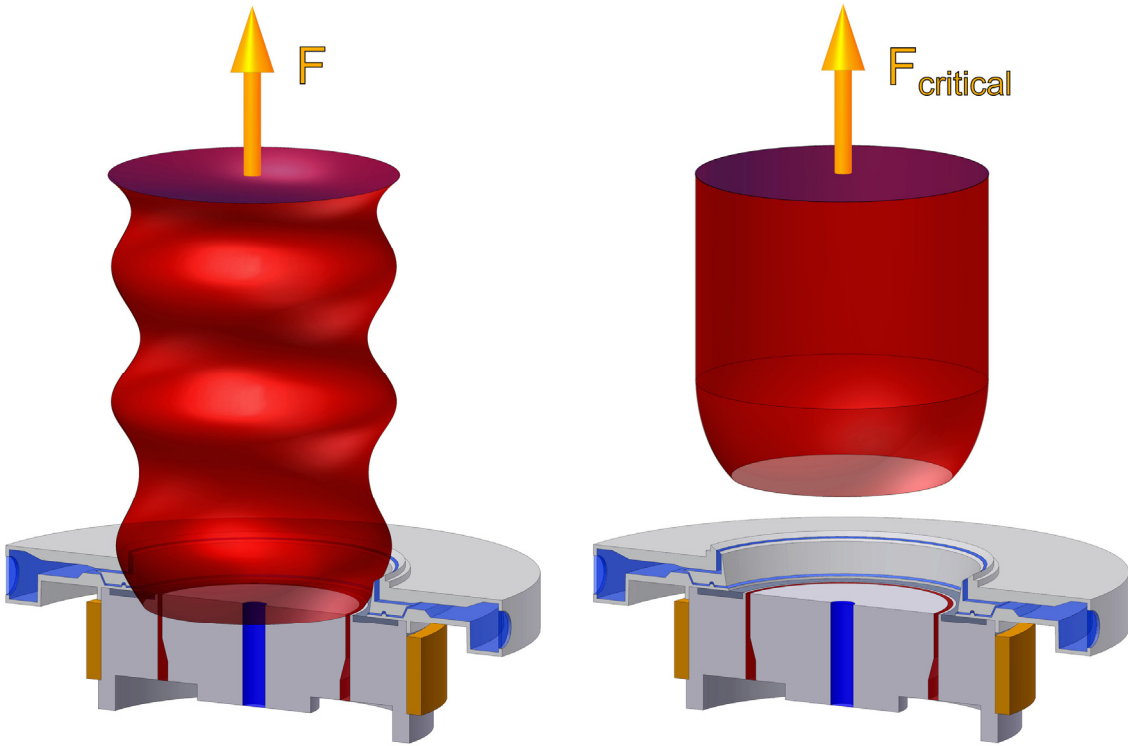


Figure 3. Draw resonance and bubble tear instabilities affected by the forces, F , and F_{critical} , respectively, where $F < F_{\text{critical}}$.

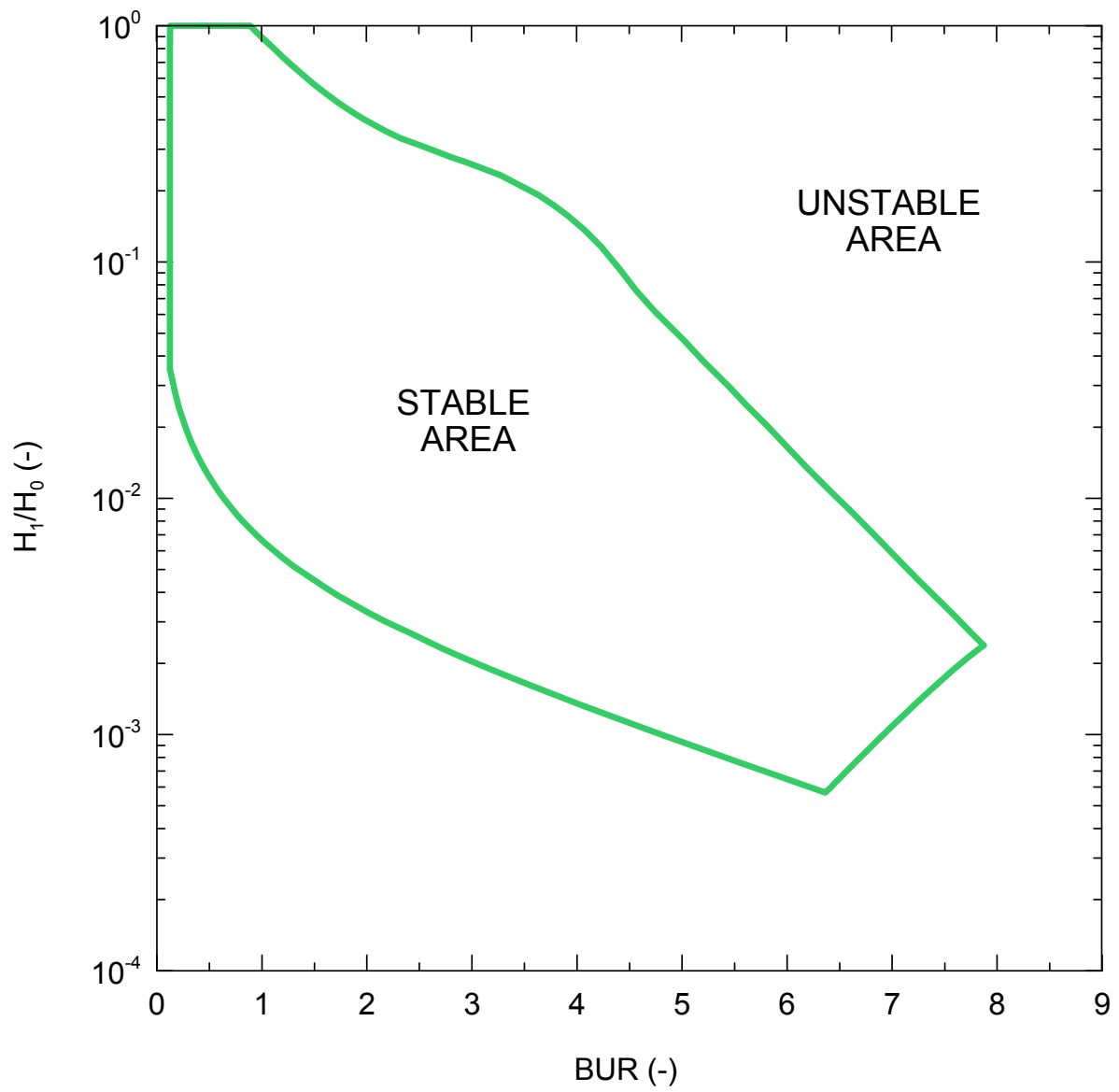


Figure 4. Description of the stability processing window predicted by the Zatloukal-Vlcek model.

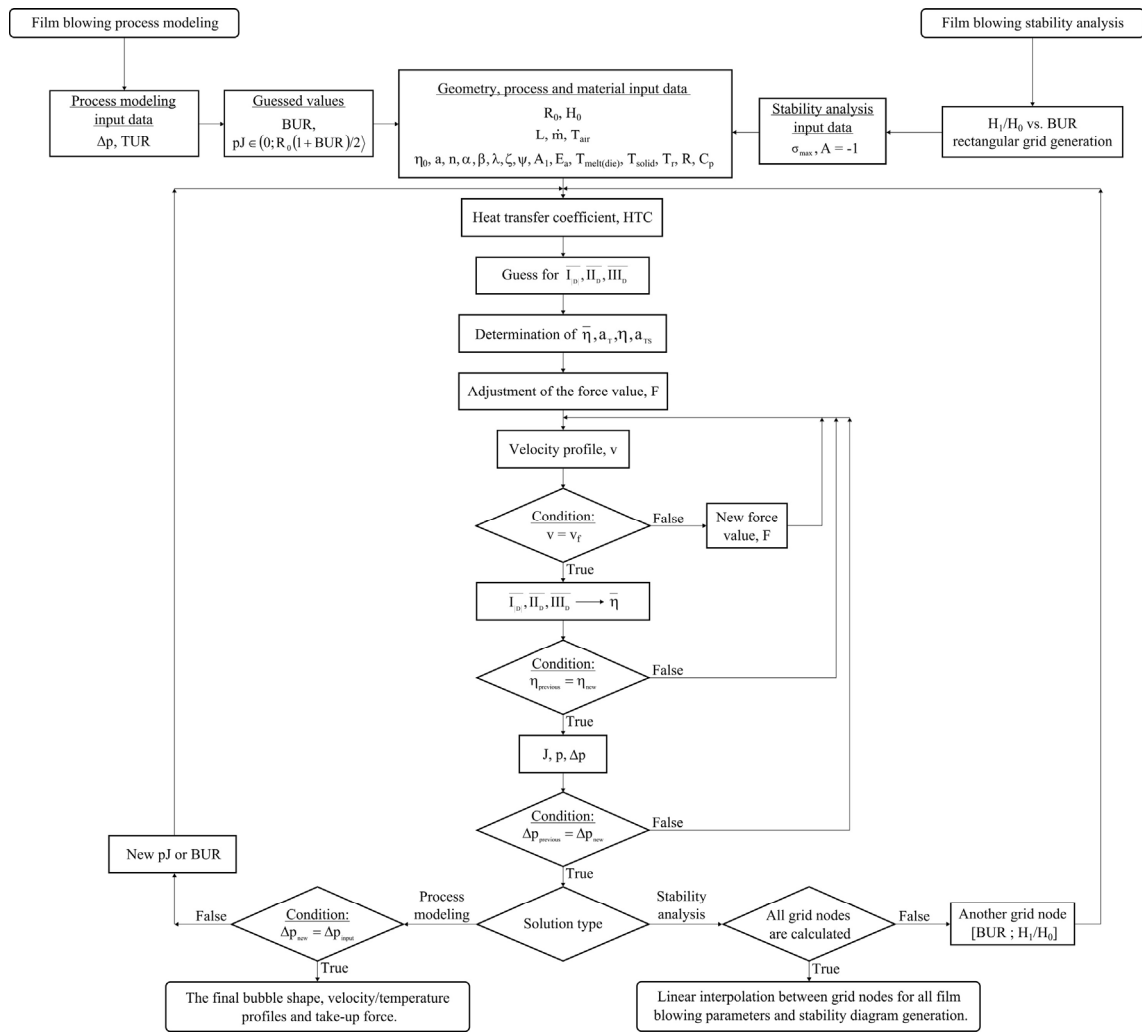


Figure 5. Iteration scheme of the Zatloukal-Vlcek model utilized for the film blowing process modeling (left branch) and film blowing stability analysis (right branch).

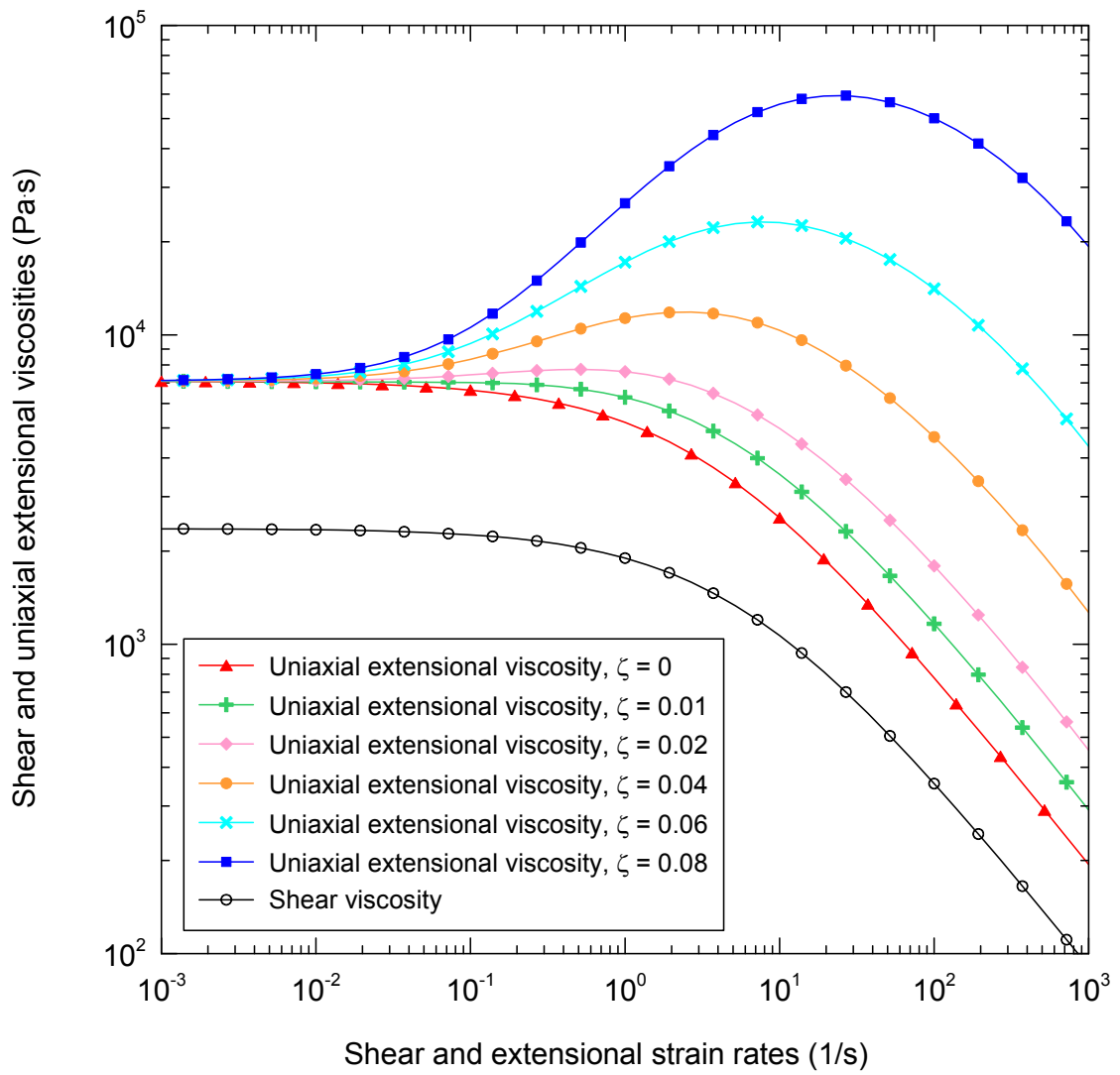


Figure 6. Effect of extensional strain hardening parameter ζ in the utilized generalized Newtonian model on the uniaxial extensional viscosity.

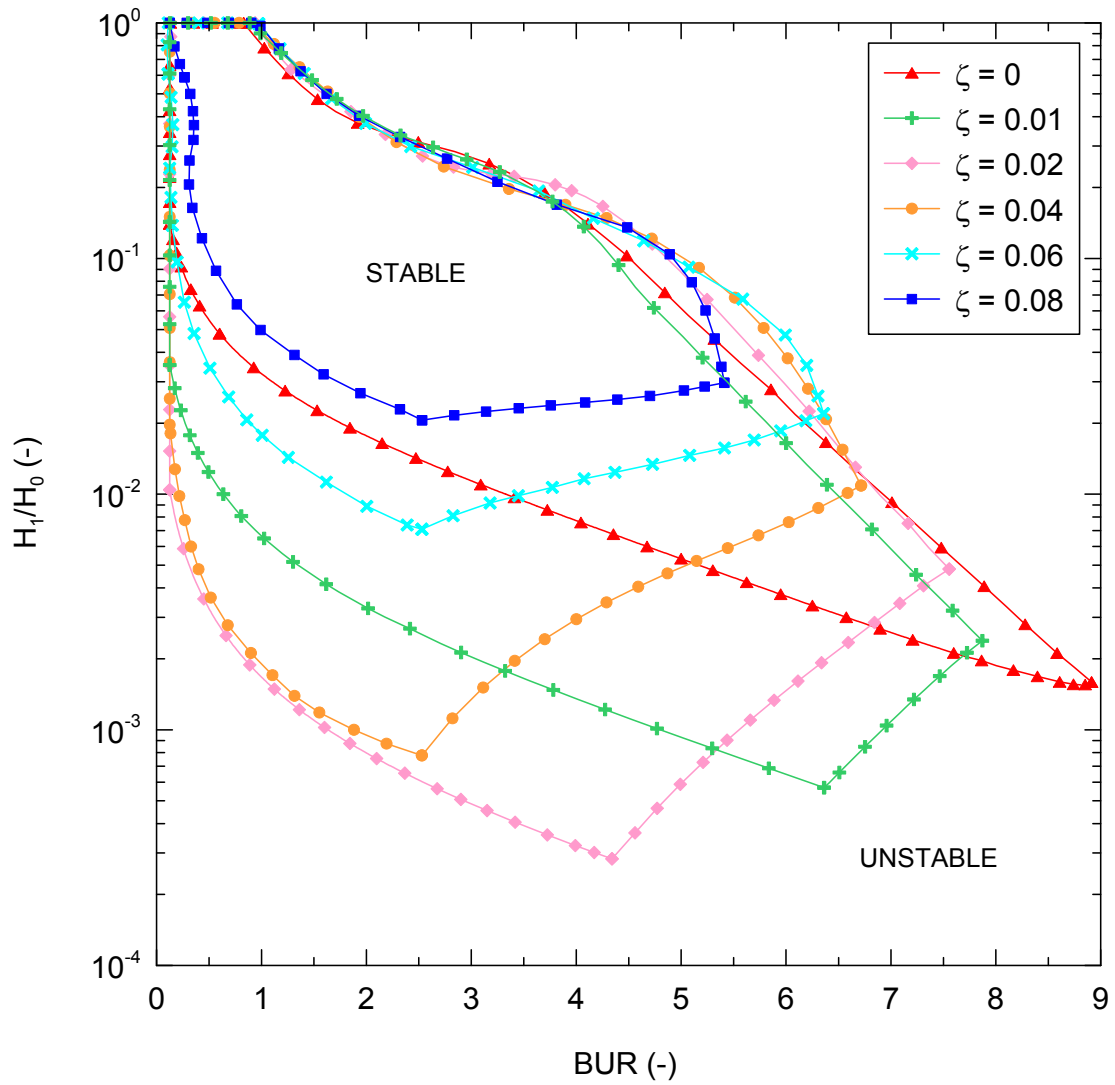


Figure 7. Predicted film blowing stability window shapes for different levels of the extensional strain hardening parameter ζ at constant melt strength, $\sigma_{\max} = 1$ MPa.

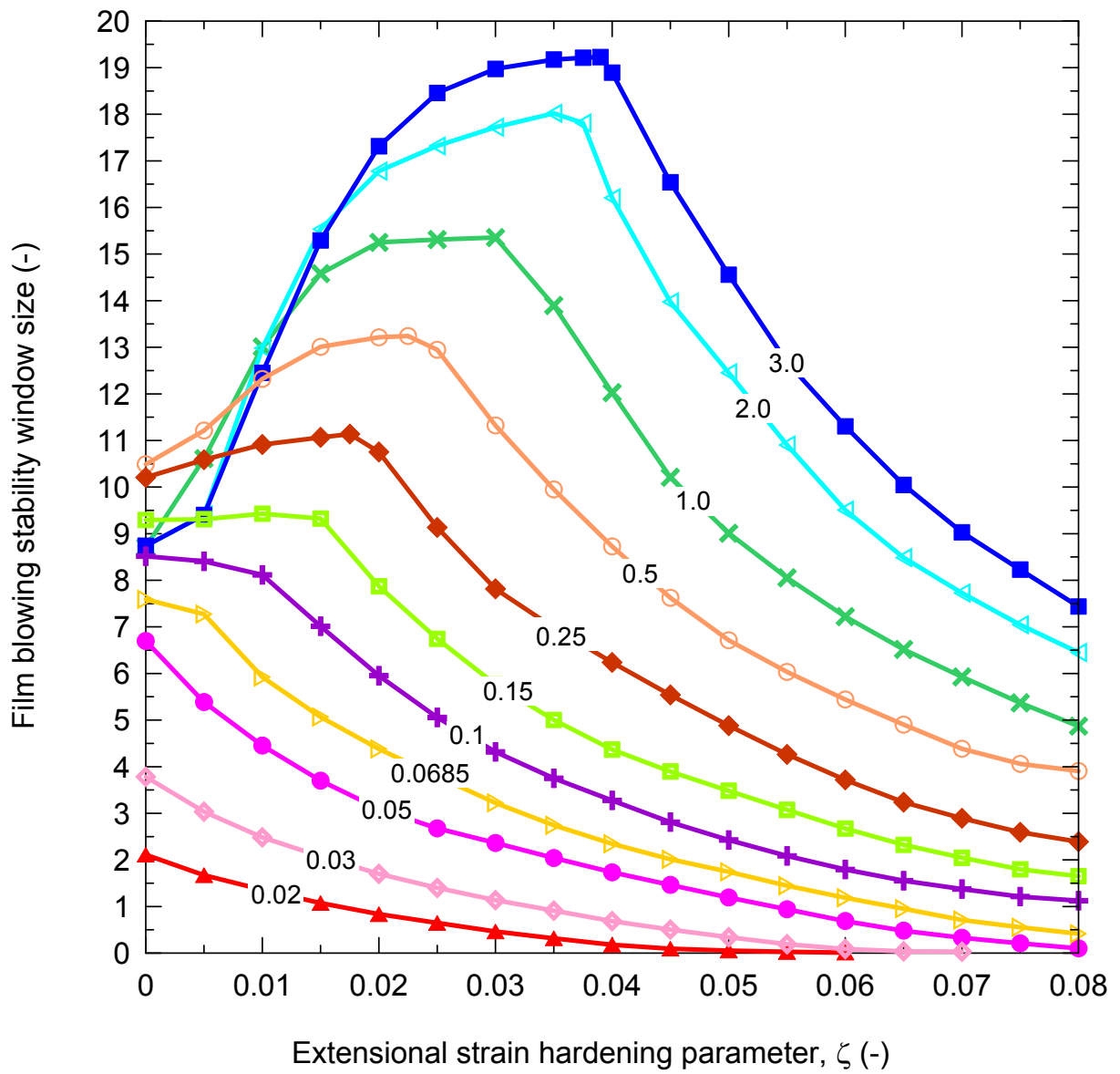


Figure 8. The effect of extensional strain hardening parameter ζ on the film blowing stability window size for given melt strength values, which are provided for the each curve in MPa.

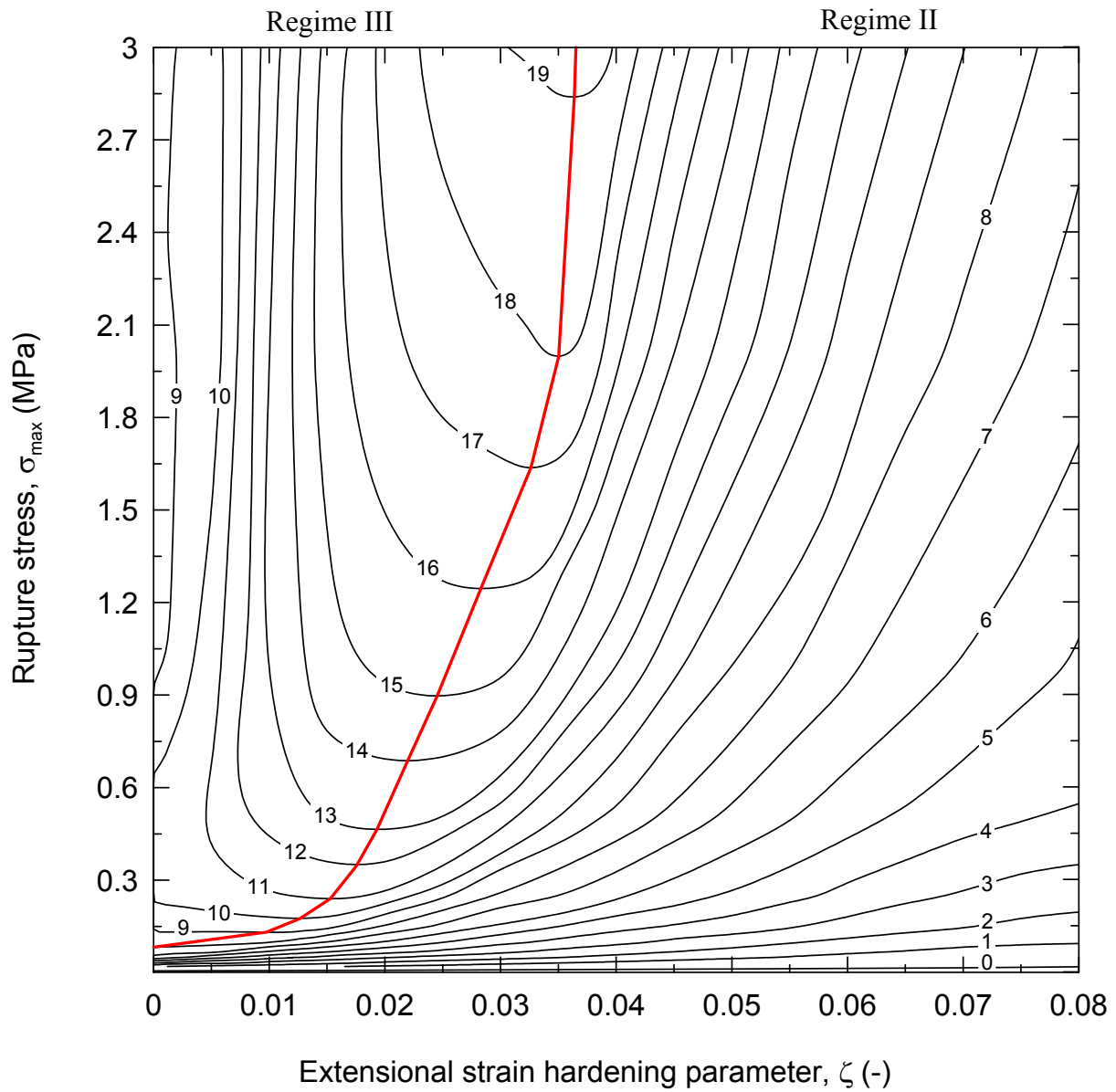


Figure 9. Iso-stability contour map for the rupture stress vs. extensional strain hardening parameter dependence. Here, the iso-stability contour value is given by the film blowing stability window size.

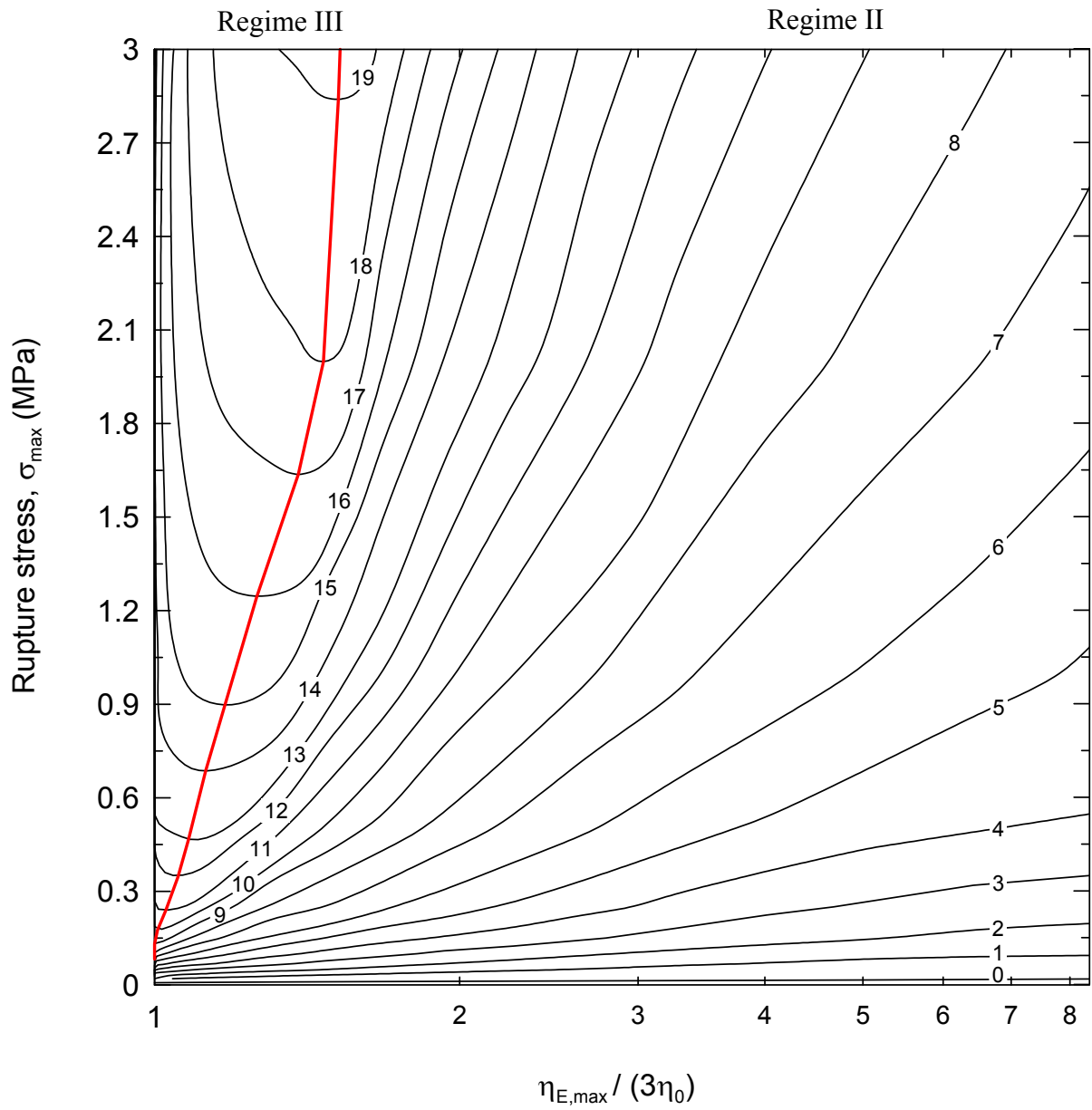


Figure 10. Iso-stability contour map for the rupture stress vs. $\frac{\eta_{E,\max}}{3\eta_0}$ dependence. Here, the iso-stability contour value is given by the film blowing stability window size.

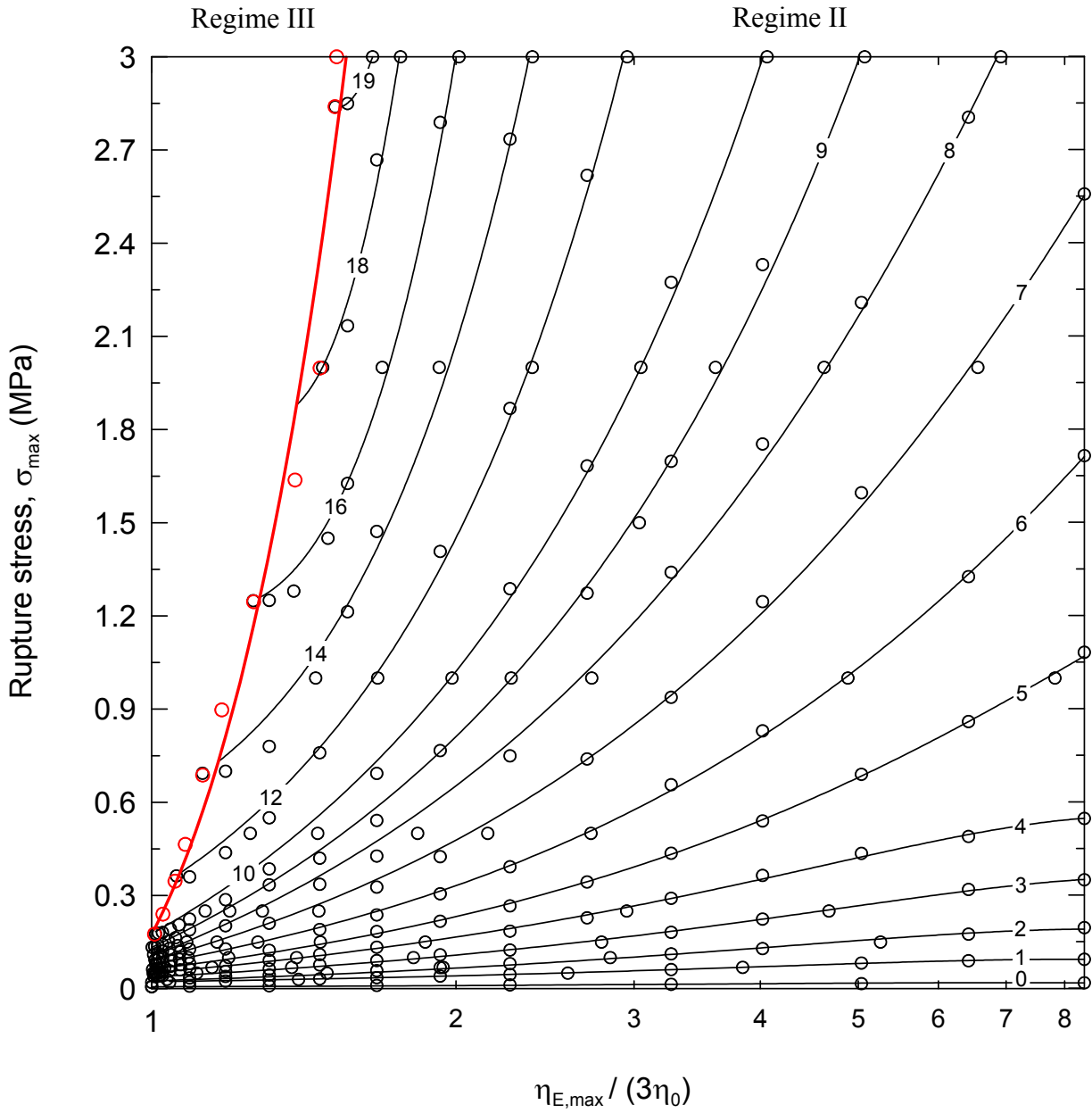


Figure 11. Comparison between the numerically determined iso-stability contour map for the rupture stress vs. $\frac{\eta_{E,\max}}{3\eta_0}$ dependence (open symbols) and approximation function given by Eq. (22) and parameters summarized in Tables 4 and 6. Here, the iso-stability contour value is given by the film blowing stability window size.

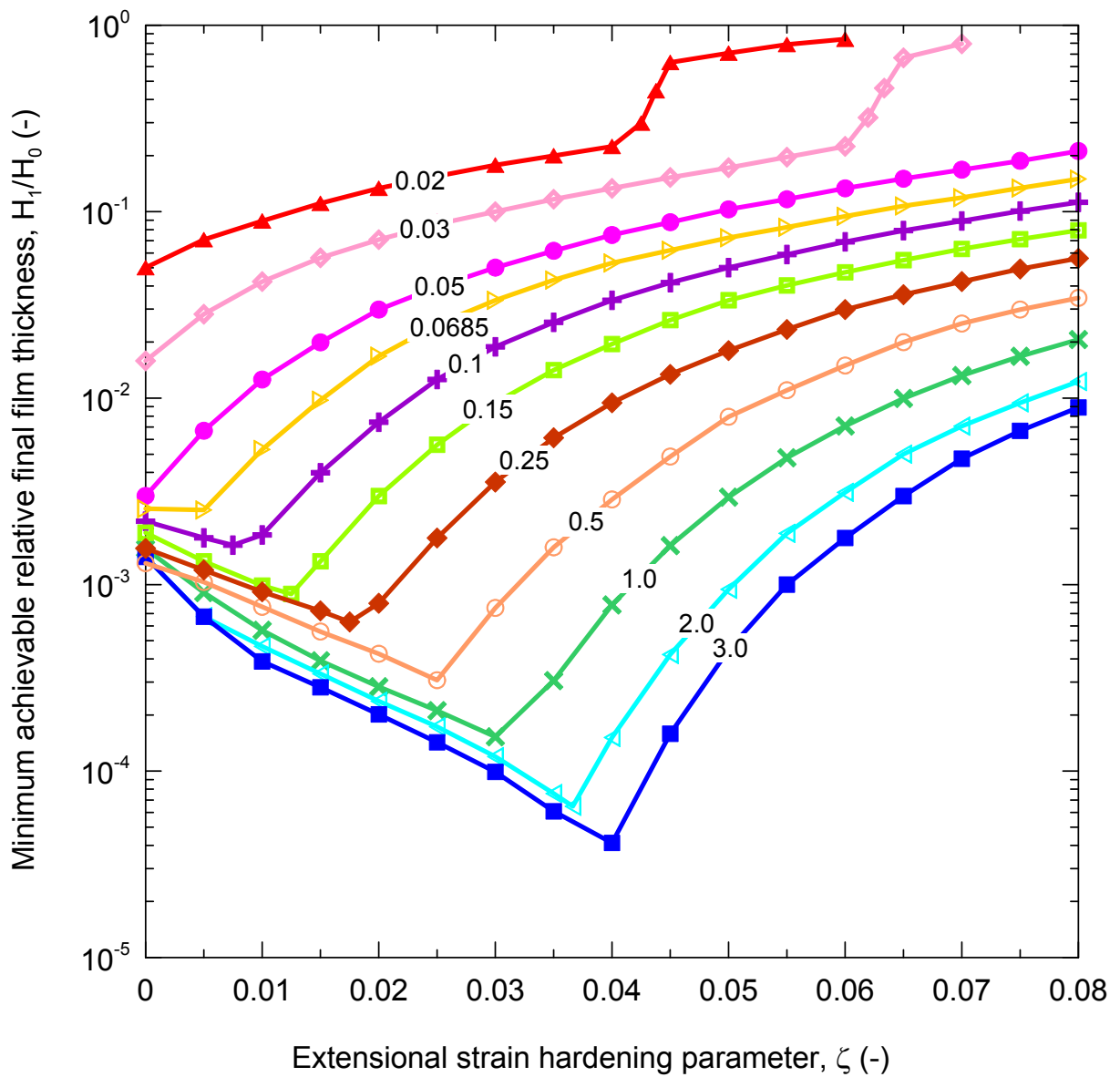


Figure 12. The effect of extensional strain hardening parameter ζ on the minimum achievable relative final film thickness for given melt strength values, which are provided for the each curve in MPa.

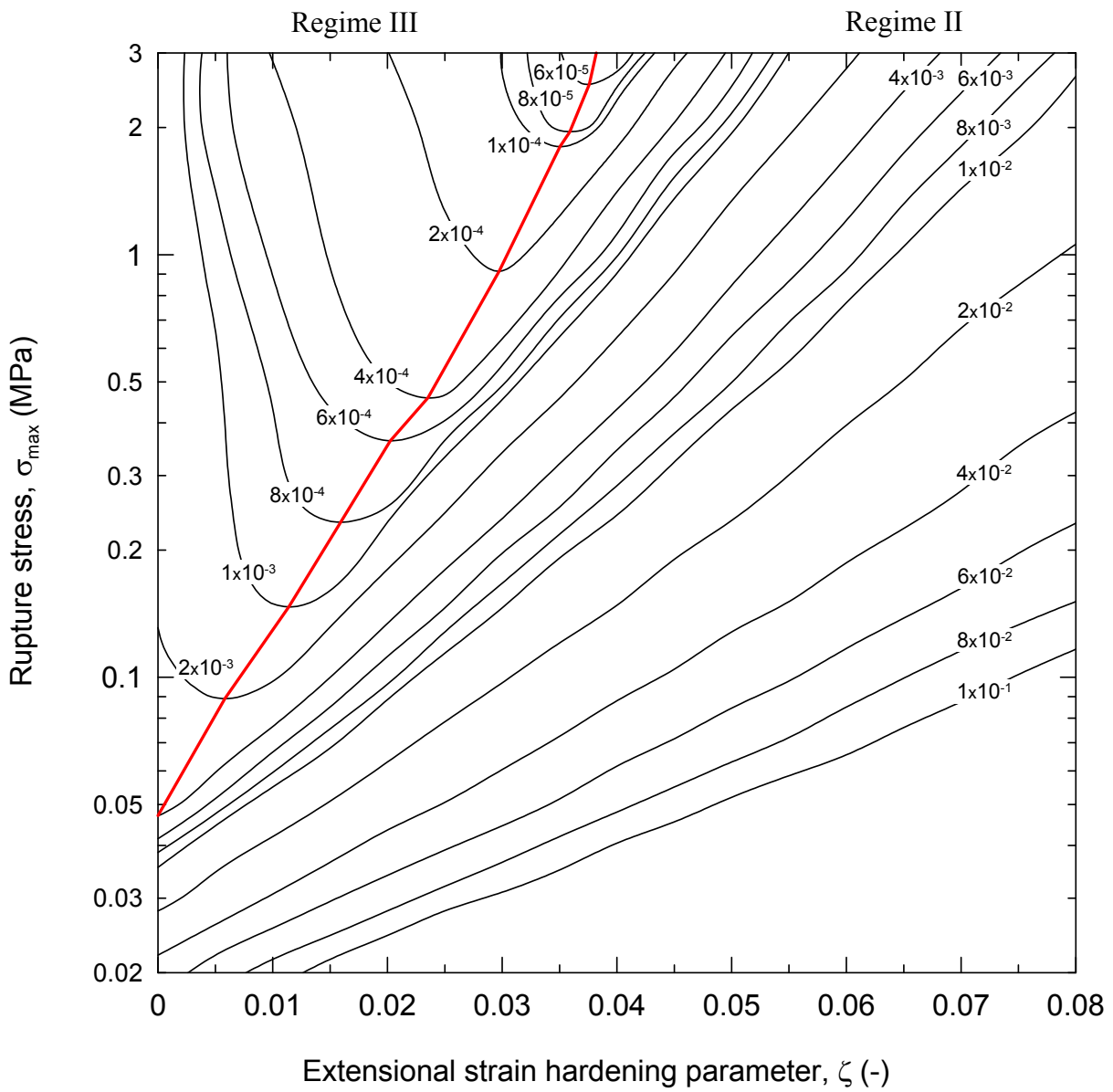


Figure 13. Iso-minimum relative final film thickness contour map for the rupture stress vs. extensional strain hardening ζ parameter dependence. Here, the iso-minimum relative final film thickness contour value is given by the H_1/H_0 ratio.

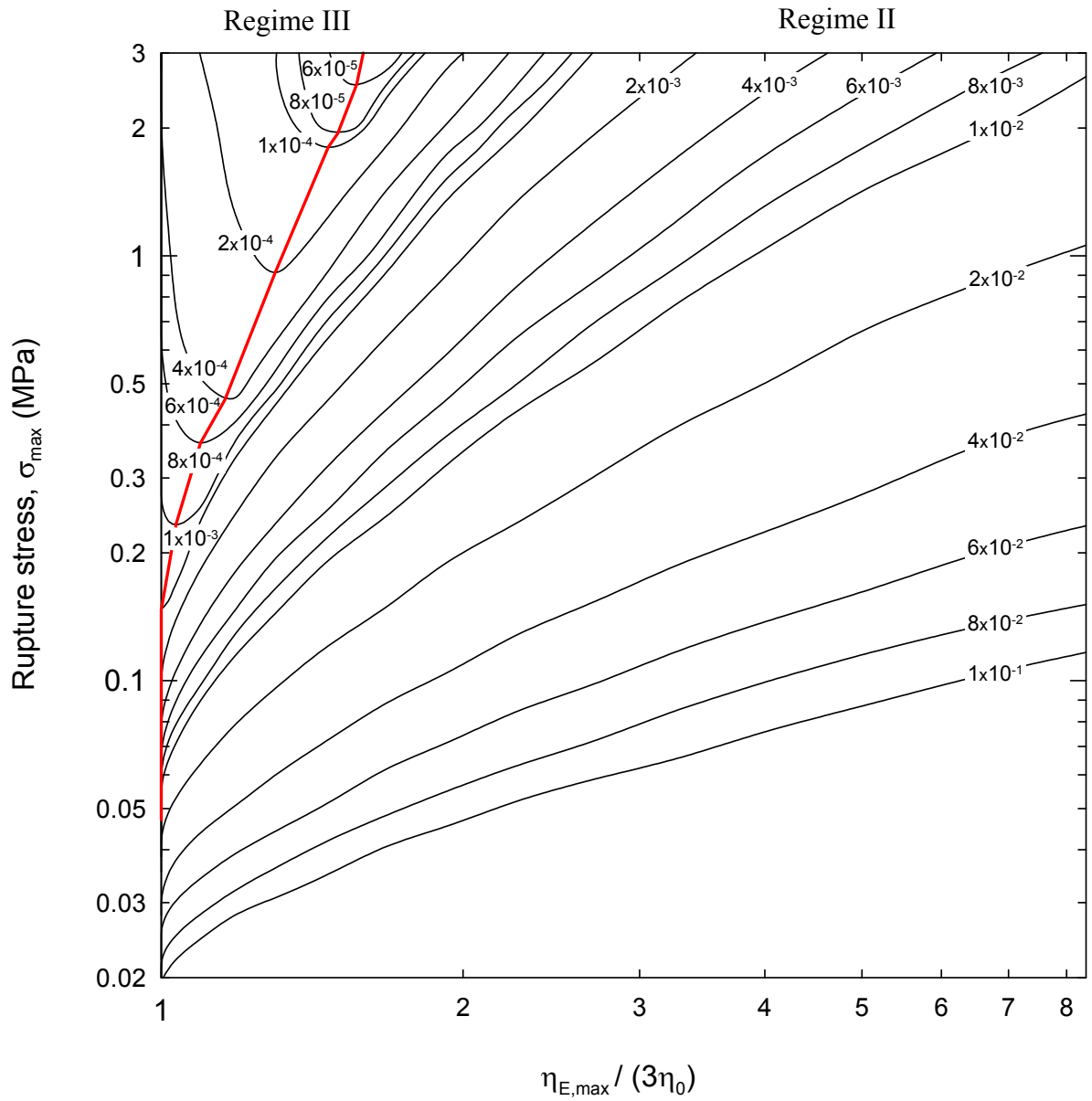


Figure 14. Iso-minimum relative final film thickness contour map for the rupture stress vs. $\frac{\eta_{E,\max}}{3\eta_0}$ dependence. Here, the iso-minimum relative final film thickness contour value is given by the H_1/H_0 ratio.

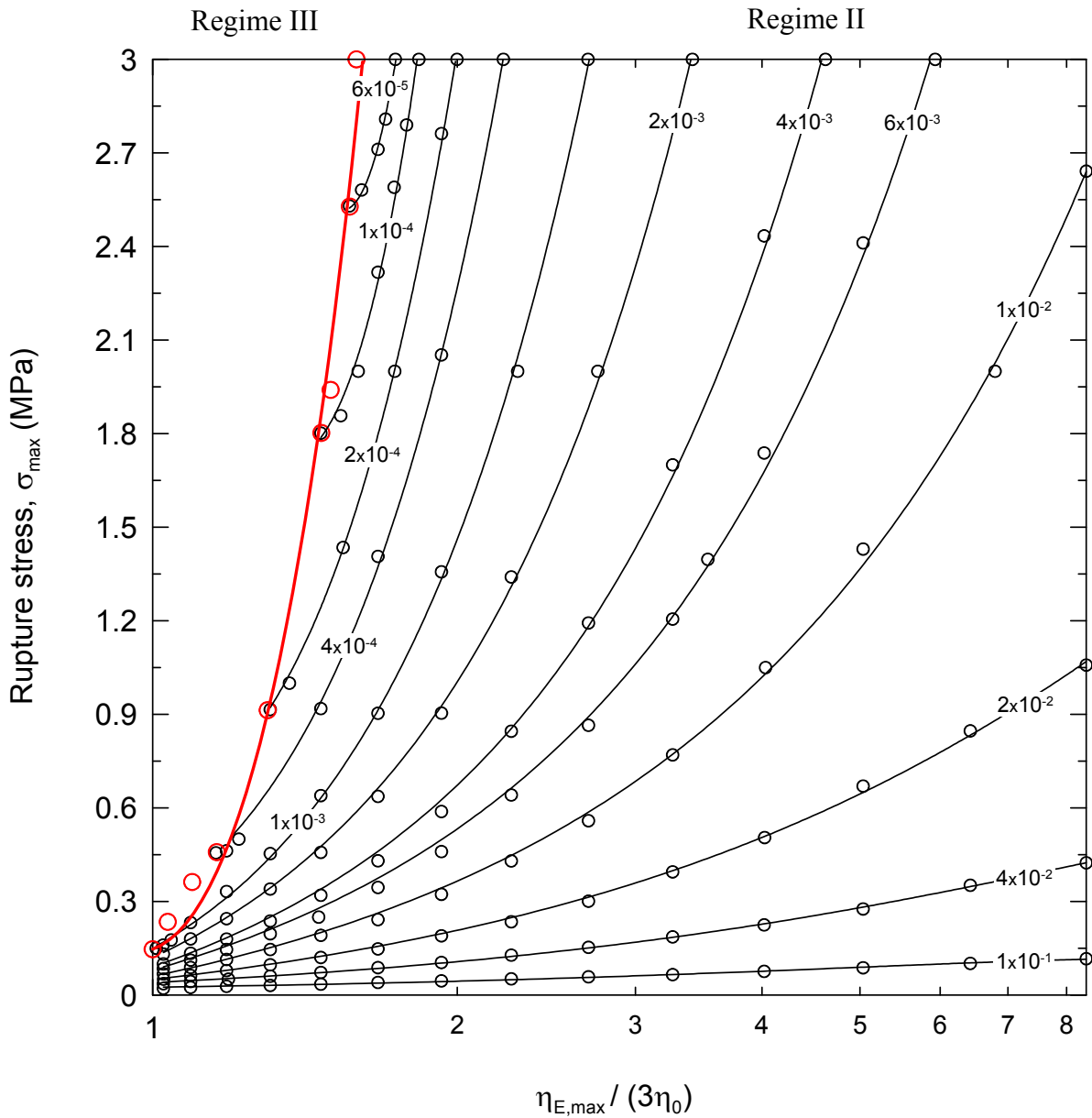


Figure 15. Comparison between the numerically determined iso-minimum relative final film thickness contour map for the rupture stress vs. $\frac{\eta_{E,\max}}{3\eta_0}$ dependence (open symbols) and approximation function given by Eq. (22) and parameters summarized in Tables 5 and 6. Here, the iso-minimum relative final film thickness contour value is given by the H_1/H_0 ratio.

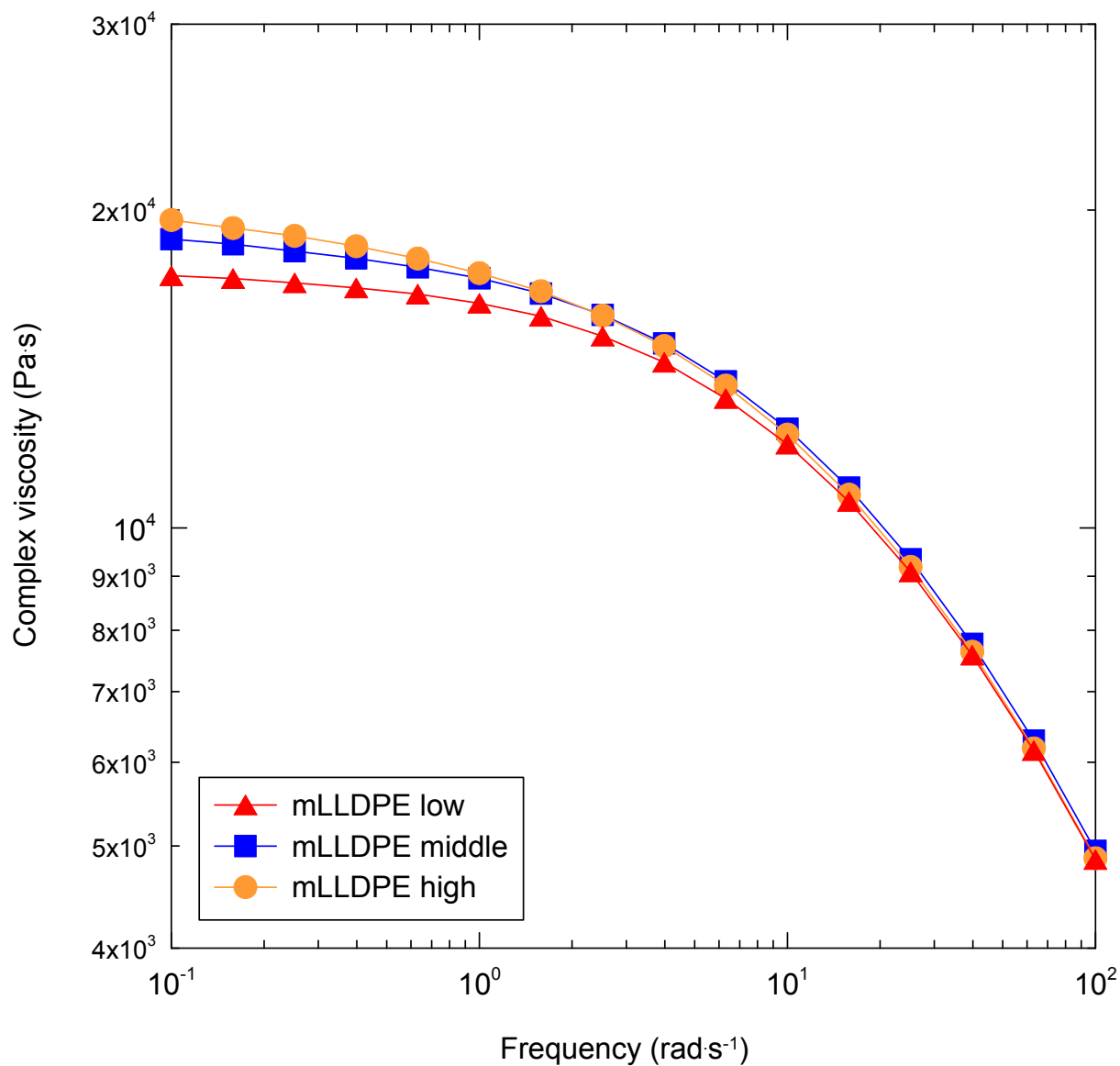


Figure 16. Complex viscosity data for three mLLDPEs having different levels of long chain branching obtained experimentally by ARES rotational rheometer at 140°C.

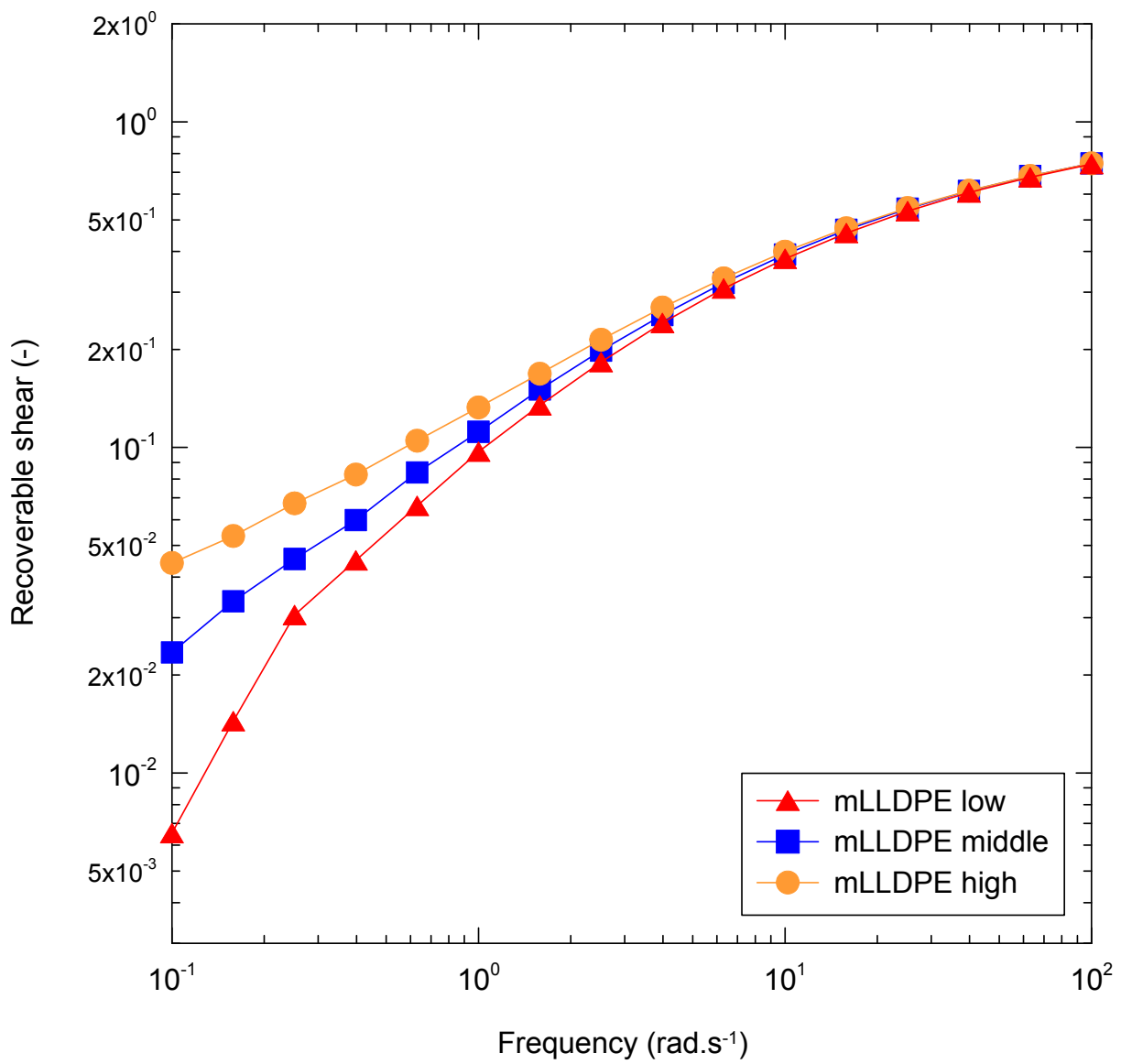


Figure 17. Recoverable shear data for three mLLDPEs having different levels of long chain branching obtained experimentally by ARES rotational rheometer at 140°C.

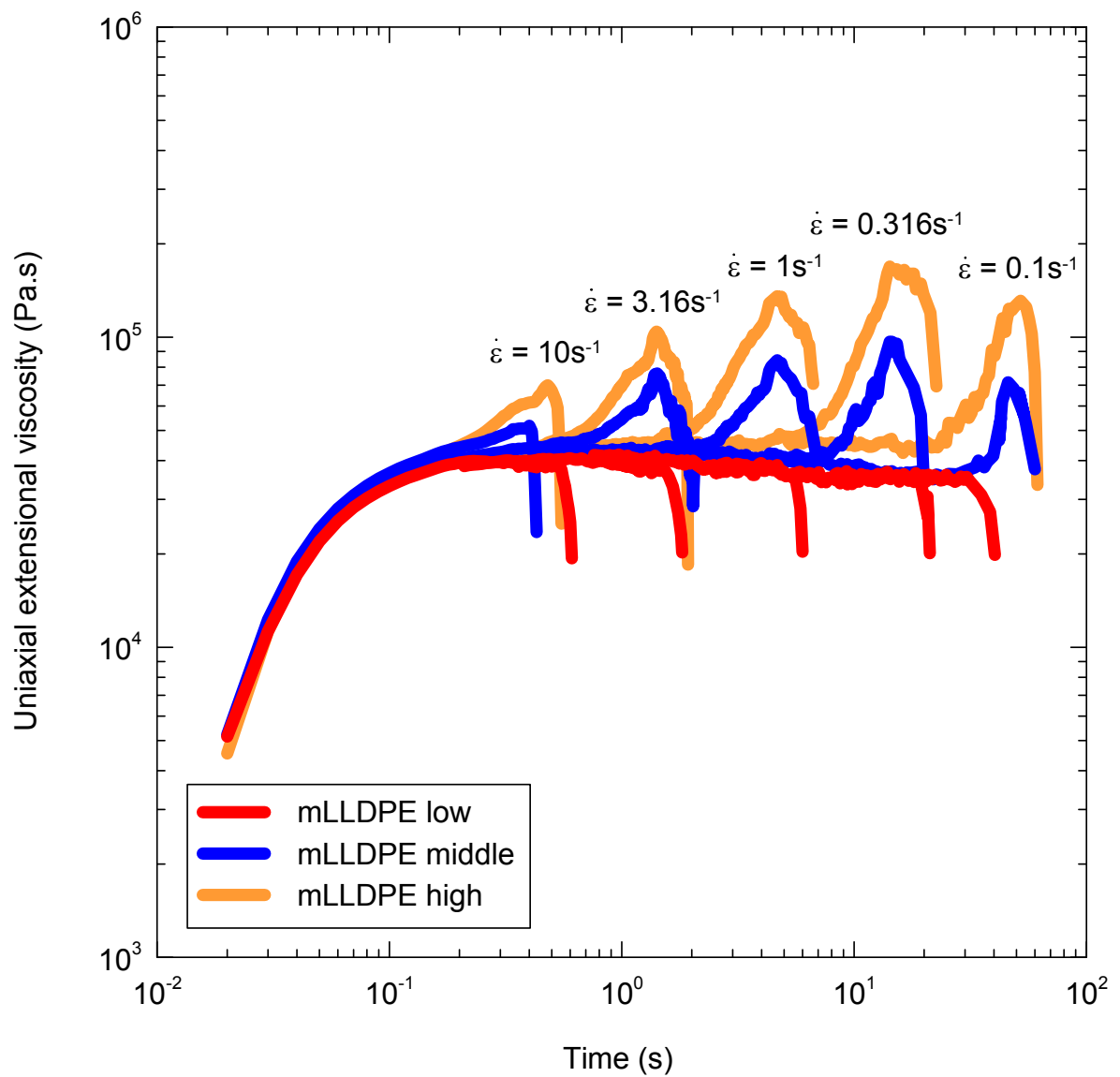


Figure 18. Time-dependent uniaxial extensional viscosity $\eta_E^+(t)$ data for three mLLDPEs having different levels of long chain branching obtained by SER at 140°C.

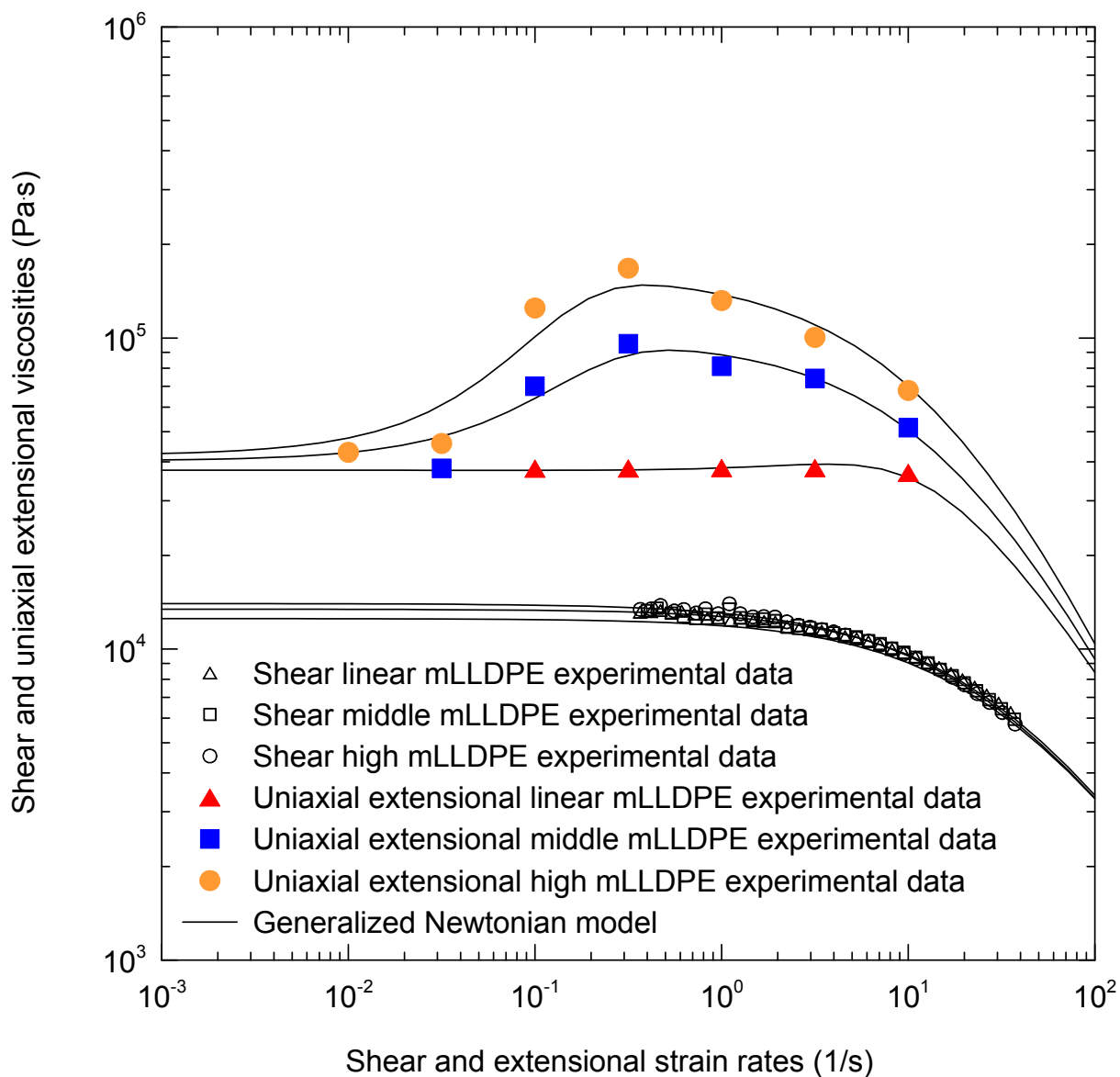


Figure 19. Comparison between the utilized generalized Newtonian model fits (solid lines) and measured shear and steady uniaxial extensional viscosities for all tested polymer samples.



Figure 20. Film blowing experimental set-up. 20a) General view of the experimental film blowing line; 20b) Closer view of the film blowing die; 20c) Used spiral mandrel; 20d) DSBMT barrier screw with a 24:1 L/D and barrier flighted with spiral Maddox mixer; 20e) Detail picture of the Maddox mixer (egan type).

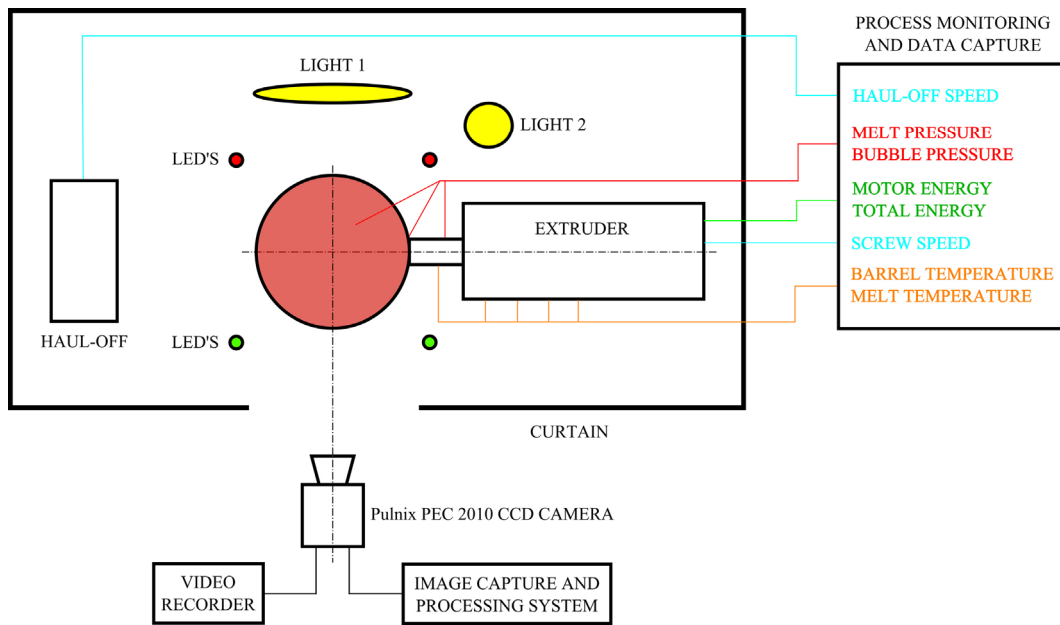


Figure 21. Schematic of the experimental setup for the film blowing stability analysis.

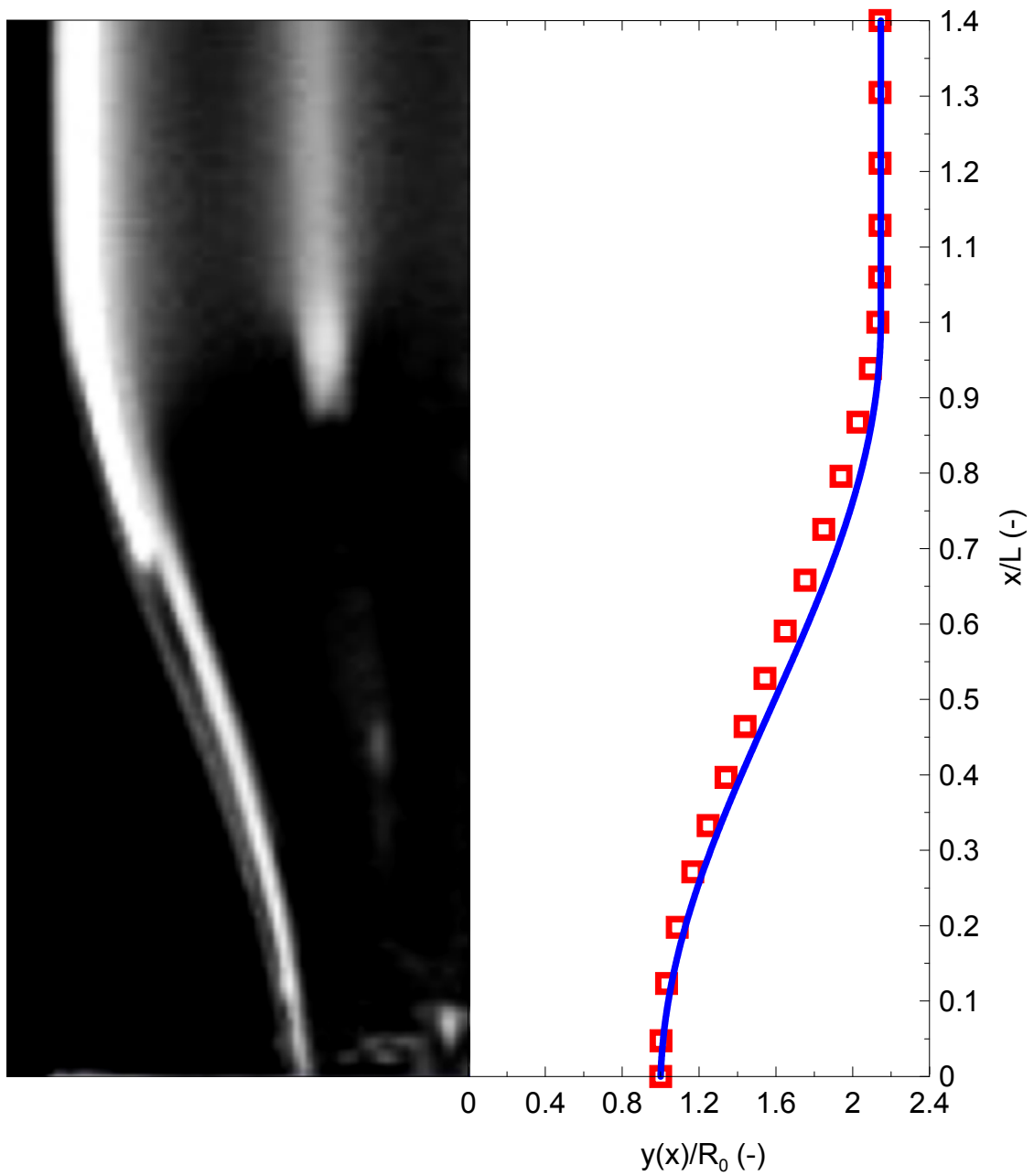


Figure 22. Comparison between experimental data (open symbols) and the model prediction (solid line) for linear mLLDPE low. Processing conditions are summarized in Table 6.

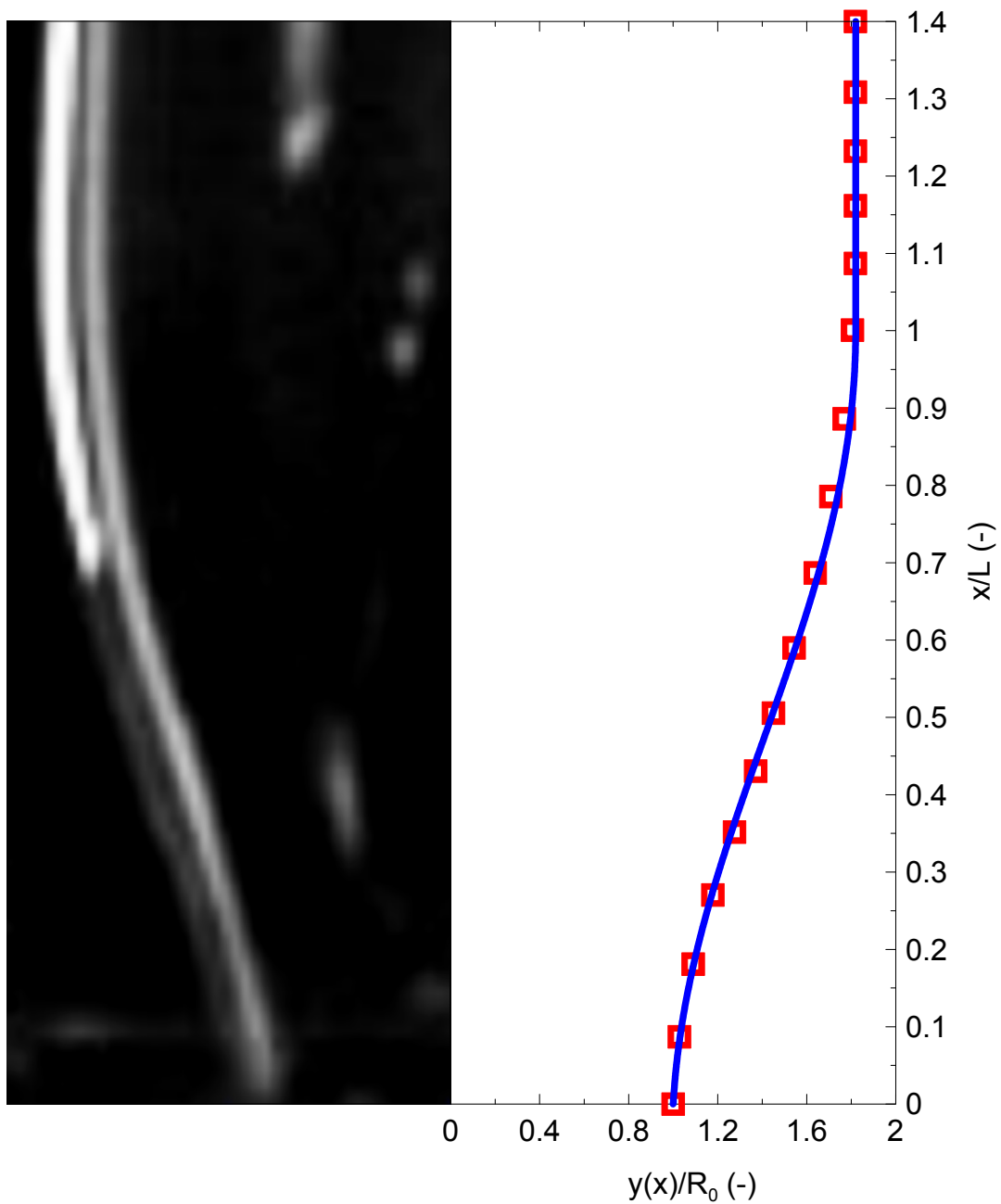


Figure 23. Comparison between experimental data (open symbols) and the model prediction (solid line) for slightly branched mLLDPE middle. Processing conditions are summarized in Table 6.

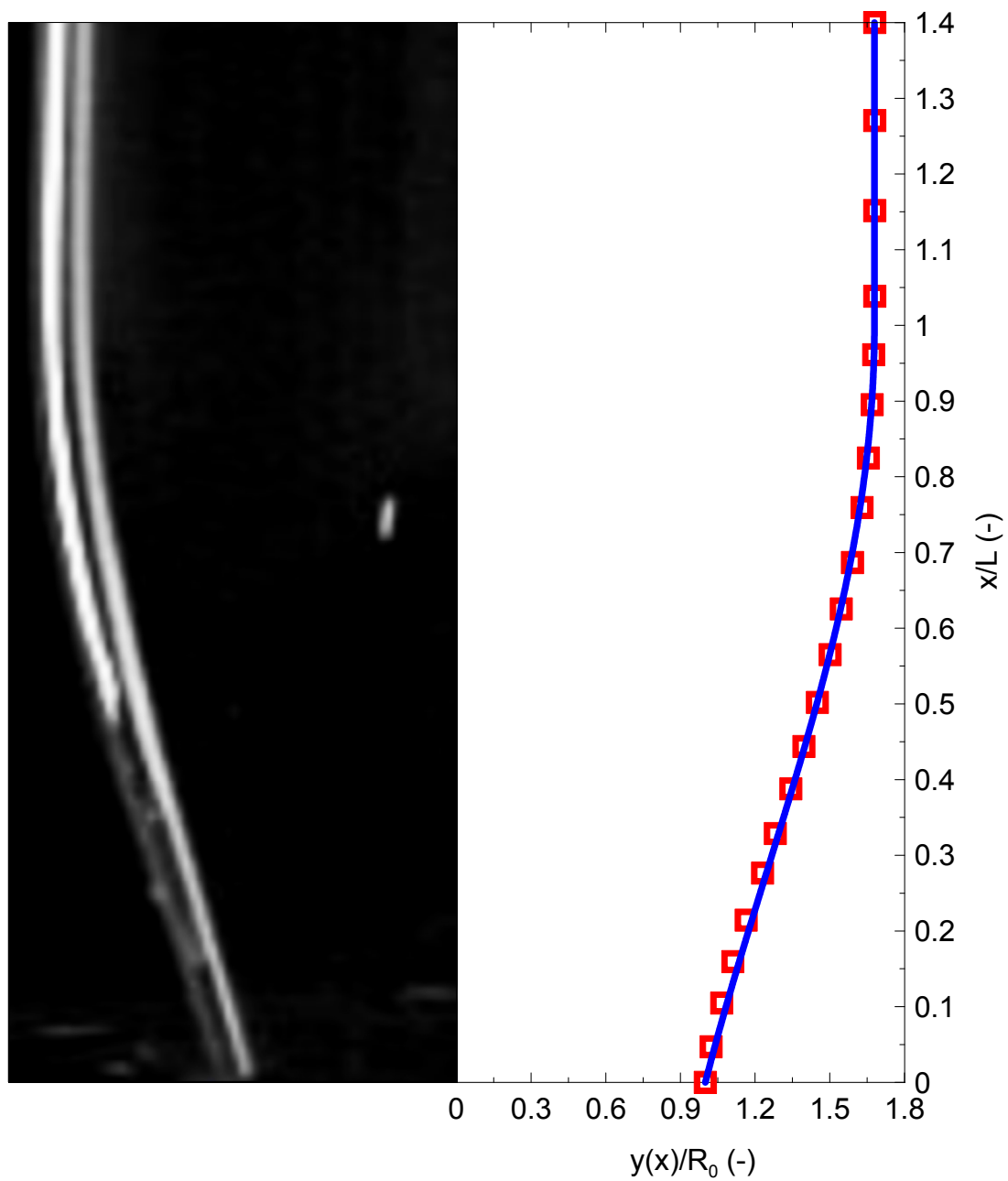


Figure 24. Comparison between experimental data (open symbols) and the model prediction (solid line) for highly branched mLLDPE high. Processing conditions are summarized in Table 6.

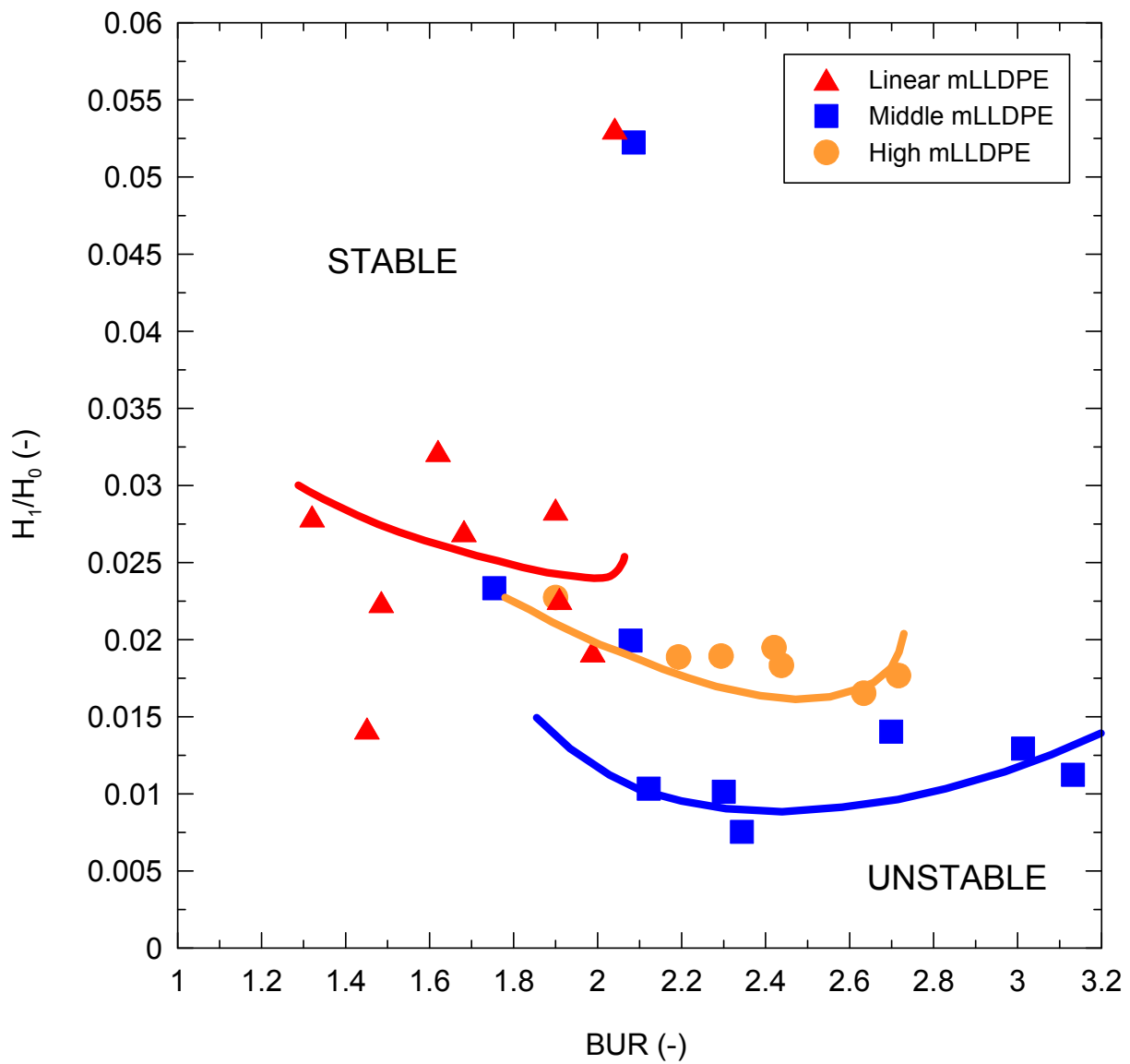


Figure 25. The experimentally determined stability contours for both, linear and branched metallocene LLDPE samples (freezeline height 0.18m and temperature 190°C).

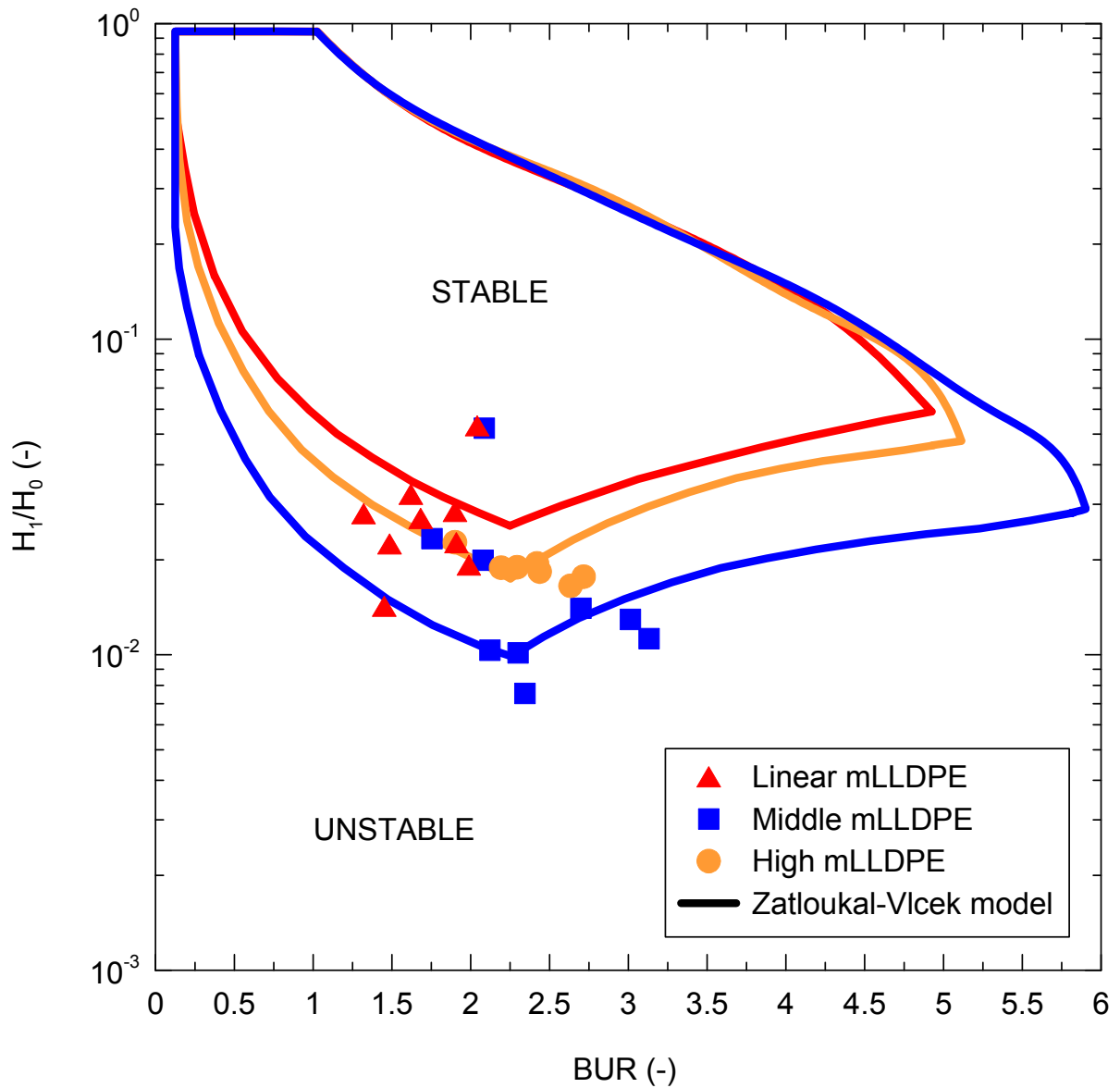


Figure 26. Comparison between experimentally determined stability points (full symbols) and theoretically predicted stability contours (solid lines). Processing parameters: freezeline height 0.18 m, cooling air temperature 25°C, linear mLLDPE mass flow rate 0.003258333 kg s⁻¹, middle mLLDPE mass flow rate 0.00223888 kg s⁻¹, high mLLDPE mass flow rate 0.00385 kg s⁻¹.

PAPER IV

Evaluation of the 9-Layer Film Blowing Process by using Variational Principles

Roman Kolarik^{1,2}, Martin Zatloukal^{1,2} *

*¹Centre of Polymer Systems, University Institute, Tomas Bata University in Zlin,
Nad Ovcirnou 3685, 760 01 Zlin, Czech Republic*

*²Polymer Centre, Faculty of Technology, Tomas Bata University in Zlin,
TGM 275, 762 72 Zlin, Czech Republic*

*Corresponding author: mzatloukal@ft.utb.cz

ABSTRACT

In this work, coextrusion experiments utilizing an industrial 9-layer Brampton Engineering coextrusion film blowing line for LDPE/LDPE/tie/PA6/EVOH/PA6/tie/LDPE/LDPE film production has been performed under different processing conditions (different air cooling intensity and mass flow rate) in order to evaluate variational principles based modeling approach for the multi-layer film blowing process. It has been revealed that the variational principle based model can describe the bubble shape and predict internal bubble pressure reasonably well for all applied processing conditions even if the multi-layer film has been viewed as the static elastic membrane characterized only by one material parameter - bubble compliance J , which was not allow to vary along the multi-layer bubble.

Keywords: Variational principle, Coextrusion, Multi-layer film blowing, Polymer, Modeling.

INTRODUCTION

Production of thin polymer films is mostly introduced by the film blowing process. Although this process is widely used, the single layer films do not reach specific properties required especially in a food packaging industry, such as barrier properties (low permeability to oxygen or carbon dioxide), heat-seal ability, high film strength, printability, adhesion and low costs [1-2]. All these properties are easily and economically achievable in multi-layer films produced by coextrusion.

In coextrusion (see Figure 1), two or more different polymer melts (having various rheological properties and temperatures) are extruded from individual extruders, through a coextrusion die, to a continuous tube which is cooled by an air ring and internal bubble cooling system, *IBC*, axially stretched by the take-up force, F , and circumferentially inflated by the internal bubble pressure, Δp , to required bubble dimensions. Then, above the freezeline height, the stable solidified bubble is folded by the collapsing frames and consequently drawn upward by the nip rolls to a wind-up roll. Then, the final lay-flat coextruded multi-layer film, which represents a combination of the best properties of each used polymers, can be applied for example in food packaging, medical and electronic industry. The most frequently used materials in coextrusion are polar barrier polymers, such as nylon (PA), ethylene vinyl alcohol (EVOH), polyvinyliden chloride (PVDC), and non-polar polyolefines, i.e. polyethylene (PE), polypropylene (PP), polystyrene (PS) [1-2].

In spite of a rapid growth of a blown film coextrusion in the last decades, the number of experimental and modeling studies of the multi-layer process is very limited. In 1978, Han and Shetty [3] experimentally and theoretically investigated blown film coextrusion of two polymers in various combinations, i.e. low density polyethylene (LDPE) with ethylene-vinyl acetate (EVA), LDPE with high density polyethylene (HDPE), LDPE with polypropylene (PP) and HDPE with EVA. Further, they performed a theoretical study where the experiment was theoretically analyzed by using a power-law non-Newtonian model included in a computational procedure predicting the number of layers, layer thickness and the volumetric flow rate compared with the experiment. Theoretical investigation of two-layer coextruded blown film was also studied by Yoon and Park [4] in 1992. In their work, considering isothermal

processing conditions, two film layers are described by a Newtonian and an Upper-Convected Maxwell fluid (UCM). In order to evaluate influence of viscous and viscoelastic forces on the flow mechanics of the process, the various flow rate ratio values of the fluids are applied for numerical determination of the bubble radius and the film thickness profiles. It was revealed, that in the case of the small relaxation time the flow mechanics of UCM layer is similar to a Newtonian single-layer. On the other hand, increasing relaxation time supports the viscoelasticity effect of the UCM layer leading to dominance of bubble dynamics. In 2000, Yoon and Park [5] performed a linear stability analysis of the above presented polymer system. It was observed that the critical film thickness decreases with increasing blow-up ratio which makes the process unstable. In more detail, in case of a Newtonian single-layer flow, there exists an upper unstable region where the bubble is unstable when the BUR is greater than a certain critical value. On the other hand by the presence of a thin viscoelastic layer this restriction can be removed resulting in enhanced stable area at higher values of BUR. In 2000, Stasiek [6] studied the heat transfer between three-layer blown film and cooling medium. In his work, mathematical model, estimating length of a cooling path and taking into account crystallization effect, was developed and used to describe the relationship between the temperature changes in each layer and the thermal energy. In 2005, Elkoun et al. [7] investigated effect of composition and layout of layers on end-use properties of a coextruded LLDPE five-layer blown film. For coextruded structure, a conventional Ziegler-Natta LLDPE gas phase butene copolymer, an advanced Ziegler-Natta LLDPE solution octene copolymer, and a single site LLDPE solution octene copolymer were used and compared with mono-layer blended film. It was observed, that combination of the LLDPE butene and the single site LLDPE in a five-layer coextruded film reveals improved tear resistance due to a presence of interfacial transcrystalline layers. Further, combination of coextruded single site LLDPE and the Ziegler-Natta octane copolymers leads to enhanced tear strength, too. Finally, significant haze reduction, caused by placing the single site LLDPE on the outside layers of the multi-layer films, was observed. In 2005, Gamache et al. [8] performed experimental and theoretical study evaluating stresses in a two-layer coextruded blown film of LDPE, ultra low density polyethylene (ULDPE),

LDPE/ULDPE and ULDPE/LDPE. Then, the axial and transverse stresses were experimentally measured under various processing conditions, which were then successfully compared with theoretically calculated ones by the non-isothermal Newtonian model. In 2007, Gururajan and Ogale [9] studied effect of coextrusion on the orientation and morphology of the coextruded films of PP and LDPE by using Raman spectroscopy. In the case of multi-layer films, no significant difference in overall molecular orientation of PP and LDPE was found. On the other hand, single-layer LDPE films indicated existence of some row-nucleation of crystals which was not observed in the LDPE layer in coextruded film. In 2009, a 2-D model describing non-isothermal two-layer blown film process was developed by Xu and McHugh [10]. This model is based on the 1-D model of Henrichsen and McHugh [11] taking to account viscoelasticity and flow-enhanced crystallinity. The 2-D model presents numerical results showing influence of the rheological, thermal and crystallization properties on the crystallinity development and stresses in particular layers. It was observed, that the individual layers of the same materials contain significantly different stresses due to the temperature difference. Further, different material properties in a certain layer affect stresses and crystallinity in its own layer as well as in another layer through heat transfer. Finally, stresses and semi-crystalline phase orientation at the freezeline, i.e. final film properties, are affected by the layer arrangement.

As can be seen from the literature overview, the number of theoretical studies of the multi-layer film blowing process is rather rare, considering maximally 3 layers and laboratorial processing conditions only due to extremely high mathematical and rheological complexity of the problem. Due to this, the multi-layer film blowing process for high number of layers and industrial processing conditions is not fully understood yet. Recently, it has been found that utilization of the variational principle based single-layer film blowing process modeling leads to very stable numerical schemes allowing qualitative as well as quantitative description of the experimental reality [12-17]. The main goal of this work is to investigate whether it is possible to utilize the variational principles based modeling approach for the multi-layer film

blowing process. For the model validation purposes, industrial 9 layer film blowing line has been utilized to produce multi-layer bubbles under different processing conditions.

MATHEMATICAL MODELING

Zatloukal-Vlcek Formulation

The variational principle based Zatloukal-Vlcek formulation [12] describes a stable film blowing process as a state when the bubble shape satisfies minimum energy requirements. In more detail, the bubble during blowing is viewed as a bended elastic membrane due to the internal load, p , and the take-up force, F , (see Figure 2), considering that the membrane potential energy, E_p , takes into account both, elastic strain energy increase and negative work done by the applied load:

$$E_p = \frac{F}{2} \int_0^L (y')^2 dx - p \int_0^L y dx \quad (1)$$

Having the bubble volume, $V = \pi \int_0^L y^2 dx$, as the main geometrical constrain, the equation for the bubble shape, y , can be derived through minimization of the potential energy functional, I , in the following form:

$$I = \left[\frac{1}{2} F (y')^2 - p y \right] + \lambda_1 (\pi y^2) \quad (2)$$

i.e., $I = f(x, y, y')$ where λ_1 is the Lagrange multiplier. The functional I is minimized if the following equation is satisfied:

$$\frac{\partial I}{\partial y} - \frac{\partial}{\partial x} \frac{\partial I}{\partial y'} = 0 \quad (3)$$

Eqs. (2) and (3) yield the following differential equation:

$$F y'' - \frac{1}{J} y + p = 0 \quad (4)$$

where J is the compliance of the membrane defined as positive constant taking the following form:

$$J = \frac{1}{2\pi\lambda_1} \quad (5)$$

The following boundary conditions for the bubble shape can be considered:

$$\frac{\partial y(x=L)}{\partial x} = 0, \quad y(x=0) = R_0 \quad (6)$$

and

$$y(x=L) = R_0 BUR \quad (7)$$

where R_0 is the extrusion die radius, L the freezeline height, which represents transition between the liquid and solid phases where no bubble deformation above this height is assumed, BUR the blow-up ratio defined as a ratio of the final bubble diameter at the freezeline height to the die diameter and $R_0 BUR$ is the bubble radius at the freeze line, i.e. $x=L$. Since above the freezing line there is no deformation, it can be assumed that $y(x>L) = const. = y(x=L)$. It is not difficult to show (see reference [12] for detailed derivation) that the solution of Eq. (4), considering the above mentioned boundary conditions, takes the following form:

$$y = (R_0 - pJ) \cos\left(\frac{x\varphi}{L}\right) - \alpha'(pJ - BURR_0) \sin\left(\frac{x\varphi}{L}\right) + pJ, \quad x \in \langle 0; L \rangle \quad (8)$$

where the take-up force F is given by the following expression:

$$F = -\frac{L^2}{J\varphi^2} \quad (9)$$

Here α' and A are given below and the value of $\varphi(A)$ is calculated according to Table 1:

$$\alpha' = \sqrt{\frac{2pJ - R_0 - BURR_0}{pJ - BURR_0} \left| \frac{R_0(BUR - 1)}{pJ - BURR_0} \right|} \quad (10)$$

$$A = \frac{pJ - R_0}{pJ - BURR_0} \quad (11)$$

The total number of parameters needed to describe the bubble shape, y , is equal to four (pJ , L , R_0 , BUR). It should be noted that the total deformation (curvature) of the bubble is determined according to the pJ/R_0 value (dimensionless form of pJ expressing relationship between the external load, membrane compliance and deformation).

According to [12], the internal bubble pressure and the take-up force for a 3D bubble can be directly calculated from parameters of the proposed model and the force balance by taking the 3D nature of a real bubble into account through following equations:

$$\Delta p = \frac{pL}{2\pi \int_0^L y \sqrt{1 + (y')^2} dx} \quad (12)$$

$$F_{\text{total}} = |F| \quad (13)$$

where the term $2\pi \int_0^L y \sqrt{1 + (y')^2} dx$ in Eq. (12) means the bubble surface and the term pL is the force acting in the thickness direction of the bubble, $F_{\text{thickness}}$. Eq. (12) represents the calculation of the internal bubble pressure in such a way that the bubble is represented by an equivalent cylinder, which has the same surface as the real bubble. Force F in Eq. (13) is defined by Eq. (9).

EXPERIMENTAL

In this work, coextrusion experiments were carried out on an industrial 9-layer Brampton Engineering coextrusion film blowing line (Figure 3 and 4) equipped with a 350 mm diameter flat spiral dies ($R_0 = 0.1626$ m) with a die gap of 2.032 mm ($H_0 = 0.002032$ m). During the process, the bubble was cooled by an air ring as well as by an internal bubble cooling system. The coextruded structure was LDPE/LDPE/tie/PA6/EVOH/PA6/tie/LDPE/LDPE with following layer thicknesses: 17.5 % for LDPE, 5% for tie, 5% for PA6 and 10% for EVOH. In all experiments, the following parameters were kept to be constant: die exit temperature, $T_{\text{die}} = 250^\circ\text{C}$, overall film thickness (gauge), $H_1 = 100$ μm , (which corresponds to draw-down ratio $DDR = 11.17$), blow-up ratio, $BUR = 1.8$, and lay-flat film, 1000 mm. During the experimental work, firstly, different bubble cooling intensity was applied at the constant overall mass flow rate, 300 kg/h, (i.e. constant line speed 25.9 m/min) and secondly, overall mass flow rate was varied from 225 kg/h to 375 kg/h (i.e. from 19.4 m/min to 32.3 m/min for the line speed) by keeping the bubble cooling intensity the same.

For given processing conditions, the bubble shape was monitored by the EOS digital SLR photo camera Canon EOS 450D model (Canon, Inc., Japan) with resolution of 12.2 Mpx equipped with Canon lens EF-S 18-55mm f/3.5-5.6 IS whereas the average bubble temperature was measured by the heat gun, model camera: INFRACAMTM using calibration site FLIR SYSTEM, AB SWEDEN and corresponding software (ThermaCAM QuickReport 1.0).

RESULTS AND DISCUSSION

At the beginning, three unknown film blowing model parameters L , BUR and pJ (for the known die radius $R_0 = 0.1626$ m) were determined by the least square minimization method through application of Eq. (8) on all experimentally obtained bubble shapes and they are summarized in Table 2. In order to calculate the take-up force and the internal bubble pressure for given processing conditions, p and J parameters were separated from the particular pJ value in the same way as described in [12] i.e. parameter J (which is viewed as constant characterizing the bubble compliance) was determined from pJ value for one reference processing conditions for which the load p was chosen to get equal predicted and measured internal bubble pressure. The reference processing conditions are provided in the second column of Table 2.

The comparison between the experimentally determined bubble shape and internal bubble pressure for all tested processing conditions are summarized in Figures 5-8 and Table 2, respectively, and as it can be seen, the agreement between the measured data and model predictions is very good. In more detail, the model can describe the bubble shape and predict internal bubble pressure reasonably well for both, decreased freeze line height and the bubble curvature due to increased air cooling intensity or decreased mass flow rate under highly non-isothermal conditions, which are quantified through average bubble temperature measurements in Figures 9 and 10, even if the assumption about the constant bubble compliance J along the multi-layer bubble has been used. This suggests, that the variational principle based modeling approach proposed in [12] can be used and explored for the multi-layer film blowing process in the similar way as shown in [12] for single-layer film blowing process. Moreover, it is believed, that such theoretical approach can be used to understand complex heat transfer and crystallization effects occurring in multi-layer film blowing process resulting in highly non-linear average temperature profile along the multi-layer bubble, depicted in Figures 11 and 12 for the studied experimental conditions, which is not the case of the single-layer film blowing process at which the average temperature profile along the bubble is strictly linear as shown in [18-25].

CONCLUSION

In this work, coextrusion experiments utilizing an industrial 9-layer Brampton Engineering coextrusion film blowing line for LDPE/LDPE/tie/PA6/EVOH/PA6/tie/LDPE/LDPE film production has been performed under different processing conditions (different air cooling intensity and mass flow rate) in order to evaluate variational principles based modeling approach for the multi-layer film blowing process.

It has been revealed that the variational principle based model can describe the bubble shape and predict internal bubble pressure reasonably well for both, decreased freeze line height and the bubble curvature due to increased air cooling intensity or decreased mass flow rate under highly non-isothermal conditions even if the multi-layer film has been viewed as the static elastic membrane characterized only by one material parameter - bubble compliance J , which was not allow to vary along the bubble. Thus, it is believed, that the variational principle based modeling approach can be used and explored for the multi-layer film blowing process to understand complex rheological, heat transfer and crystallization phenomena occurring in multi-layer film blowing process with respect to process stability and final film properties.

ACKNOWLEDGMENTS

The authors wish to acknowledge the Grant Agency of the Czech Republic (grant No. P108/10/1325) for the financial support. This article was written with support of Operational Program Research and Development for Innovations co-funded by the European Regional Development Fund (ERDF) and national budget of Czech Republic, within the framework of project Centre of Polymer Systems (reg. number: CZ.1.05/2.1.00/03.0111).

The authors would also like to thank Brampton Engineering Inc. which allows us to perform all experimental work on their complete commercial size 9-layer AeroFrost air cooled blown film line.

REFERENCES

- [1] CANTOR, K. *Blown Film Extrusion*. Munich: Carl Hanser Verlag, 2006. ISBN 3-446-22741-5.
- [2] BUTLER, T.I. *Film Extrusion Manual: Process, Materials, Properties*. Atlanta: Tappi Press, 2005. ISBN 1-59510-075-X.
- [3] HAN, C.D., SHETTY, R. Studies on Multilayer Film Coextrusion III. The Rheology of Blown Film Coextrusion. *Polym. Eng. Sci.* 1978, vol. 18, no. 3, pp. 187-199.
- [4] YOON, K.-S., PARK, C.-W. Analysis of Isothermal Two-layer Blown Film Coextrusion. *Polym. Eng. Sci.* 1992, vol. 32, no. 23, pp. 1771-1777.
- [5] YOON, K.-S., PARK, C.-W. Stability of a Two-layer Blown Film Coextrusion. *J. Non-Newtonian Fluid Mech.* 2000, vol. 89, no.1-2, pp. 97-116.
- [6] STASIEK, J. Review of a Mathematical Treatment of the Heat Transfer in Multi-layer Film Blowing. *Prog. Rubber Plast. Recycl. Technol.* 2000, vol. 16, no. 3, pp. 183-192.
- [7] ELKOUN, S., HUNEAULT, M.A., McCORMICK, K., PUTERBAUGH, F., KALE, L. LLDPE-based Mono- and Multilayer Blown Films: Property Enhancement Through Coextrusion. *Polym. Eng. Sci.* 2005, vol. 45, no. 9, pp. 1222-1230.
- [8] GAMACHE, E., AGASSANT, J.-F., DEMAY, Y., LAFLEUR, P.G. Evaluation of Stresses in a Two-layer Co-extruded LDPE Melt Blown Film. *J. Plast. Film Sheeting* 2005, vol. 21, no. 2, pp. 127-144.
- [9] GURURAJAN, G., OGALE, A.A. Effect of Coextrusion on PP/LDPE Bicomponent Blown Films: Raman Spectroscopy for Real-time Microstructural Measurements. *J. Plast. Film Sheeting* 2007, vol. 23, no. 1, pp. 37-49.
- [10] XU, F., McHUGH, A.J. A Model for the Two-layer Blown Film Process with Flow-enhanced Crystallization. *Chem. Eng. Sci.* 2009, vol. 64, no. 22, pp. 4787-4795.
- [11] HENRICHSEN, L.K., McHUGH, A.J. Analysis of Film Blowing with Flow-enhanced Crystallization: part 1. Steady-state Behavior. *Int. Polym. Proc.* 2007, vol. 22, no. 2, pp. 179-189.

- [12] ZATLOUKAL, M., VLCEK, J. Modeling of the Film Blowing Process by using Variational Principles. *J. Non-Newton. Fluid Mech.* 2004, vol. 123, no. 2-3, pp. 201-213.
- [13] KOLARIK, R., ZATLOUKAL, M. Modeling of Non-Isothermal Film Blowing Process for Non-Newtonian Fluids by Using Variational Principles. *J. Appl. Polym. Sci.* 2011, vol. 122, no. 4, pp. 2807-2820.
- [14] KOLARIK, R., ZATLOUKAL, M. Modeling of non-isothermal film blowing process for polyolefines by using variational principles. *AIP Conference Proceedings* 2009, vol. 1152, pp. 251-269.
- [15] ZATLOUKAL, M., KOLARIK, R. Non-Isothermal Film Blowing Process Stability Analysis by using Variational Principles. *Annual Technical Conference - ANTEC, Conference Proceedings* 2009, vol. 3, pp. 1587-1595.
- [16] ZATLOUKAL, M., KOLARIK, R. Modeling of Non-Isothermal Film Blowing Process for Non-Newtonian Fluids by using Variational Principles. *Annual Technical Conference - ANTEC, Conference Proceedings* 2011, vol. 2, pp. 1317-1322.
- [17] KOLARIK, R., ZATLOUKAL, M. Variational Principle Based Stability Analysis of Non-Isothermal Film Blowing Process for Non-Newtonian Fluids. *AIP Conference Proceedings* 2011, vol. 1375, pp. 56-74.
- [18] WAGNER, M.H. Ein Rheologisch-thermodynamisches Prozessmodell des Folien-blasverfahrens. *Ph.D. Thesis*, IKT Stuttgart, 1976.
- [19] FISHER, E. Ein Rheologisches Modell zur Beschreibung der Produktqualität bei der Verarbeitung von Hochdruckpolyethylen. *Ph.D. Thesis*, IKT Stuttgart, 1983.
- [20] CAO, B., SWEENEY, P., CAMPBELL, G.A. Simultaneous Surface and Bulk Temperature Measurement of Polyethylene during Film Blowing. *J. Plast. Film Sheeting* 1990, vol. 6, no. 2, pp. 117-130.
- [21] KANAI, T., WHITE, J.L. Kinematics, Dynamics and Stability of the Tubular Film Extrusion of Various Polyethylenes. *Polym. Eng. Sci.* 1984, vol. 24, no. 15, pp. 1185-1201.

- [22] AST, W. Extrusion von Schlauchfolien. Theoretische und experimentelle Untersuchungen des Abkühlvorganges. *Ph.D. Thesis*, IKT Stuttgart, 1976.
- [23] MUSLET, I.A., KAMAL, M.R. Computer Simulation of the Film Blowing Process Incorporating Crystallization and Viscoelasticity. *J. Rheol.* 2004, vol. 48, no. 3, pp. 525-550.
- [24] BEAULNE, M., MITSOULIS, E. Effect of Viscoelasticity in the Film-Blowing Process. *J. Appl. Polym. Sci.* 2007, vol. 105, no. 4, pp. 2098-2112.
- [25] SARAFRAZI, S. SHARIF, F. Non-Isothermal Simulation of the Film Blowing Process Using Multi-Mode Extended Pom-Pom Model. *Int. Polym. Proc.* 2008, vol. 23, no. 1, pp. 30-37.

LIST OF SYMBOLS

A	Zatloukal-Vlcek model function	1
BUR	Blow-up ratio	1
dx	Element length in x direction	m
E_p	Membrane potential energy	J
F, F_{total}	Take-up force	N
$F_{\text{thickness}}$	Force acting in the thickness direction of the bubble	N
H_0	Bubble thickness at the die exit	m
H_1	Bubble thickness at the freezeline height	m
J	Membrane compliance	Pa ⁻¹
I	Potential energy functional	N
L	Freezeline height	m
L_{CRH}	Cooling ring height	m
\dot{m}	Mass flow rate	kg·s ⁻¹
p	Internal load	Pa·m
R_0	Inner die radius	m
r_f	Bubble radius at the freezeline height	m
$r(x)$	Local bubble radius	m
TUR	Take-up ratio	1
V	Bubble volume	m ³
v_{die}	Bubble velocity at the die exit	m·s ⁻¹
v_f	Bubble velocity at the freezeline	m·s ⁻¹
x	Particular distance from the die exit	m
$y(x), y$	Local bubble radius	m

Greek symbols

α'	Zatloukal-Vlcek model function	1
Δp	Internal bubble pressure	Pa
Δp_{exp}	Experimentally measured internal bubble pressure	Pa
Δp_{calc}	Predicted internal bubble pressure	Pa

λ_1	Lagrange multiplier	Pa
π	Ludolf's number	1
φ	Zatloukal-Vlcek model function	1

Table 1. Parameters A and φ for different bubble shapes (y) [12].

<i>Equation</i>	A	φ	y
1.	1	0	R_0
2.	$0 < A < 1$	$\arctan \left(\frac{\sqrt{1 - A^2}}{A} \right)$	The form of Eq. (8).
3.	0	$\pi/2$	$R_0 \left\{ 1 - \sin \left(\frac{x\pi}{2L} \right) (1 - BUR) \right\}$
4.	$-1 < A < 0$	$\pi + \arctan \left(\frac{\sqrt{1 - A^2}}{A} \right)$	The form of Eq. (8).
5.	-1	π	$\frac{R_0}{2} \left\{ 1 + \cos \left(\frac{x\pi}{L} \right) (1 - BUR) + BUR \right\}$

Table 2. Summarization of the model parameters and model predictions (by keeping the bubble compliance J the same for all the cases equal to $0.00028221 \text{ Pa}^{-1}$) for all tested processing conditions including the measured value of the internal bubble pressure Δp_{exp} .

<i>Air ring</i>	Low cooling 300 kg/h	High cooling 300 kg/h	High cooling 225 kg/h	High cooling 375 kg/h
<i>BUR</i> (-)	1.79554	1.79934	1.82050	1.77169
<i>pJ/R₀</i> (-)	1.06416160	1.35021986	1.41020	1.1500010
<i>L</i> (m)	0.7570395	0.5530498	0.4469456	0.7038099
Δp_{exp} (Pa)	489.05	489.05	684.67	684.67
Δp_{calc} (Pa)	417.89	489.05	554.07	390.38
<i>F</i> (N)	738.17	178.37	72.74	533.13

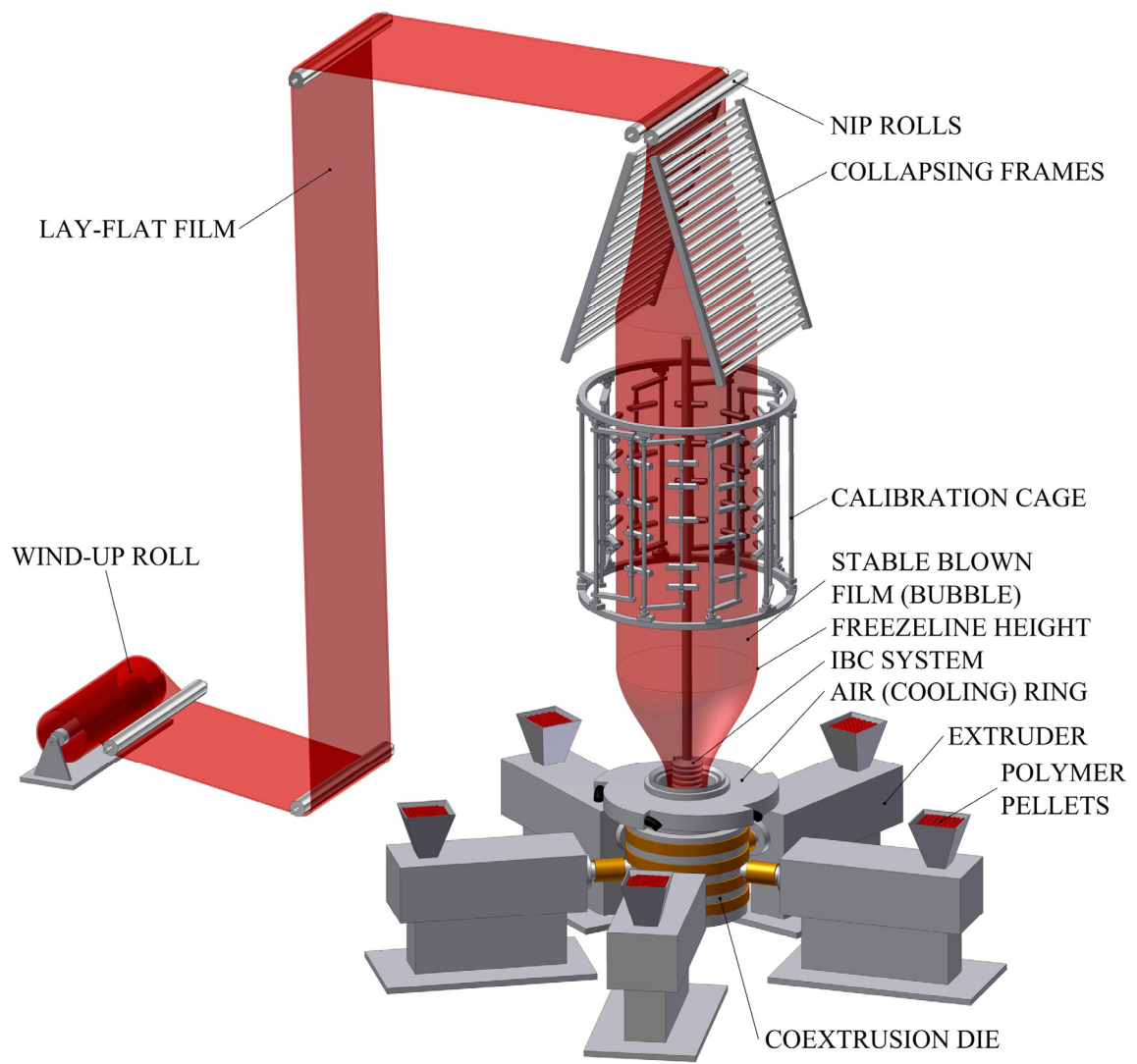


Figure 1. Sketch of the multi-layer film blowing line.

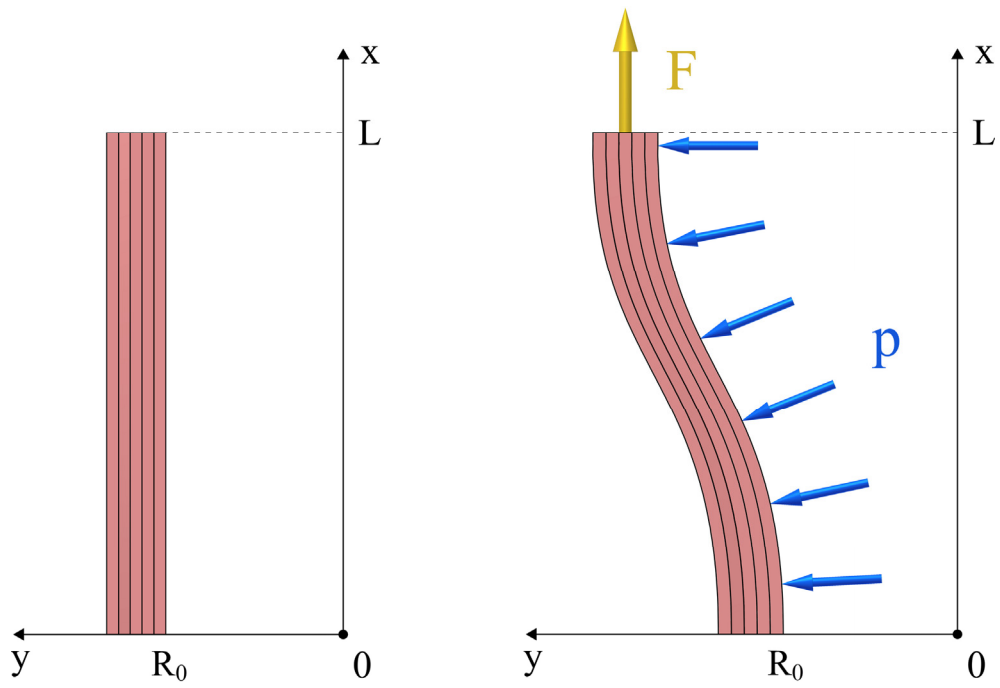


Figure 2. Multi-layer membrane before deformation (left), multi-layer membrane after deformation (right).

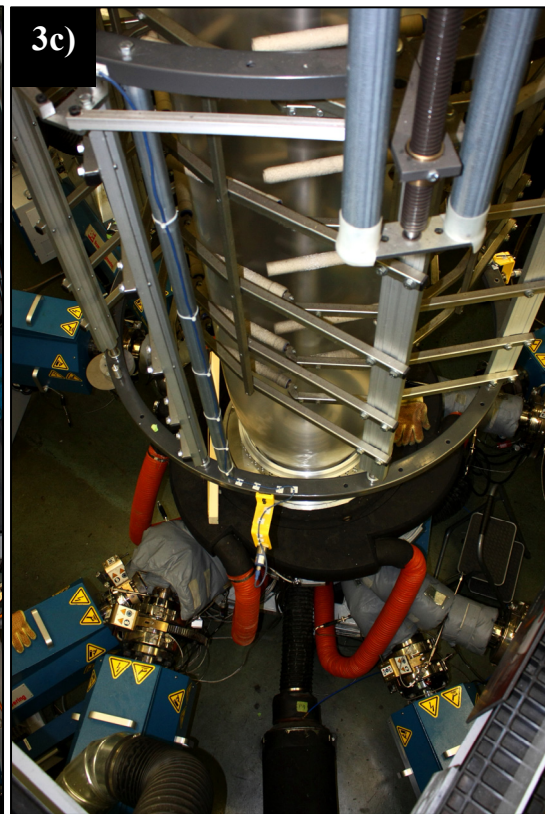
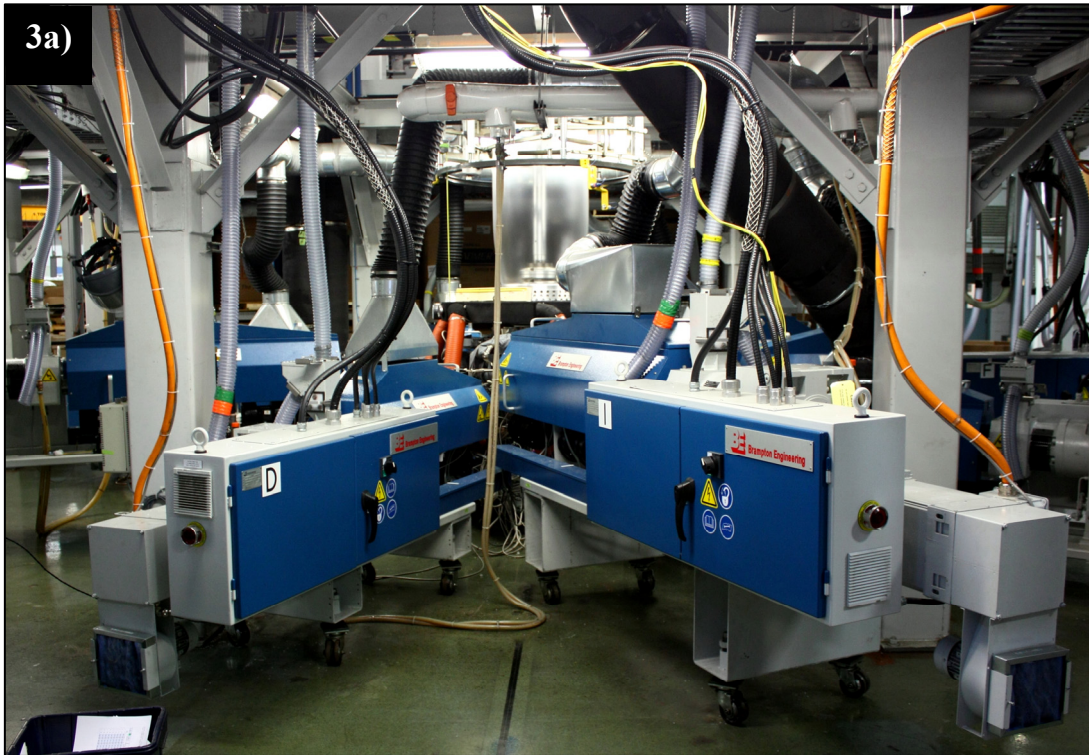


Figure 3. Brampton Engineering 9-layer air cooled blown film line.

3a) and 3b) Side view. **3c)** Top view.



Figure 4. Detail view of the 9-layer film formation at Brampton Engineering multi-layer die exit region including the scale for precise bubble shape determination by using digital image analysis.

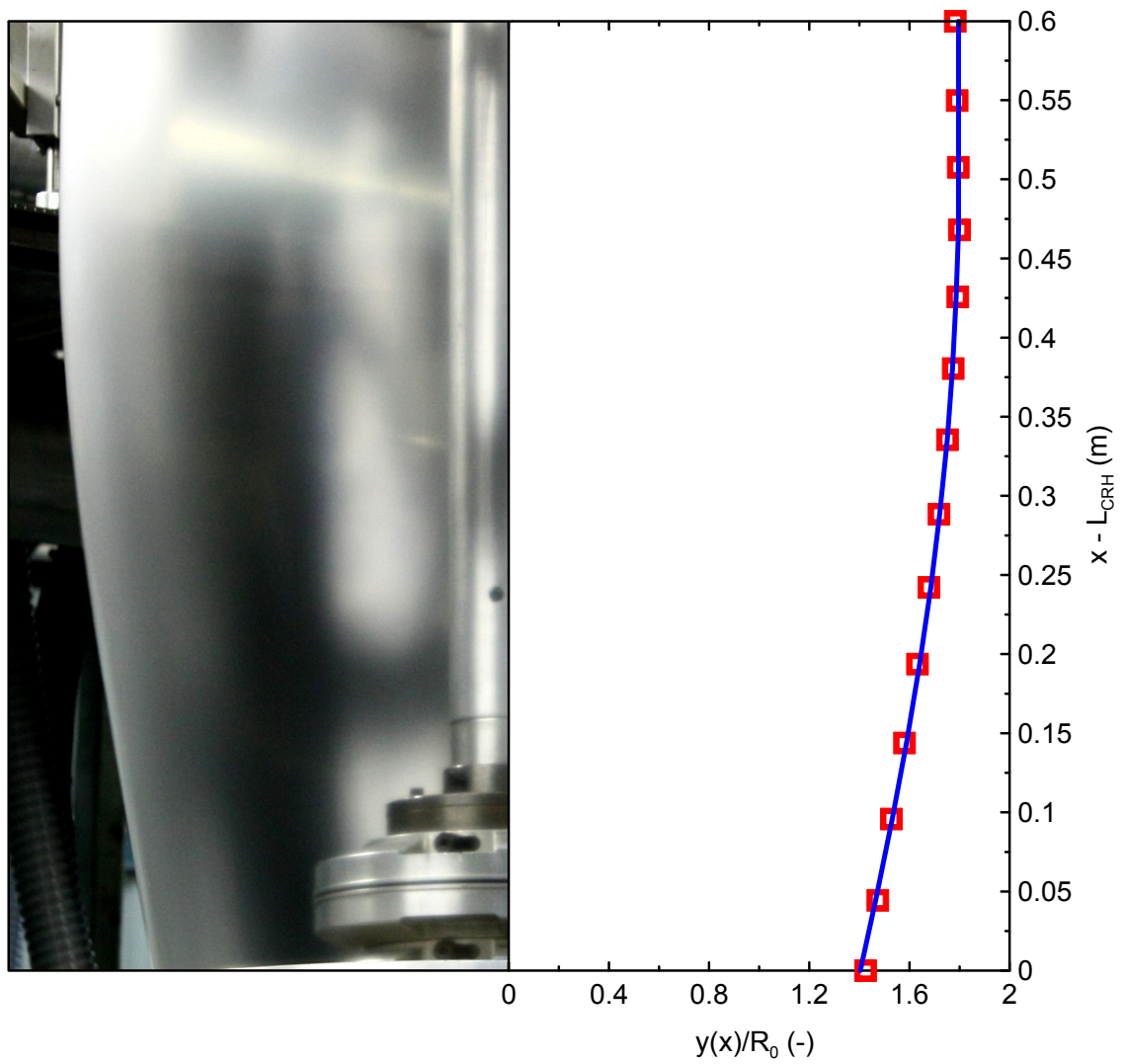


Figure 5. Comparison between experimentally determined multi-layer bubble shape (open symbols) and model prediction (line) for low air cooling processing conditions and mass flow rate equal to 300 kg/h (cooling ring height, $L_{CRH} = 0.26$ m).

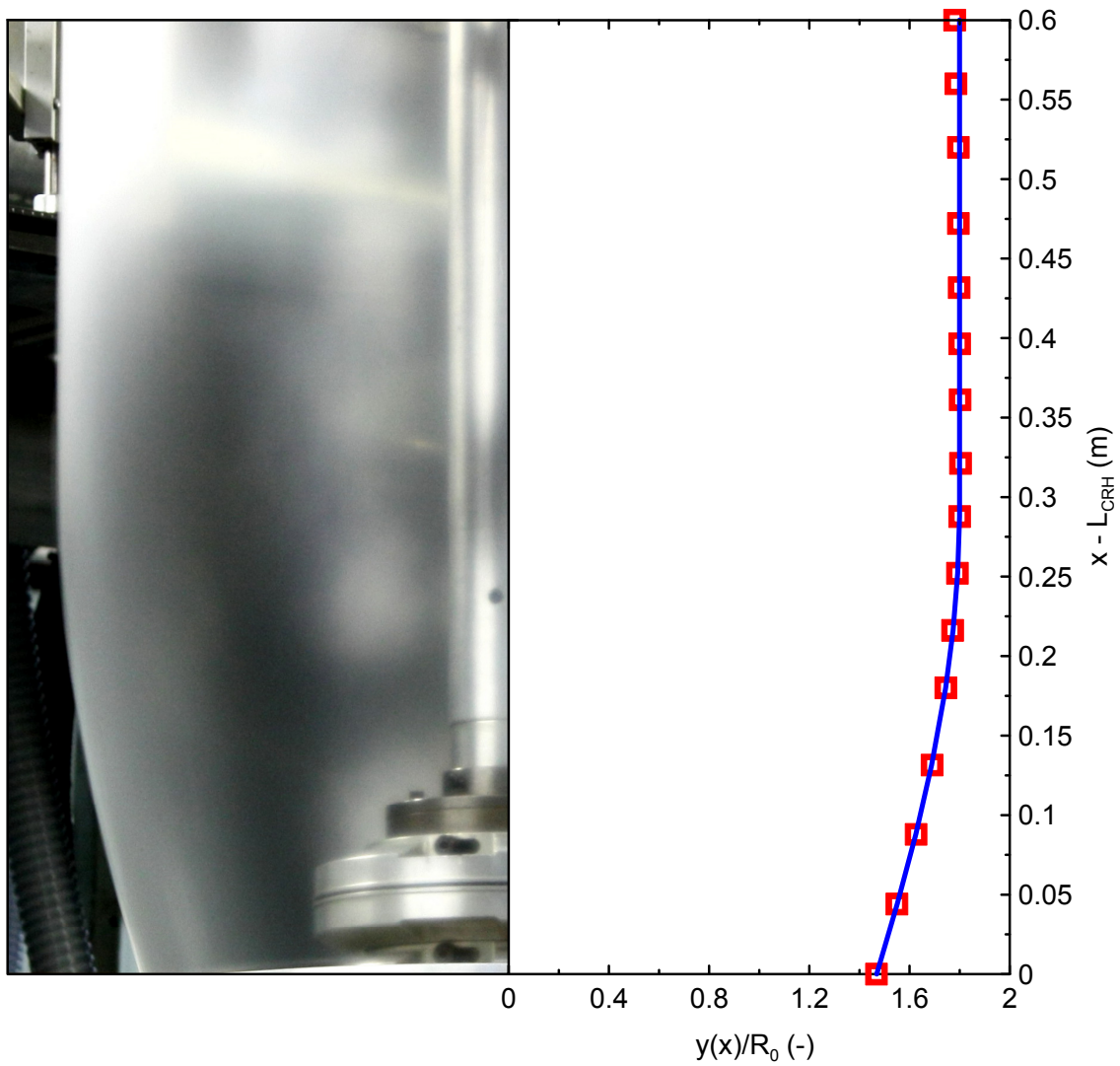


Figure 6. Comparison between experimentally determined multi-layer bubble shape (open symbols) and model prediction (line) for high air cooling processing conditions and mass flow rate equal to 300 kg/h (cooling ring height, $L_{CRH} = 0.26$ m).

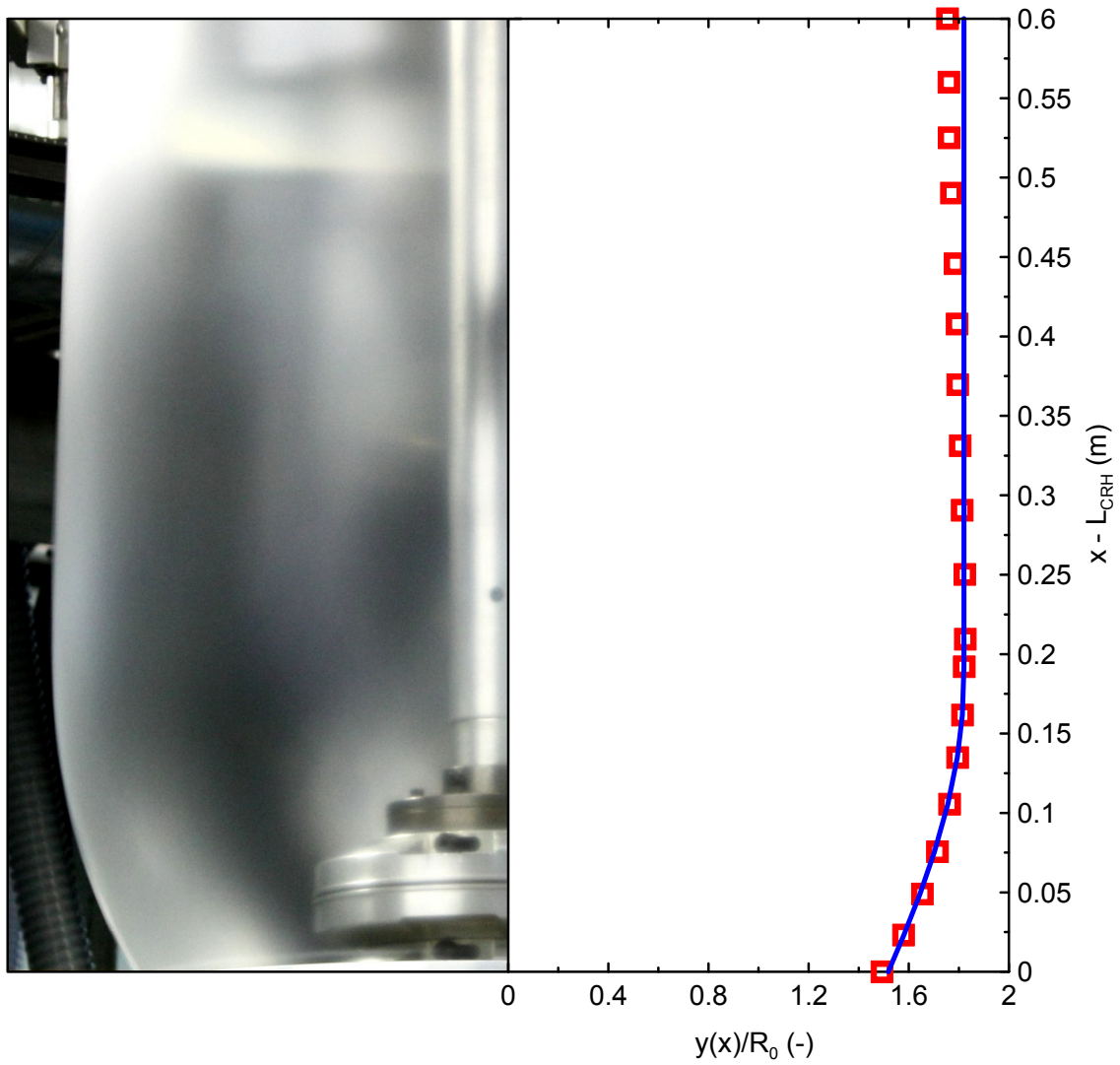


Figure 7. Comparison between experimentally determined multi-layer bubble shape (open symbols) and model prediction (line) for high air cooling processing conditions and mass flow rate equal to 225 kg/h (cooling ring height, $L_{CRH} = 0.26$ m).

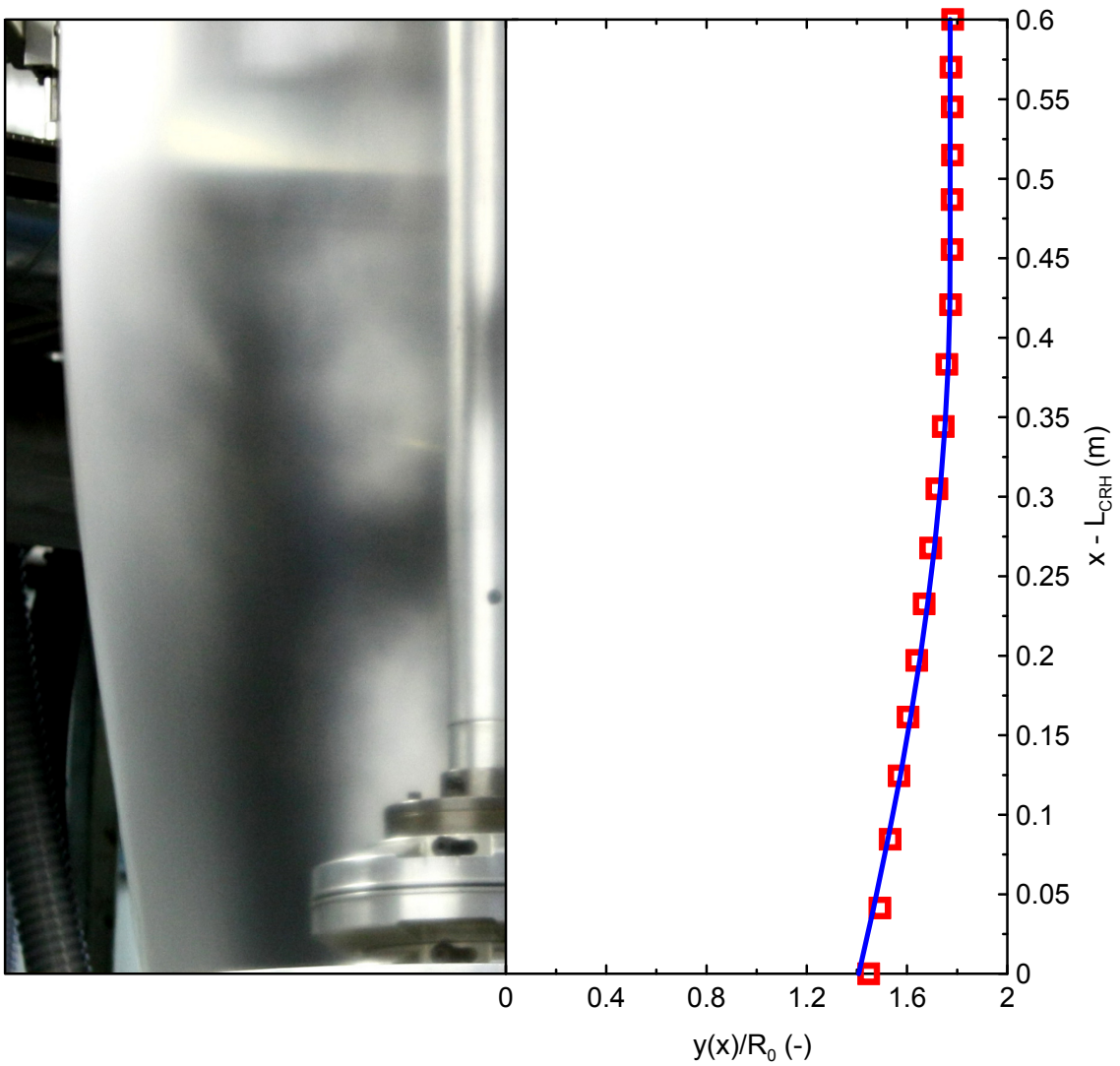


Figure 8. Comparison between experimentally determined multi-layer bubble shape (open symbols) and model prediction (line) for high air cooling processing conditions and mass flow rate equal to 375 kg/h (cooling ring height, $L_{CRH} = 0.26$ m).

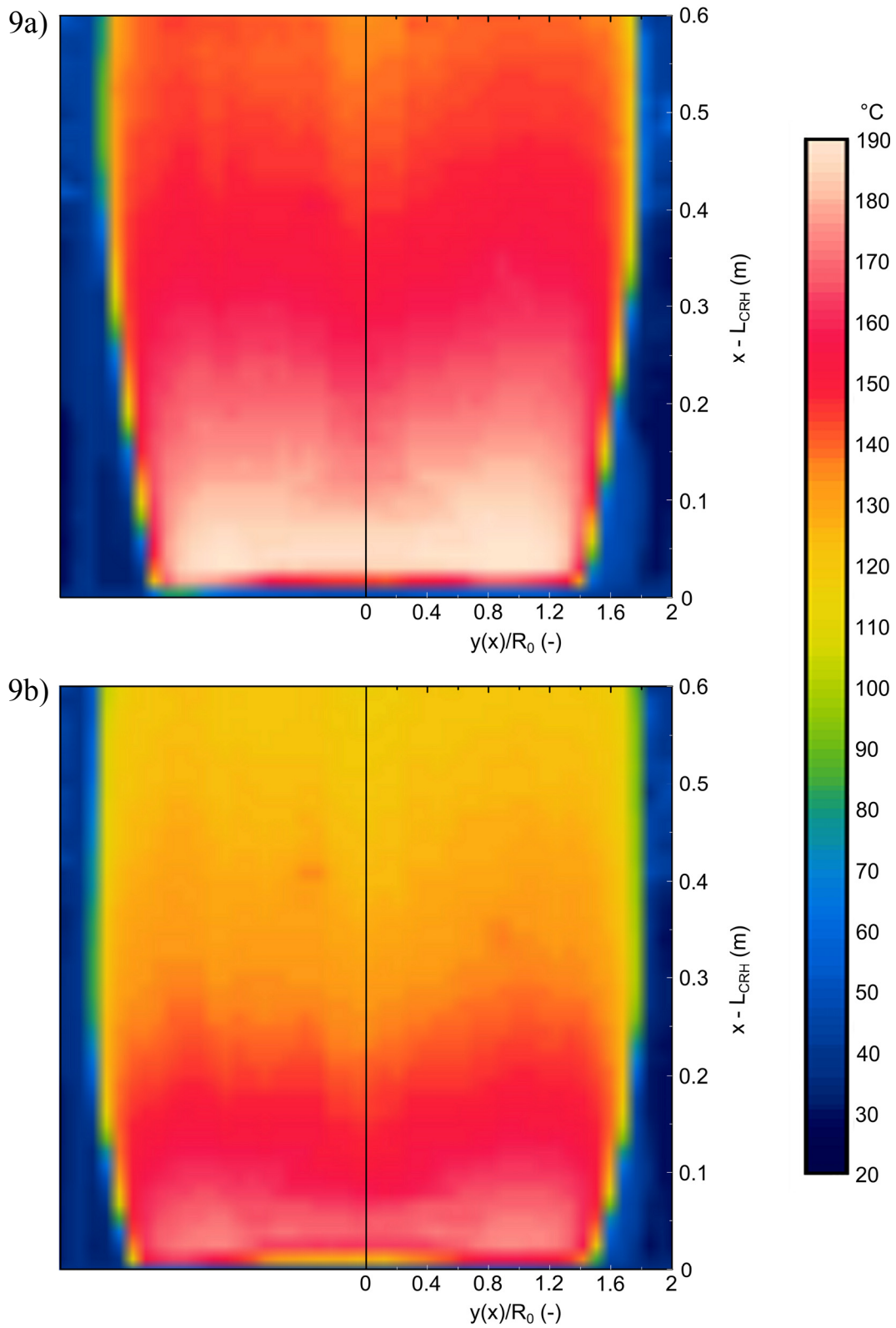


Figure 9. The effect of air bubble cooling intensity on the average multi-layer bubble temperature filed at fixed mass flow rate (300 kg/h). **9a)** Low air cooling intensity (cooling ring height, $L_{CRH} = 0.26$ m). **9b)** High air cooling intensity (cooling ring height, $L_{CRH} = 0.26$ m).

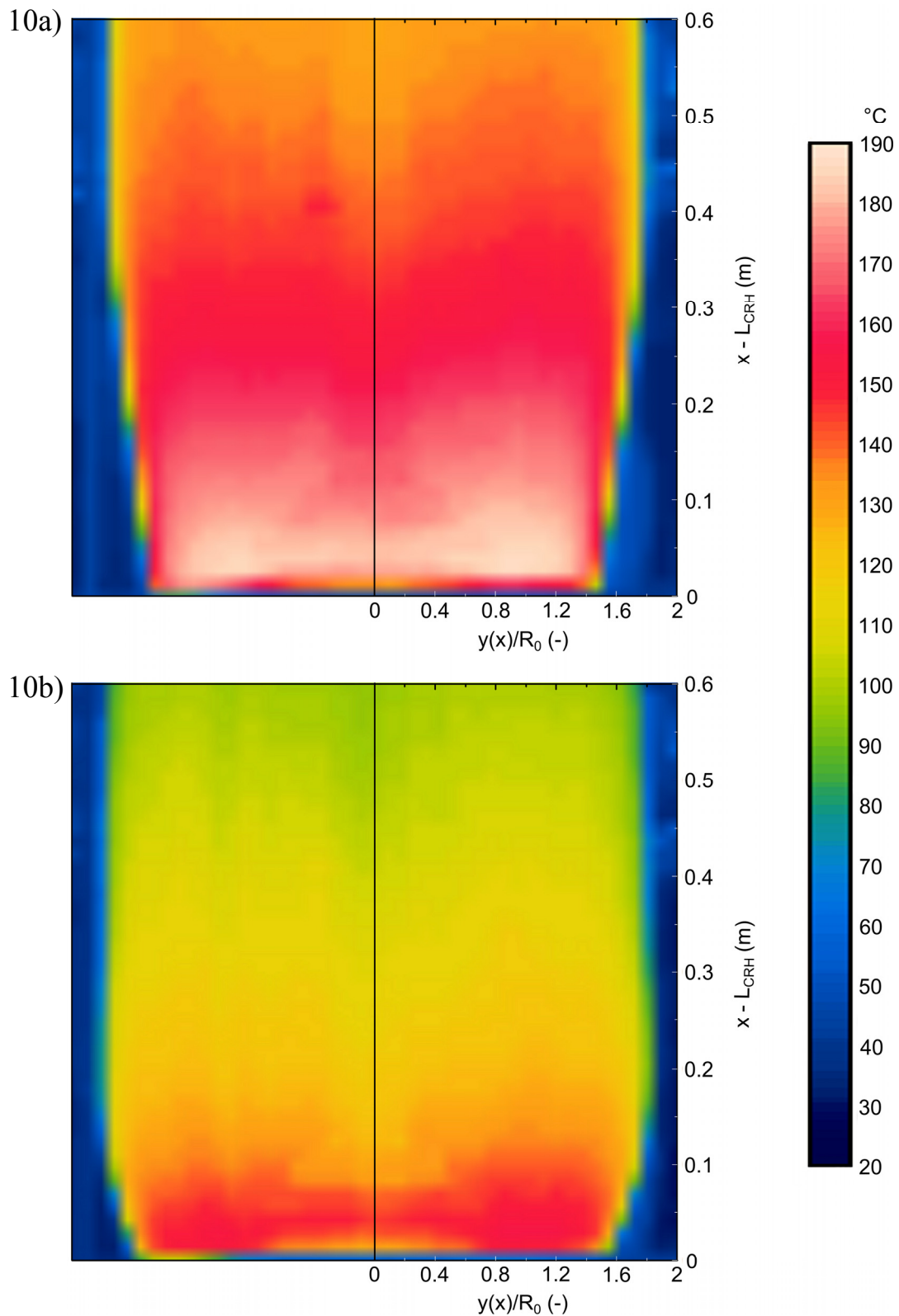


Figure 10. The effect of mass flow rate on the average multi-layer bubble temperature filed at the fixed high air cooling intensity. **10a)** Mass flow rate equal to 375 kg/h (cooling ring height, $L_{CRH} = 0.26$ m). **10b)** Mass flow rate equal to 225 kg/h (cooling ring height, $L_{CRH} = 0.26$ m).

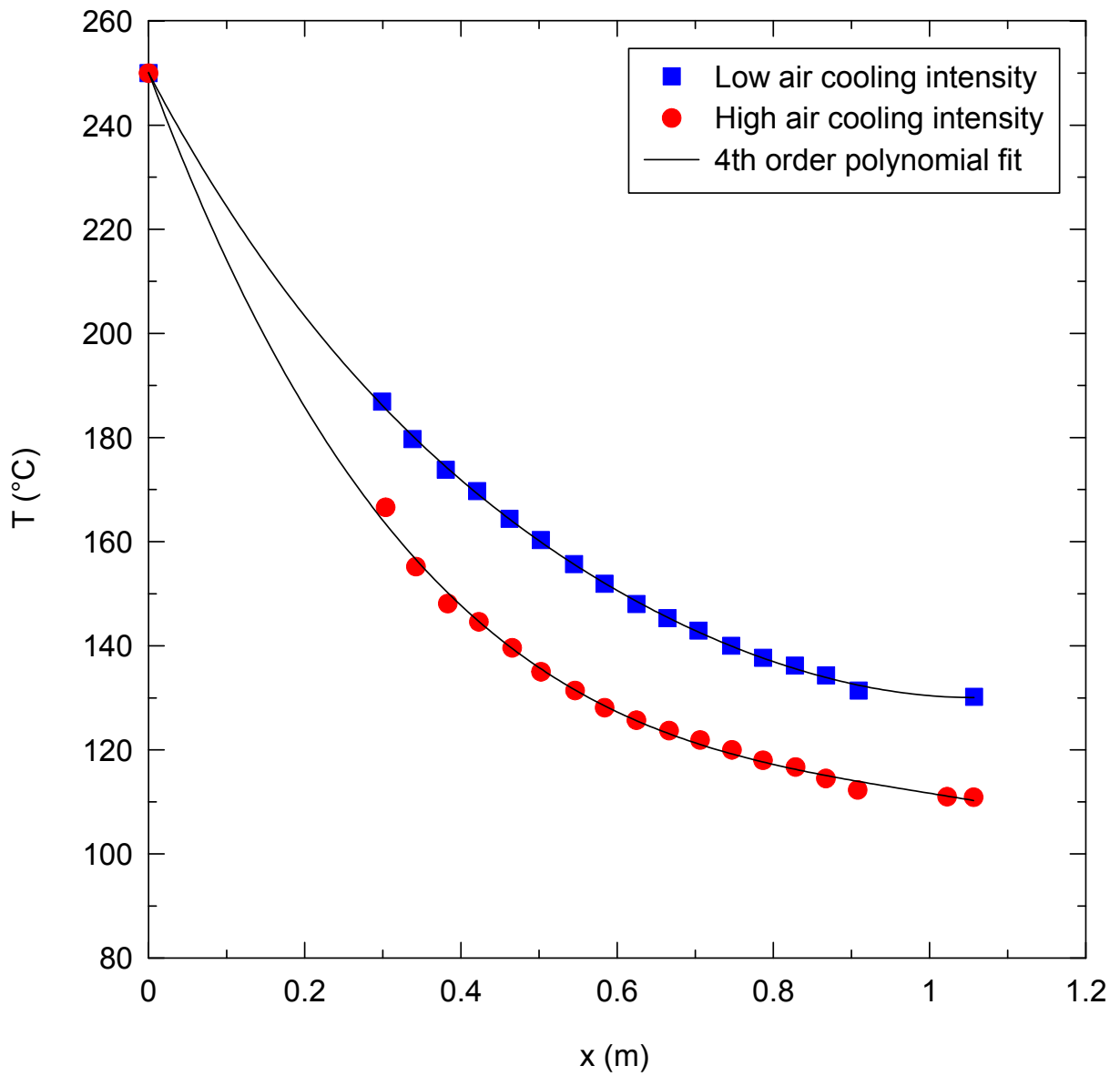


Figure 11. The effect of air bubble cooling intensity on the average multi-layer bubble temperature profile (taken from the bubble centre) at the fixed mass flow rate (300 kg/h).

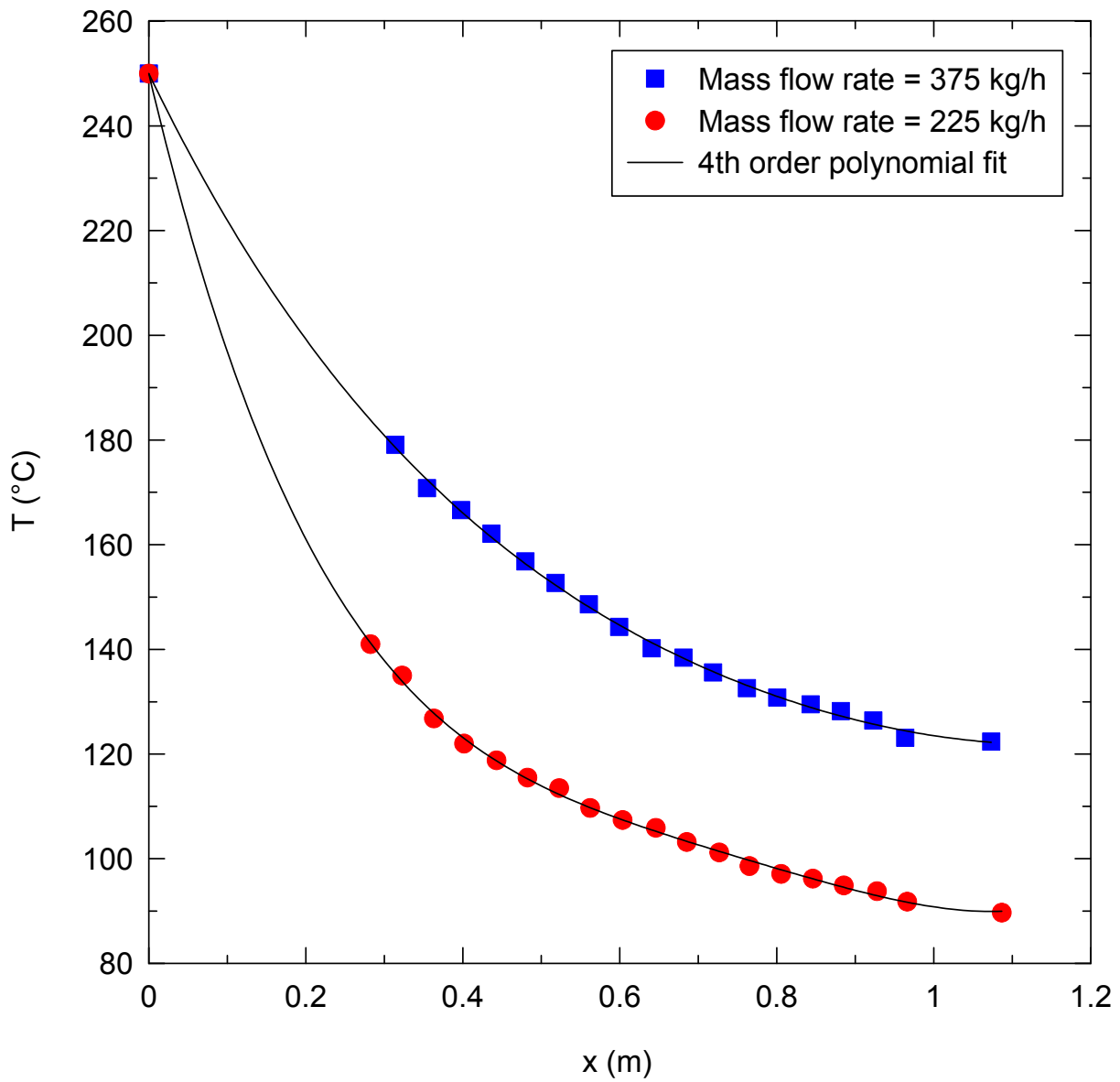


Figure 12. The effect of mass flow rate on the average multi-layer bubble temperature profile (taken from the bubble centre) at the fixed high air cooling intensity.

Personal data

CURRICULUM VITAE

Personal Information

First name / Surname	Roman Kolařík, Ing.
Address	Tomas Bata University in Zlín, Faculty of Technology, Polymer Centre, TGM 275, Zlín 762 72 Czech Republic
Telephone	+420 57 603 1322
E-mail	roman.kolarik@email.cz
Nationality	Czech
Date of birth	14.7. 1983
Birthplace	Zlín, Czech Republic

Education

Period	2008 – present
Title of qualification awarded	Ph.D.
Principal branch	Technology of Macromolecular Substances
Organisation providing education	Tomas Bata University in Zlín, Faculty of Technology Polymer Centre
Period	2006 – 2008
Title of qualification awarded	Ing.
Principal branch	Technological Equipments Design
Organisation providing education	Tomas Bata University in Zlín, Faculty of Technology, Department of Production Engineering
Period	2003 – 2006
Title of qualification awarded	Bc.
Principal branch	Technological Equipments
Organisation providing education	Tomas Bata University in Zlín, Faculty of Technology, Department of Production Engineering
Period	1999 – 2003
Principal branch	Engineering
Organisation providing education	Secondary Technical School Zlín

Training Abroad

Date	2010 (8 months)
Place	Canada, Ontario, Waterloo
Organisation providing training	University of Waterloo, Faculty of Engineering Department of Chemical Engineering

Work on Projects

2011-2014	Project CZ.1.05/2.1.00/03.0111 <i>Centre of Polymer Systems</i> Part-time employee
2010 – 2014	Grant GA ĀR P108/10/1325 <i>Applied Rheology for Advanced Polymer Processing</i> Member of research team
2011-2013	Project CZ.1.07/2.200/15.0363 <i>Innovation Education in Technology and Applications of Polymers</i> Member of research team
2009 – 2013	Grant GA ĀR 103/09/2066 <i>Analysis and Development of Constitutive Equations for Description of Non-Newtonian Fluids</i> Member of research team
2011	Grant UTB IGA/2/FT/11/D <i>Investigation of Negative Die Drool Phenomenon During Polymer Extrusion</i> Member of research team
2007 – 2011	Grant GA AV ĀR IAA200600703 <i>Investigation of Flow Behavior for a Novel Class of Metallocene- Based Polymers</i> Member of research team

2010 Grant UTB IGA/3/FT/10/D
Modeling of the Vortex Development During Polymer Extrusion Process
Member of research team

2008 – 2010 Grant MSMT ME08090
Analysis of Extrusion Post-Die Instabilities for Advanced Viscoelastic Macromolecular Substances
Member of research team

LIST OF PUBLICATIONS

Impact Factor Journal Papers Abstracted on Web of Science Database

1. KOLARIK, R., ZATLOUKAL, M., TZOGANAKIS, C. Stability Analysis of Non-Isothermal Film Blowing Process for Non-Newtonian Fluids using Variational Principles. *Chem. Eng. Sci.* 2012, vol. 73, pp. 439-453.
2. KOLARIK, R., ZATLOUKAL, M. Modeling of Non-Isothermal Film Blowing Process for Non-Newtonian Fluids by Using Variational Principles. *J. Appl. Polym. Sci.* 2011, vol. 122, no. 4, pp. 2807-2820.

Non Impact Factor Journal Papers Abstracted on Scopus Database

1. KOLARIK, R., ZATLOUKAL, M. Variational Principle Based Stability Analysis of Non-Isothermal Film Blowing Process for Non-Newtonian Fluids. *AIP Conference Proceedings* 2011, vol. 1375, pp. 56-74, ISSN: 0094243X.
2. KOLARIK, R., ZATLOUKAL, M. Modeling of Non-Isothermal Film Blowing Process for Polyolefines by Using Variational Principles. *AIP Conference Proceedings* 2009, vol. 1152, pp. 251-269, ISSN: 0094243X.

Conference Papers Abstracted on Web of Science and/or Scopus Databases

1. ZATLOUKAL, M., KOLARIK, R. Investigation of Processing and Rheological Parameters Effect on Film Blowing Process Stability by using Variational Principles. *Annual Technical Conference - ANTEC, Conference Proceedings* 2012.
2. KOLARIK, R., ZATLOUKAL, M. Variational Principle based Modeling of Film Blowing Process for LDPE Considering Non-Isothermal Conditions and Non-Newtonian Polymer Melt Behavior. *Recent Advances in Fluid Mechanics, Heat & Mass Transfer and Biology - Proc. of the 9th WSEAS Int. Conf. on FLUIDS'12* 2012, pp. 168-173, ISBN: 978-1-61804-065-7.
3. KOLARIK, R., ZATLOUKAL, M. Investigation of Polymer Long Chain Branching on Film Blowing Process Stability by using Variational Principle. *Recent Advances in Fluid Mechanics, Heat & Mass Transfer and Biology - Proc.*

- of the 9th WSEAS Int. Conf. on FLUIDS'12* 2012, pp. 174-179, ISBN: 978-1-61804-065-7.
4. ZATLOUKAL, M., KOLARIK, R. Modeling of Non-Isothermal Film Blowing Process for Non-Newtonian Fluids by using Variational Principles. *Annual Technical Conference - ANTEC, Conference Proceedings* 2011, vol. 2, pp. 1317-1322, ISBN: 978-161782960-4.
 5. ZATLOUKAL, M., KOLARIK, R. Non-Isothermal Film Blowing Process Stability Analysis by Using Variational Principles. *Annual Technical Conference - ANTEC, Conference Proceedings* 2009, pp. 1587-1595, ISBN: 978-161567327-8.
 6. ZATLOUKAL, M., KOLARIK, R. Film Blowing Process Stability Analysis for Non-Newtonian Fluids by Using Variational Principles. *Technical Papers, Regional Technical Conference - Society of Plastics Engineers* 2008, vol. 3, pp. 1370-1375, ISBN: 978-160560320-9
 7. ZATLOUKAL, M., KOLARIK, R., MARTYN, M., COATES, P. Investigation of Film Blowing Process Stability for Metallocene Based LLDPE with Different Level of Long Chain Branching. *Annual Technical Conference – ANTEC, Conference Proceedings* 2007, pp. 1565-1570, ISBN: 978-160423214-1.

Conference Papers Not Abstracted in Research Databases

1. ZATLOUKAL, M., KOLARIK, R., SAHA, P. Progress in Viscoelastic Modeling of Polymer processing with Respect to Free Surface Flow Instabilities. In: *Novel Trends in Rheology II*. Edited by M. Zatloukal, Tomas Bata University in Zlin. 2007, pp. 68-81, ISBN: 978-80-7318-591-6.
2. ZATLOUKAL, M., KOLARIK, R., MARTYN, M., COATES, P. Application of Variational Principles in Film Blowing Stability Analysis for Metallocene Based Polyolefines. *PPS Europe/Africa Regional Meeting* 2007, CD-ROM.
3. ZATLOUKAL, M., KOLARIK, R., MARTYN, M., SAHA, P. Theoretical and Experimental Investigation of Film Blowing Process Stability for Metallocene Based LLDPE with Different Level of LCB. *3rd Annual European Rheology Conference* 2006, vol. 195.

Book Chapters

1. ZATLOUKAL, M., CHALOUPKOVA, K., KOLARIK, R., MARTYN, M., COATES, P. Progress in Strongly Nonlinear Viscoelastic Modeling of Polymer Processing with Respect to Free Surface Flow Instabilities. In Polymer Process Engineering 07: Enhanced Polymer Processing. Edited by PD Coates, University Press, Bradford, UK, 2007, pp. 176-232, ISBN: 1-85143-248-5.

Theses

1. KOLARIK, R. Non - Isothermal Film Blowing Process Stability Analysis for Non - Newtonian Fluids by using Variational Principles. *Master Thesis*, Zlín, Tomas Bata University in Zlín, Faculty of Technology, 2008.
supervisor: prof. Ing. Martin Zatloukal, Ph.D.
2. KOLARIK, R. Modeling of the Film Blowing Process by using Variational Principles. *Bachelor Thesis*, Zlín, Tomas Bata University in Zlín, Faculty of Technology, 2006.
supervisor: doc. Ing. Martin Zatloukal, Ph.D.

Roman Kolařík

**Modeling of Film Blowing Process for Non-Newtonian
Fluids by using Variational Principles**

Modelování procesu vyfukování fólií pro neneutonské
kapaliny s využitím variačního počtu

Doctoral Thesis Summary

Published by Tomas Bata University in Zlín,
Nám. T. G. Masaryka 5555, 760 01, Zlín.

This publication has not been edited.

Year of publishing 2012